Horizon 2020
European Union Funding
for Research & Innovation

In2Rail

In2Rail

Project Title:	**INNOVATIVE INTELLIGENT RAIL**
Starting date:	01/05/2015
Duration in months:	36
Call (part) identifier:	H2020-MG-2014
Grant agreement no:	635900

Deliverable D3.1

Investigation of Repair Methods and Welding Techniques

Due date of deliverable	Month 32
Actual submission date	31-12-2017
Organization name of lead contractor for this deliverable	Trafikverket
Dissemination level	PU
Revision	FINAL

Authors

		Details of contribution
Author(s)	**Trafikverket (TRV)** Stefan Kallander	Structuring the whole document.
Contributor(s)	**ACCIONA** Carlos Hermosilla Carrasco Rafael Sanchez Villardon	Co-writing Chapters 5.1 and 5.5 together with UoH Review of Chapters 3 and 5-8
	British Steel Sandra Fretwell-Smith Frédéric Fau Chen Zhu	Writing Appendix 1. Co-writing Chapter 5.2 together with UoH. Review of Chapters 3-8.
	Chalmers University of Technology (CHALMERS) Anders Ekberg Elena Kabo Michele Maglio	Structuring the whole document. Writing Appendix 2. Writing Chapters 5.3 and 7.3. Given input to Chapters 3, 5-8. Review of Chapters 1-8. Writing Executive summary and Conclusions
	Network Rail (NR) Robert Cox	Co-writing Chapter 3 together with UoH, TRV and SNCF. Review of Chapters 1-8.
	Trafikverket (TRV) Stefan Kallander	Writing Chapters 1 and 2. Co-writing Chapter 3 together with UoH, NR and SNCF. Given input to Chapter 8. Review of Chapters 1-8.
	University of Huddersfield (UoH) Yann Bezin Jay Jaiswal Matin Sichani	Writing Chapter 4. Writing Chapter 6. Writing Chpater 3.2 and the co-writings see above. Given input to Chapters 3, 5, 7 and 8. Review of Chapters 1-8.
	Société Nationale des Chemins de fer Français (SNCF) Charles Voivret	Co-writing Chapter 3 together with UoH, TRV and NR. Review of chapters 1-8..

Executive Summary

Repair of running surface defects provides a cost-effective alternative to expensive rail replacement. The report demonstrates and supports further development and assessment of existing and upcoming rail head repair methods.

To this end, chapter 3 sets out with an in-depth overview of different rail head defects with a focus on which defects that can be mitigated by repair welding. This is combined with a statistical analysis of the occurrence of the different defects on major European networks. The charting of repairable rail head defects is contrasted to an overview of existing repair welding methods.

Repair welding relates to a number of challenges. The first is to ensure a smooth and aligned running surface. Chapter 4 investigates this issue by analysing consequences of imperfect weld geometries. Standards for allowed irregularities are described, and simulations of dynamic wheel–rail interactions are carried out to assess how imperfect longitudinal geometries (so-called weld dip) affect the contact forces at different operational conditions. The fact that not only the longitudinal, but the entire 3D geometry affects the dynamic wheel–rail interaction is acknowledged and assessed. Further, the altered mechanical properties of the weld may lead to local wear in the vicinity of the weld (so-called weld cupping). This will deteriorate the contact geometry over time. This phenomenon is investigated through numerical simulations.

The overview assessment of repair methods in chapter 3 is taken further in chapter 5 where operational aspects of the different methods are assessed in detail. This includes the need for equipment, productivity issues, and potential challenges in further development of the method.

The metallurgical integrity of welds is crucial since material defects, pores and phase transformation can drastically reduce the operational life and the structural integrity of the weld. Detailed tests have been undertaken and are reported in Chapter 5.2 and Appendix 1. This also relates to the steel grade of the rails to be repaired, a topic that is discussed in Chapter 5.3.

The quality of the weld is highly influenced by the thermal stress field induced by the welding process. This topic is investigated in detail in Chapter 5.4 and Appendix 2. The study shows the possibility of numerical simulations and investigates in detail requirements and sensitivities of numerical models. In particular it highlights the sensitivity that relate both to simulation parameters and to experimental testing to establish the temperature fields at a repair weld. The thermal analysis is then extended to a thermomechanical analysis that is able to investigate the residual state of stress after repair welding. It is noted that such analyses can be used to compare repair methods and also investigate the sensitivity to different operational parameters.

Chapter 6 takes the study in chapter 5 a step further by more in detail addressing the possibility of further development of methods based on aluminothermic welding and fluxed cored arc welding (FCAW). Recommendations for further development and investigations are detailed.

The recommendations for future studies are elaborated in chapter 7. Here first the desired attributes of a rail defect repair system are outlined. Based on this the discrete defect repair (DDR) method is considered to have the largest potential of the methods investigated. The most important scopes for development of this method are highlighted in chapter 7.2.

One crucial issue in developing innovative repair techniques is to have a "streamlined" approval process where requirements are clear and the evaluation process features a combination of numerical simulations, laboratory testing and validating field tests. The outline of such a process is presented in chapter 7.3.

Finally, it is noted that the current studies have focused on repair welding of plain rails. The methods could however be more widely deployed. Potentials and challenges with a wider application are discussed in chapter 7.4.

The report ends with a summary of the main conclusions in chapter 8.

TABLE OF CONTENTS

Abbreviations and acronyms

Abbreviation / Acronyms	Description
60E1	Rail profile
60E2	Rail profile
ABAQUS/CAE	Software for simulations
AREMA	American Railway Engineering and Maintenance-of-Way Association
AT	Aluminothermic weld
C4R	Capacity for rail – European funded project
CEN	European committee for standardization
DB	Deutsche Bahn
DDR	Discrete Defect Repair
EN	European norm
ESAB	Manufacturer of welding consumables (wires, rods etc)
EU	European Union
FP7	Seventh Framework Programme for Research and Technological Development – European funded project
FCAW	Fluxed Cored Arc Welding
FE	Finite Element
GB	Great Britain
GPa	Gigapascal (Unit of pressure)
HAZ	Heat Affected Zone
Hz	Hertz (Unit of frequenzy)
HB	Brinell (Unit for hardness)
HV	Vickers (Unit for hardness)
IBJ	Insulated Block Joint
INNOTRACK	Innovative track Systems – European funded project
IRR	Institute of Railway Research
LCC	Life Cycle Cost
Ltd	Limited company
MATWELD	Division of Railtech International
MGT	Million Gross Tonnes (Traffic load)
MMA	Manual Metal Arc
MPa	Megapascal (Unit of pressure)
NDT	Non Destructive Testing
NR	Network Rail
PLC	Programmable Logic Controller
PPE	Personal Protective Equipment
RCF	Rolling Contact Fatigue
S&C	Switches and Crossings
SAW	Submerged Arc Welding
SkV	Aluminothermic welding method for joining rails
SNCF	Société Nationale des Chemins de fer Français (Railway administration in France)
UoH	University of Huddersfield
UT	Ultrasonic Testing
UK	United Kingdom
WRIST	Innovative Welding Processes for New Rail Infrastructures – European funded project
UIC	International union of railways

1. Background

The present document constitutes Deliverable D3.1 “Investigation of repair methods and welding techniques” in the framework of the Project titled “Innovative Intelligent Rail” (Project Acronym: IN^{2}RAIL; Grant Agreement No 635900).

During the last 5 to 10 years the European railway networks have faced a higher amount of local rail head defects. The complex contact conditions at the rail–wheel interface can lead to the formation of local rail head defects such as squats and wheel burns. If remedial maintenance is not undertaken on such defects, they grow and can lead to transverse rail breaks, although, modern inspection techniques are sufficiently advanced to ensure early detection to prevent transverse rail breaks. If detected relatively early, the repair of such running surface defects provides a cost-effective alternative to expensive rail replacement. Rail head defects affect track possessions, maintenance cost and train disturbance. Therefore, one of the tasks included within the Horizon 2020 project IN^{2}RAIL is the development and evaluation of technologies for cost effective repair of rail head defects.

The major challenges with local repair welding are:

- to obtain a rail that has the correct geometry and finish of the running surface in the vicinity of the repair to prevent “weld dips”;
- prevent differential wear across heat affected zone, “weld cupping”;
- produce clean weld metallurgy to prevent subsequent crack initiation;
- produce a residual stress field that does not promote growth of initiated cracks.

This document has been prepared to demonstrate and support further development and assessment of existing and upcoming rail head repair methods. For further development and enhancements of the technologies recommendations are given to next stage in the Shif2Rail project.

2. Objective / Aim

The complexity and severity of the contact stresses at the rail-wheel interface coupled with operational conditions of acceleration and braking can lead to the formation of local rail head defects such as squats and wheel burns even in the best maintained railway networks. Such defects are generally detected by modern track inspection to prevent transverse breaks. Depending on their size and severity, such defects can either undergo in-situ repair or a short length of rail containing the defect is replaced.

Consequently, the primary objective of Work Package 3.1 is the "Development, assessment and validation of local rail head repair solutions". It involves:

- analysis of current problems and advantages/disadvantages of current techniques;
- analysis of feasibility and assessment of selected welding processes including establishment of tolerances;
- identification of more innovative repair methods with proposals for further development in follow up projects within Shift2Rail initiative.

3. Evaluation of current problems

3.1. Detailed technical analysis of current problems

Running of steel wheels on steel rails creates very arduous conditions within the rail wheel contact patch leading to gradual degradation of both mating surfaces. Under ideal conditions of rolling contact, the primary degradation mechanism is wear and rails would last until the worn section dimensions became incapable of supporting the load being imposed by the passing vehicles. However, the complexity of vehicle track interaction and its dependency on a wide range of track design and traffic characteristics, leads to a variety of running surface defects that can significantly reduce the life of the rail. Although a number of such defects are relatively shallow and extend over <100mm in length, their continued presence compromises the integrity of the track and their rectification imposes a cost penalty on the maintenance budget. It is, therefore necessary to establish a matrix of rail head defects that could be repaired in-situ and thereby avoid the replacement of the affected length with a short length of new rail.

Although most European Railway networks have developed their own catalogues of rail defects [1], they are largely and adaptation of the UIC Code 712 [2] on Rail Defects. Table 1, based on the UIC code with additional references to the rail defect catalogues from other European Railway Networks, list the defects that are potentially repairable using weld repair techniques. For completeness, Table 2 lists those defects that are not considered to be repairable. The location of the defects is as per UIC Code 712 and shown in Figure 3.1.

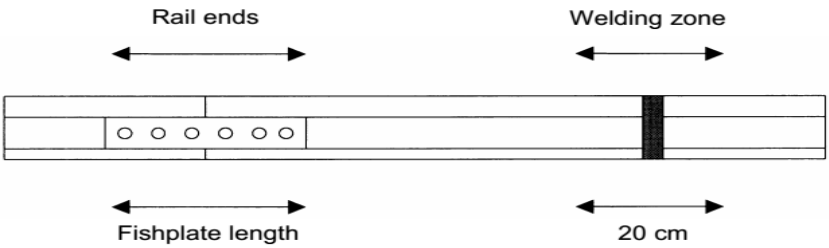

• Rail End • Welding Zone • Plain rail	• Part of the rail located within outer limits of fishplate • Part of the rail located within 100 mm on either side of the weld and within 10 to 25 mm (depending on regulations) on either side of a weld repaired area • Part of the rail located away from rail ends and welding zones

Figure 3.1: Location of defects as per UIC Code 712

Table 3.1: Weld repairable rail head defects

UIC 712 Code No. [2]	NR Defect Code [1]	Defect Description	Suitability for Weld Repair
121	*	Surface defects	Suitable for resurfacing by weld deposition of very localised defects of this type. However, this defect is rare with modern rail manufacturing methods and consequently have not been included in the defect catalogues of some railways such as NR.
122	Same	Shelling of running surface	Suitable for weld repair
123	106	Crushing	Localised crushing at rail ends may be suitable for weld repair
127	127	Squat at Rail End	Suitable for weld repair
125	129	Wheel burns	Suitable for weld repair
221	*216*	*Surface defects*	*Suitable for resurfacing by weld deposition of very localised defects of this type. However, this defect is rare with modern rail manufacturing methods and consequently have not been included in the defect catalogues of some railways such as NR.*
2203	*204*	*Lateral wear*	*Generally, not suitable for weld repair but there is potential for weld repair in specific locations to impart lower coefficient of friction and increased wear resistance*
2221	*222*	*Shelling of the running surface*	*Suitable for weld repair if very localised*
2222	*221*	*Shelling of the gauge corner*	*Suitable for weld repair if very localised*
2251	2291	Isolated wheel burn	Suitable for weld repair
227	227	Squat / Cracking and local depression of the running surface	Suitable for weld repair
301	241	Bruising	Some shallow bruises on the surface of the rails are suitable for weld repair
*	423	Gauge Corner cracking or Head checking at weld	Potentially weld repairable if detected early
*	427	Squat at weld	Suitable for weld repair
*	429	Wheel burn on a weld	Potentially weld repairable if detected early
472	482	Detachment or shelling of resurface portion	Suitable for weld repair
*	705	Crossing nose wear	Suitable for weld repair
*	721	Shelling of the gauge corner of a cast crossing	Suitable for weld repair
* = No equivalent defect code			

Table 3.2: Rail head defects that are not weld repairable

Table 2

UIC 712 Code No.	NR Defect Code	Defect Description	Suitability for Weld Repair
111	Same	Progressive transverse cracking	Not suitable for weld repair
112	Same	Horizontal cracking	Not suitable for weld repair
113	Same	Longitudinal vertical cracking	Not suitable for weld repair
*	123	Gauge Corner cracking or Head checking at rail end	Not suitable for weld repair
124	*	Local batter of running surface	Not suitable for weld repair
*	207	Localised Head Loss	Not suitable for weld repair
*	208	Insufficient rail depth	Not suitable for weld repair
*	209	Lipping	Not suitable for weld repair
211	Same	Progressive transverse cracking	Not suitable for weld repair
212	Same	Horizontal cracking	Not suitable for weld repair
213	Same	Longitudinal vertical cracking	Not suitable for weld repair
2201	202	Short-pitch corrugation	Not suitable for weld repair
2202	203	Long-pitch corrugation	Not suitable for weld repair
2204	205	Abnormal vertical wear	Not suitable for weld repair
2223	223/224	Head checking at the gauge corner	Not suitable for weld repair
2252	2292	Repeated wheel burns	Not suitable for weld repair
223	206	Crushing	Not suitable for weld repair
224	217	Local batter of the running surface	Not suitable for weld repair
302	*	Faulty machining	Not suitable for weld repair
303	243	Permanent deformation	Not suitable for weld repair
411	Same	Transverse cracking of the profile (Electric Flash-butt welding)	Generally, not suitable for weld repair since sub-surface fatigue can be deep and well developed when detected
421	*	Transverse cracking of the profile (Thermit welding)	Generally, not suitable for weld repair since sub-surface fatigue can be deep and well developed when detected
431	*	Transverse cracking of the profile (Electric arc welding)	Generally, not suitable for weld repair since sub-surface fatigue can be deep and well developed when detected
471	481	Transverse cracking of the profile (weld repair)	Generally, not suitable for weld repair since sub-surface fatigue can be deep and well developed when detected
* = No equivalent defect code			

3.1.1. Statistics of rail defects from Network Rail

Although Table 3.1 1 identifies rail head defects that could be weld repaired, it is necessary to establish the frequency of occurrence of these defects so as to better justify the development of cost effective repair techniques. This is shown in Figure 3.2 using data from Network Rail for the year 2015-16.

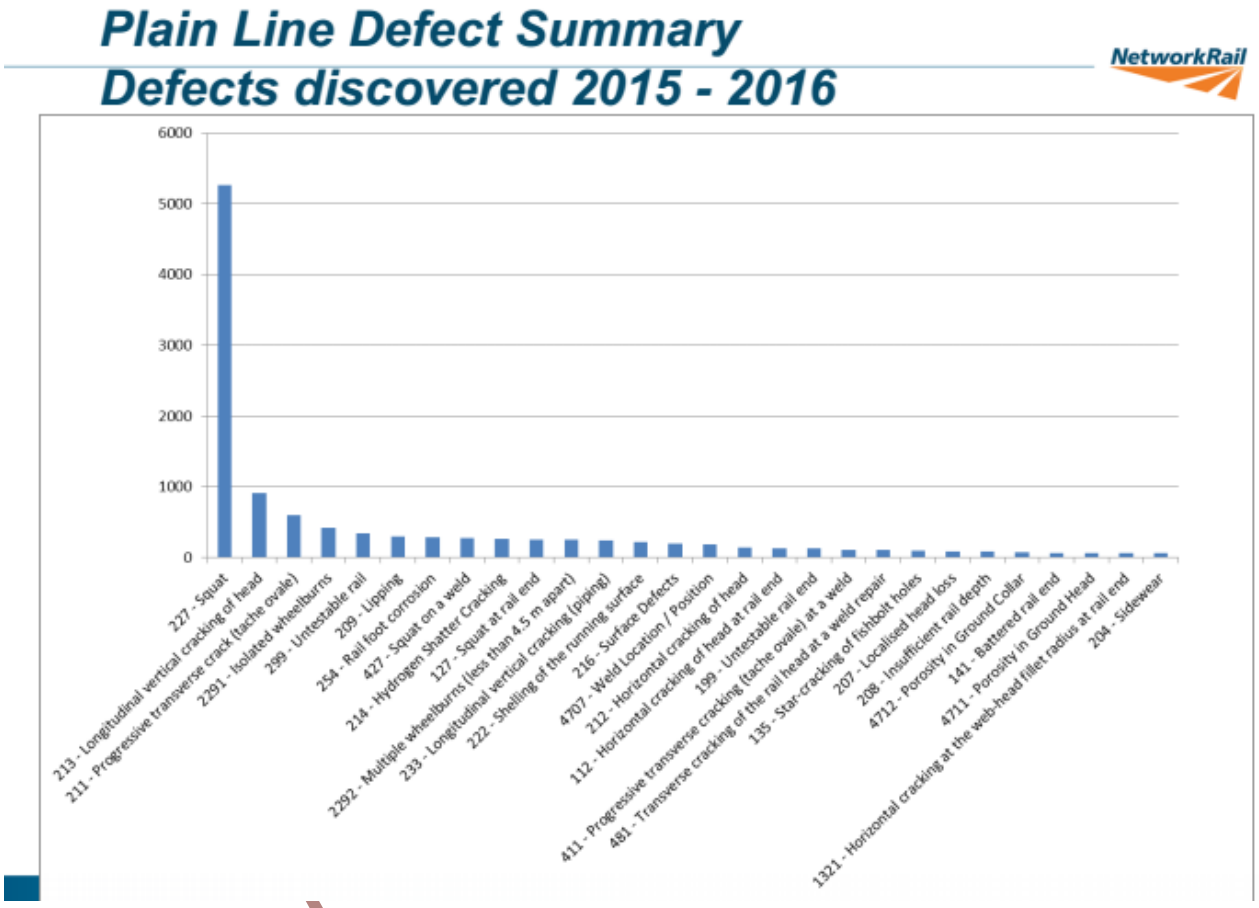

Figure 3.2: Frequency of occurrence of various rail defects

Information and data from Table 3.1 and Figure 3.2 indicate that annually there are ~6 300 defects within the 33 000km network of NR that have the potential of being restored by weld repair techniques. However, it is likely that the lengths and depths of a proportion of the defects detected make them unsuitable for cost effective repair with rail replacement being the preferred option. Hence, an estimate of 60% of the ~6 300 defects of the appropriate defect code detected is suggested as a pragmatic approximation of repairable defects in a 33 000km modern railway network. Figure 3.2 also indicates that squat defects in mid rail, weld, or rail end locations is the predominant defect type that is considered weld repairable. Consequently, additional information that would be useful in the assessment of the various weld repair techniques are the length and depth dimensions of such squat defects. Historical information of

the length and depth of Squat defects detected in NR network is provided in Table 3.3 and Table 3.4.

Table 3.3: Length of squat defects detected in NR network

Year	% of Defects in Size Range				
	No <51 mm long	No >50 <101 mm long	No >100 <201 mm long	Blanks & Erroneous Entries	Total
2016	40.7	44.3	8.4	6.5	100.0
2015	58.7	28.5	5.7	7.0	100.0
2014	66.0	21.9	4.5	7.6	100.0
2013	62.7	26.5	5.0	5.8	100.0
2012	64.7	24.3	3.8	7.2	100.0
2011	59.9	29.1	4.4	6.6	100.0
Average	**58.8**	**29.1**	**5.3**	**6.8**	**100.0**

Table 3.4: Depth of squat defects detected in NR network

Year	% of Defects in Size Range					
	1-10 mm deep	11-15mm deep	16-20 mm deep	21-30 mm deep	Blanks	Total
2016	54.6	30.6	4.4	2.0	8.4	100.0
2015	49.8	35.4	4.5	1.8	8.5	100.0
2014	37.9	43.0	7.6	2.8	8.6	100.0
2013	30.0	51.4	7.9	3.0	7.7	100.0
2012	23.1	58.5	7.2	2.3	8.9	100.0
2011	21.8	57.7	8.9	3.1	8.6	100.0
Average	**36.2**	**46.1**	**6.7**	**2.5**	**8.4**	**100.0**

Data in Table 3.3 and Table 3.4 suggest that >80% of the squat defects were <101 mm long and <15 mm deep with a small % being up to 200 mm long and 20 mm deep. Consequently, weld repair techniques must be capable of restoring defects that are <100 mm in length and <15 mm deep but preferably defects up to 200 mm long and 20 mm deep in the most cost-effective manner in the minimum time on site. It is expected that the above repair dimensions will also fulfil the requirements for the repair of the other rail head defects identified in Table 3.1.

3.1.2. Statistics of rail defects from Trafikverket

Sweden´s railway network is just over 16 500 track kilometres. Of this, Trafikverket manages the infrastructure of 14 100 track kilometres. As a part of the safety work and maintenance of certain track standard, a large proportion of rails and rail components are checked with non-

destructive testing. The non-destructive test consists mainly of ultrasonic testing, but trials are also being undertaken with eddy current in order to detect rail defects. The ultrasonic inspections are both automated and manually and are performed at intervals according to the actual track sections inspection class.

Detected defects are divided in two different groups, group one and group two. Group one defects must be remedied within a maximum of three months. Group one defects have three different action priorities, A – immediate action, V – two weeks action time, M – three months action time. Group two defects, B, are allowed to be left in track but are inspected at all security inspections until the defects have been removed.

Summary of detected rail defects in Plain line (S&C excluded) is shown in Table 3.5 and Figure 3.3. The defects are as per UIC code 712 [2].

Table 3.5: Number of defects in plain line detected by ultrasonic testing 2011 – 2016

Plain line	2011	2012	2013	2014	2015	2016
Group 1 (A/V/M)	1718	1934	1755	1917	2360	1817
Group 2 (B)	368	509	544	302	633	372
Total per year	**2086**	**2443**	**2299**	**2219**	**2993**	**2189**
Inspected track kilometer	12 000	12 875	13 143	15 117	16 130	13 369
Defects per track kilometer	0,17	0,19	0,17	0,15	0,19	0,16

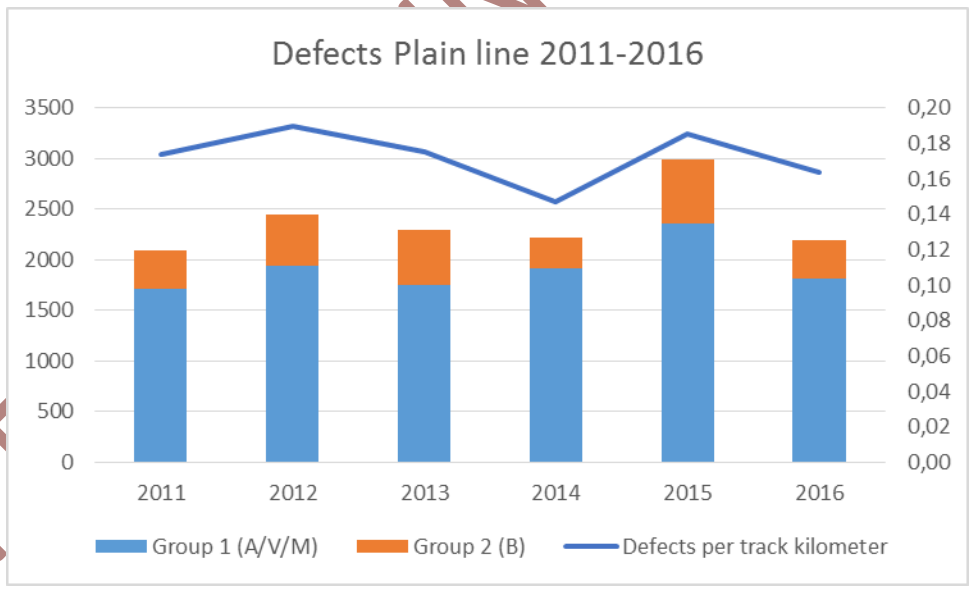

Figure 3.3: Number of defects in plain line from ultrasonic testing in year 2011 – 2016 and number of defects per track kilometre, within Trafikverket network

Although the length of track inspected has increased every year, the number of defects detected has remained broadly constant at 0.15-0.19 defect per track kilometre, with the higher end being comparable to the corresponding value from NR.

Comparing repairable defects listed in Table 3.1, the result is quite similar and is shown in Table 3.6 and Figure 3.4.

Table 3.6: Repairable defects in plain line detected by ultrasonic testing 2011 – 2016

Repairable rail defects Plain line	2011	2012	2013	2014	2015	2016
Squat/ 127, 227	522	643	815	948	914	820
Squat alu. weld/ 427	30	58	89	61	98	67
Wheel burns/ 125, 2251	11	6	9	5	4	3
Detachment or shelling of the resurfaced portion/ 472	10	9	6	4	8	4
Surface defects/ 121, 122, 123	9	28	26	18	26	18
Total per year	**582**	**744**	**945**	**1036**	**1050**	**912**
Inspected track kilometer	12 000	12 875	13 143	15 117	16 130	13 369
Repairable Defects per track kilometer	0,05	0,06	0,07	0,07	0,07	0,07

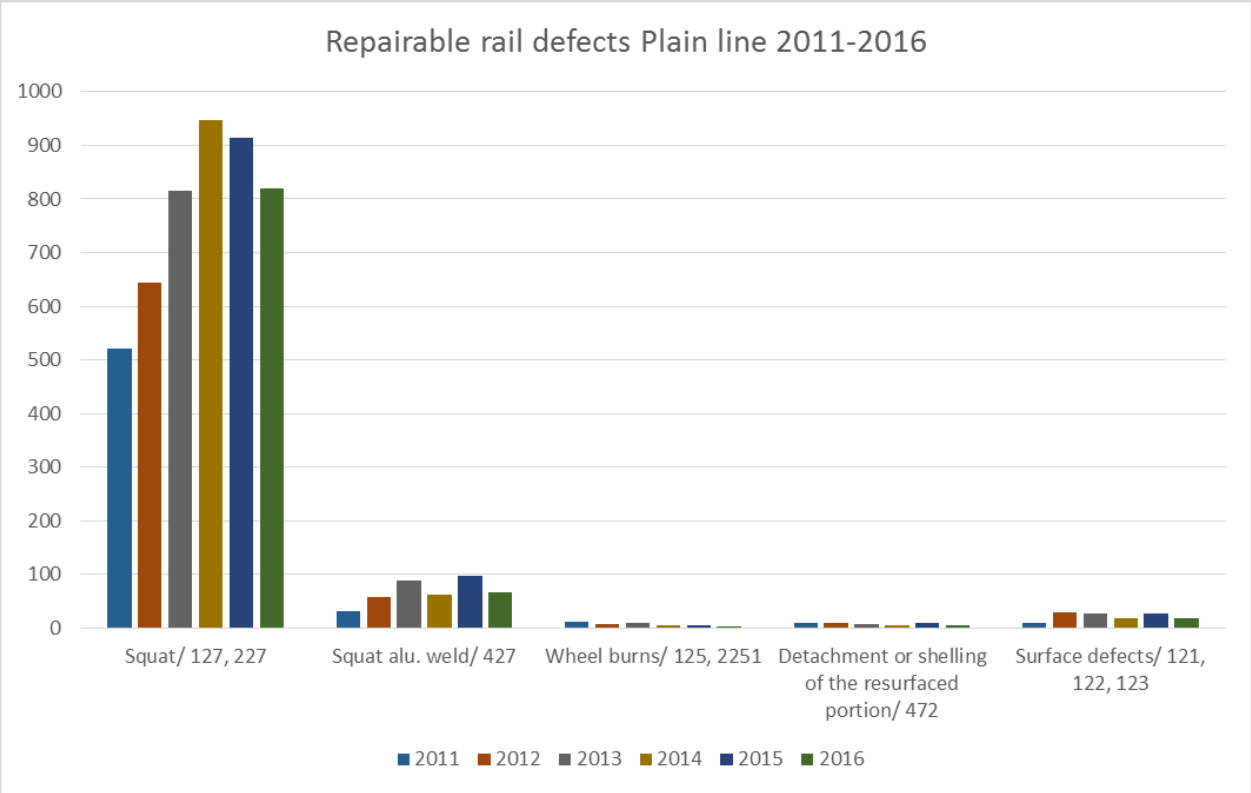

Figure 3.4: Number of repairable defects in plain detected by ultrasonic testing 2011 – 2016

The above data refers to defects in plain line and addition of similar data for repairable rail defects in switches and crossings would increase the above total by ~150 per year bringing the total to around 1150.

3.1.3. Statistics of rail defects from SNCF

France´s railway network is composed of 49 250 track kilometres including nearly 4 100 kilometres of high speed lines. The rail is inspected through visual examination and non-

destructive ultrasonic testing. Ultrasonic inspections are both automated and manually done. Over the period 2013–2016, the average number of defect per kilometre is 2.67 including all classes of defects in terms of size. The repartition of these detected defects is presented in Figure 3.5. The number of defect falling in category eligible for repair (squat, shelling and weld) is stable and close to 100 000. An internal study carried out several years ago concluded that the effective number of repairable defects, considering defect size and repairing method capacity, is around 10 000 (10%). The data for SNCF appears to be higher than that for both NR and TRV in terms of the number of defects detected per unit length of track but significantly lower in terms of the proportion that are considered repairable. Such differences suggest the need for a pan European standard for the recording of rail defects and the criteria for the identification of repairable defects.

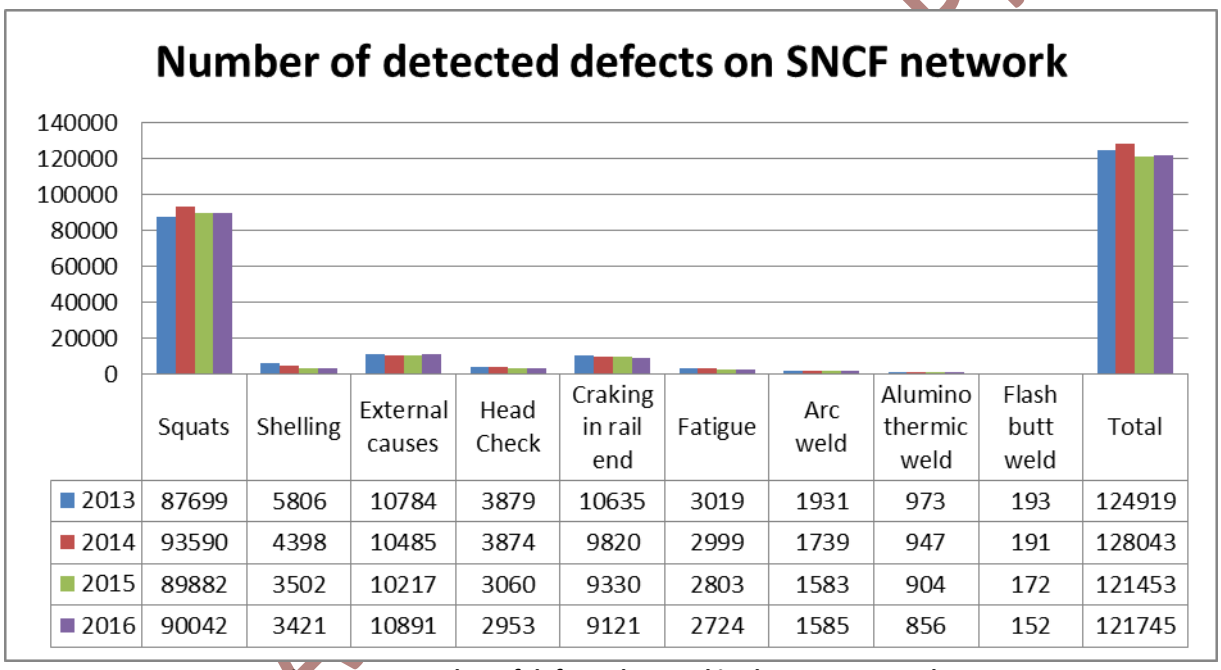

	Squats	Shelling	External causes	Head Check	Craking in rail end	Fatigue	Arc weld	Alumino thermic weld	Flash butt weld	Total
2013	87699	5806	10784	3879	10635	3019	1931	973	193	124919
2014	93590	4398	10485	3874	9820	2999	1739	947	191	128043
2015	89882	3502	10217	3060	9330	2803	1583	904	172	121453
2016	90042	3421	10891	2953	9121	2724	1585	856	152	121745

Figure 3.5: Number of defects detected in the SNCF network

3.2. Advantages and disadvantages of current techniques

The following are the key maintenance actions that are available to affect the repair of local rail head defects on the running surface of rails:

1. “Plug Rail”;
2. Manual Metal Arc repair;
3. Flux Cored Arc Welding (FCAW);
4. Wide Gap aluminothermic weld;
5. Flash Butt Wedge Repair;
6. Thermit Head Repair (THR) process / Railtech Head Wash Repair (HWR);
7. British Steel / ARR Discrete Defect Repair.

Brief description of these processes together with their advantages and disadvantages are provided in subsequent chapters.

3.2.1. "Plug Rail"

The process involves the replacement of the defective rail with a new length of rail. In view of the requirements of a minimum distance between two track welds of 4.5m, a 9m length of rail is generally used to replace the defective portion.

The key advantages of this approach are:

- uses well established procedures for rail replacement.

The key disadvantages of this approach are:

- two new aluminothermic welds (AT) are introduced into the network for every defective length replaced with the associated risks of geometrical irregularities and weld defects;
- time consuming and costly.

3.2.2. Manual Metal Arc (MMA) Repair

Manual Metal Arc (MMA) welding [3-5], technically known as Shielded Metal Arc Welding (SMAW), is a well-established technique used in many industries and was introduced into the railway track industry around the 1920s for the resurfacing of worn parts crossings and plain line rails. Since then the process has been used widely in the vast majority of railways throughout the world.

The complexity and severity of contact conditions demand extremely high integrity of weld repairs to avoid the dangers associated with rail breaks. Consequently, the industry has recognised the need for standardised approvals of the consumables and procedures used as well as the qualification of the welders undertaking the welding operation. The relevant EN standards that permit the delivery of the necessary controls are:

- EN 287-1, Qualification test of welders – Fusion welding – Part 1: Steels;
- EN ISO 544, Welding consumables – Technical delivery conditions for welding filler materials – Type of product, dimensions, tolerances and markings;
- EN 571-1, Non-destructive testing – Penetrant testing – Part 1: General principles;
- EN 1290, Non-destructive examination of welds – Magnetic particle examination of welds;
- EN ISO 15609-1, Specification and approval of welding procedures for metallic materials - Welding procedure specification - Part 1: Arc welding;
- EN ISO 15613, Specification and qualification of welding procedures for metallic materials - Qualification based on pre-production welding test;

- EN ISO 15614-1, Specification and qualification of welding procedures for metallic materials - Welding procedure test - Part 1: Arc and gas welding of steels and arc welding of nickel and nickel alloys.

The three critical aspects of the above standards are the approval of the consumables which come together with recommendations of control parameters and care instructions, the training of the welders, and the procedures to be adopted on site. Hence the above standards and translated into the Railway Company Standards [6] such as NR/L2/TRK/0132 – Issue 6 (4 December 2010) for Network Rail. Although a more up to date version of this document may now be available, reference to this version is considered adequate to demonstrate the degree of manual control that needs to be exercised with this process. Although not an exhaustive comparison, Table 3.7 compares some selected aspects of recommended procedures for the use of MMA welding for the repair of rail head defects on plain line for two networks [7-12].

Table 3.7: Key elements of MMA welding practice

Parameter	UK Practice [7-9]	Swedish Practice [10-12]
Consumables (Normal Grade Rail Group)	Filarc, KV3L Bohler, CM 2 KB Oerlikon, Chromoly 21 WB Alloys, 9009E (for repairs to Bainitic steels only) Murex, Armoid 1 (for track-circuit deposits only) Eutectic, 'Ductrode' XHD 646 (includes track-circuit deposits) Note: Stick electrodes need to be redried and kept at ~120°C when not in use	Rail steels <1175 MPa: ESAB OK 83.28, or OK 83.29, or Oerlikon-Citorail Note: Stick electrodes need to be redried and kept at ~120°C when not in use
Preheat Temperatures	Normal Grade Group (This probably refers to Grade R220 but could also be applicable to Grade R260): The temperature of the rail over the area to be welded, including an additional 75 mm at each end, shall be subjected to an initial preheat of 343°C minimum, maintained throughout welding. Alloyed and heat-treated rail groups: The welding of alloyed rails (wear-resisting grade B, 90 and 110 kg/mm2 chromium, microalloyed head hardened [MHH] and high performance [HP]), is not permitted without the prior written approval of Network Rails' Senior Technology Engineer (Welding).	R220 Grade: 300° – 350°C R260/R260Mn Grade: 350° – 400°C R320Cr Grade: 400° – 450°C R350HT/LHT Grade: 350° – 400°C Note: 1. Area to be repaired + 100 mm on either side must be preheated. 2. Temperature maintained throughout welding may not go under 50°C of the preheat temperature.
Deposition Techniques	Only the stringer bead technique shall be used. The use of the weave technique is not permitted. Weld beads shall be deposited such that they	

Parameter	UK Practice [7-9]	Swedish Practice [10-12]
	overlap one another by approximately one third	
	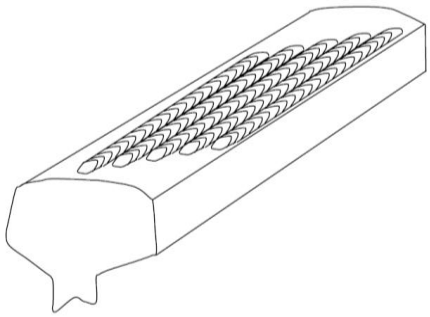	
Maximum dimensions of repair	Length: 200 mm. The maximum lengths specified include the tapered ends at the stop/start positions. Longer defects may be repaired. The 250, 200 or 125 mm length shall be completed and ground to profile on each occasion, prior to cutting back into the previously repaired length and continuing to completion Width: 50 mm. If defect extends to full head width, cut back into the head of the rail from the opposite side already repaired to remove fully. Repairs shall always commence on the non-running edge of the rail. See figure below. Depth: 15 mm from crown (red zone), 25 mm from crown (green zone). If defect cannot be removed at the maximum specified depth, a temporary repair shall be made, the rail fitted with emergency fishplates and clamps where practicable and rail replaced within 4 weeks	Length: Maintaining the temperature when welding over longer distances are difficult. The demand is to split up the welding areas in smaller sections (preheated section) when welding over longer distances. No specific distance is mentioned. Dimensions: Practically, it is often the time effort or existing track possessions that are controlling the dimensions of repair.
	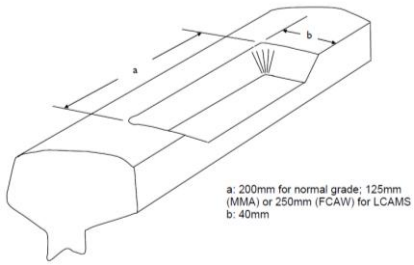	When a contractor is doing the procedure specification for MMA this geometry is used. 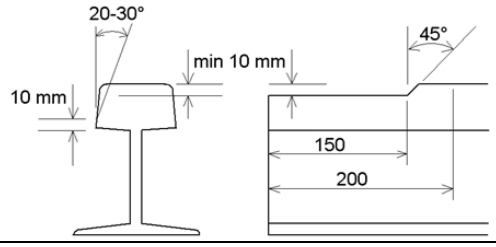
Welding parameters	Set as per manufacturers' recommendations and approved as per the relevant EN standards (EN ISO 15609-1 and EN ISO 15613)	

It is apparent that the consumables and welding parameters are approved according to the procedures detailed in the relevant EN standards. However, the integrity of the resultant weld repair is adjudged only on the static basis of hardness profile and microstructural constituent

within the HAZ and the weld metal. Since the weld repaired area and, particularly the interface with the parent metal, is subjected to cyclic loading and experiences a stress range, it would be prudent to include the assessment of repair integrity under dynamic loading such as in 4-point bend fatigue tests with the repaired head in tension. Nevertheless, it is acknowledged that MMA repairs of defects in rail have been undertaken over many decades and its short comings are apparent in the many rail breaks associated with weld repairs every year. This aspect is covered later in this chapter.

Based on the assessment of welding practices described above, the key advantages and disadvantages of MMA welding for the repair of local rail head defects are:

- Advantages:
  1. the process is long established and widely used in many industries;
  2. it offers flexibility of operation to permit cost effective repair over small areas and under complex access conditions;
  3. power sources for MMA welding are portable and robust and are used with diesel driven generators for site work.
- Disadvantages:
  1. the process details summarised in Table 3.7 depict many variables whose control is largely dependent on the diligence and competence of the welder. Some examples are:
     a. manual excavation, inspection to confirm defect removal, and the removal of slag after each layer of deposition can be a source of inconsistency,
     b. the permissible variation in preheat temperature of +150°C or -50°C appears large, although it is recognised that the aim is to slow down the cooling rate within the HAZ,
     c. the range of deposition patterns could lead to inconsistencies in HAZ width and microstructure as the dimensions of the patterns cannot be too precise in practice,
     d. the length of the weld deposit is largely governed by the durability of the electrode and the deposition rate achieved – manual control of the process can result in inconsistencies from one location to another and from one welder to another;
  2. quality of repair is very dependent on the competence and diligence of the welder;
  3. requires a mandated preheat temperature of at least ~350°C. – heating to extend to ~75-100 mm beyond the area to be repaired. Use of only a single burner is permitted and consequently attaining the required preheat temperature is relatively time consuming;
  4. audit trail of the process route is generally a paper check list and is, therefore, subjective;

5. time consuming and costly – MMA repair can take up to 8 hours;
6. although the rail is not cut through which is used as a justification for not undertaking rail re-stressing, the high and prolonged preheating of the rail coupled with the heat input during the process will alter the local residual stress pattern in the rail;
7. the lack of any process monitoring and the variability of the ground excavated surface have historically lead to inconsistency of quality with tiny defects at the weld-parent metal interface which subsequently lead to fatigue failure. The two most common flaws are porosity and slag entrapment. Such defects are generally tiny (but can also be large) and not detectable using conventional NDT techniques but are sufficiently critical to initiate fatigue. The fatigued area grows with the passage of traffic and reaches a size that is detectable by ultrasonic testing and the only remedial action is replacement of a short length of rail. If undetected, the fatigued area results in a loss of section strength and a transverse rail break. A pictorial representation of the most common types of defects associated with MMA weld repair are shown in Figure 3.6.

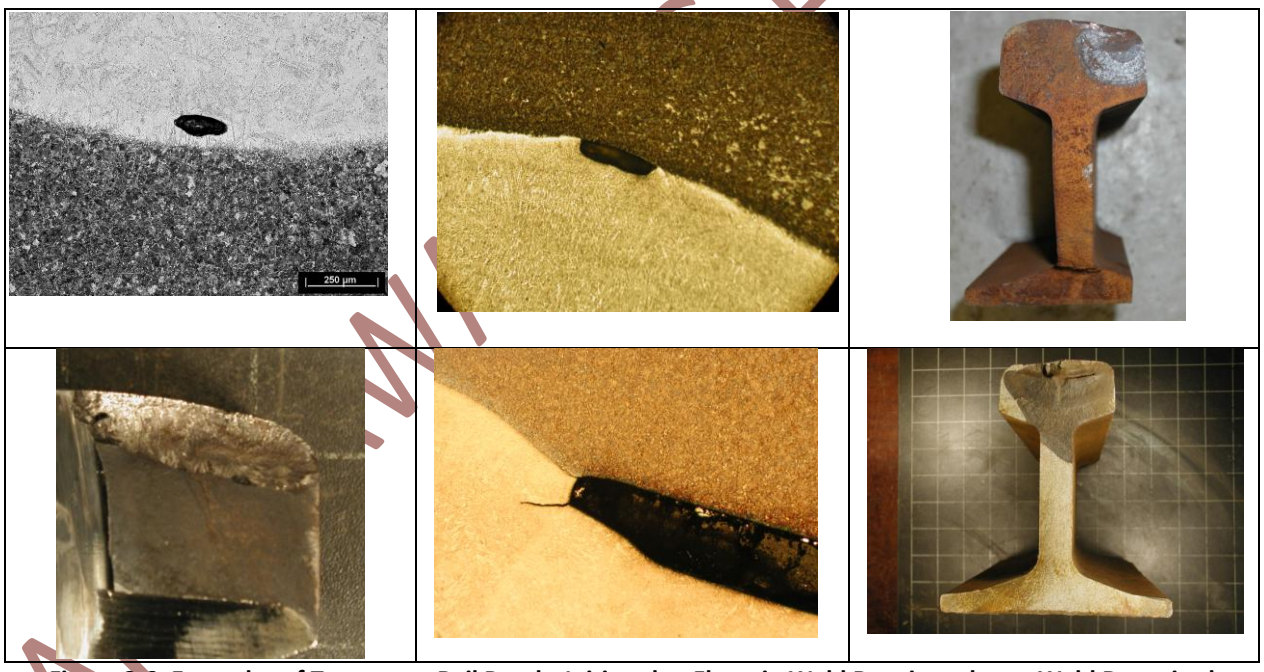

Figure 3.6: Examples of Transverse Rail Breaks Initiated at Flaws in Weld Repairs - above: Weld Deposited Layers;below: Slag entrapment at weld metal-parent rail interface revealing cracks and eventually leading to transverse fracture

3.2.3. Flux Cored Arc Welding (FCAW)

Flux cored arc welding (FCAW) is an arc welding process in which the heat for welding is produced by an arc between a continuously fed tubular electrode wire and the work. The basic principles of the process are identical to the MMA process except that the welding operation is semi-automatic using a continuous wire feed. The process utilises “flux-cored wires” that are

tubular electrodes that have flux on the inside. There are two types of flux-cored wires: gas-shielded and self-shielded, Figure 3.7[13].

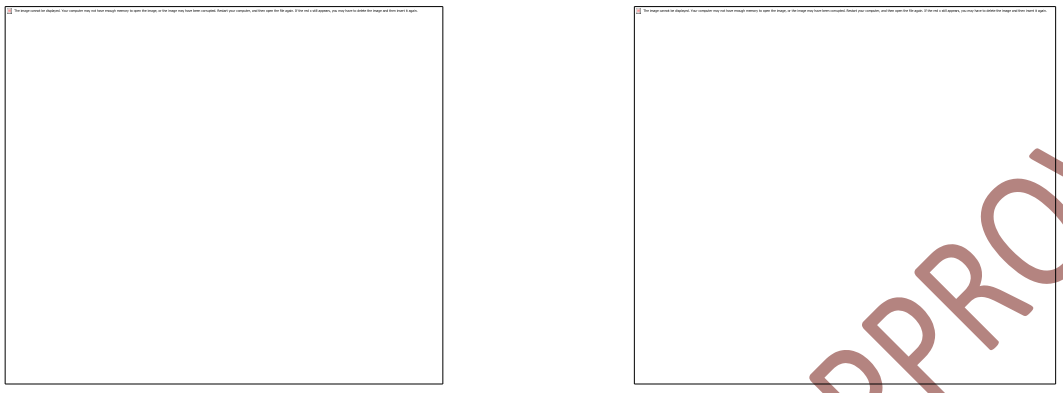

(a) FCAW-G (b) FCAW-S

Figure 3.7: Flux Cored Arc Welding [13]

As the name suggests, the former (FCAW-G) uses the flux inside the wire to form the protective slag layer but also relies on an external shielding gas to protect the arc from the atmosphere. In contrast, FCAW-S uses just a self-shielded flux cored wire and could be described as a process that employs "a stick electrode that is inside out". Just like stick electrodes, the process relies on the inherent slag system and the molten metal is protected from the atmosphere by the gases generated from the decomposition of gas-forming ingredients contained in the electrode's core. In addition to the gas shield, the flux-cored electrode produces a slag covering for further protection of the weld metal as it cools, which must be manually removed using a wire brush or similar. It is the FCAW-S process that is used for weld restoration of worn rail and other track components because of the convenience of not needing the availability of gases for on-site repairs.

The equipment for undertaking FCAW-S process comprises a power source, welding cables, consumables (flux cored wire), wire feeder, welding gun, process control equipment, and wire brushes or peening gun to remove slag. The need for standardised approvals of consumables and welding procedures, and the qualification of the welders to ensure weld integrity was emphasized with reference to MMA welding and these are equally applicable to FCAW-S. The relevant EN standards that permit the delivery of the necessary controls have also been translated into the Railway Company Standards [6] such as NR/L2/TRK/0132 – Issue 6 (4 December 2010) for Network Rail. Furthermore, a very comprehensive arc welding procedural document [8] was also prepared by a weld repair provider.

Although significant research and trials were undertaken by BR Research, the active commercial deployment of the FCAW-S process has been somewhat slow in the UK railway network. Network Rail purchased [14] ~70 BV1000 welding units from ESAB in ~2010 equipped with

Mobilemaster IV wire feed units. In addition to the welding units, the company acquired 140 Arcgen-165 generator sets and 70 Matweld hydraulic grinding units. Two of these generators, when connected in parallel, are capable of supplying power for the welding units, the grinder, and site lighting. Preheating is undertaken using heating units supplied by Trueflame Rail Equipment. For plain line rail repairs, the heaters are 800 mm long while a specially designed 1000 mm long heater is used for the repair of switch blades. The switch blade heaters are clipped to the back of the blade and can be operated if the interpass temperature falls below the critical limit of 300°C.

Initially, the units were targeted at the repair of crossings but subsequently extended to the repair of switch blades. The switch blade repair process [14] utilises the P4 stringer bead programme with a preheat of 343°C, welding travel speed of 35cm/min, and the voltage amperage settings at the bottom of the range specified for the wire. The weld beads are deposited on a 4mm offset, starting at the bottom of the wear scar and finishing right at the top of the switch blade. Network Rail [15] are also promoting the replacement of MMA repairs with FCAW-S for plain line repairs using Miller welding equipment, Arcgen-165 generators, and Trueflame preheaters. The process routes adopted are specific for the rail grade or crossing steel to be repaired and the associated approved consumables. Although full details of the process routes are not in the public domain, available details [15] for plain line repairs suggests preheating temperatures of between 350°C and 500°C, and welding currents of between 150 and 190 amps. The welding gun is manoeuvred manually as per agreed weld bead placement patterns.

The process appears to have found greater acceptance in Scandinavian countries and process details are available in published literature [11,12,16]. A brief summary of the process recommended by ESAB and used in Sweden and Denmark is shown in Table 3.8 for plain line rail, switch blade, and C-Mn crossings.

FCAW-S process is also used in the Australian network under the proprietary process of Hedkote [17]. However, details of the procedure are not available apart from the defect being removed by grinding, use of hardfacing wires, use of conventional preheat temperatures, and using either a stringer or weaving beads or a combination. The process is available for repairs on track or for refurbishment of components back within a workshop.

FCAW-S is also deployed on the French network and the CTF-Sauron process is being evaluated in the current project.

The CTF-Sauron process is a semi-automatic electric arc welding process delivered using the TRANSLAMATIC series of machines employing SAF-FRO Steel cored 54 flux cored 1.6mm Ø welding wire. The TRANSLAMATIC units are defined by their working strokes in the X-Y

directions and comprise the TRANSLAMATIC frame, a “Charlie” control unit, a “Roll n Roll” wire feed unit, and the PLUTONELEC generator unit. The preheating of the rail is undertaken using a designed frame with two fixed burners. The “Charlie” control unit has two programs, although facility exists to add further bespoke programs. The programs are capable of weld deposition in various shapes and sizes. Further details of the equipment are available in the manufacturers brochure [18],

Table 3.8: Brief summary of the FCAW process recommended by ESAB and used in Scandinavian Countries

Parameter			Note
Plain Rail			
Preheat Temperature	Steel Grade: R200 R260/260Mn R320Cr	 300°C-350°C 300°C-350°C 400°C-450°C	• For stringer beads of <30 mm width, preheat temperatures should be raised by 50°C • 100 mm on either side of area to be repaired is preheated
Welding consumables	ESAB OK Tubrodur 15.41 or 15.43 ø 1.6 mm		
Welding parameters	200-240A 28-30V		• To avoid distortion rail is unclipped from 1-3 sleepers on either side of the repair area and the rail raised by 5 mm • Welding is undertaken longitudinally with a weaving of 30-35 mm. • Last welded layer is hammered and ground immediately • Slow cooling is mandatory for higher hardness grades
Switch Blade			
Preheat Temperature	Steel Grade: R200 R260	 400°C 400°C	• 100mm on either side of area to be repaired is preheated
Welding consumables	OK Tubrodur15.43 ø 1.6 mm		
Welding parameters	140-300A 24-30V		• The area to be welded should be raised by ~20 mm to form the shape of a curve • Bead placement technique is shown in Ref 9.
C-Mn Crossings			
Preheat Temperature	Steel Grade: R200 R260Mn	 300°C 400°C	• For stringer beads of <30 mm width, preheat temperatures should be raised by 50°C • Entire area to be repaired and 100 mm on either side is preheated
Welding consumables	OK Tubrodur 15.43 ø 1.6 mm		
Welding parameters	200-240A 28-30V		• To avoid distortion rail is unclipped underneath the damaged area and raised by 5-10 mm • Longitudinal beads along most worn parts (edges) made first and weaving across pattern is used in subsequent welding. Further details in Ref 11 and 16

Although, the basic process is utilised in many other industries outside the railways, widespread application for rail head repair is not yet apparent. The key advantages and disadvantages of this process are:

- Advantages:
  1. the process overcomes the disadvantages of the intermittent/discontinuous operation of the MMA process but would benefit from automation to control the movement of the welding gun;
  2. the small diameter wire (e.g. 1.6 mm) gives the welder greater control of the weld pool;
  3. a wider range of compositions of wires could be available to produce matching hardness and wear resistance to those of premium grade rails;
  4. metal deposition rate is higher resulting in greater productivity at reduced costs;
  5. as welded appearance is better than with MMA and hence requires less grinding.
- Disadvantages:
  1. the process is reliant on excavation of defective area using manual grinding or flame cutting methods that are more susceptible to inconsistencies of shape, surface roughness, and the presence of detrimental sharp corners;
  2. the process also follows the conventional practice of preheating the rail to a minimum of 343°C as in the case of MMA repair. The magnitude of preheating is even greater for premium grade rails;
  3. welding gun is manually operated which allows flexibility for location of welding but lacks the standardised control of reproducibility;
  4. current practice lacks traceability of the procedures followed – no process data logging;
  5. finish profile grinding is manual and hence.

3.2.4. Wide Gap Aluminothermic Weld

The process is effectively an extension of the aluminothermic welding process but utilises a wider gap to permit the bridging of gap created by the removal of the defect. Thus, a very short rail length affected by the defect is cut out and the two rail ends re-joined by an aluminothermic weld. Although the process has been used to join dissimilar rail profiles, it is not generally used to repair rail head defects. Its inclusion in this list is more for completeness rather than a serious contender for further development within the project.

The key advantages and disadvantages of this approach are:

- Advantages:
  1. the basic technology of aluminothermic welding is long established within the rail industry and hence can claim proven status.
- Disadvantages:
  1. although more precise control of process parameters and welder training and approval has reduced the incidence of AT weld breaks very significantly, the process has the inherent disadvantages of casting technology;
  2. significant heating of the rail ends is likely to change the residual stress pattern the consequences of which may not be corrected through re-stressing of the rail and needs to be studied;
  3. there is a desire to reduce the width of the heat affected zone and the variation of hardness and the resistance to wear, plastic deformation, and rolling contact fatigue (RCF) – this is made far more difficult in a wide gap AT weld;
  4. the concept of comprehensive automatic monitoring of the aluminothermic welding process remains a desire and development task and hence consistency will be influenced strongly by the competence and diligence of the welder;
  5. the productivity of defect repair using this technology is likely to be relatively low unless the defects are reasonably close together to permit rapid transportation of equipment from one location to another.

3.2.5. Flash Butt Wedge Repair

This is a relatively newly developed process details of which were presented at the AREMA 2011 Conference (David Workman of Edison Welding Institute) [19]. The process employs flash butt welding to place a wedge of the actual rail material into a slot cut out from the rail head to remove the defect. Although details of the process can be obtained from the paper, a pictorial representation is shown in Figure 3.8.

FIGURE 1. SLOT CUT IN RAIL HEAD TO REMOVE DEFECT

FIGURE 2. WEDDGE BLANK SITING IN RAIL Slot CUT-OUT

FIGURE 3. FLASH BUTT WEDGE WELDING MACHINE

FIGURE 4. COMPLETED FLASH BUTT WEDGE WELD

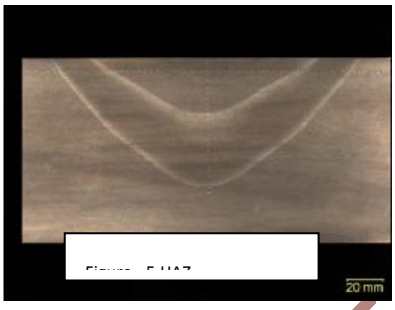

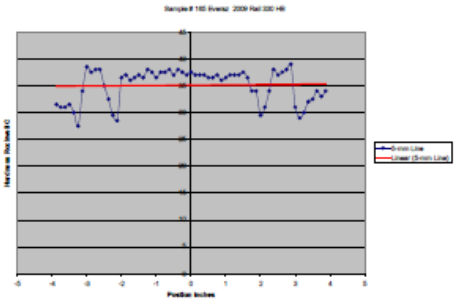

Figure 3.8: Pictorial description of Flash Butt Wedge Repair (Photographs from Paper by D Workman – AREMA 2011)

The key advantages and disadvantages of this process appear to be:

- Advantages:
  1. it is a solid phase welding technique with the inherent advantages for internal integrity that are already well known to the industry;
  2. the claimed properties of bend strength, uniformity of hardness, and fatigue strength are all impressive;
- Disadvantages:
  1. the process requires large and specialist equipment and even accepting all the technical merits of the process at face value, there is need to examine the logistics of process delivery, productivity, and the impact on track availability;
  2. in view of the newness of the process, there is a need to undertake a critical evaluation of the technical and operational merits within the context of high volume mixed traffic railway network.

3.2.6. Rail head repair, aluminothermic welding

The use of the conventional aluminothermic welding technology to repair an isolated rail head defect was first examined by Elektro-Thermit around 50 years ago [20] and was subsequently evaluated by British Rail Research [21] in 1974 and again in 1983. The technology did not gain acceptance primarily because of problems with control of preheating and the lack of fusion but the development was continued by Thermit Australia. More recently (2006), Network Rail

approached Thermit GB to resurrect the development employing improved preheating techniques and consumables [21-24]. Similar development has also been undertaken in parallel by Railtech International [25,26]. Repairs made by both the above companies have also undergone testing on the FAST test track [27,28] and the key mode of degradation was shelling. However, their behaviour under heavy haul operating conditions is not considered directly relevant to their performance in mixed traffic. Hence, the two processes that are currently being deployed in some mixed traffic railway networks are:

1. Head Repair Weld (HRW) / Thermit Head Repair (THR) from Thermit GB / Elektro-Thermit;
2. Head Wash Repair (HWR) from Railtech International.

In view of the similarity of the underlying technology, the above two processes are discussed briefly according to the process stages employed, see Table 3.9.

Table 3.9: Aluminothermic welding processes for repair of rail surface defects

Process Stage	Thermit – HRW	RailTech – HWR
Defect Removal Scope (Based on Network Rail approval	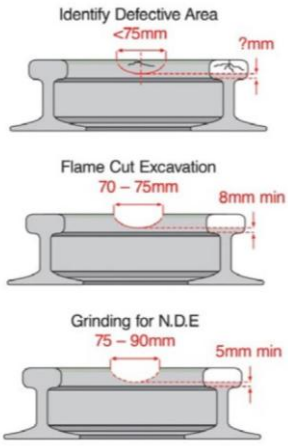	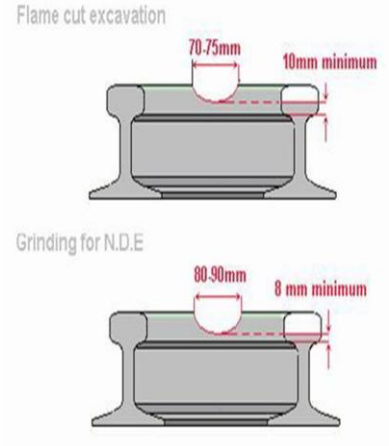
	• The defect removal scope [23,24] of the two processes show minor differences. Scope defines maximum but not minimum excavation depth. At maximum depth, the interface between cast and wrought metal is well below the depth that experiences the maximum shear stresses from wheel contact. • The excavation shape results in a variable depth to the interface and process approval tests do not assess the consequences for the longevity of the repairs.	
Defect detection process	• Although published literature on the Railtech HWR process does not provide details of defect detection, it is presumed that standard ultrasonic techniques approved by the network would be employed. Thermit HRW process indicates the use of 0° probe to record defect length and a 70° probe for defect depth. The length and centre of the defect are clearly marked on the field side of the rail head with a scribed line on a sprayed paint background. However, what has not been made apparent is where the responsibility of defect detection lies – whether it is with the expertise of the Infrastructure Manager or does the weld repair service provider needs to add ultrasonic inspection expertise with the service delivery team. Furthermore, no auditable control procedure for the confirmation of the detected defect has been given.	

Process Stage	Thermit – HRW	RailTech – HWR
Defect excavation process		
	• A bespoke designed oxy-fuel gas cutting template and torch is used to excavate the desired shape which is then ground to prepare it for MPI examination.	• Although Raitech offer the option of oxy-fuel cutting for their approval by NR, other process brochures favour the use of a precision Matweld frog grinder. Excavation completed in 11 minutes.
Rail Alignment	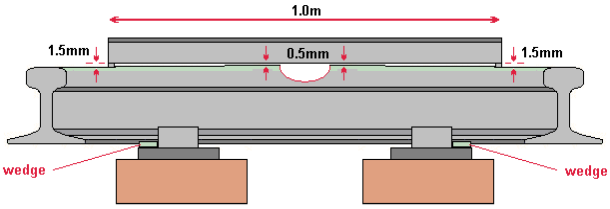	

	• Based on Network Rail approval, rail alignment requirements are set at:
	  • Line speed of <100 mph: lift = 0.5 mm over 1 m
	  • Line speed of >100 mph: lift = 1.0 mm over 1 m
		• Although no details of rail alignment are available for the Railtech HWR process, it is likely to be similar to that used in the HRW process

Process Stage	Thermit – HRW	RailTech – HWR
Moulds	 	 Front View  Side View 
	• Two-piece mould design with the molten steel tapped directly into the mould as in standard aluminothermic weld	• Moulds used are the same as wide gap welds. • Mould suitable for 110 & 113 lb rails for use in UK but the process has approval from SNCF so would also be capable of repairing 60E1 rails. The mould sits on the foot of the rail. Sand steps provided to accommodate rail wear
Preheating		
	• An angled preheat torch with a stainless reflector avoids overheating of the torch and permits the use of either propane or acetylene fuel gases. • Preheating employs standard SkV pressures (O_2 – 3 bar, Propane – 0.7 bar) • Preheating time – 3 minutes	• Preheater holder height – 110 mm • Standard 22-hole RTI preheater • Oxygen – 1.2 bar • Propane – 0.6 bar • Preheating time – 4 minutes

Process Stage	Thermit – HRW	RailTech – HWR
Pouring & Trimming		 
	• A 6kg single use crucible with Z80 portion is used • Following pour, the weld is allowed to cool before the equipment is stripped and trimming undertaken using a standard weld trimmer. • Weld is left undisturbed for 30 minutes before wedges are removed and pads and clips refitted.	• A smaller 8.5 kg portion is employed • No information available on time to be allowed for cooling but demoulding and trimming is considered to take ~20 minutes
Finish Grinding		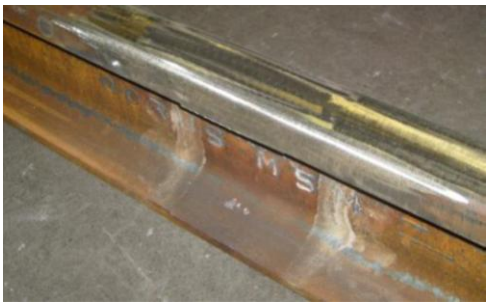
	• The trimmed weld is ground using a conventional profile grinder – the company brochure suggests that grinding is carried out after the weld is allowed to cool for 30 minutes before re-clipping and grinding • Grinding tolerances are categorised by line speed	• Finish grinding is undertaken using a precision MatWeld frog grinder.

Process Stage	Thermit – HRW	RailTech – HWR
Integrity testing – Macrograph	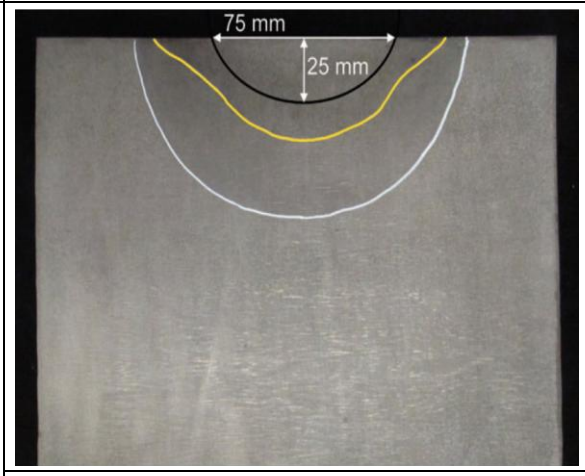	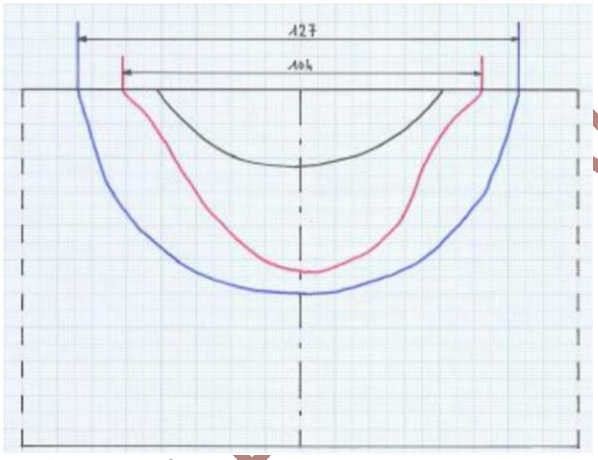
	• The approximate dimensions available on the macrographs suggest the distance between parent rail to parent rail to be between 125 to 150 mm and hence the wear resistance over such a distance needs to be similar to that of the parent rail. • Also of interest are the interfaces and their behaviour under wheel-rail contact conditions. Supporting micrographs revealing the integrity of the microstructure at the interfaces would be useful	
Integrity testing – Hardness Traverse	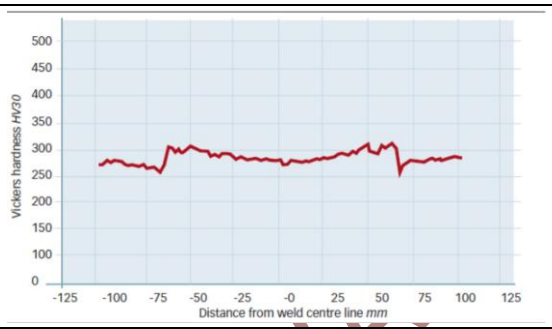	
	• The above traverse is for rail Grade R260. Although the traverse appears relatively uniform, a comparative hardness traverse through a conventional aluminothermic weld joint would be useful to assess the expected wear performance. The depth at which the traverse was measured should be given. • A hardness traverse through the depth of the repair should also be provided • The assessment of integrity under cyclic loading within the stress range experienced in the head has not been undertaken (until a single test within the current project) to establish any susceptibility to sub-surface initiation.	• Hardness traverses in either a longitudinal or transverse section was not included in the report submitted to Network Rail. Instead 3 individual test results of running surface hardness of 285 HB were quoted. • The assessment of integrity under cyclic loading within the stress range experienced in the head has not been undertaken to establish any susceptibility to sub-surface initiation.
Other key features	• An UT procedure (U18) has been developed[17] to detect HRWs. • Process is approved[17] by Network Rail for rail profiles 98lb, 110lb, 56E1, 60E1/E2 in steel grades R220, R260, R350HT, R370CrHT (Tata 400 MHH), and Tata HP335. • Overlapping repairs are permitted for	• The HWR process is not considered suitable for long wheelburns but a variant of the process (triple HWR) was being developed. • A variant to permit the use of the process to repair squat defects on Flash Butt welds is also under development.

Process Stage	Thermit – HRW	RailTech – HWR
	wheelburns allowing for maximum length of 160 mm to be removed • By December 2011, ~1300 HRW had been installed in NR track	

The key advantages and disadvantages of the head defect repair processes based on aluminothermic welding are:

- Advantages:
  1. the process has been approved by NR and several hundreds of defects have been repaired using the process and although no serious problems have been highlighted, no data from structured monitoring is available;
  2. the behaviour of a cast microstructure under rail wheel contact is known from the degradation of aluminothermic welded joints and hence differential wear is likely to happen;
  3. the process permits excavation to a depth that leaves just 10 mm of the rail head remaining measured from the bottom of the rail head. Hence very well developed defects could be repaired using this technique, although it is worth raising the question as to how such large defects were allowed to remain within the network;
  4. the process is capable of repairing squat defects up to a length of 90 mm and overlapping repairs are permitted for wheel burns allowing a maximum length of 160 mm to be repaired;
  5. processes from both companies mainly utilise existing consumables and equipment;
- Disadvantages:
  1. although the technology of aluminothermic casting is well understood, the kit required to implement the head repair process appears quite intricate and requires careful assembly and hence the need for expert human interface;
  2. no bending fatigue tests with the repaired head in tension had been undertaken to determine the integrity of the interface between the cast and the original rail structure until the single test completed successfully within the current project; further tests are needed for the two processes to gain confidence;
  3. since the process is permitted to repair relatively large lengths (up to 160 mm), the cast structure is very visible to the wheel and it is therefore necessary to establish the wear and RCF resistance of the cast structure, such data is not currently available;
  4. the need for a reliable seal between the rail and the mould precludes the repair of defects on top of existing flash butt or aluminothermic welds;

5. the underlying technology is old and the process is highly dependent on the fallible human interface suggesting the need for precise and easily auditable control of the process.

3.2.7. British Steel / ARR Discrete Defect Repair (DDR) Process

The British Steel / ARR Rail Discrete Defect Repair Process is an innovative technique that has been designed to address the key technical imperatives established through critical assessment of the main available techniques. The process is effectively a FCAW process using welding consumables already approved for use on rail steels by UK and other European railway Infrastructure Managers. The novelty of the process, described below, arises out of the following three key aspects that ensure the integrity of the repair:

1. the process uses low preheat of just 60°C to 80°C which when combined with the welding parameters and the weave pattern ensures a tough microstructure within the Heat Affected Zone (HAZ) surrounding the repair. The use of low preheat is covered by an existing British steel patent [29].
2. excavation of the identified defect is undertaken using computer controlled milling to deliver a cavity of prescribed dimensions. Weld deposition to restore the milled cavity is also computer controlled and ensures reproducible repair quality with proven integrity.
3. comprehensive traceability of the adherence to the prescribed and approved welding procedures provides positive verification of weld repair integrity.

3.2.7.1. The DDR Process

The key steps in the developed process are:

1. **Defect Detection and Verification:** The detection of the defect to be repaired is considered outside the scope of the current development. Instead reliance is placed on the inspection systems of the Infrastructure Manger to identify clearly the location of the defect to be repaired.

2. **Defect Removal:** The process of defect removal is a key part of the developed process that underlines the emphasis on consistency of operation by creating a standardised cavity around the defect. Currently, the process is programmed for a standardised cavity of 100 x 72 x 10 (Length x Width x Depth) where the length extends equally on either side of the centre of the identified defect while the width represents the full width of 60E2 rail section. The choice of both the length and depth of the cavity can be altered to be compatible with the “minimum Action” rules of the Infrastructure Manager.

   A reduction in the length of the cavity will reduce the total repair time while an increase in the depth dimension will increase repair time. Coverage of the full head

width remains the recommended approach, and the welding unit is equipped with a laser edge detection system to recognise the edges of even side worn rails.

The process involves controlled milling using a bespoke design cutting tool to ensure the radii at the bottom and the angle of the side walls of the cavity do not compromise the integrity of the deposit. A milled cavity is shown in Figure 3.9.

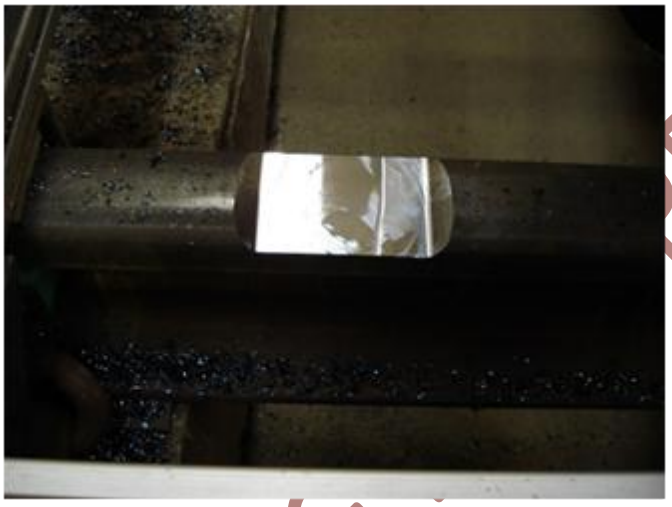

Figure 3.9: Milled cavity

3. **Preheating:** The uniqueness of the developed process arises out of the avoidance of the standard practice of preheat of ~350°C for the weld restoration of high carbon steels. Instead, the developed process employs a low preheat of just 60°C to 80°C. The maintenance of this temperature provides a safety net that prevents the completion of martensite transformation in the HAZ and retains a high proportion of untransformed austenite until the heat from an adjacent bead or the next layer of deposit raises the temperature and tempers any martensite that may have formed. As will be shown later, the use of optimised welding parameters and weave pattern reduces the cooling rate in the HAZ sufficiently to ensure transformation to pearlite.

4. **Semi-automatic Open Arc Weld Deposition:** The creation of a standard cavity provides the ideal platform for a programmed semi-automatic welding operation. The developed process employs the well proven Open Arc welding process with a flux cored arc wire. The success of the developed process centres around the control of the metallurgical transformation through the use of optimised welding parameters and an oscillating weave pattern. The 10mm deep cavity is fully restored with a 3-layer deposit and a carefully positioned final sacrificial layer to ensure that the HAZ created by the penultimate layer is fully tempered and no new HAZ is created at the edges of the cavity. The second factor controlling the integrity of the deposit is the removal of the surface slag formed after each pass using a peening needle gun. Weave pattern

details are encapsulated in the automation programme while the welding parameters are included in the accompanying process manual and displayed on the control unit. Photographs showing the as deposited layers are shown in Figure 3.10.

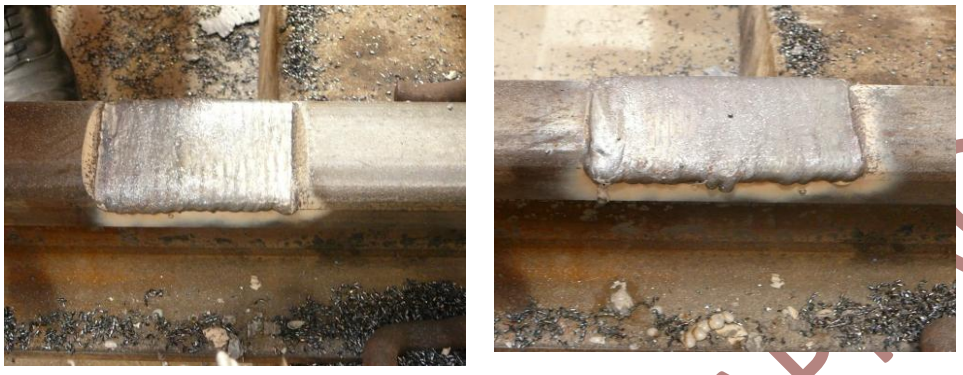

Figure 3.10: Weld deposited layers

5. **Profile Grinding:** Grinding of the as weld repaired rail is undertaken using a rail mounted grinder approved by the Infrastructure Manager. The process has the facility to use the milling tool to remove part of the sacrificial layer leaving a flat surface to be blended using a rail mounted grinder. This requires the welding head to be replaced with the milling tool at the end of the welding cycle and the time taken for this activity needs to be assessed against the time saved in profile grinding.

6. **Quality Assurance:** The integrity of the weld repair is assured through precise control of the process parameters that are embedded into the programming for automation. The validity of the process parameters is fully demonstrated through commissioning trials and independent metallurgical testing to achieve process approval from Railway Infrastructure Managers. A certificate of conformity provided at the end of each repair demonstrates the compliance to the approved procedure and hence the integrity of the repair.

7. **Inspection:** Inspection of the weld repair will be subject to the inspection procedure specified by the Infrastructure Manager and has been shown to be fully capable of meeting the criteria specified in Network Rail (NR-SP-TRK-132 v4).

3.2.7.2. The DDR Equipment

A bespoke prototype unit has been designed and manufactured to deliver the Discrete Defect Repair service. The equipment has been designed for the specific needs of the developed process and includes technological developments to maximise process automation to ensure strict adherence to specified procedures to deliver the desired integrity of repair. The salient features of the equipment are:

- the equipment comprises a linear support frame measuring 2410 mm x 800 mm x 690 mm that spans both running rails to provide a stable platform for the mounting of all the equipment needed to deliver the two key functionalities of milling and welding, as shown in Figure 3.11. The milling and welding heads can be interchangeably housed in a single moving head the operation of which is controlled by a process computer to ensure accuracy of positioning and reproducibility. The framed design ensures rapid deployment of the unit on the track within ~10 minutes;

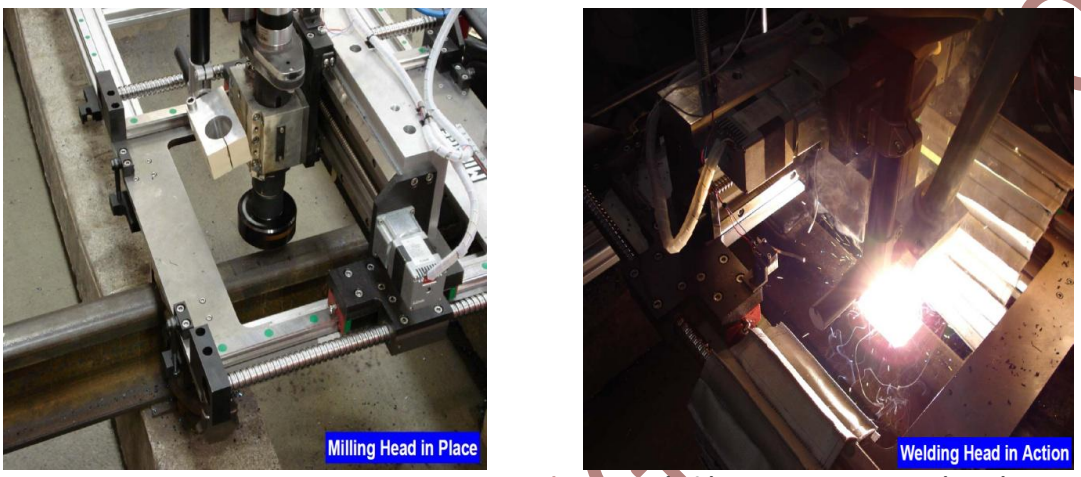

Figure 3.11: The DDR process: DDR milling head (left); DDR welding head (right)

- the weight of the assembly, excluding the generator, welding set, and cables, is 176 kg;
- the current design of the frame assembly is compatible with the standard track gauge of 1435 mm. However, the unit can be designed for other track gauges;
- the design of the housing to accommodate the milling and welding heads permits rapid changeover from one operation to another and has a common home position to ensure accuracy of positioning;
- the frame is secured to the track rails using specially designed clamps. Once secured in position, both milling and welding operations can be completed without relocating the DDR unit;
- the milling tool utilises appropriately designed cutters with 6 carbide inserts each of which has 3 useable cutting edges. The design of the cutters is critical to ensure the radii at the bottom corners and the angle of the sides. A cavity measuring 100 mm x 72 mm x 10 mm can be milled out in ~25 minutes. The control programme can be adjusted to excavate different lengths and depths;
- the unit is equipped with skirts and a tray to collect the milling swarf and prevent ballast contamination;
- a Kempe welding power source and feed unit with appropriate cables and 20 kVA generator has been employed in the current unit. Electrical supply for milling and

welding functions (240 volts milling / 415 volts welding) is provided by the diesel powered generator weighing ~ 350 kg;

- the welding process comprises 4 layers of weld deposits, including the sacrificial layer, and is completed in ~21 minutes;
- 25 kg wire spool, containing 1.6 mm FCAW wire, is mounted on the frame assembly. Network Rail approved wires from 2 different manufacturers have been successfully used in the process;
- all operations are controlled through a PLC unit supported by laser identification of rail edges to ensure precise control of excavated cavity was reduced from 100 to 50 mm since this would be sufficient to ensure removal of most commonly occurring defects.

The key advantages and disadvantages of the Discrete Defect Repair process are:

- Advantages:
  1. the process is largely automated with the two key process stages of milling and welding fully automated under the control of the process PLC to provide unparalleled consistency of operation;
  2. the process utilises milling to excavate a cavity of prescribed dimensions that overcomes the inconsistencies of manual grinding out of the defect;
  3. the process requires a low preheat within the range of 60oC to 80oC for the repair of discrete defects in Grade R260 compared to the mandated preheat requirement of >343oC for the other weld repair processes;
  4. the use of a prescribed weld parameters combined with the set square weave pattern instead of the stringer beads used in all currently conventional weld repair processes provides precise control of temperature and cooling rates in the HAZ to result in a fully pearlitic microstructure in R260 grade rails;
  5. the provision of data logging of all welding and operational parameters provides much needed traceability of repairs that is not available in current processes. However, further development is required to establish a database of repairs that is compatible with the rail management system of the network;

- Disadvantages:
  1. although the process has been demonstrated under controlled trial conditions, it has no proven pedigree under truly track conditions, particularly any potential degradation of the repair under traffic;
  2. the developed equipment requires vehicular access to the track and the logistics of delivery of the equipment has to be established;

3. the process has been demonstrated for the standard rail grade of R260 which suggests that it should also be suitable for the leaner grades of R200 and R220. However, the process requires further development to identify welding wire and the associated parameters for the repair of defects in premium grade steel rails such as R350HT, R370CrHT, R400HT, and HP335.

4. Consequences of imperfect repair geometry

The local rail repair welding may potentially introduce two sources of concern that can cause wheel-rail dynamic loading amplification and eventually rail damage formation and track degradation. These are the relatively short-wave geometrical irregularity and the material inhomogeneity of the rail running surface along the weld repair.

In Chapter 4.1, the consequences of imperfect repair geometry along the rail running surface are studied. Methods of measuring the finished weld geometry are introduced along with relevant standards on rail longitudinal profile. Moreover, results and conclusions of a parametric study on rail damage due to imperfect longitudinal geometry are presented.

In previous chapter, the effect of metallurgical variations along the repaired surface which implies a variation in hardness and wear resistance is also studied. Such variations cause differential wear of the rail surface which in turn results in a geometric irregularity that give rise to variation in contact forces and further differential wear. Figure 4.1 shows potential deterioration loop after introducing the railhead weld repair.

A methodology is proposed to calculate the wear along the rail, taking into account the vehicle-track dynamic interaction and material inhomogeneity along the rail within a feedback loop. Using this, the effect of material inhomogeneity introduced by the weld on the long-term rail surface irregularity is studied.

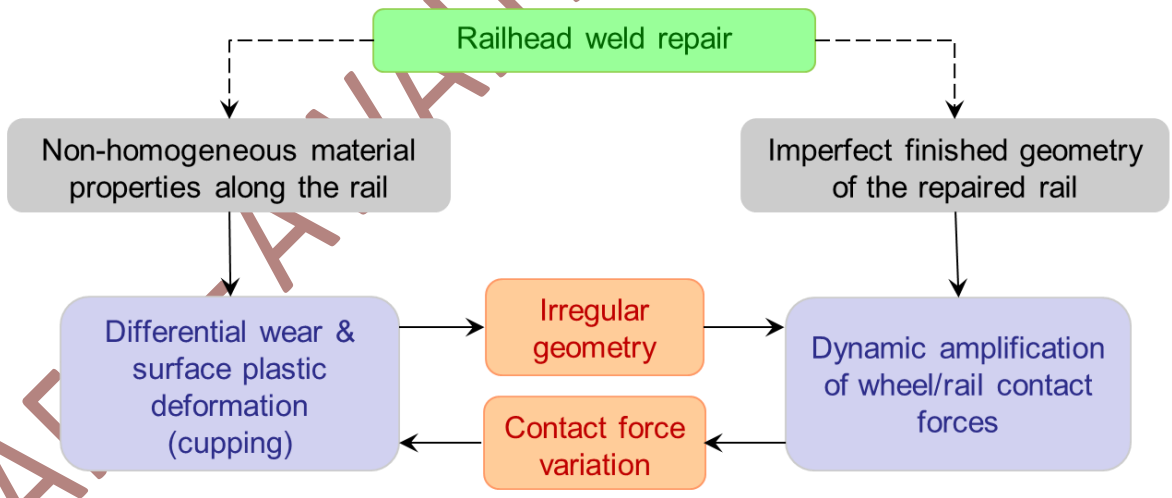

Figure 4.1: Deterioration loop due to material and geometrical imperfections in weld repairs

4.1. Effect of imperfect geometry

An imperfect geometry of a finished rail repair may arise due to various reasons and there is a need to consider the geometry in the “as-installed/repaired” condition and the “degraded geometry” after the passage of traffic.

In the “as-installed/repaired” condition, the geometry is governed by the manual grinding operation that overrides any influence of heat and metallurgical transformation after the welding/weld repair operation. Nevertheless, the practice of allowing the repaired/welded area to cool down prior to grinding to avoid loss of profile due to the inhomogeneous material shrinkage after cooling is necessary [1]. Manual grinding after the repair is likely to leave a short wavelength irregularity on the running surface the magnitude of which is influenced by the competence of the operator and site conditions.

The degradation of profile with the passage of traffic is more strongly influenced by the welding/weld repair operation. The heat of welding leads to re-austenitisation and re-transformation of the steel in the immediate vicinity of the weld fusion line and this leads to metallurgical inhomogeneity and the property variation across a weld is the root cause of the often observed “weld cupping”. It is reported [2] that these local dips coincide with the fall in the hardness value in the heat-affected zone (HAZ).

Hence, there are two drivers for weld geometry profile optimisation: firstly, improvement to the weld finishing/grinding operation such that it imparts the same longitudinal and transverse geometry as available on parent rail either side of the rail. Secondly, reduction in property variation and the length over which it occurs such that the rate of profile degradation through wear is the same in the weld region as it is for the parent rail either side of the rail.

The unevenness of the running surface results in variations in the contact force and cause impact loading. These variations in the contact force, in combination with material inhomogeneity, result in differential wear (and work hardening) of the surface which worsens the rail surface geometry progressively. It is due to this cycle that imperfect rail welds, and presumably rail head repairs, are observed to be the initiating cause of other damage mechanisms on the rail surface such as corrugation [3] and squats [4].

Field measurements [2] show that there is a linear relationship between the maximum impact force arising at welds and the vehicle speed (for a specified track condition and unsprung mass). This is shown by simulations in time [5] and frequency domain [6] for measured weld profiles. A similar conclusion is derived by simulation and experiment for dipped rail joints [7] too. It is also shown by simulations and partly validated by field measurements that the maximum impact force is linearly related to the rail joint dip angle [7]. Inspired by this, Steenbergen [1] has proposed a linear relation to estimate the maximum dynamic force from vehicle speed and the maximum profile gradient of the welded rail surface.

The magnitude of the impact force may be considered as a rail damage indicator; however, the track deterioration may be better expressed in terms of the energy released due to the impact

which should be dissipated by the system. Damage occurs as the system components reach their limit of energy absorption.

4.1.1. Relevant standards on geometry of welded surface

Requirements are specified for finished weld geometry and material properties in the welding vicinity by standards. Most of these regulations address the welding of continuous rails however there exists some standards specific to rail head repairs. In this chapter, the standards relating to welding geometry set by CEN (European committee for standardization) as well as the ones adopted by the Dutch infrastructure manager ProRail and Australian infrastructure manager ARTC are presented.

4.1.1.1. European standards

There are two standards addressing the acceptance of the rail welding and one specifically on rail repairs by electric arc welding.

EN14730-2 standard [8] regulates the alumina-thermic welding process of rails. It specifies the alignment and flatness of the rail surface within the welded region. The vertical alignment tolerance concerns with aligning of the two rail ends before welding and is not of interest in case of rail head repair. However, the flatness limit is applicable for repairs too. Flatness is measured using straightedge and feeler gauge over the grinding length for peaked welds. Figure 4.2 shows the definition of flatness according to the standard.

Dimensions in millimetres

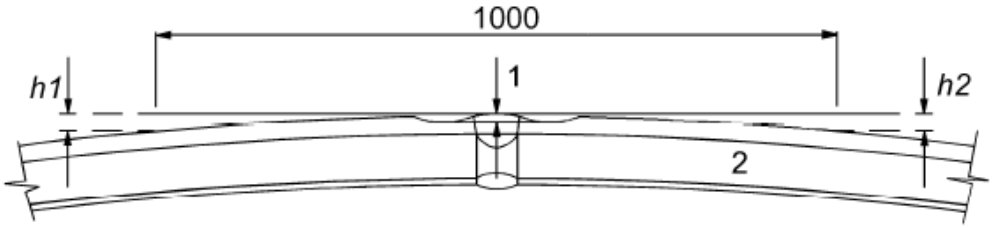

Key

1	Flatness
2	Rail
*h*1,*h*2	Values at the rule extremity

Figure 4.2: Weld flatness definition according to EN14730-2 (taken from [8])

The flatness limit is set for different categories to be specified by the railway authority. The limit is 0.2 mm for most categories with 0.1 mm and 0.15 mm for higher categories.

EN14587-1 standard [9] specifies regulations for flash butt welding. The flatness measurements should be done similar to the alumina-thermic welds. The limits are categorized in three classes as 0.1 mm, 0.15 mm and 0.2 mm.

In addition to the rail surface geometry, the size of the HAZ and hardness variation along the weld is also regulated for various rail grades. Figure 4.3 shows the HAZ for Flash-butt, aluminothermic, and the DDR weld repair process. It is apparent that the HAZ, in the case of flash butt weld, lies on either side of the central fusion line and the total width between the two parent rails on either side needs to be between 25mm and 45mm as specified in EN 14587-1 [9]. In contrast, there are two regions of HAZ in an Aluminothermic weld lying between the weld metal and the parent rail on either side as shown in Figure 4.3. As per EN14730-1 [8], the width of the HAZ must not exceed 20mm, 30mm, or 40mm as specified by the Infrastructure Manager. Similarly, the HAZ in a weld repaired section, lies between the parent rail and the edge of the weld metal on either side of the repaired area. Thus, there is a need for consistency of definition of the HAZ with reference to the difference in the microstructure and material properties that the wheel will encounter as it traverses across the weld. Simulation of the wear behaviour with the passage of traffic across the weld requires knowledge of the material properties in these regions. There is ample evidence of the relationship between hardness and resistance to wear of rolled pearlitic rail steels. However, as the microstructure of the weld metal and that within the HAZ is different to that of the parent rail, their dependence on hardness may also be different. Consequently, there is need to acquire the material property data required.

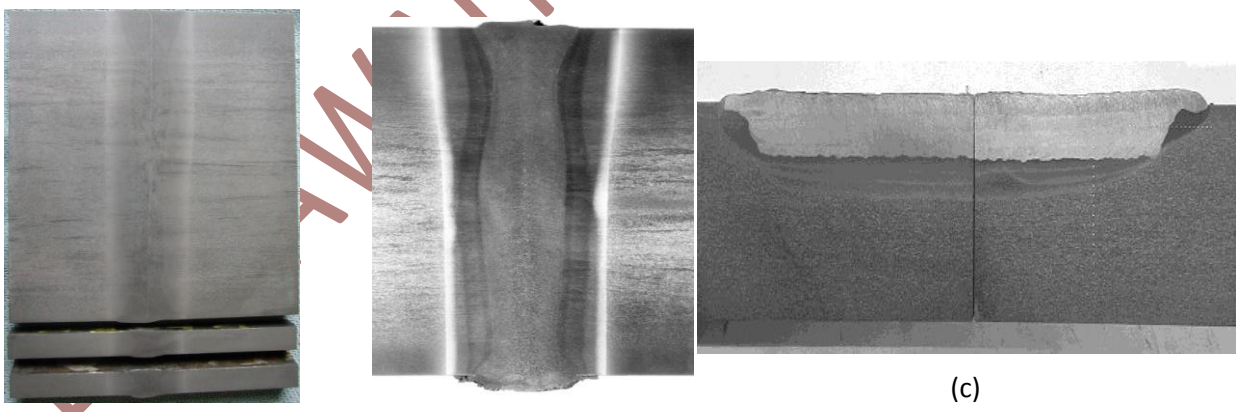

(a) (b) (c)

Figure 4.3: Visible HAZ width in different weld types: (a) flash-butt, (b) aluminothermic and (c) DDR weld repair

The hardness values across the HAZ shall not be more than 30 HV_{30} below or 60 HV_{30} above the average hardness of the parent rail. This applies to Flash-butt welds made in non-heat treated rail grades of R220, R260 and R260Mn while a minimum of 325 HV_{30} and a maximum of 410 HV_{30} is specified for heat treated grade R350HT within 10 mm from both sides of the weld line.

EN 15594 [10] standard addresses the restoration of rails by electric arc welding. It specifies the hardness requirements for various rail grades and single or multilayer welding repair. Table 4.1 summarizes the hardness requirements for both surface and subsurface hardness testing.

Table 4.1: Hardness requirements for surface and sub-surface hardness testing (taken from [10])

Grade	Position	Single layer	Multi-layer
R200, R220, R260, R260Mn, R320Cr	surface	380 max. HBW	290 HBW – 340 HBW
	sub-surface	not applicable	400 HV10 max.
R350HT	surface	400 max. HBW	340 HBW – 390 HBW
	sub-surface	not applicable	400 HV10 max.

Regarding the geometry, the standard specifies that flatness tests should be done for deposit and rail over 1 m to detect local deformation. It also requires for frequent inspections in 1 day, 1 month, 6 and 12-month time. The standard states that no surface deviation (flatness) measured over 1m shall exceed 0.2 mm.

4.1.1.2. Australian standard

The ETM-01-01 rail weld geometry standard [11] provided by Australian infrastructure manager ARTC specifies the limits for finished welds of any kind including head repair welding. The surface deviation of rail is limited in terms of change in weld ramp angle (surface inclination). The limit is 7 mrad over 50 mm base. This corresponds to a 0.35 mm of vertical deviation. The rail running surface should be checked with a so called P1 gauge or an approved device capable of measuring weld surface angle. shows the P1 gauge instrument [12].

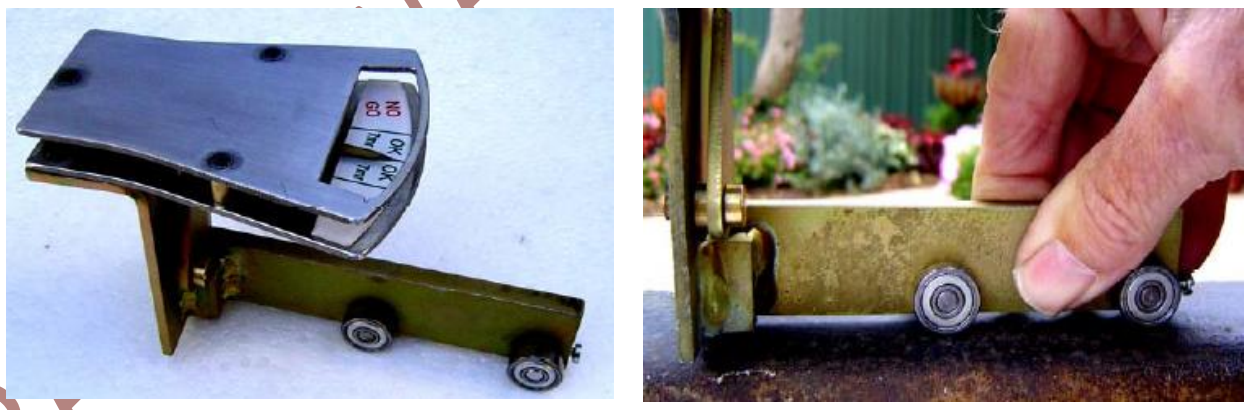

Figure 4.4: P1 gauge instrument (taken from [12])

Unlike the EU standard, the limitation is applied on the rate of change of the surface rather than the magnitude of the vertical deviation. In fact, the Australian standard allows for higher vertical deviation (0.35 mm) than the one allowed by the EU standard (0.2 mm).

4.1.1.3. Dutch standard

The studies in [5, 13] shows that maximum dynamic force arising due to weld geometrical irregularities is better correlated to the surface gradient than vertical deviation. Thus, a so-called weld quality index (QI) is proposed to evaluate the rail weld geometry. The index is defined as the ratio between the maximum absolute gradient of the actual weld and the allowable gradient for that line. The maximum allowable absolute gradient on a 25mm basis is categorized based on the line speed as shown in Table 4.2.

Table 4.2: Norm values of the maximum absolute inclination adopted for the QI determination [14]

Line speed [km/h]	Allowable gradient (25 mm basis) [mrad]
0-40	3.2
40-80	2.4
80-140	1.8
140-200	1.3
200-300	1.0

The Dutch standard enforces considerably tighter limits on the surface inclination compared to the Australian standard. The weld geometry measurements are carried out using a 1m digital straightedge similar to the one in Figure 4.5.

Figure 4.5:RAILPROF digital straightedge (taken from [15])

4.1.2. Parametric study of dynamic loads due to imperfect geometry

In order to study the effect of various vehicle and track parameters on the impact loads arising at rail weld irregular geometry, a parametric study is carried out using a vertical vehicle/track interaction (VTI) model. The model is validated and described in details in [16]. Figure 4.6 illustrates a schematic of the VTI model.

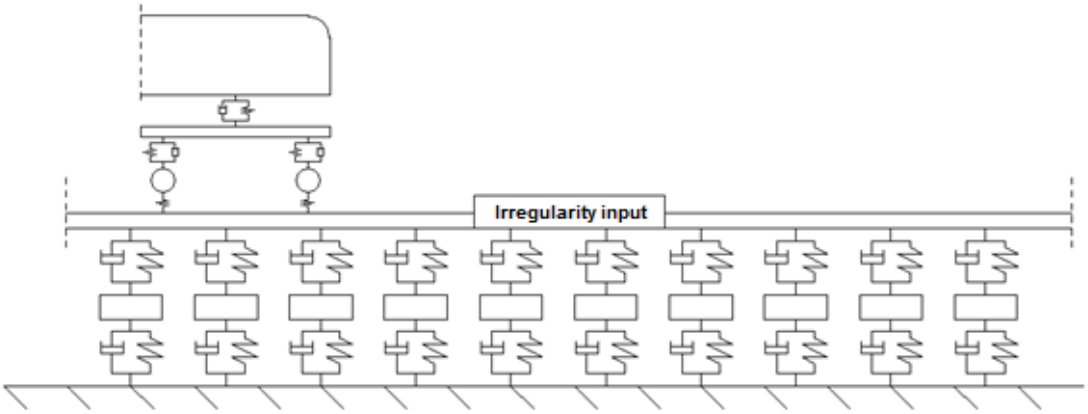

Figure 4.6: Vertical VTI model with an arbitrary irregularity along the rail [17]

Initially, a theoretical weld irregularity as a sinusoidal wave over 1m with a maximum height W and a triangular wave over L with a maximum height V is studied, as illustrated in Figure 4.7. The aim is to quantify the effect of different vehicle and track components on desired outputs through parameter variation. The desired outputs of the model are:

- P1 and P2 impact forces as a measure of rail damage and track deterioration;
- ballast force;
- bending stresses on rail foot to assess possible fatigue failure.

The system parameters studied includes traveling speed, unsprung mass, vehicle primary stiffness, rail mass and area moment of inertia, sleeper mass and spacing, support stiffness and gap under hanging sleepers. The parameters are varied within a realistic range and several extreme cases in terms of type of vehicle and track condition are considered as well. Six different geometrical irregularities are produced to represent a range of vertical deviation and surface inclination.

The study shows that the most influential parameters on the outputs are the speed, unsprung mass and support stiffness. The effect of hanging sleepers is also crucial especially with respect to bending stresses on rail foot. In terms of P1 force, the speed and the irregularity gradient are the crucial parameters whereas in terms of P2 force the unsprung mass and support stiffness play an important role. Figure 4.8 shows influence of these parameters on P1 and P2 forces for the studied geometries.

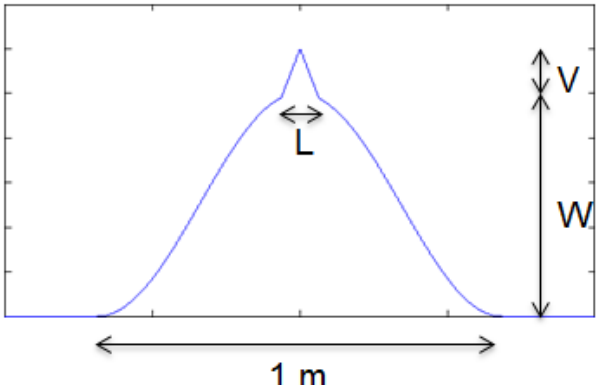

Figure 4.7: Defined theoretical weld irregularity

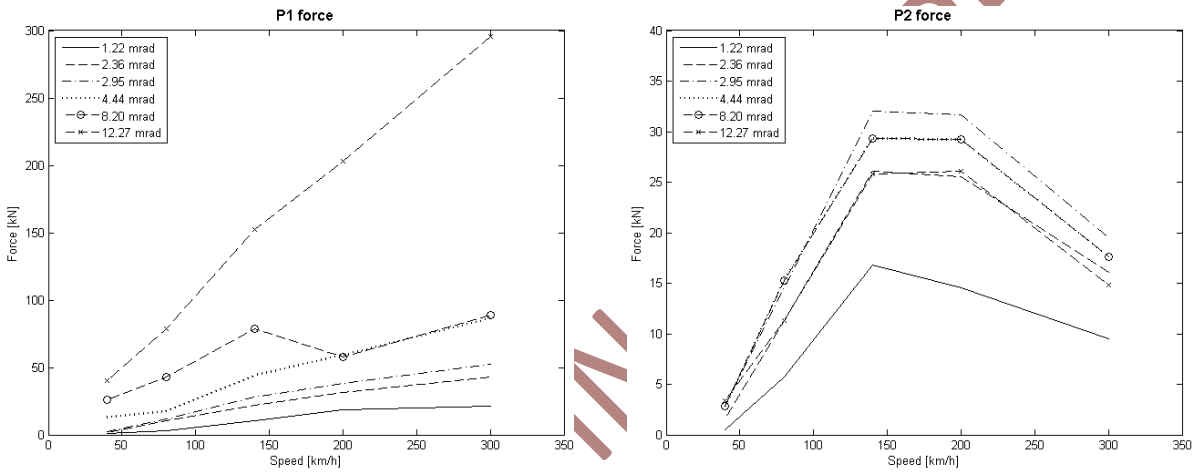

(a) influence of speed

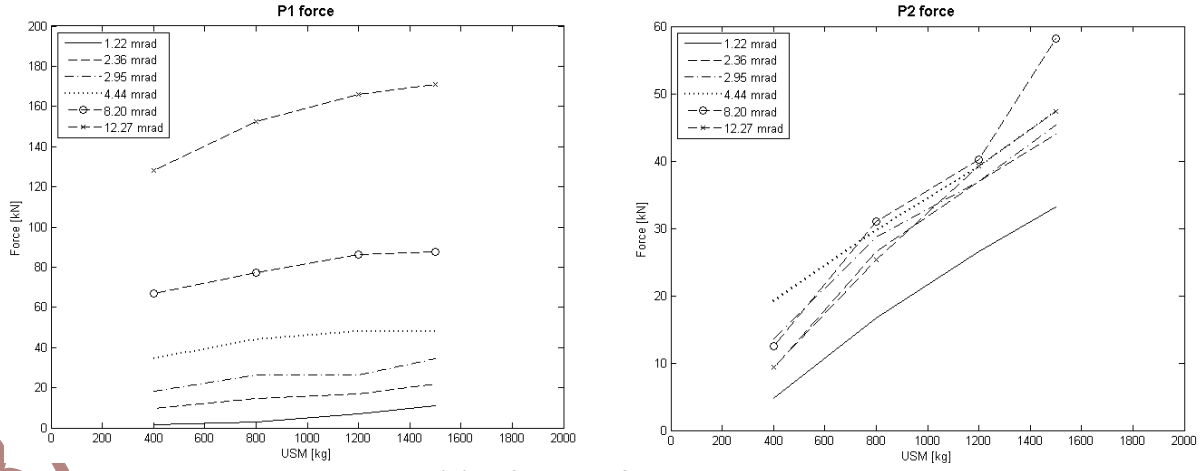

(b) influence of unsprung mass

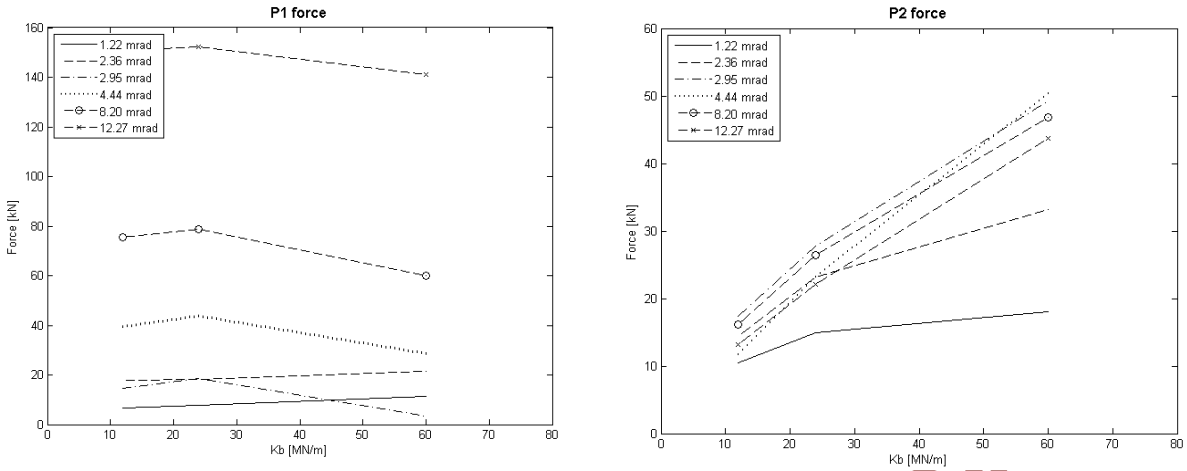

(c) influence of support stiffness

Figure 4.8: The influence of (a) speed, (b) unsprung mass and (c) support stiffness on impact forces for various irregularity geometry

In terms of ballast force the support stiffness has the major role. When it comes to bending stresses on rail foot, apart from the rail area moment of inertia, the sleeper spacing and gap of hanging sleepers play a more important role than the support stiffness.

The results from this theoretical study show that:

- increasing speed requires better weld geometry to limit, principally, the P1 force;
- increasing the unsprung mass has a moderate effect on all quantities considered;
- a better weld geometry is essential for track with a higher support stiffness to lower or minimize the magnitude of P2 and ballast forces;
- in case of low speed and high axle load, changing the support conditions has a moderate effect only on the ballast forces and the bending stresses;
- in case of high speed and low axle load, changing the support conditions has a remarkable effect on P2 force, ballast forces and a moderate effect on bending stresses.

In conclusion, good weld geometry (i.e. low maximum absolute gradient) is strongly required in case of high speed lines. It is also concluded that the effect of support conditions on track degradation is more crucial in high speed lines.

In addition to the above work, 110 measured weld geometries were acquired which were measured using RAILPROF digital straightedge [15] on the Dutch network [17]. To study the effect of major role-playing parameters and their correlation with desired outputs a new study is carried out using the measured weld geometries. The range of parameters studied is presented in Table 4.3.

Table 4.3: Parametric variations considered in the present study. The nominal values are in bold

Parameter	Values
Speed [km/h]	40/80/**140**/200/300
Wheel unsprung mass [kg]	400/**800**/1200/1500
Ballast support stiffness per sleeper end [MN/m]	15/20/**30**/40/60/80

The main findings from this study is summarised in Table 4.4.

Table 4.4: Summary of findings (▲▲▲ highly, ▲▲ moderately, and ▲ slightly affected by the weld geometry and the parameter. The data is slightly (upward) or moderately (downward) dispersed.)

Output / Parameter	Speed	Unsprung mass	Support stiffness
P1 force	▼▼▼	▼	▼
P2 force	▲▲▲	▲▲	▲▲
Rail bending stresses	▼▼▼	▼▼▼	▲▲
Ballast forces	▼▼	▼	▼▼▼

The main conclusions drawn from the findings in Table 4.4 are as follows,

- the P1 force is more influenced by the travelling speed rather than unsprung mass and support stiffness;
- increasing unsprung mass requires a better weld geometry to limit P2 force and rail bending stresses;
- increasing the support stiffness requires a better weld geometry to limit, principally, the P2 force and the ballast force.

The findings are generally in line with the ones drawn from the study on theoretical irregularities. From the parametric study with theoretical and measured weld profiles it is concluded that tighter weld geometry restrictions are required with respect to high speed routes. Moreover, for a track with low support quality, it is crucial to improve the weld geometry in order to lower the risk of rail breaks.

4.1.3. Three-dimensional evaluation of surface geometry

In current practice the evaluation of the rail surface geometry along the welds are limited to a single line measurement of the surface usually made on the top of rail position. However, it is evident from field observations that the contact band, where the wheel contacts the rail, is not always a straight line. For instance, Figure 4.9, shows that the contact band location is disrupted after passage over the weld. The geometrical imperfections over the weld may cause a sudden change in rolling radius and contact angle, which leads to lateral movement of the wheelset locally. Sometimes, significant wheelset movement cause gauge corner damage such as lipping as seen in Figure 4.10.

Figure 4.9: Change in contact band location near the weld

Figure 4.10: Lipping at a weld due to severe wheelset steering

To investigate the three-dimensional weld surface geometry, a series of rail transverse profile measurements are obtained along the weld surface using MiniProf device [18]. Each measurement set consisted of 13 transverse profiles taken across the 500 mm either side of the weld centreline. The measurement resolution was increased around the centre of the weld with a profile spacing of 50 mm. In order to single out the effect of three-dimensional geometry variation for a weld with hypothetically perfect rail top (fully complied with norms), profiles are then aligned with respect to top of the rail. An example data set is shown in Figure 4.11.

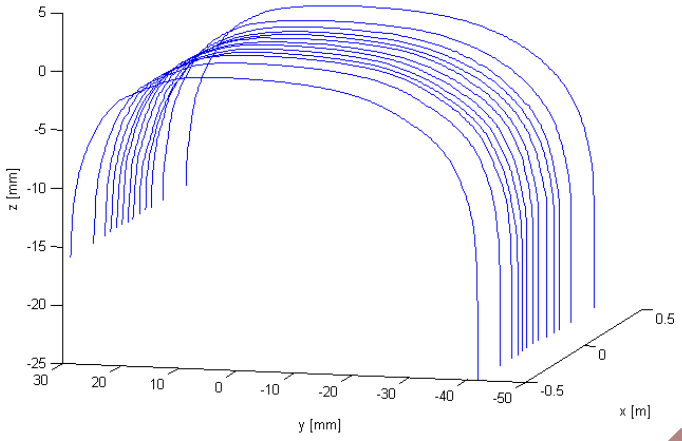

Figure 4.11: An example of a measured rail surface over a weld

Weld profiles are measured at 3 different locations on the track: tangent section, end of an exit transition and within a 2600 m curve. The welds on both high and low rails are measured. Thus, in total, 6 weld surface profiles are achieved.

The variation of the contact conditions as the wheelset passes over the measured geometries is studied using a three-dimensional vehicle-track interaction model as shown in Figure 4.12 and described in details in [19]. The vehicle is modelled as a quarter of the carbody, half bogie and a single wheelset. Single contact point at each wheel is assumed and Hertz method for normal and Shen-Hedrick-Elkins method [20] for tangential contact solution is used.

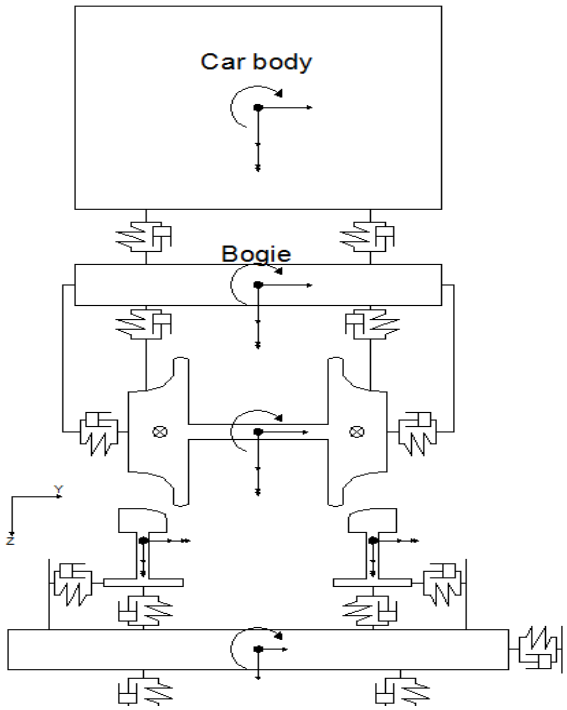

Figure 4.12: Vehicle-track interaction model in plane view. taken from [19]

Figure 4.13 shows the wheelset being slightly displaced after passing over one of the measured welds. The contact location variation along the weld is also shown in Figure 4.14. The actual

vertical displacement of the wheel due to geometrical irregularity over the weld is experienced at contact location. For the geometry studied here, the straight edge measurement will show a perfect geometry since the profiles are aligned to have same rail top position. However, the vertical deviation experienced by the wheel at the point of contact is different.

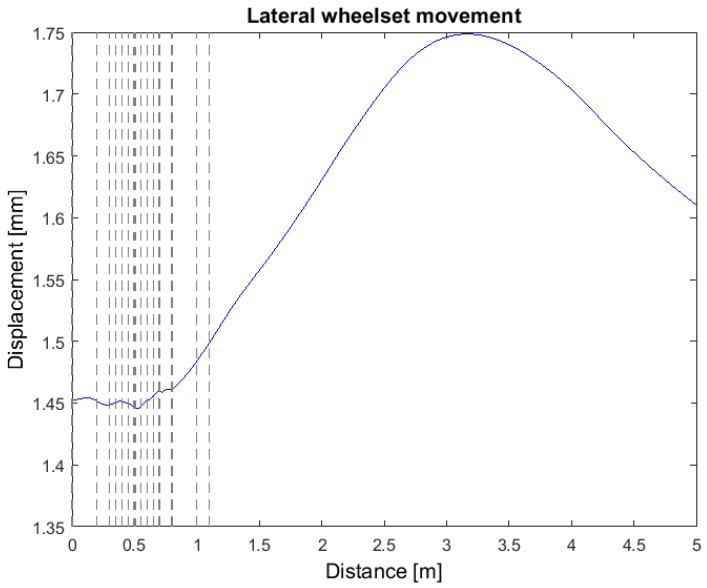

Figure 4.13: Lateral wheelset movement after passing the welded region

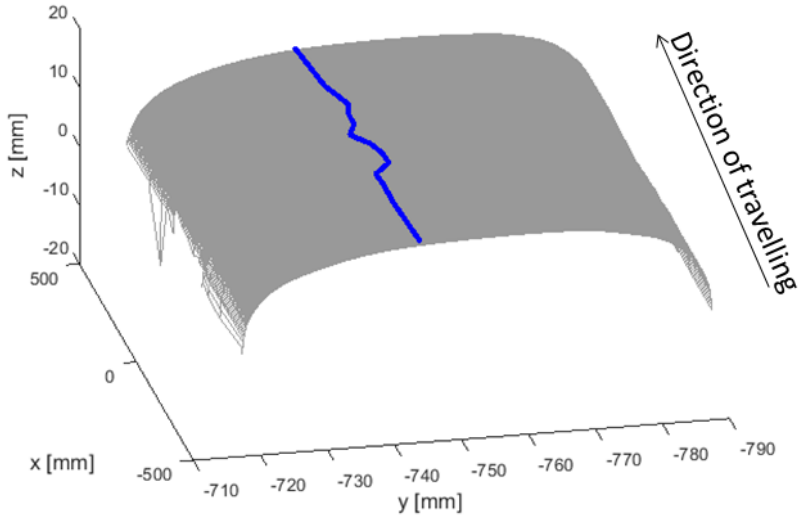

Figure 4.14: Contact point location within the welded region

Figure 4.15 shows the vertical deviation of the surface geometry along the weld at the actual point of contact. Same quantity is shown for a virtually centred wheelset. As seen, the actual deviation experienced by the wheel may rise up to 0.15 mm for an approved weld geometry using a straightedge measurement on top of the rail. This hypothetical example indicates the

necessity of a three-dimensional measurement (or straightedge measurement at more than one location) of the weld surface for geometry approvals.

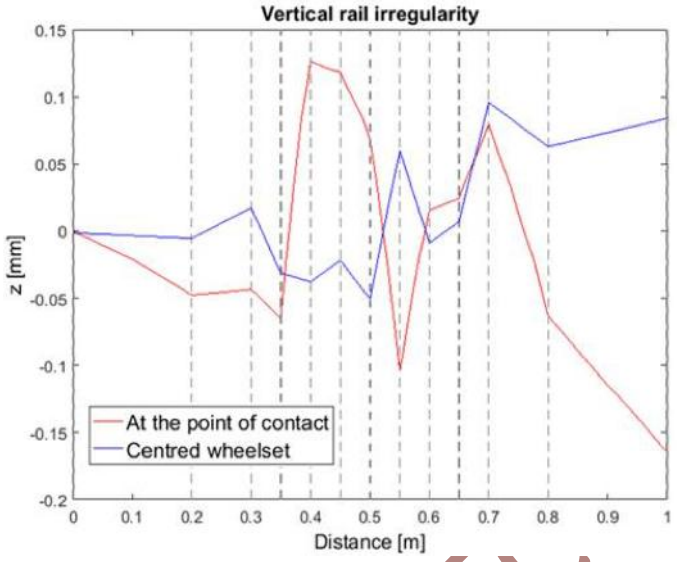

Figure 4.15: Vertical rail profile variation as experienced by a virtually centred wheelset versus the one experienced at the actual point of contact (moving wheelset)

4.1.4. Recommendation on 3D weld profile evaluation

Based on the simulation above it is shown that, the effective wheel-rail contact on the 3D rail surface might impose additional lateral and vertical movement to the wheel of the same order of magnitude as those limits currently specified in the EN standard (for controlling the weld vertical profile quality), even if the weld is perfectly flat horizontally.

Recommendations for future work are therefore to:

- acquire a representative number of welds from track (new and worn) using advanced 3D surface measurement system, for example that developed by University of Huddersfield during the WRIST (weld) and C4R (S&C) projects based on a laser measurement (Figure 4.16);
- carry out a range of parametric wheel-rail contact and vehicle dynamic analysis using this input data, and estimate the impact of the 3D quality of the weld on the vertical dynamics response. Compare this to the current EN and Dutch assessment methods. The parametric study would involve the use of an advanced contact algorithm accounting for material flexibility in the contact and a range of vehicle speed, curve radius, vehicle primary yaw stiffness and wheel shapes;
- evaluate the merits and added benefits of introducing a 3D based control and monitoring method for welds, and propose a suitable methodology for its deployment.

Figure 4.16: UoH Laser measurement trialled on crossing welded leg end (left) and on full S&C Assembly (right)

4.2. Effect of material inhomogeneity

Material inhomogeneity is influenced by the type of welding process. The inhomogeneity may arise either due to the use of a material with similar but different composition to the rail steels or due to the high thermal input that results in a heat affected zone either side of the weld.

In Flash butt welding, a solid phase joining process take place and no external material is introduced. Consequently, there is little chemical inhomogeneity unless the compositions of the two rails being joined are vastly different to promote chemical diffusion. However, there is material property inhomogeneity resulting from the thermal input that results in a heat affected zone either side of the fusion line. It is this zone that has different material properties that will lead to differential wear. In aluminothermic welding, a material of similar composition to the rail steels being joined is used with some modifications to give the desired hardness. Material property inhomogeneity also arises out of high heat input creating a wide HAZ either side of the cast weld metal.

4.2.1. Estimation of profile evolution

The material inhomogeneity implied by the welding process can result in differential evolution of the rail profile in different ways. The hardness variation within the heat affected zone cause differential wear and possibly surface plastic deformation along the rail. Moreover, the difference between the microstructural characteristics of the weld and the parent rail may imply a variation in wear resistance along the rail.

As mentioned earlier, differential rail surface evolution results in a geometric irregularity that give rise to variation in contact forces and further surface damage. In fact, the running surface

irregularity and wear mechanism act in a feedback loop connected through dynamic wheel/rail interaction (see Figure 4.1).

Therefore, in order to predict the profile evolution, a methodology is needed to combine the dynamic response of the vehicle/track system due to geometry excitation with profile evolution due to wear and surface plastic deformation.

Limited to two-dimensional vertical dynamics, including traction, a methodology is proposed in Figure 4.17 to study the effect of inhomogeneous hardness along the repaired rail.

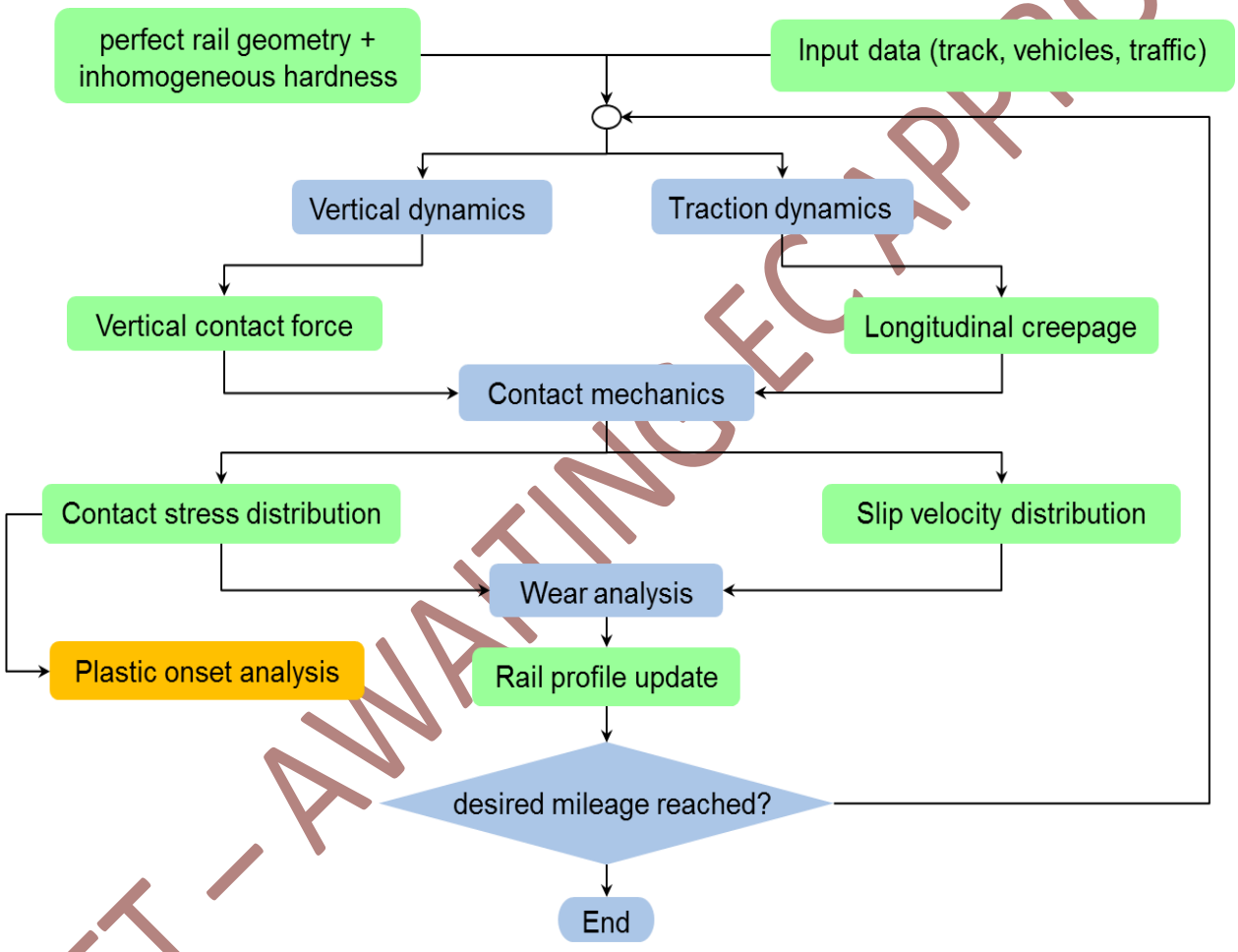

Figure 4.17: Methodology for calculation of differential wear due to material inhomogeneity

In the following chapters each module of the proposed methodology is discussed in more details.

4.2.1.1. Vertical dynamics

To incorporate the variation of normal force, a vertical dynamic model of the unsprung mass and track is needed. However, a detailed finite element model of the discretely supported track is too time-consuming to be used for parametric studies of rail wear. A simple mass-spring-damper equivalent track model is used here instead. Figure 4.18 illustrates the vertical dynamics

model with three degrees of freedom excited by surface irregularity. The input track parameters (presented in Table 4.5) are modified according to [21], for better correspondence to more sophisticated track models (e.g. discretely-supported beam models) within the frequency range of interest (~ 50-1000 Hz). The vehicle representation is limited to unsprung mass since the primary suspensions isolate it from the rest of the vehicle within this frequency range. The track model consists of two degrees of freedom representing rail and sleeper connected to pad and ballast characterized by spring-damper elements. Wheel-rail interaction is modelled by non-linear Hertzian spring including contact damping.

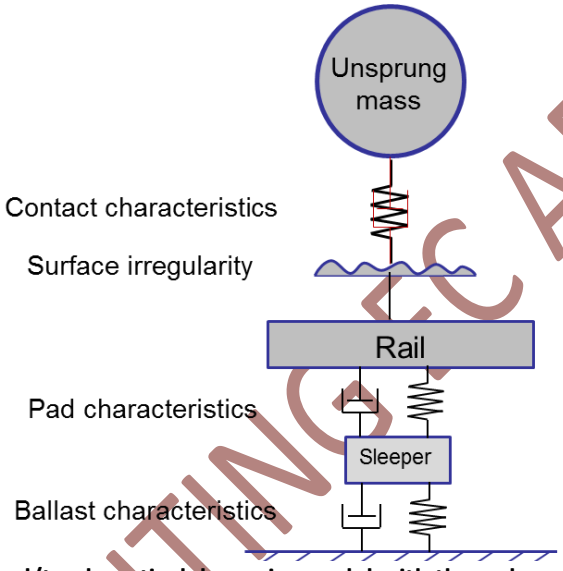

Figure 4.18: Wheel/track vertical dynamics model with three degrees of freedom

4.2.1.2. Traction dynamics

To generate wear, wheel should slip over the rail. For simplicity, lateral vehicle dynamics is discarded and the study is limited to straight track assuming the contact position does not change considerably. The longitudinal creepage due to acceleration-braking of a driven wheel is therefore considered as the source of slip. The longitudinal creepage is however not considered to be constant. For a driven wheel with constant tractive torque, longitudinal creepage is calculated taking into account the varying contact conditions. Figure 4.19 depicts the simplified driven wheel model. The wheel is assumed to be in rotational and longitudinal equilibrium. The longitudinal creepage and creep force is calculated as the normal force varies.

The creepage-creep force relation is provided using Carter's solution for line contact. Figure 4.20 illustrates the creep curve.

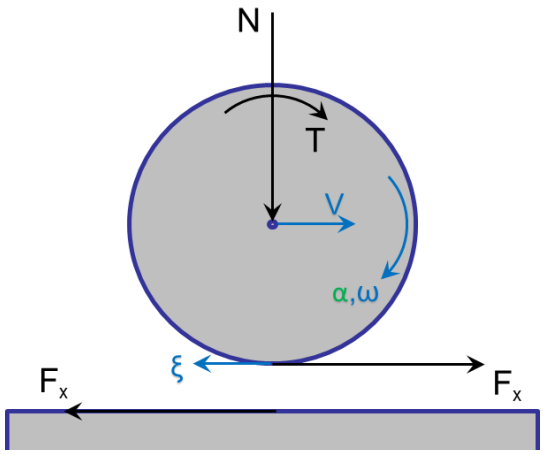

Figure 4.19: Traction dynamics model of a driven wheel

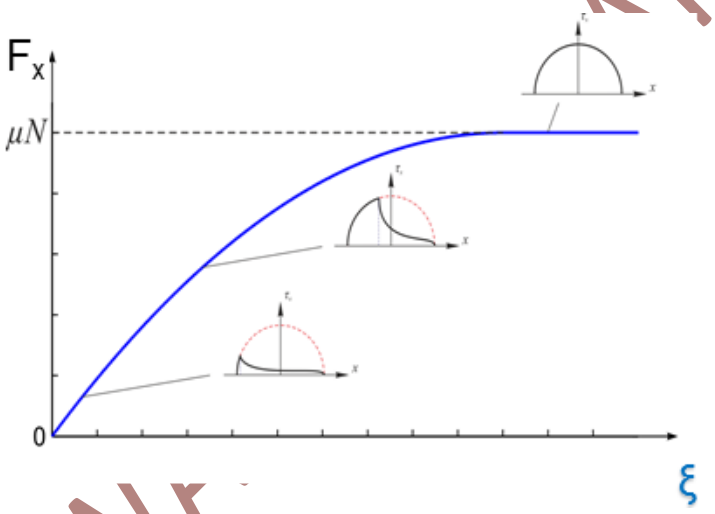

Figure 4.20: Creep force – creepage curve according to Carter's solution

4.2.1.3. Contact mechanics

When it comes to wheel-rail contact, several features that are essentially important in profile evolution estimation are taken into account. These features include contact filtering effect, geometrical contact shift and rail curvature variation.

Surface irregularities with wavelength lower than the typical contact length are supressed due to filtering effect of the contact elasticity. Thus, contact filter considering a typical contact length of 15 mm is applied to the rail profile.

Due to non-flat rail surface the contact point is not directly located under the wheel centre. There is a geometrical shift of the contact point location with respect to the wheel's centre. This implies a torque on the wheel which is negligible. However, the geometrical shift of the contact patch centre is important when it comes to applying the calculated worn depth at the right location. An exaggerated illustration of this shift, denoted as S, is shown in Figure 4.21.

The irregular rail surface in the longitudinal direction presents a non-zero curvature, therefore, rail curvature is calculated at each point along the rail.

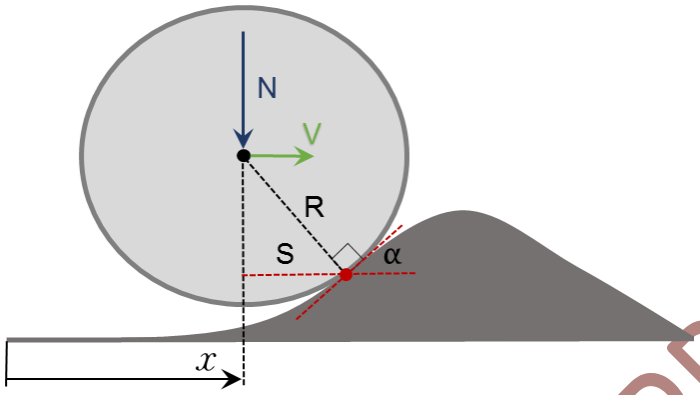

Figure 4.21: Schematic illustration of contact point shift (S) due to irregular rail surface

One-point contact is assumed. Thus, to make sure two-point contact (in the longitudinal direction) does not occur it is checked whether the longitudinal wheel curvature is greater than rail curvature at each point along the rail.

To calculate the maximum contact pressure, it is assumed that the wheelset stays centred, thus, contact semi-axes ratio is calculated for the given wheel/rail pair at wheelset's central position.

4.2.1.4. Wear analysis

The wear depth along the rail is calculated by applying Archard wear model locally [22] at each contact patch. The slip distance is calculated within the slip area from the Carter's solution for tangential traction. Wear coefficient is dependent on slip velocity and contact pressure and is categorized into areas representing mild, severe and catastrophic wear according to the wear map presented in Figure 4.22. The calculated wear depth is then applied to the rail profile considering the slip area location of each patch and the contact point geometrical shift with respect to wheel centre position along the rail.

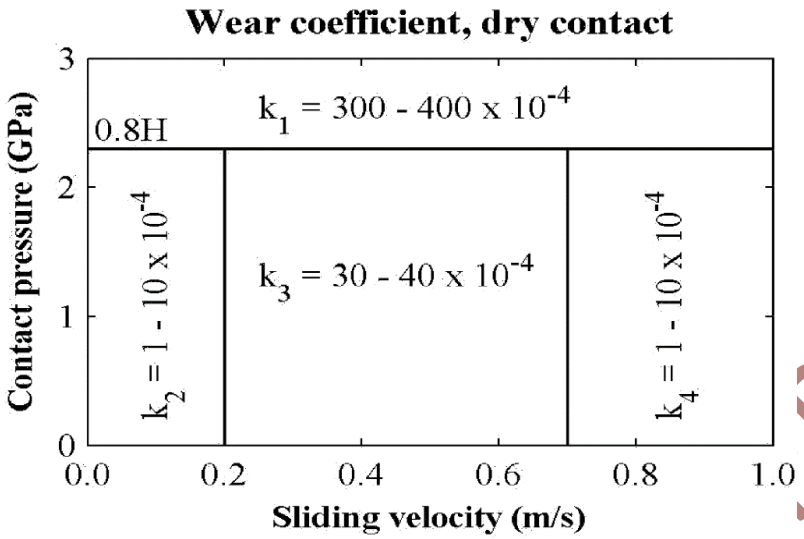

Figure 4.22: Wear map for wheel-rail contact in dry conditions (H = Vickers hardness in GPa) [22]

Wear distribution within a single contact patch, calculated using contact pressure and slip distance distribution, is illustrated in Figure 4.23. The calculated wear distribution is then smoothed using a moving average filter (with length of 15 mm). This slightly lowers the peaks in wear distribution but has negligible effect on worn profile shape.

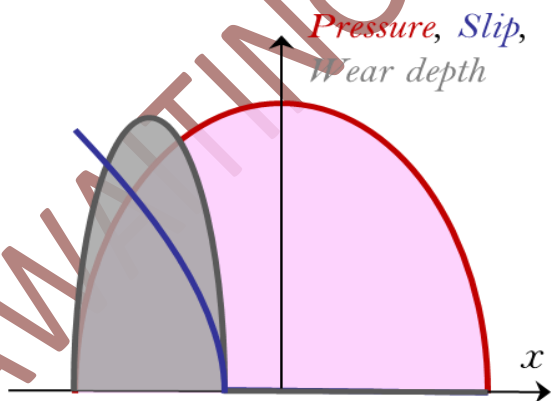

Figure 4.23: Distribution of contact pressure, slip distance and wear depth in a partial slip case

4.2.1.5. Plastic onset analysis

The evolution of the running surface may not only be caused by wear. Plastic flow of the material in the normal direction may also contribute to geometry variation along the rail. It should be noted that here only plastic deformation of the material on the running surface and in the normal direction is of interest. Material may undergo plastic deformation below the surface which does not contribute to rail profile variation.

The variation in material properties of the rail within the HAZ may result in parts of the rail having lower elastic limit and more prone to plastic flow on the surface. To study the possibility of having plastic flow on the surface along the weld repair, the elastic limit along the rail is estimated at each point along the rail from the hardness variation using an empirical

relationship [23]. It is then checked if the loading at each point would lead to onset of plastic deformation, in accordance to von Mises criterion, for two-dimensional tractive rolling [24]. Figure 4.24 depicts the elastic limits dependent on friction coefficient and tractive to normal load ratio (adhesion utilization).

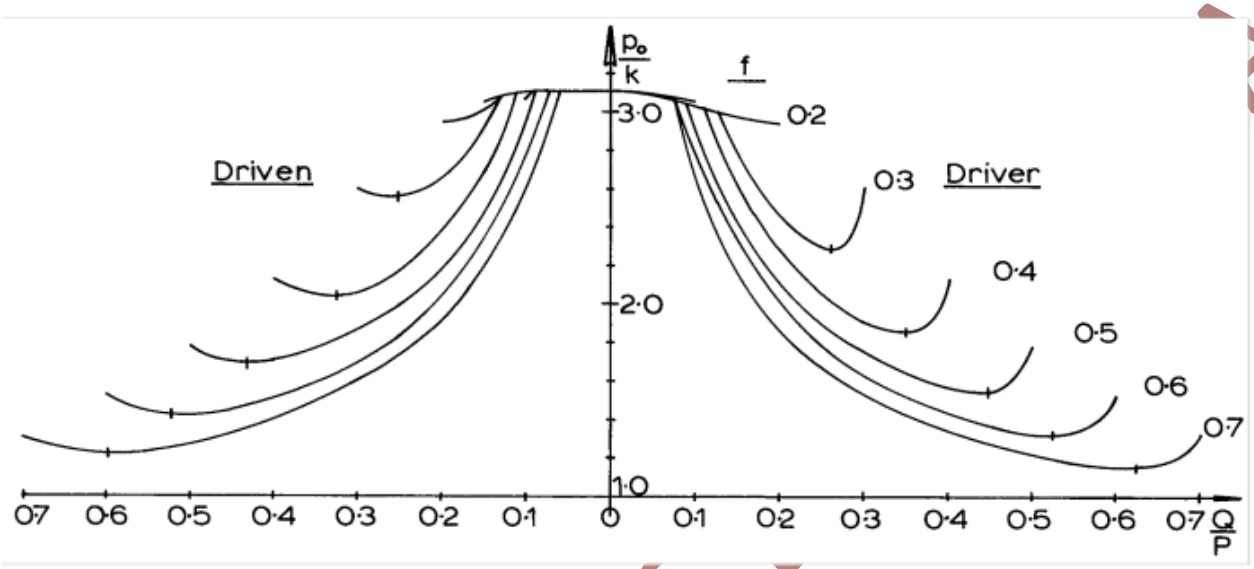

Figure 4.24: Elastic limits in 2D tractive rolling for different friction coefficients (f) and adhesion utilization (Q/P) where p0 is the maximum Hertzian pressure and k is the von Mises shear strength

According to [25], for frictionless contacts, initially the material yields under the surface and the plastic deformation is confined to a small enclave below the surface. Only after an appreciable load increase the plastic zone expands to the surface. However, in presence of friction, yield occurs at all points on the surface if the friction coefficient is above 0.3.

4.2.2. Case study

To study the long-term effect of the HAZ characteristics on the surface quality of the rails, the evolution of the rail profile due to differential wear along the weld repair is investigated. For this aim the methodology presented in the previous chapter is implemented.

In order to characterize the hardness variation within the HAZ, the measured hardness profiles along the HAZ resulted from aluminothermic or DDR head repairs [26] are considered. Figure 4.25 shows the measured hardness profiles along the HAZ as well as simplified representations of the hardness profiles for each of the repair techniques. It should be mentioned that the HAZ area specified in the measured data refers to the visible HAZ area. However, in this study, the HAZ length corresponds to the transition from one hardness region to the other.

A generalization of the hardness profile along the HAZ irrespective of the repair technique may be considered as depicted in Figure 4.26. Thus, hardness variation along the HAZ may be quantified by three parameters; the HAZ length (λ), hardness peak-to-peak variation (Δ) and weld-to-parent rail hardness difference (δ). The measured hardness data presented in Figure

4.25 may be represented by λ ≈ 60 mm, Δ ≈ 60 HV, δ ≈ 0 HV for alumino-thermic repair and by λ ≈ 10 mm, Δ ≈ 140 HV, δ ≈ 60 HV for DDR repair. However, as explained later in the document, the composition of the weld metal in the case of the DDR process has been specifically designed to achieve a wear resistance similar to that of parent rail despite the difference in hardness.

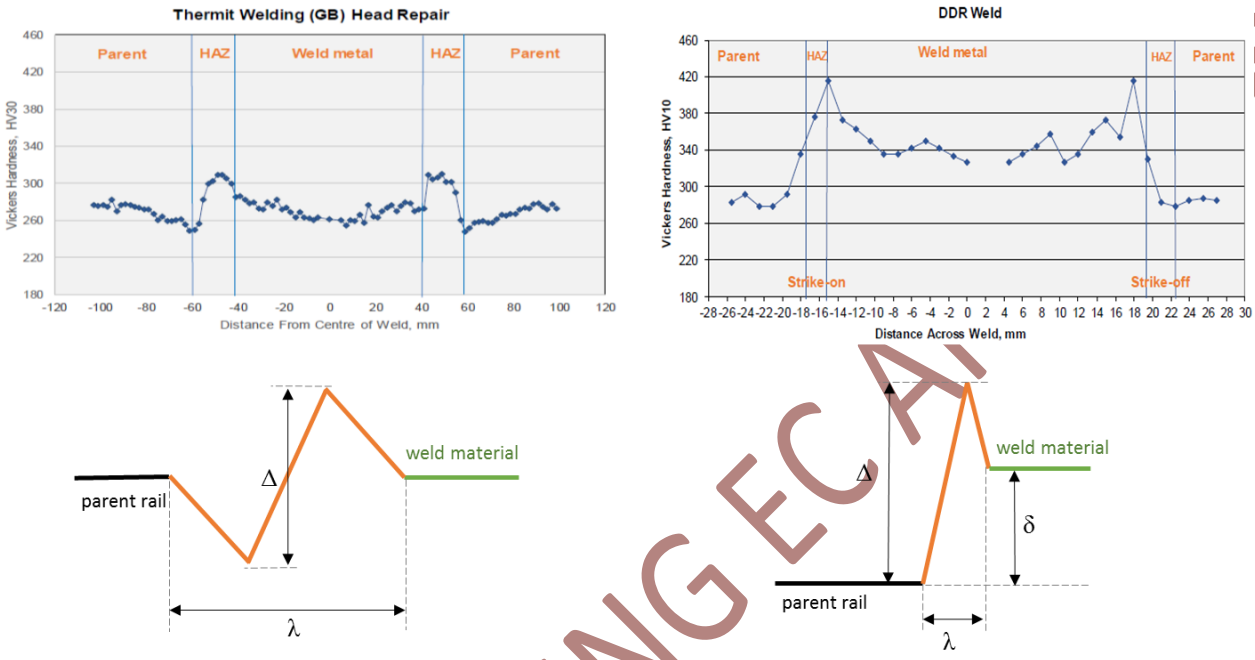

Figure 4.25: Measured hardness profiles along the HAZ [26] and schematic representations resulted from different weld repair techniques

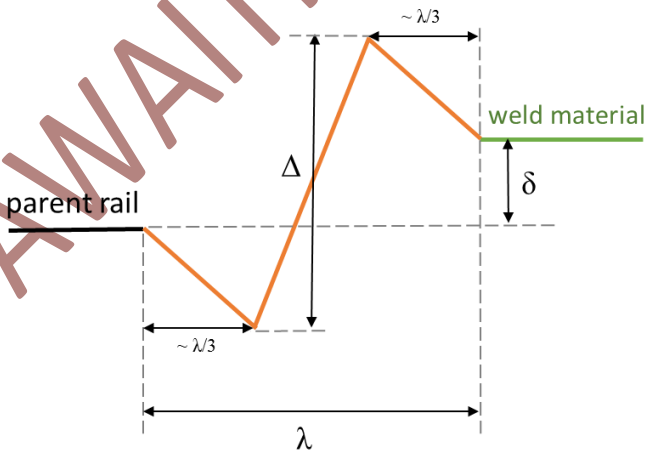

Figure 4.26: Generalization of the hardness profile along the HAZ

To study the effect of HAZ length (λ) and hardness variation (Δ) within it on rail profile evolution a case study is conducted in which a weld repaired rail on straight track is considered. The wear due to the mixed traffic of typical passenger and freight locos are considered. The characteristics of the track as well as the locos are listed in Table 4.5. The loco wheels are driven. The wear due to longitudinal slip of free rolling wheels in trailer cars and wagons is negligible and thus discarded.

Table 4.5: Track and vehicle input data

Track data:	
Sleeper spacing	0.65 m
Rail pad stiffness	195 MN/m
Rail pad damping ratio	0.1
Sleeper mass	325 kg
Ballast stiffness	65 MN/m
Ballast damping ratio	0.5
Simulated distance	1 m
Rail data (60E1):	
Density	7850 kg/m^3
Cross-section area	7.67 m^2
Second moment of inertia	3.038 m^4
Profile radius	300 mm
General properties:	
Young's modulus	210 MPa
Poisson ratio	0.3
Friction coefficient	0.3

Vehicle data:	
Passenger loco:	
Speed	120 km/h
Axle load	20 tonnes
Unsprung mass	1800 kg
Tractive torque	4500 Nm
Wheel moment of inertia	120 kgm^2
Wheel radius	460 mm
Wheel profile	P8
Freight loco:	
Speed	80 km/h
Axle load	22 tonnes
Unsprung mass	2500 kg
Tractive torque	6500 Nm
Wheel moment of inertia	250 kgm^2
Wheel radius	600 mm
Wheel profile	P10

The evolution of the rail surface for 100 million gross tonnes (MGT) of traffic is simulated and the profile is updated after each 1 MGT. Since field and laboratory measured wear coefficients show a rather wide range of variation, the simulations are repeated for two sets of wear coefficients representing upper and lower bounds in Figure 4.22. Table 4.6 summarizes the input data used within the wear analysis module.

Table 4.6: Wear model input data

Overall simulated gross tonnage	100 MGT
Wear-step (profile updating)	1 MGT
Wear coefficients (mild, severe, catastrophic)	Low: 1, 30, 300 x 10^{-4}
	High: 10, 40, 400 x 10^{-4}

A track length of 1 meter is simulated which contains a weld repair of 100 mm length with its centre located at 30 cm. The parent rail is taken to be of R260 grade. The estimated evolution of the rail profile along the track, using two sets of wear coefficients, is shown in Figure 4.27, for a HAZ characterized by λ = 60 mm, Δ=60HV and δ=0HV.

For low wear coefficients, the rail profile directly follows the hardness profile along the weld repair. This implies that the imperfection introduced on the surface geometry does not provoke drastic dynamic load amplification and further damage due to impact loading.

However, using high wear coefficients, the predicted rail profile is deteriorated into a more irregular shape and it initiates some sort of corrugation ahead of the repair. The main reason to it is the high force variation due to dynamic response of the system to dynamics loads of P1 and P2.

Figure 4.28 shows the evolution of surface wavelength spectrum for both sets of simulation. The high wear set shows formation of corrugation with wavelength of about 110 mm which is close to the size of weld repair.

Relevant standards mentioned in Chapter 4.1.1 specify upper and lower bounds on hardness values within the HAZ. For welded rails, the limits are specified according to the rail grade with about 30-45 HV below and 40-60 HV above the parent rail. In terms of weld repairs, the limit is dependent on number of deployed layers as well as rail grades. There is also a different set of limits on surface and sub-surface measured hardness. However, only limits for maximum hardness values are identified. The limits are generally higher for single layer welds going up to about 125 HV and 85 HV for standard rail grades. No specific limitations are set on HAZ length of weld repairs. For welded rails, the apparent HAZ should be symmetrical on both sides of the weld and should be within 25 to 45 mm.

(a) Low wear coefficients:

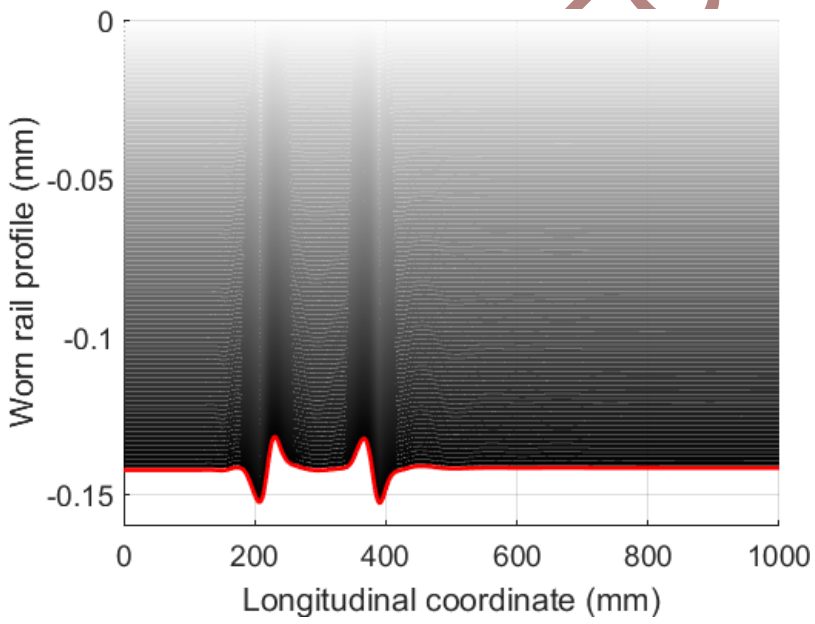

(b) High wear coefficients:

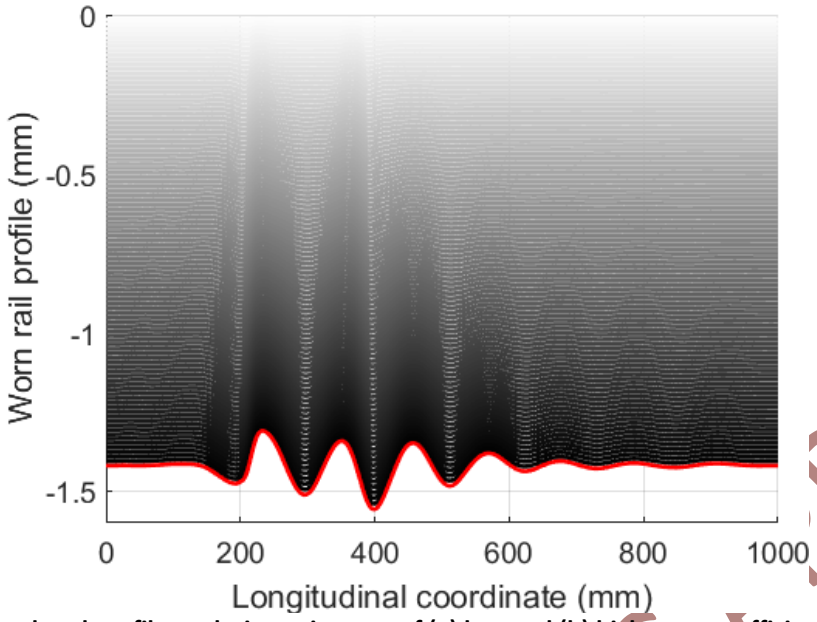

Figure 4.27: Simulated profile evolution using sets of (a) low and (b) high wear coefficients (Table 4.5) for a weld repair having a symmetrical HAZ with λ = 60 mm, Δ = 60HV and δ = 0 HV

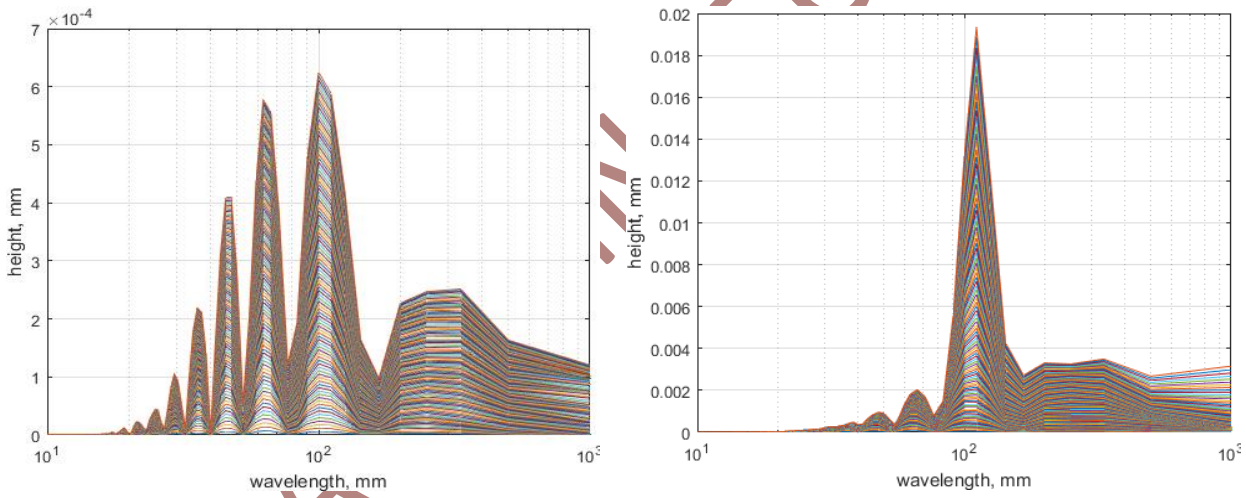

(a) Low wear coefficients **(b) High wear coefficients**

Figure 4.28: Wavelength spectrum of the rail surface irregularity corresponding to plots in Figure 4.27

To study the effect of HAZ characteristic on long-term surface geometry degradation, a set of wear analysis is conducted using a combination of HAZ length and hardness variation within it. The Hardness variation range is of 20-100 HV is considered with a HAZ length range of 20-100 mm. Lower HAZ lengths are not considered since the simple dynamic model, used for time efficiency, may not be valid for higher frequency ranges (lower wavelengths).

In total, 25 cases of different HAZ characteristics are simulated for 100 MGT and the maximum deviation on the surface as well as maximum absolute gradient of the surface are calculated according to the relevant standards. Figure 4.29 shows the contour plots of the maximum

surface deviation over the possible HAZ domain using both low and high wear coefficients (as in Table 4.6). Figure 4.30 shows the contour plots for maximum absolute gradient of the surface.

Both figures show that increasing the HAZ length (hardness variation length) worsens the surface degradation for a constant hardness variation within the HAZ. Therefore, it is concluded that any limitation specification on hardness variation should be imposed in combination with the HAZ length. Thus, for welding methods that result in shorter HAZ length (comparable to contact size) a higher hardness variation within the HAZ may be tolerated.

Using higher wear coefficients, the limiting effect of HAZ length on vertical deviation (Figure 4.29) is more pronounced. However, rather similar constant surface gradient curves (Figure 4.30) are obtained for both low and high wear coefficients.

For the cases studied, no two-point contact in longitudinal direction occurs. The plastic onset analysis shows that only for very extreme HAZ conditions and in wear-steps near 100 MGT, the elastic limit is exceeded on the surface. Usually when loss of contact occurs the dynamic load arising from the wheel impacting the rail may cause plastic deformation. However, in early stages, no plastic deformation due to low hardness zones within the HAZ is predicted.

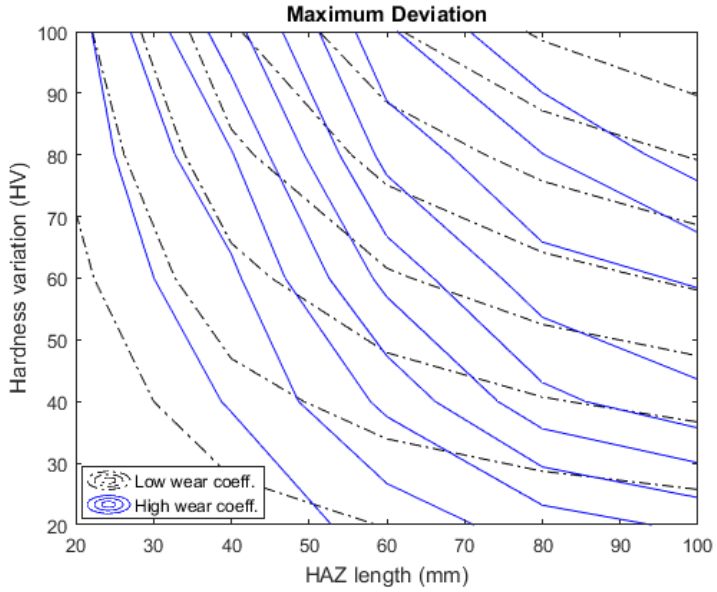

Figure 4.29: Contours of maximum vertical deviation on rail surface using either low or high wear coefficients

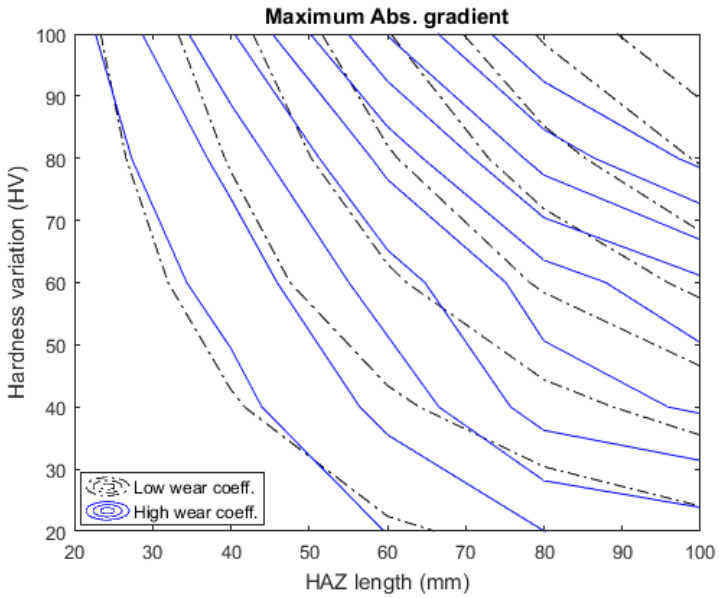

Figure 4.30: Contours of maximum absolute gradient of rail surface using either low or high wear coefficients

4.2.3. Conclusions on wear analysis of weld repairs and recommendations

The conclusions drawn here are based on a single case study using a specific set of track and vehicle and wear input data. Therefore, no quantitative limitation criterion for HAZ characteristic is recommended. However, the parameter variation studied allows for drawing insights into better understanding of the damage due to material inhomogeneity imposed by weld repairs.

A logical methodology to study the evolution of wear profile across a weld has been developed. It is considered suitable for use to the study the evolution of wear on Flash-butt welds, aluminothermic welds, aluminothermic head repair, conventional high preheat FCAW repair, or the recent DDR weld repair process. However, it is necessary to point out that in the case of aluminothermic weld repairs, the wear degradation of the weld material may not follow the hardness dependence of wear in parent pearlitic rails. Similarly, in the case of conventional FCAW and the DDR process, the hardness dependence of wear will be governed by the choice of the welding wire composition and the resultant microstructure of the deposit – these may not be similar to that for the parent rail – consequently further controlled tests are required to generate the required relationship between hardness and wear behaviour of different microstructures.

It is based on the Archard wear model that is able to distinguish between the effect of hardness, commonly attributed to wear performance, and wear resistance (through wear coefficients) and provides the advantage that a consumable with high hardness but lower wear resistance (e.g. carbide-free bainitic microstructure) may be studied more accurately. Therefore, the proposed

methodology for rail profile evolution may be used in future to facilitate the choice of consumable in the welding process in order to minimize differential wear.

However, the methodology requires reliable and comparable input data of wear coefficient – consequently there is need to generate a specification for the acquisition of such data. There are three potential sources that could be considered: Wheel-rail interface rig at DB where a rail length with a weld in the centre can be tested for given contact conditions to determine the wear RCF behaviour across the weld. Voestalpine also have a rig to test a full section rail in contact with a full-scale wheel. This rig could also test welds and provide comparative values for the resistance to wear of the HAZ and the weld metal compared to that for the parent rail. A third option is the large twin disc facility at IRR at the University of Huddersfield; this facility can accommodate a 16mm thick slice cut from the full rail section and would provide comparative values for the resistance to wear of the HAZ and the weld metal compared to that for the parent rail for a range of contact conditions encountered in service.

The tool could be developed further to establish the comparative importance of the influence of HAZ width and the absolute magnitude of hardness differential across the HAZ or the weld metal.

It should be noted that in this study, it is assumed that the wear resistance of parent rail and weld material are identical. However, in case of DDR method, the consumable in use forms a bainitic microstructure which is shown to be less wear resistant than pearlitic one with same hardness value [27]. In this case, a different set of wear coefficients should be used when calculating the weld material wear. At present such coefficient are not available and it is recommended that material testing for wear using representative wheel-rail contact conditions be carried out with such material and compared to typical parent rails steels. The University of Huddersfield is engaged in such testing using scaled twin disc rig and full-scale bogie roller rig facilities, and future research including weld samples would enable further recommendations in this area.

In case of DDR, a lower resistance to wear of bainitic weld material is compensated by its higher hardness compared to the parent rail. Therefore, in this case a higher maximum hardness limit may be permitted. A possible use of the proposed methodology for worn profile prediction is to help optimizing the consumable used in DDR method with respect to differential wear performance.

It should be emphasized that the choice of the composition in the case of the aluminothermic process is based on practical experience of the wear behaviour of the cast weld metal and is generally targeted to be slightly harder than the parent rail. In the case of the DDR process, the bainitic welding wire was chosen deliberately to give a higher hardness than the parent rail

because past assessments of the behaviour of this composition had indicated that its hardness needed to be ~20 points higher than standard pearlitic steel to achieve an equivalent rate of wear It should also be noted that the weld metal in both processes can be modified to give a flatter hardness profile if it can be demonstrated that similarity of hardness will lead to more uniform wear regardless of microstructure.

5. Assessment of operational and quality aspects

The processes available for the repair of discrete defects on rails have been discussed in an earlier chapter together with their advantages and disadvantages. Assessment of the operational and quality aspects of selected processes and their potential for further development are discussed in the following chapters.

5.1. Assessment of operational aspects

The purpose of this chaptern is to carry out an evaluation of the different rail head repair methods from the operational, practical point of view. This evaluation has been carried out taking into account the analysis of some parameters such as: equipment, installation, repair process, weather conditions, risk of welders, etc.

5.1.1. Manual Metal Arc (MMA) welding

Manual metal arc welding process has been very well established for many years in many industries and hence is backed by a wealth of practical experience. It is the benchmark defect repair process that has been used widely in virtually all railway networks. The key operational attributes and potential development challenges of the process are:

1. **equipment, installation, and set up**: the equipment required to undertake MMA repair comprises welding power source, dry electrodes, gas bottles and rail heater, rail grinder for defect excavation and finish grinding, necessary equipment for magnetic particle and/or dye penetrant inspection. The equipment is considered relatively portable using a trolley but individual units could also be carried to site. The setup time at site is short and some Infrastructure Managers permit repairs in between trains but this practice is discouraged in view of the safety of workers;
2. **defect repair process**: the process is well established and used in many industries but the two important criteria of repair quality and shift productivity are almost entirely reliant on the diligence and competence of the welders. This reliance is reflected in the quality of the repair that is frequently found to contain porosity within the deposit and, more importantly, at the interface with parent rail. Such welding flaws act as the site for fatigue initiation and the eventual transverse failure of the rail. Examples of such flaws is discussed further in the metallurgical assessment of weld repaired samples detailed in Appendix 1. The mandated requirement of a preheat temperature of >343^{0}C (300^{0}C -450^{0}C, depending on rail grade) is time consuming and the lack of a process monitoring system results in this aspect of the procedure not being rigidly followed. Consequently, cooling rates within the HAZ can be high resulting hard brittle microstructures and subsequent failures. This aspect is also covered in the

metallurgical assessment of weld repaired samples detailed in Appendix 1. As for other defect repair processes, MMA repair is adversely affected by weather conditions resulting poor quality of repair. In particular, damp electrodes lead to deterioration of electrode coating and cold cracking resulting from the introduction of excessive hydrogen into the weld deposit;

3. **shift productivity**: a minimum of two welders are required to carry out the repair safely excluding those involved to provide safety look out. Shift productivity with this process is low with a single MMA repair taking between 4-8 hours;
4. **worker safety:** potential hazards that require appropriate safety measures are electric shock, fumes, radiation burns to eyes or body, body burns due to hot or molten materials or flying sparks;
5. **potential development challenges:** although MMA welding continues to be suitable for selected applications in other industries, the availability of FCAW and well-established process automation and control technologies signals the demise of MMA welding for the repair of rail head defects.

5.1.2. CTF Sauron - Flux cored arc welding

The CTF Sauron process is the conventional semi-automatic FCAW process discussed in detail in Chapter 3. It is employed by the company (CTF Sauron) for the repair of rails in plain line and switches and crossings. Although details of operational procedures are not available apart from those in the company brochure [5-1], the key operational attributes and potential development challenges of the process are:

1. **equipment, installation, and set up**: the equipment required to undertake repair of discrete defects is based on the TRANSLAMATICs Range of the Automatic Robotic Welders produced by J. SAURON S.A.. The TRANSLAMATICs unit is composed of a frame called TRANSLAMATIC, a programmed process controller called Charlie, a wire feed unit call Roll n Roll, and the PLUTONELEC generator unit. All equipment is carried to site on a TRANSHYDRO 600S unit fitted with caterpillar track and shown inFigure 5.1.

Figure 5.1: TRANSHYDRO 600S [3–18], Translamatic 1252.350, & Translamatic 400-350

The TRANSHYDRO 600S unit appears compact and well organized which should facilitate setup at the track site with the caterpillar tracks providing easier maneuvering. However, the means of transportation of the TRANSHYDRO 600S unit itself to the work site is not apparent;

2. **defect repair process**: the CTF Sauron process is a FCAW process that is used widely in many industries but relatively sparsely used in the railway track industry. Although no details of how the rail defect area is excavated is available, it is believed to be manual and hence dependent on the competence of the operator. However, the influence of the condition of the excavated surface on the integrity of the weld metal-parent rail interface will become apparent in the metallographic examination of samples repaired using this process as discussed in Appendix 1. The process complies with the mandated requirement of a preheat temperature of >343^{0}C (300^{0}C -450^{0}C, depending on rail grade) which is time consuming and it is not apparent whether the control system (Charlie) for the welding process includes the monitoring of the preheat and interpass temperatures. Furthermore, the CTF company brochure does not clarify whether the process controller also serves as a data logger to provide verification and traceability of the process parameters used. As for other defect repair processes, the CTF Sauron repair process would be adversely affected by weather conditions, particularly the influence of moisture absorption into the flux cored wire and flux;

3. **shift productivity**: a minimum of two welders are required to carry out the repair safely excluding personnel required to provide safety look out. Shift productivity with this process is expected to be 3 times higher than that of the MMA process;

4. **worker safety: p**otential hazards that require appropriate safety measures are electric shock, fumes, burns to eyes or body due to hot or molten materials or flying sparks;

5. **potential development challenges:** although FCAW is a long-established technique, its application in the railway track industry has been relatively slow and a few challenges need to be addressed to facilitate wider acceptance into the industry:
    a. logistics of delivery of equipment to site,
    b. development of an automated means of excavation of the defect area such as the use of milling to produce options for standard sizes of cavities depending on defect type,
    c. automation of the operation of the welding gun and although automation of finish grinding would be very useful, the difficulty of blending of the repaired are to various wear profiles that could be encountered in track is recognized,
    d. auditable traceability of the process parameters employed to undertake the repair – process monitoring and data logging,
    e. development/identification of welding consumables and parameters to enable repair of defects in premium grade steels with uniform resistance to degradation through wear and RCF across the length of the repaired area.

5.1.3. Aluminothermic Weld Head Repair Processes – Thermit HRW and Railtech HWR

The two rail head defect repair processes (Thermit-HRW and Railtech-HWR) based on the aluminothermic welding process have already been discussed in detail in Chapter 3 and although there are differences in equipment and operation between the two suppliers, it is appropriate to consider their key operational attributes and future development challenges together. These are listed below:

1. **equipment, installation, and set up:** equipment required to undertake repair includes 0 and 70 degrees ultrasonic probes for defect detection, template for defect cut out shape and oxy-fuel gas cutting torch, gas bottles, manual grinders, MATWELD frog grinders (in the case of Railtech HWR process), preheating torches, appropriate moulds and associated aluminothermic welding equipment, welding portions, and grinders for finish grinding. Although the process manufacturers believe the equipment to be light-weight and portable, the above list highlights the complexity. Hence, the ease of their safe delivery to site has to be considered and evaluated with data on time and motion study to establish operational efficiency obtained;
2. **defect repair process:** in the case of the Thermit process, excavation of the defect is carried out by a flame cutting template and torch followed by manual grinding to achieve a reasonably smooth surface and shape. In the case of the Railtech process, the use of a MATWELD frog grinder is preferred to excavate the defect. Thus, both processes depend on the diligence and competence of the operator and there is no auditable and verifiable traceability of the defect excavation process. Both defect repair processes require careful assembly of the welding moulds and equipment and hence highlight the

need for expert human interface. There appears to be no automated process monitoring but adherence to standard operating practice is believed to be through paper check lists. Both processes would be adversely affected by weather conditions;

3. **shift productivity**: a minimum of two welders are required to carry out the repair safely with both the above processes. Although shorter repair times have been claimed by the process owners, it is believed that the total time required at site is around 3 hours per repair but this could be shortened if two repairs are required at the same site;
4. **worker safety**: worker safety requirements are similar to those for the manufacture of conventional aluminothermic welds requiring similar PPE for protection against hot metal, flames, and sparks;
5. **potential development challenges:** both processes have been approved for use on the UK mainline railway network (NR) with a large number of repairs undertaken using the above processes. However, there is not enough information to indicate its acceptance and use on other European networks. The key developmental challenges that remain are:
    a. the kit required to implement the head repair process appears quite intricate requiring careful assembly – would benefit from simplification, particularly for their applicability for the repair of defects on top of existing flash butt or aluminothermic welds,
    b. although both processes are believed to have been used relatively extensively to repair defects on R260 grade rails, there is little data to support their use for premium grade rail steels,
    c. since the process is permitted to repair relatively large lengths (up to 160 mm), the cast structure is very visible to the wheel and it is therefore necessary to establish the wear and RCF resistance of the cast structure, such data is not currently available,
    d. a large number of repairs have been in-service on the UK network; detailed examination of the microstructure and properties after significant tonnage of traffic would increase understanding and prediction of degradation rates,
    e. the underlying technology is old and the process is highly dependent on the fallible human interface suggesting the need for precise and easily auditable control of the process.

5.1.4. British Steel / ARR Discrete Defect Repair (DDR) Process

The novel process combines two computer controlled operations of milling to excavate the defect followed by FCAW for weld restoration of the cavity. The key operational attributes and potential development challenges of the process are:

1. **equipment, installation, and set up: a** prototype equipment is available to demonstrate the feasibility of the novel process. The unit comprises a welder generator, programmed process control monitoring and data logging computer, a frame containing an interchangeable milling and welding head and wire feed unit, peening gun, and preheating torch. It is expected that low temperature preheating will be undertaken using a bespoke designed infrared heating unit powered by the welder generator. The frame assembly spans both rails and is secured into position through specially designed clamps and weighs 176 kg which makes it impractical for manual handling onto track. However, several design improvements are under consideration for the commercial unit including the logistics of delivery to site. Once placed on track, the setup procedure involves securing the clamps and connecting the power cables and is considered to take ~10 minutes;

2. **defect repair process: t**he process has been described in detail in Chapter 3 but the key attributes that need to be emphasized are:

   - high degree of automation, process monitoring, and data logging capability to ensure verifiable control of the prescribed process,
   - as the process equipment is a prototype, the methodology for getting it to repair location remains to be finalized and this will further enhance automation into the execution of the process,
   - currently, the prototype equipment is capable of one standard size of cavity but the planned new version of the equipment will provide a range of sizes for area to be excavated which can be selected from a drop-down menu,
   - another aspect of the process that is being considered for automation is the preheating stage. Currently this is undertaken using a gas burner but the use of a bespoke design of an infrared heating unit powered by the welder generator is planned so as to remove the manual element in the preheating stage,
   - similarly, the manual procedure of changing the milling and welding heads is to be designed out,
   - finally, a sacrificial layer needs to be deposited very precisely to avoid the creation of new HAZ while at the same time ensuring that the HAZ microstructure of the penultimate layer is sufficiently tempered.;

3. **shift productivity:** although actual on-site experience is required to establish the productivity expected from the process, a minimum of two welders would be required to carry out the repair safely. A trial repair undertaken under audit control conditions concluded that a 100m long and 10mm deep repair could be completed within 1 hour inclusive of the finish grinding operation. This duration could be reduced to ~30 minutes if the length of repair was reduced to 50mm which would be sufficient to cater for most of the observed defects;

4. **worker safety**: worker safety requirements should be similar to FCAW welding processes, although the magnitude of automation reduces the exposure of the workers;

5. **potential development challenges:** the novelty of the process arises out of the use of the low preheating temperature of just 60^0C to 80^0C compared to the current specified minimum temperature of 343^0C. Although not a development challenge, the need to change long-established specifications will be a challenge for process approval. The key developmental challenges that remain are:
   - the current prototype equipment is heavy at 176kg excluding a welder generator weighing ~350kg. Although some light weighting could be achieved through design and material selection for the frame, the process requires a robust and rigid frame to ensure accuracy of milling and subsequent welding. Thus, the challenge lies in the choice of vehicular transportation of the kit to site,
   - further design modifications such as interchangeability of the milling and welding heads, and infrared preheater are required to improve shift productivity,
   - the process has been demonstrated for the repair of defects on Grade R260 and further development is required to adapt the process for premium rail steel grades,
   - development of data communication system to permit the issue of certificate of conformance to agreed procedures after the repair of each defect,
   - development of appropriate process and training manuals to facilitate acceptance by Infrastructure Managers.

5.2. Assessment of metallurgical integrity of repairs

Weld repairs made by the various processes described in preceding chapters have been examined to establish their metallurgical integrity. The tests undertaken are shown in Table 5.1 and the report discussing the results is attached in Appendix 1.

Table 5.1: Assessment of metallurgical integrity of weld repairs

Repair Process	**Macro Examinations**	**Microstructural Examinations**	**Hardness Traverse**	**Fatigue Test**
MMA	Based on previous examinations			
CTF Sauron – FCAW	☐	☐	☐	
Thermit GB HR	☐	☐	☐	☐
Railtech HWR	☐	☐	☐	
DDR	☐	☐	☐	☐

It is important to point out that the depth of repair was different in the processes assessed. The CTF-Sauron technique was applied to a very shallow excavated are with just a single layer of deposit. It is important to note that The Goldschmidt Thermit Group, of which Thermit Welding (GB) is a member, have two head repair welding procedures, the HR procedure used by Thermit Welding (GB) Ltd, which partially excavates the rail head, and the HRW process, which excavates the full rail head. The repaired sample examined in the current project was a HR weld from

Thermit Welding (GB) Ltd. The Railtech HWR process makes the deepest excavation extending beyond the lower fishing radius and into the top of the web. In comparison, the DDR process used a standard excavation depth of just 10mm. Nevertheless, the assessments provide a good insight into the capabilities of the techniques. The key findings of the above assessment are:

- high levels of porosity are an acknowledged characteristic of MMA weld repairs and are known to initiate fatigue and subsequent transverse failure of the rail. In comparison, the internal soundness of both the DDR weld and the aluminothermic head repair welds was excellent, with all having levels of porosity well below the maximum levels permitted in EN 15594:2009. However, some areas of porosity in the Sauron welds exceeded the levels specified in the above standard. The interface between the weld metal and parent rail for all head repair techniques assessed was continuous with no evidence of lack of fusion. The consistency of the shape of the excavated cavity in the DDR process coupled with the use of peening to prevent slag entrapment between the deposited layers is considered to be better for avoiding porosity and slag inclusions than the excavation of a cavity by grinding or gas burning as in the case of the aluminothermic weld repairs (HRW & HWR);
- control of preheating and interpass temperatures in both FCAW and MMA welding is dependent on the competence and diligence of the welder and this human interface is a source of variation that can frequently fall below the desired levels. In comparison, only a minimal preheat is required for the DDR process and maintenance of interpass temperature is not necessary as the weave technique inputs sufficient heat to slow the cooling rate to avoid low temperature transformation phases, e.g. martensite, within the HAZ. The principles of metallurgical transformation underlying the DDR process were clearly demonstrated through examination of the partially repaired samples from the audit trial. In particular, the importance of deposition of a 4th (sacrificial) layer to not only temper the weld metal/HAZ of the penultimate layer but also imparts sufficient heat to further temper the earlier layers;
- the exposure of the rail to the higher temperatures in the aluminothermic weld repair processes is reflected in the widest and deepest HAZ. Consequently, the wheel traverses over a longer length between the parent rail microstructures and it is the degradation resistance of the HAZ and weld metal microstructures that dictates the long-term performance of these repairs, particularly in terms of differential wear across the weld repaired section. In comparison, the HAZ of the CTF-Sauron repair is at a very shallow depth and hence strongly influenced by the wheel-rail contact conditions and, therefore, emphasizes the need for tough microstructure free of hard brittle microstructural phases. The low preheat DDR process produces narrow HAZ either side of the repair and at the bottom of the repair and hence less exposed to wheel-rail contact stresses;

- the hardness traverses across the weld repaired section reflected the composition of the consumables and the processing conditions. However, the rate determining factor is the resistance to wear and RCF that may not have a similar dependence on hardness as that for the pearlitic parent rail. Thus. the choice of a bainitic consumable in the case of the DDR process and a resulting hardness that is higher than the pearlitic R260 grade rail is a deliberate design feature to achieve comparable resistance to wear between the weld metal and parent rail on either side. Although the Sauron process also uses a bainitic consumable but with a different composition to that used by the DDR process, the hardness targets are similar. However, the wear resistance of such bainitic deposits need to be established. The portions used in the aluminothermic weld repair processes are the same as those used in the joining of rails, and hence, their wear behavior would also be expected to be similar to that of welded joints. However, comparative controlled tests need to be undertaken to determine the wear resistance of the cast microstructure present in the aluminothermic weld repair processes;
- the integrity of the DDR and Thermit HR weld repairs was tested under cyclic loading at a stress range of up to 230 MPa, effectively representing over six times that experienced in service by the top layers because of the bow wave effect. Both welds completed 5 million cycles at a stress range of 105MPa (3 times that in-service) but the Thermit HR sample failed from an internal flaw after a further ~176 000 cycles at the higher stress range of 230 MPa. The DDR sample completed a further 3.3 million cycles before failure which was subsequently attributed to a sharp grinding facet on the surface rather than any internal flaw within the repair deposit.

5.3. Applicability to different rail steel grades

As part of the derivation of rail degradation algorithms, the FP7 project “INNOTRACK” [?] developed a methodology for segmentation of railway networks based on their susceptibility to degradation. Although based on limited data, the study estimated that ~57% of European railway network was tangent track and this proportion increased to ~70% if curves and transition curves with radii between 3000 and 6000 m were included. Since the dominant degradation mechanism in such track is vertical wear, it is reasonable to assume that at least this proportion of track or even as high 90% utilise plain carbon-manganese grades with a hardness of <300 HB. Thus, any repair procedure should be capable of repairing defects in Grade R260 or the leaner compositions. However, in view of the increasing realisation of the lower life cycle costs of the use of premium grade rail steel grades in locations more susceptible to degradation through RCF, it is essential that repair processes are also capable of repairing defects in the currently available premium grades. A more detailed discussion of the metallurgical attributes of the currently available rail steel grades is available in a deliverable

D5.2 of the European project Capacity4Rail. The assessment, with reference to the process of weld repair, is discussed briefly in subsequent chapters. The capability of the various repair processes being assessed within the current project is summarized in Table 5.2.

Table 5.2: Rail grades for which the studies welding methods are applicable

	MMA	CTF SAURON	HWR, HEAD WASH REPAIR (RAILTECH)	HWR, HEAD REPAIR WELD (Elektro-Thermit GmbH & Co)	DISCRET DEFECT REPAIR (DDR)
RAIL GRADE	R220, R260, R260Mn, R320Cr, R350HT, R350LHT	R260	R220, R260,	R220, R260	R260

5.3.1. Grades R200, R220, and R260

Although the leanest and softest of all rail steels, they are high carbon-manganese steels with a Carbon Equivalent of >0.7% which puts them into the category of "difficult to weld". Nevertheless, Manual Metal Arc welding of these grades has been practiced for a long time but requires a mandated preheat temperature of >343^{0}C. The primary reason for the use of such a high level of preheat is to slow the rate of cooling of the HAZ and the weld metal to prevent transformation to hard and brittle microstructures with high susceptibility to cracking. Thus the MMA procedure for the weld repair of these grades forms the benchmark against which any proposed weld repair procedure can be evaluated.

5.3.2. Grade R260Mn

This grade is a variant of Grade R260 with a slightly lower carbon range but with a significantly higher content of Manganese. Although the improved hardenability from the increased concentration of Manganese refines the pearlitic interlamellar spacing, the strength and hardness requirement mandated by EN 13674-1 remains the same as that for Grade R260. The argument often put forward in favour of the use of this grade is that the finer interlamellar spacing, resulting from the higher Manganese content, provides a desirable increase in toughness. However, this theoretical improvement is not reflected in the observed performance of this grade. Furthermore, the increase in hardenability brings about greater challenges in welding, and particularly in repair welding. It should also be emphasized that the usage of this grade is limited to very selected railway networks such as the Dutch network.

5.3.3. Grade R320Cr

The desire to increase hardness and thereby increase its resistance to wear led to the development of this grade that is alloyed with levels of Silicon and Chromium much higher than in all other rail steels to develop a hardness of up to 360 HB in the as-rolled condition. The enrichment of the composition raises its Carbon Equivalent to well over 1% with the resultant difficulties for a robust quality weld repair. However, although the grade remains included

within the current EN standard, its usage has largely been overtaken by the availability of heat treated grades. Hence, there is little merit in assessing the capability of the weld repair process with reference to this grade.

5.3.4. Grade R350HT

The original heat treated rail steel was the same composition as the standard R260 grade but used accelerated cooling to increase hardness and tensile strength. Although specifications permit alloying with up to 0.15% Chromium, the required properties can be equally achieved in accelerated cooled plain carbon-manganese variants. Consequently, the grade could be considered as weld repairable as Grade R260. However, the following factors make weld repairing of this grade far more difficult are:

- hardness of the parent rail is between 350 HB and 390HB giving a level of wear resistance that is considered to be 3.5 times greater than that of R260. Consequently, the composition of weld metal used in the repair also needs to develop a matching level of resistance to both wear and RCF. No data was available to verify whether appropriate electrode/wire consumables for MMA and FCAW have been approved by Railway authorities. In the case of aluminothermic weld repair techniques, it may be possible to use the same welding portions used for joining this grade of rail;
- the effect of high preheat temperatures on the microstructure and properties of the parent rail adjacent to the repair remain to be established for each of the repair processes;
- similarly, the need for post weld heat treatment, if any, to develop microstructure and properties that match those of the parent rail need to be established.

The low preheat DDR process that has precise control of the welding parameters could be suitable for the repair of this grade but the consumable capable of developing the properties similar to the parent rail need to be identified.

5.3.5. Grade R350LHT

This is a variant of the R350HT grade in which the level of Chromium content has been increased from a maximum of 0.15 to 0.30%. The metallurgical contribution of this change in composition is a finer interlamellar spacing of the pearlite, although a similar microstructure could be achieved in R350HT grade with a slightly increased rate of cooling. The benefits of a marginally finer microstructure under the demanding rail-wheel contact conditions is yet to be proven.

Although European homologation exists for the flash-butt and aluminothermic welding of this grade, there does not appear to be any commercially available or approved processes for weld repair of this grade. The factors that make weld repair more difficult are the same as those for Grade R350HT but the higher Chromium content of this grade increases its susceptibility to non-pearlitic microstructures in the vicinity of the weld metal parent rail interface. As for R350HT grade, the low preheat DDR process is likely to have the capability to repair this grade but appropriate consumables and welding parameters remains to be identified.

5.3.6. Grade 370CrHT

The desire to develop harder rail steels lead to combined use of additional alloying elements and accelerated cooling to achieve the finest pearlitic microstructure. This approach is reflected in the design of this composition which permits the enrichment of the eutectoid steel composition with up to 0.6% Chromium combined with up to 1.1% Manganese, and 1% Silicon resulting in a Carbon Equivalent of ~1.3%. The higher carbon equivalent of the composition makes welding more challenging, but satisfactory procedures are available for both aluminothermic and flash butt welding of this grade. Although the rail manufacturers claim that the steel is weld repairable, the degree of control required and the need for high temperature post welding heat treatment make the policing of the procedures deployed and the quality of the repair achieved very questionable. Further development of weld repair procedures is necessary for such hardenable grades.

5.3.7. Grade R400HT

This is a heat treated hypereutectoid steel that has been used more extensively by the heavy haul networks. Its inclusion in the Euro Norm (EN13674-1 2011) for conventional and high speed lines is more recent and its application is likely to be restricted to the most demanding segments of mixed traffic networks Since the specification does not incorporate any compositional mitigation measures to avoid the formation of grain boundary cementite, it is reliant on the control of cooling rate within narrow limits to prevent the formation of this deleterious phase. However, the non-uniform nature of the rail section leads to a wide variation in cooling rate and hence increases the probability of the formation of this phase in the slower cooled parts of the rail, away from the active surface of the head. This requirement of closely controlled cooling rate is particularly important for weld repair processes as it will dictate both the preheat temperatures and post weld heat treatment to achieve the desired properties. Similarly, the electrode/wire consumables for the MMA/FCAW processes and the weld portions for the aluminothermic weld repair processes need to be identified.

5.3.8. Grade HP335

Grade HP335 [7] is a naturally cooled hypereutectoid steel from British Steel that has been approved for use by Network Rail but not yet included in EN13674-1 2011. ic ferrite.

In contrast to the R400HT grade included in EN specification, the steel has tailored the composition to prevent the formation of grain boundary cementite and thereby achieve the desired property combination of high resistance to both wear and RCF at the modest as-rolled hardness of ~350 HB. However, the high Carbon Equivalent of the composition makes wed repair extremely challenging and impractical. It is believed that MMA procedure developed for this grade by British Steel involves a high temperature preheat and a post weld heat treatment at around 450^0C for several hours. Although precise details of the developed process are not available, the long post weld treatment times necessitate development of alternative procedures.

5.4. Assessment through numerical simulations

Operational parameters of railhead repair methods involving welding may have an adverse effect on the base- and repair materials. In particular, high temperatures followed by rapid cooling may induce unwanted martensitic phase transformations. There is a possibility to investigate the metallurgy of test samples, however this is not a feasible procedure to obtain a sufficient statistical basis to ensure the feasibility of the method. Further, such analyses cannot be used to investigate the parametric influence since it would result in an unrealistic amount of test samples.

Instead, work has been carried out to investigate the novel discrete defect repair method through numerical simulations. In this investigation, we have studied the Discrete Defect Repair (DDR) Process described in Chapter 3.2.7.

The numerical study essentially has two objectives. Firstly, it is a pilot investigation on the possibility to employ numerical simulations in the homologation process. This would pave the way for much more streamlined, (cost) efficient and exact approval processes. This topic will be discussed further in chapter 7.3.

The second objective is to investigate the DDR method more in detail. In particular, the effect of the significantly lower preheat temperature (60–80 °C) on the evolution of the thermal field during welding and subsequent cooling has been analysed. Through such simulations cooling curves for critical locations (or in fact any location) in the rail head can be evaluated and the risk of weld related defects and metallurgical transformations to hard microstructures can be assessed. As a basis for the simulations, numerical models of a milled rail head were created in ABAQUS/CAE. The repair welding procedure was then simulated and the results compared to experimental data from the literature.

In short, the simulations featured an FE model of a railhead of a 60E1 rail worn down to a rail head height of 44 mm. The repair welding was applied to a 10 mm deep and 100 mm wide cavity, see Figure 5.2.

To ensure the stability of the model, a mesh sensitivity analysis was carried out. A FE mesh that provided sufficient accuracy with reasonable computational effort was selected.

To further investigate the sensitivity of the numerical model, the transition from the inclined walls to the horizontal bottom layer was modelled using a radius of 5 mm (standard), 10 mm, and without radius. The numerical results showed little difference between these geometries, which led to the conclusion that the numerical model was robust. Note that this does not generally imply that the physical results are insensitive to the transition radius – a sharp transition may cause insufficient filling, which may lead to the formation of pores etc.

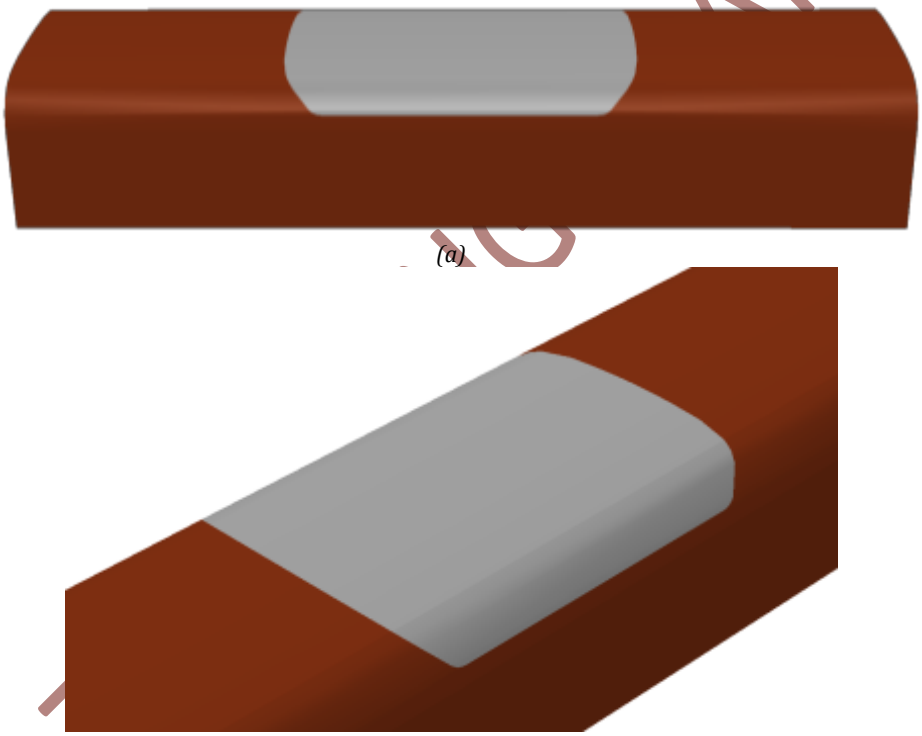

(a)

(b)

Figure 5.2: Geometry of the milled cavity to be filled with repair welding. From (Maglio 2017)

As mentioned, the simulations featured the thermal loading. Thermal boundary conditions were applied as room temperature at the head/web interface of the rail and at two vertical cross-sections 125 mm from the centre of the cavity. This rail head section was ensured to be sufficiently long through convergence studies.

Temperature dependent material properties of the rail head and the filler material were provided within the project by British Steel. The application of the filler was simulated as a discretised application of three passes for each bead, see Figure 5.3. Each pass was timed to

four seconds to match the total weld time at trials. A “cooling time” of 180 seconds is added after each weld layer.

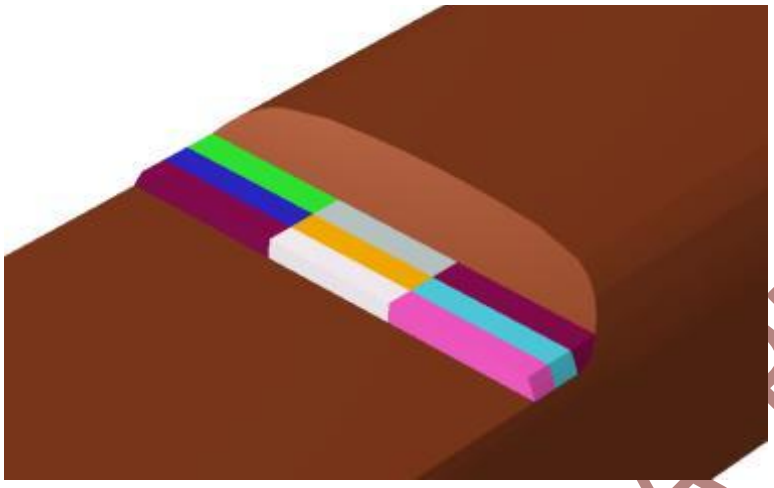

Figure 5.3: Color-coded representation of the discretised weld beads. From (Maglio 2017)

Results were collected in positions corresponding to thermocouples in physical tests. It should here be noted that there is an uncertainty in the physical position of thermocouples in the physical tests since they will depend on the accuracy of drilling etc.

The results show temperature trends that are in line with temperature measurements from trials carried out some years ago. Initial investigations showed the preheating to 80°C to have a small effect on the thermal behaviour of the material. The simulations show the sensitivity to parameters such as the temperature of the molten filler and cooling times. In particular the influence of the temperature of the filler material (which is very hard to measure in field) was investigated. Similar peak temperatures were obtained when the temperature of the molten material was set to 1700°C. Comparisons between measured and simulated temperature histories are provided in Figure 5.4. The results from the simulations clearly show the influence of the temperature of the molten filler material.

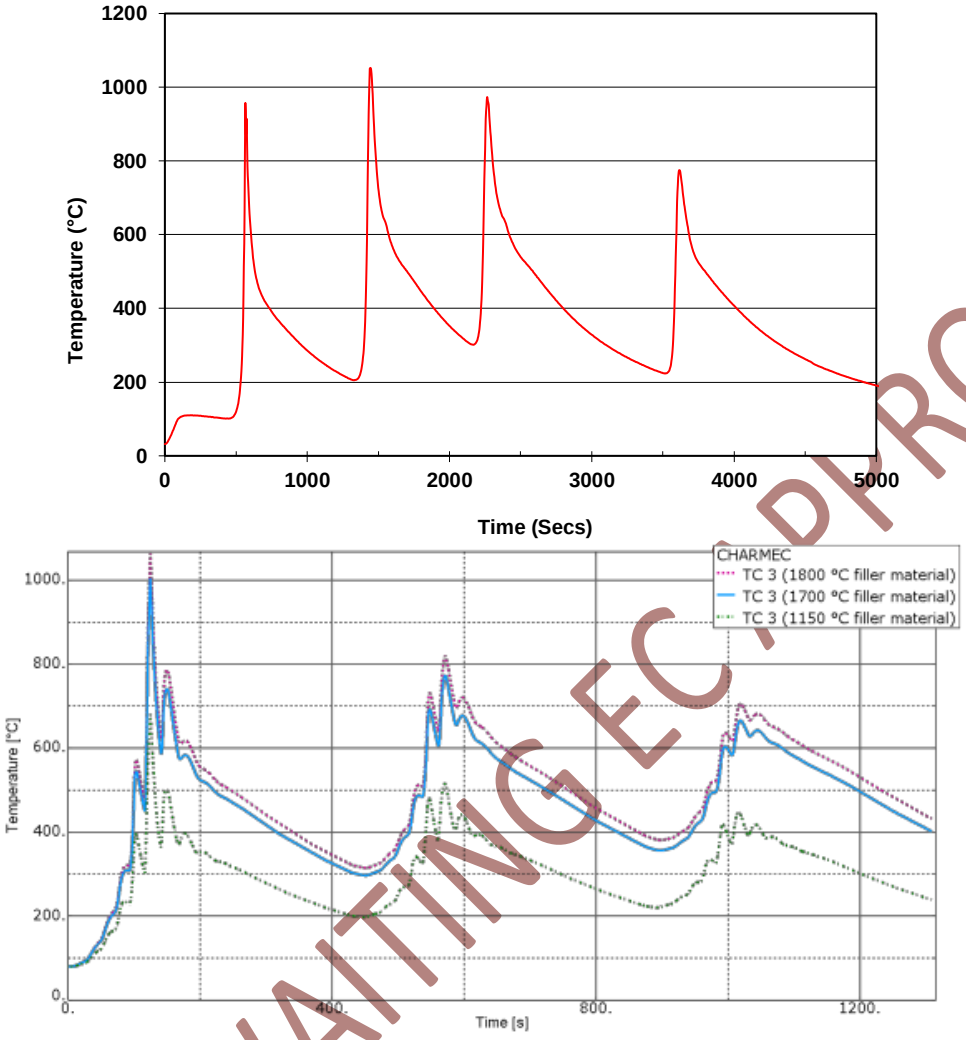

Figure 5.4: Thermal history from experiment (top) and from numerical simulations (bottom), From (Jaiswal 2016) and from (Maglio 2017)

As discussed above, the location of thermocouples is uncertain. Further, the evaluation of temperatures in the simulations are carried out at discrete locations. Since the temperature gradients were found to be very high, in particular at instants in time corresponding to peak temperatures, the influence of the exact location where temperature is measured/evaluated may be crucial. Results from the numerical simulations were employed to quantify this influence. Figure 5.5 shows the points in the numerical model where temperatures are evaluated and the corresponding temperature evolutions. It is seen that between the highest and lowest point (a distance of 1.51 mm), the difference in peak temperature reaches more than 200°C.

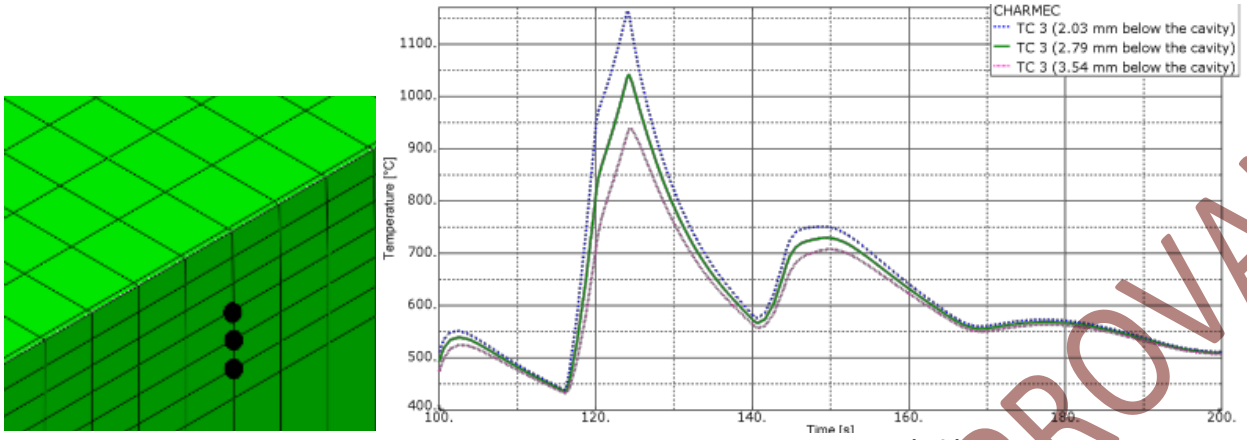

Figure 5.5: Points in the numerical model where temperature is investigated (left) and corresponding temperature histories (right). From (Maglio 2017)

The study has revealed the high potential in simulating operational procedures and thereby be able to e.g. investigate effects of various process parameters. However, to validate and calibrate the numerical models, the study has shown that more high-quality test data are required. In particular the simulations show how sensitive a calibration is to the exact position of thermocouples and the timing of the welding process. On the other hand, the thermal simulations have shown that small variations in the geometry of the numerical model of the repair process do not have a significant influence on the predicted cooling curves.

Detailed descriptions of the thermal simulations are presented in Appendix 2.

In addition to the numerical analyses of the evolution of the thermal fields during the DDR process, a thermomechanical analyses were carried out. This analysis evaluates the stress fields during the repair process. In particular, residual stresses after welding are evaluated. The main reason for such analyses is to get deeper awareness of the (residual) stress field in the rail material due to elevated temperatures followed by cooling phase at the end of DDR process. The thermomechanical analyses were also performed using the commercial software ABAQUS. The only way of evaluating residual stresses due to welding in ABAQUS is to performing a so-called consequential thermomechanical analysis. Such an analysis is very demanding in terms of time, memory and space requirements.

The main input to the stress (structural) analysis is here the temperature fields from each step of the thermal (heat transfer) analysis. As described above, this consists of establishing an initial temperature of 80 °C, addition of weld beads (by so-called model change to simulate the welding process) and finally the cooling stage. It should be noted here that no changes to the geometry or FE-mesh were made after the thermal analysis. To avoid rigid body motions in the structural analysis, encastre boundary conditions (where all displacements and rotations at a node are locked) are employed at a 21 mm wide central strip of the bottom part of the rail. The heat transfer and consequent structural analyses are carried out in 576 load steps. The input

data correspond to some 1 800 000 lines of text. The wall-clock simulation times on a powerful workstation were 3 hours for the heat transfer and 12 hours for the structural analyses, respectively. Storage of results required in total some 80 Gb.

The thermomechanical analysis presented was carried out for the DDR process featuring a 1700 °C filler material. The geometry etc. are the same as for the thermal analyses described above and in Appendix 2. The material was modelled as elastoplastic with temperature dependent characteristics following Appendix 2. In addition, the material was modelled with an initial yield stress of 835 MPa at 25 °C and isotropic hardening. Phase transformations were not considered in the current analysis. Residual stress fields after cooling are presented in Figure 5.6 and Figure 5.7 in terms of von Mises stresses and maximum principal stress, respectively.

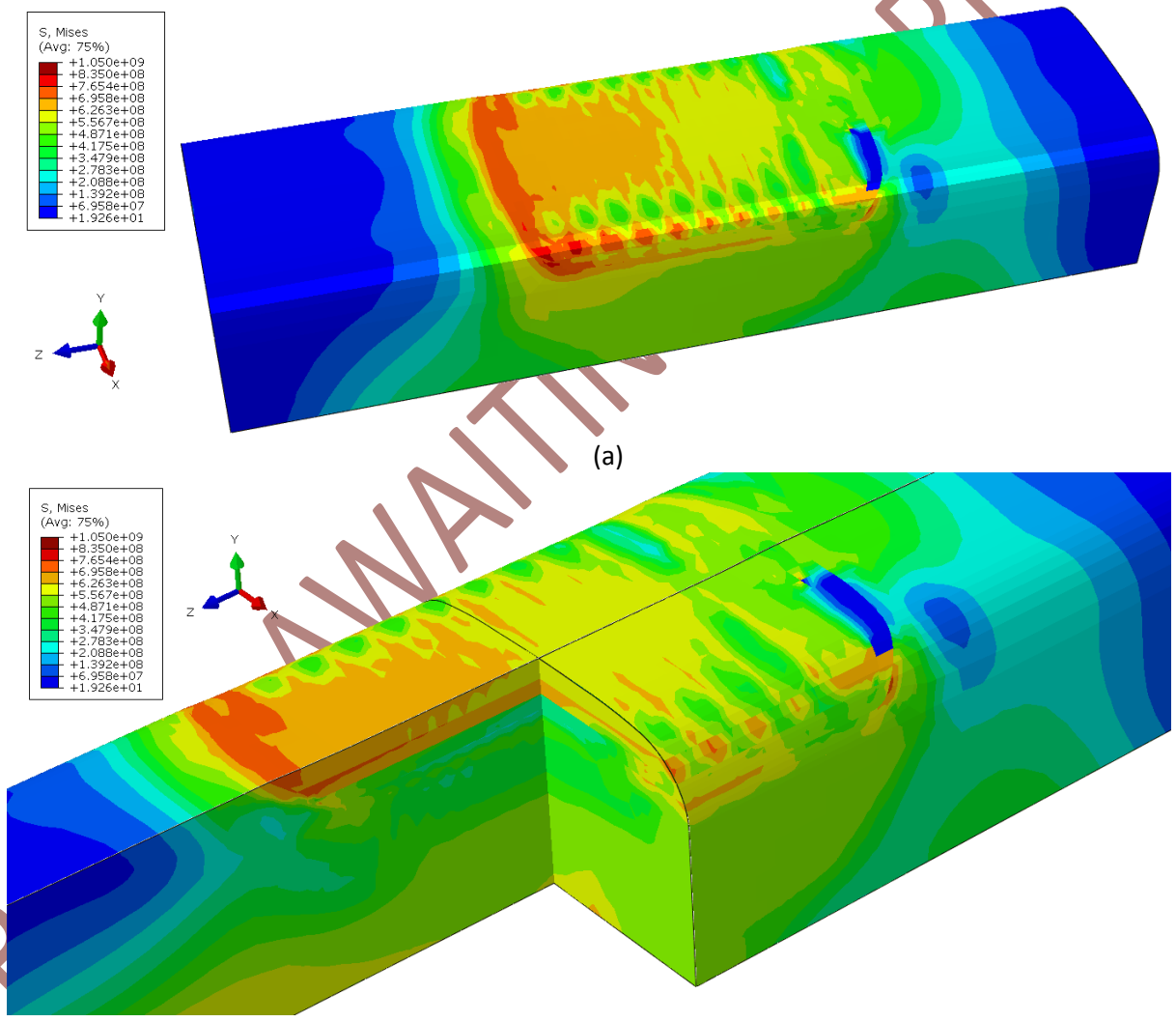

Figure 5.6: von Mises residual stress in the welded rail at the end of the cooling stage in the thermo-mechanical analysis of the DDR process (a) global view and (b) cut-out view

It is seen that residual von Mises stresses are somewhat higher towards the bottom and sides of the cavity where they reach some 750 MPa. Maximum residual principal stresses show that high

tensile stresses exist at the bottom of the cavity, at the top welding layer and at the side of the cavity. Peak magnitudes reach some 800 MPa.

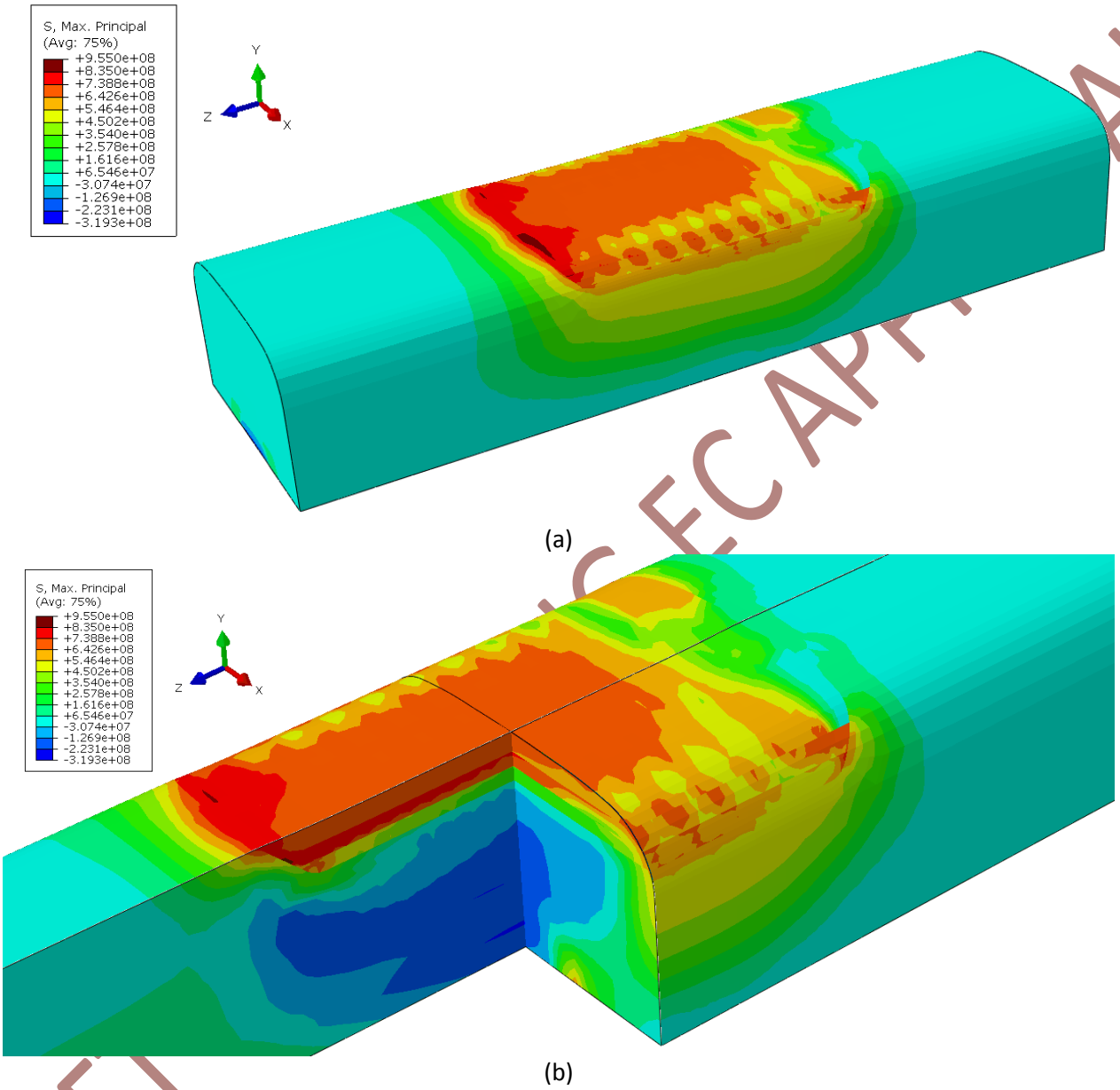

Figure 5.7: Maximum principal residual stress in the welded rail at the end of the cooling stage in the thermo-mechanical analysis of the DDR process in (a) global view and (b) cut-out view

The current study has demonstrated the possibility of numerical simulations of the repair welding process. This can be employed in the further development of repair welding e.g. by investigating the influence of operational parameters. Further development includes improved modelling of the material properties of rail and filler material especially at very high temperatures. These types of numerical simulations can also be employed to investigate the residual stress field resulting from different repair methods. Such a comparison can be a valuable part in the (virtual) homologation of repair welding methods.

5.5 Assessment of cost-effectiveness

The cost-effectiveness of the different rail head repair techniques has been assessed taking into account the following parameters:

- operational cost (includes track possession time);
- labour cost;
- material cost and
- expected failure rate.

The weight of every parameter has been assumed to be equal to arrive at the global cost effectiveness of the different repair techniques.

Since it is difficult to make meaningful comparison of material and personnel costs from different countries, this analysis of cost-effectiveness is not based on absolute costs but instead on a ranking of the various repair processes against the above parameters. The Manual Metal Arc process has been established as a benchmark as it has been used in the railway sector for many years and the costs are well known by most European Railway Infrastructure Managers.

The operational costs have been assessed for the repair of one rail head defect and comprise the equipment installation and setup time i.e. preparation time before the start of the welding process, defect excavation, rail preheating, weld deposition, and profile grinding.

For every parameter, a weighting has been established according to the opinions of welding experts.

Labour costs take account the working hours required to repair one defect (travelling time included) and the qualification level of the welder. This parameter takes productivity into account.

The material costs have been classified into equipment and consumables required for the repair of one rail head defect. Equipment costs take account of the required capital investment and the years of pay-back time. The weighting of both parameters has been established according to the opinions of welding experts.

Assessment of expected failure rate reflects the quality, reliability (evaluation from fatigue test), and efficiency of the repair process and, consequently, influences the total cost of delivery.

The overall ranking of costs (cheapest to most expensive), based on the assessment scores shown in Table 5.3:

- Discrete Defect Repair (DDR) process;
- Thermit Head Weld Repair (HWR) and Railtech Head Was Repair (HWR);
- CTF Sauron semi-automatic FCAW process;

- Manual Metal Arc (MMA) process.

Table 5.3: Assessment of Cost effectiveness of the different rail head repair methods – Comparative scores with MMA as benchmark process

PARAMETERS		WEIGHT (%)	PARAMETERS DETAILS	MMA	CTF SAURON	HWR, HEAD WASH REPAIR (RAILTECH)	HRW, HEAD REPAIR WELD (Elektro-Thermit GmbH & Co)	DDR
OPERATIONAL COST (Track Possession , COST = TIME)	INSTALLATION	30%	*Installation time-consumption on track. Preparation before starting welding process (portability, light - weight, time required to establish an effective procedure)*	0	-1	0	0	-1
	EXCAVATION	20%	*Excavation time-consumption. Defect removal process .Good quality is assumed.(50 mm depth could be made by DDR method)*	0	0	0	0	1
	PREHEATING	10%	*Preheating time-consumption.*	0	0	1	1	1
	WELDING PROCESS	30%	*Welding process time-consumption. Welding deposition process.*	0	1	0	0	1
	PROFILE FINISHING	10%	*Profile finishing time-consumption. Profile grinding process.*	0	0	0	0	0
	TOTAL COST	**100%**	*Cost =Time that it takes the welders to carry out one repair process on track. Track possession.*	**0**	**0**	**0,1**	**0,1**	**0,3**
LABOUR COST	**TOTAL COST**	**100%**	*Labour cost per one rail head repair. Taking into account working hours (travelling time included) per one repair (productivity) and the welder qualification level required*	0	1	1	1	1
MATERIAL COST	EQUIPMENT	20%	*Equipment cost per one rail head repair (Machines for electricity supply, rail heaters, automatic welding machine, etc) .Taking into account the capital investment and the years of pay back time*	0	-1	0	0	-1
	CONSUMABLES	80%	*Consumables cost per one rail head repair (Electrodes, head repair mould, dye penetrant, power, etc)*	0	0	0	0	0
	TOTAL COST	**100%**		**0**	**-0,2**	**0**	**0**	**-0,2**
EXPECTED FAILURE RATE	**TOTAL COST**	**100%**	*Efficiency, reliability of repair process (evaluation from fatigue tests)*	**0**	**1**	**1**	**1**	**1,5**
TOTAL COST (OPERATIONAL COST+ LABOUR COST+MATERIAL COST+ FAILURE RATE COST)				**0,00**	**0,45**	**0,53**	**0,53**	**0,65**

-2	Significantly more expensive than MMA
-1	Sligthly more expensive than MMA
0	Same as MMA
1	Slightly cheaper than MMA
2	Significantly cheaper than MMA

Labour cost and requirements are important factors of estimation of cost, however these are largely unknown and varied between countries.

6. Evaluation and development of innovative methods

Running steel wheels on steel rails leads to very arduous conditions at the rail wheel interface which has been further exacerbated by the increasing density of both passenger and freight traffic, higher speeds and effective axle loads. Such demanding contact conditions lead to discrete running surface defects even in the best maintained railway networks. Thus, sustainability of railway transportation requires the life of rail and associated components to be enhanced and life cycle costs reduced through the use of innovative products and processes. It is this context that highlights the need for a robust, reliable, and cost-effective process for the in-situ repair of these discrete defects.

The incumbent mitigation measure to address the occurrence of discrete defects is improved and frequent inspections to detect the defects followed by either in-situ repair or by replacement of a short length of rail containing the defect. Manual Metal Arc repair is the long-established technique for the in-situ repair of defects and hence formed the benchmark against which other processes could be assessed.

The current project has evaluated two processes based on aluminothermic welding technology and a further two that employ the long established FCAW technology. The operation and technical aspects of all these four processes have been discussed in earlier chapters highlighting their advantages, disadvantages, and the potential for further development. The salient factors that need to be considered in the choice of innovative methods are discussed below.

6.1. Aluminothermic welding based repair techniques

1. The underlying technology of the two processes approved for use on selected European Railway networks is old and highly reliant on the variable human interface that is very susceptible to errors and does not lend itself to objective auditable monitoring of the process and the resulting product quality.
2. The setup procedure for the two processes is relatively intricate and dependent of the dexterity and diligence of the welder. Furthermore, the current design of the moulds prevents their use for the repair of defects on flash butt and aluminothermic welded rail joints.
3. As the wear behaviour of the cast material at the wheel-rail interface would be expected to be similar to that observed on existing aluminothermic welds, it is reasonable to assume that weld repaired area will also experience differential wear compared to the parent rail. However, controlled tests to establish this potential risk of differential wear have yet to be undertaken.

Based on the above factors, further development of aluminothermic welding based repair techniques should be left to the manufacturers of the process consumables. In addition, as repairs using these processes are already in track, controlled monitoring of their degradation

should be undertaken as well as controlled laboratory based tests to establish their susceptibility to differential wear.

6.2. Repair processes based on FCAW technology

Although both the CTF-Sauron and the DDR processes employ FCAW technology, there are very significant differences between the two processes that need to be considered in the choice of the innovative repair method. The salient differences between the two processes are:

- although details of how the rail defect area is excavated is not available for the CTF-Sauron method, it is believed to be manual and dependent on the competence of the operator. In comparison, the DDR process employs milling to excavate a cavity of prescribed dimensions and thereby ensuring reproducibility of quality;
- the CTF-Sauron method employs a preheat temperature of >3430C as per specification and practice for welding of high carbon rail steels. In comparison, a key innovation in the DDR process is the use of a preheat temperature in the range of just 60oC to 80oC while still ensuring desired microstructures in the HAZ and weld metal. The use of low preheat temperature has the key benefit of reduced process time and narrower HAZ width that is visible to the passing wheel;
- although both methods employ computer control for the welding procedure, the DDR process utilises comprehensive automation for the two processes of milling and welding and thereby ensures reproducibility. Furthermore, all key operational parameters are logged in the DDR process to provide traceability and assurance that the process was undertaken using the approved parameters;
- as observed in the weld repaired samples submitted for metallurgical evaluation, the CTF-Sauron process employs longitudinal stringer beads as is the normal practice in even MMA repairs. In comparison, the DDR process employs a square weave pattern that permits better control of temperature, cooling rate, and metallurgical transformation within the HAZ and weld metal;
- the samples examined from the CTF-Sauron process indicated that it had been used to restore a shallow excavated surface with a single layer of deposit of a bainitic composition. This application suggests its use for repair of shallow defects such as ballast imprints or the very early signs of wheel burns. The lack of the heat from a second layer increases the risk of hard microstructures in the HAZ. In comparison, the DDR process was demonstrated for a 10mm deep cavity although deeper defects can also be repaired.

Based on the above analysis, the DDR process was selected for a practical demonstration under audit control conditions. The samples generated during this trial were examined to assess the

metallurgical integrity of the repairs and the results are presented and discussed in Chapter 5.2. The demonstration trial was audited by an independent auditor and his audit report is shown in Chapter 11 (Appendix 2). The trial was deemed a successful demonstration of the innovative process as is apparent from the following quote from the audit report.

"When fully developed the process should offer a cost effective, viable alternative to conventional repair processes for 220 and 260 grades of rail, and could be a particular benefit for use with alloyed and heat treated grades of rail for which no repairs procedures have as yet been approved. If the technology can be shown to work for repairing discrete defects in high performance rails, its potential importance as a maintenance tool should not be under-estimated and further development is warranted"

7. Scenario proposals for later case studies in Shift2Rail

The primary objective of Work Package 3.1 is the "Development, assessment and validation of local rail head repair solutions" and involved the following three tasks:

- analysis of current problems and advantages/disadvantages of current techniques;
- analysis of feasibility and assessment of selected welding processes including establishment of tolerances;
- identification of more innovative repair methods with proposals for further development in follow up projects within Shift2Rail initiative.

The outcomes of the above tasks have been covered in preceding chapters and a wish list of attributes that are considered desirable in rail defect repair system is summarised in Chpater 7.1 below.

7.1. Attributes of optimum rail defect repair system

It is imperative that future developments overcome the disadvantages and barriers of the incumbent rail head repair methods. Consequently, the focus of research should be to deliver the following attributes:

- the weld repair equipment should be light-weight and portable such that it can be easily lifted onto track and setup for the repair operation in minutes. It should also offer flexibility of operation under complex access conditions;
- the repair process should be cost-effective taking into account the costs of track possession, labour, consumables, as well as that of the capital investment in equipment;
- the repair process should be largely automated to minimise the fallible human interface and to ensure that the quality of the repair is not dependent on the competence and diligence of the welder;
- excavation of defect should be carried out by using a computer controlled milling tool to deliver a cavity of prescribed dimensions but with the provision for altering the length and depth of the cavity to make it compatible with the requirements of every Railway Infrastructure Manager. The surface finish of the excavated cavity should be uniform and consist so as to minimise defects at the weld metal – parent rail interface. Provision should be made for the collection of the milling swarf;
- weld restoration employing a low temperature preheat has already been demonstrated; this technology needs to be incorporated into any repair technique to minimise the time required on site and to avoid changes in the local residual stress pattern in the rail. Appropriate guards should be designed into the equipment to protect against and collect weld spatter;

- the subjective audit trail (generally a paper check list) of incumbent repair processes should be replaced by process monitoring and detailed data logging software to provide objective assurance of the process being undertaken to approved procedures and, thereby, assure the quality of repair;
- the repair process and equipment must be compliant with the requirements of ISO 14001:2015 (Standard for Environmental Management Systems);
- appropriate design and fabrication measures should be taken to minimise noise levels and fire risks;
- the process must be capable of repairing defects in the commonly used grades of R200, R220, and R260 but should also be capable of repairing defects in the premium grade steels in use on the European railway networks.

7.2. Selection of innovative rail defect repair processes

The independent audit report concluded that when fully developed the DDR process "should offer a cost effective, viable alternative to conventional repair processes for 220 and 260 grades of rail, and could be a particular benefit for use with alloyed and heat treated grades of rail for which no repairs procedures have as yet been approved. If the technology can be shown to work for repairing discrete defects in high performance rails, its potential importance as a maintenance tool should not be under-estimated and further development is warranted". Furthermore, a comparison of the attributes of the various weld repair processes currently available with the wish list detailed in Chapter 7.1 reveals that the closest match is the DDR process. Thus, the DDR process has been recommended for further development in a follow up project within the SHIFT^{2}RAIL initiative. However, it is also acknowledged that the process requires further development to deliver a robust and cost-effective repair process for the European network. The scope of the proposed further development is detailed in Chapter 7.2.1.

7.2.1. Proposed scope of DDR process development

The key development tasks that are foreseen are:

- logistics of delivery of the system to the repair site;
- risk assessment;
- equipment redesign for robustness and ease of use;
- improved process control software with data logging;
- non-gas preheating device;
- further process development particularly for premium grade steels;
- process and welder training manuals.

7.2.1.1. Logistics of delivery

The discussions to date have revealed a conflicting set of views with reference to the methodology of transportation of the process equipment to the repair site. One view, also included in the wish list in Chapter 7.1, favours the development of "a light-weight and portable such that it can be easily lifted onto track" while a second view favours a fully assembled unit mounted on a railway or road-rail vehicle that is deployable on site without reassembly and with minimal delay. These views will be discussed and developed in partnership with Infrastructure Managers, maintenance contractors, and other stakeholders to establish the preferred method/methods of deployment. Consideration will also be given to parallel initiatives such the development of a Multi-purpose Maintenance Vehicle (MMV) and robotic rail defect repair.

7.2.1.2. Risk assessment

The developed technology introduces several new approaches that carry a risk of equipment failure. It is necessary to undertake a full risk assessment with particular focus on the impact of equipment failure as the repair process is based on the removal of the full width of the rail head. Similarly, failure of the process control software is a potential risk and designed redundancy needs to be incorporated.

7.2.1.3. Redesign and fabrication of equipment

The audit trial and the discussions that followed have highlighted several areas of equipment design to improve the robustness, reliability, ease of use, and the environmental impact of the equipment. The new version of the machine will address all the identified areas of improvement.

7.2.1.4. Improved software for process control & data logging

The automation of the process is achieved through a plc unit that controls precisely the whole process. The process control program is old and it is considered prudent to move to a Windows based program to improve reliability. Such a move will permit the recording of the operator and location identity as well as enabling the logging of all process parameters required to demonstrate compliance to the proven process. It is intended to enable the developed system to issue a compliance certificate after each repair and permit downloading of required data onto any database for statistical analysis of process control.

7.2.1.5. Non-gas preheating device

The developed process requires the rail temperature to be raised to between 600C to 800C before the commencement of weld restoration. Currently, this is achieved using an oxy-propane burner but there is desire to minimise the equipment that needs to be transported to site. Consequently, a non-gas and electrically powered solution is considered desirable provided the

rate of heating does not prolong the defect repair process. A solution based on infrared heating elements powered by the welder generator employed for weld restoration will be developed. A similar system, shown in Figure 7.1, has been successfully developed to maintain the temperature of grooved rail at the desired level at the “strike on” and “strike off” locations. This design will be modified to the requirements of the DDR process.

Figure 7.1: Infrared temperature control unit

7.2.1.6. Further process development

The developed DDR process has been demonstrated for the repair of discrete defects in the most widely used rail grade in European networks, R260. The consumable used for the repair is also already approved for use in several major European networks and generates a bainitic microstructure with a wear rate that closely matches that for R260 grade rail steels. However, continuing growth in both passenger and freight traffic has promoted greater use of premium grade rail steels such as HP335, R350HT, R370CrHT, and R400HT. Since these rail grades are also susceptible to discrete defects, there is a need to identify appropriate consumables and welding parameters to enable repair of defects in these premium rail grades. A series of trials will then be undertaken using the existing DDR machine to establish the welding parameters required to give a robust deposit.

7.2.1.7. Process and welder training manuals

The preparation of process and welder training manuals are considered an essential task that will facilitate rapid and wider acceptance of the process in European Railway networks as well as many other networks across the world.

7.3. “Streamlined” approval process

In order to get widespread adoption of innovative repair welding processes, it is crucial that the approval process is “streamlined”. In this context, “streamlined” implies that the process should be more standardised, be (cost) efficient and as fast as possible while the quality of the evaluations is maintained. In addition, the approval process should be more stringent in the sense that it should be stated clearly as to exactly what is being evaluated and what the (quantified) approval criteria are. Ideally, the approval process should also be able to investigate the robustness of the welding methods and quantify how a certain method ranks compared to other methods in different aspects. Such an approval process would also decrease cost and time to market, which are important factors in promoting innovation.

7.3.1. Potential areas for virtual homologation

The general trend to achieve these objectives is a shift towards more numerical simulations, so-called “virtual homologation”. In certain areas, simulations are now so advanced and reliable that the only physical testing that is carried out is to calibrate / validate numerical models and tests that are required by regulatory bodies. The main reasons for the extensive use of numerical simulations is that they are less costly, require less equipment, are faster, and allow testing of “what if” scenarios. The latter also allows for sensitivity analyses that would be extremely costly if carried out as physical tests.

When attempting to shift to a more simulation-based approval process it is vital to understand what simulations can capture, and even more important to understand what they cannot capture. Inherently, numerical simulations give “precise” results in the sense that for a given set of input data, the numerical model, and the evaluation of selected parameters will yield a certain result. A sensitivity analysis can, to some extent, extend this by evaluating the results from a number of varied input data sets. In addition, the influence of model parameters (e.g. boundary conditions and level of detail) can be evaluated. As an example, Appendix 2 features such investigations where the influences of boundary conditions and mesh density are investigated. Such studies can be employed to increase the reliability of the results. It should however be kept in mind that there are other uncertainties that are much more difficult to capture by numerical simulations, as will be described below.

In the case of welding, there exists a number of studies on the capabilities of numerical simulations, see e.g. [2], work in the EU-project WRIST. In the current study, numerical simulations are presented in Chapters 4.1, 4.2, 5.4 and in Appendix 2.

Numerical simulations can be employed to analyse the weld process (as in Chapter 5.4 and in Chapter 11 (Appendix 2)). More in detail, these analyses can be employed to evaluate the temperature fields during welding. As described in Chapter 5.4, this is in itself a complicated

analysis where there are a number of uncertainties in input data and model parameters as described in Appendix 2. The next step is to investigate the thermomechanical interaction, which gives rise to residual stresses etc. Such simulations are demonstrated in Chapter 5.4. They are generally an order of a magnitude more complex and require more input data such as the mechanical characteristics of the weld and base materials at different temperatures.

Numerical simulations can also be employed to investigate the operational capabilities of the weld. Examples of such simulations are presented in Chapters 4.1 and 4.2. Here, the influence of weld geometry on operational loads, and the influence of operational loads on weld geometry degradation are investigated. In the latter case, material characteristics of the weld and heat affected rail base material are important influencing factors.

What is not considered in the current report is the strength of the weld regarding fatigue and fracture. This strength is strongly influenced by the material characteristics of, and geometrical irregularities in the (heat affected) base material of the rail, and of the weld material. It is also strongly influenced by the formation of material defects (including insufficient bonding) and of local geometry faults. These are factors that are extremely difficult to capture even in extremely detailed numerical simulations. They are also severely influenced by local conditions during welding. Thus, welding processes typically employ inspections and tests to minimize the risks for such complications.[1] In addition to the influence of material and geometry defects, the strength of a weld is significantly influenced by the residual stress filed in the vicinity of the weld.

7.3.2. Outline for a streamlined approval process for repair welding

From an operational perspective, an approved weld repair process – not considering production and environmental concerns, which are discussed in Chapter 7.1 – needs to ensure a correct geometry and a sufficiently strong rail structure. More in detail, this implies that the initial geometry as well as the wear characteristics need to be sufficiently good. It also implies that the material affected by the rail has a sufficient resistance towards crack initiation and growth. The latter is as noted above highly related to the temperature evolution in the filler and base material, and also to the formation of material and geometric defects.

In the current report, we have shown how evaluation of weld repair methodologies can be carried out based on operational experience and empirical knowledge, (thermo)mechanical tests, metallurgical and metallographic investigations, and through numerical simulations. Of these, the numerical simulations are (as mentioned) often the least expensive and allow to study the influence of parameter variations. The outcomes of numerical simulations are in the

[1] Note that numerical simulations of various forms can aid also in evaluating and developing such inspections methods

current study temperature fields and their evolution over time. Furthermore, global weld geometry evolution due to wear is studied. In more advanced simulations, also stress/strain distributions and evolutions can be evaluated. Further, numerical simulations can be employed to predict phase transformations and fatigue crack initiation and growth. (Thermo)mechanical tests are generally required to obtain material parameters to calibrate the numerical simulations. They can also be used for validation purposes. Metallographic/metallurgical evaluations can further be used to increase knowledge of the microstructure and to validate/calibrate predictions of phase transformations. Finally, full-scale tests will be required to validate that the method also works as foreseen under field conditions.

With this in mind, a suggestion for a streamlined approval process is outlined in Figure 7.2.

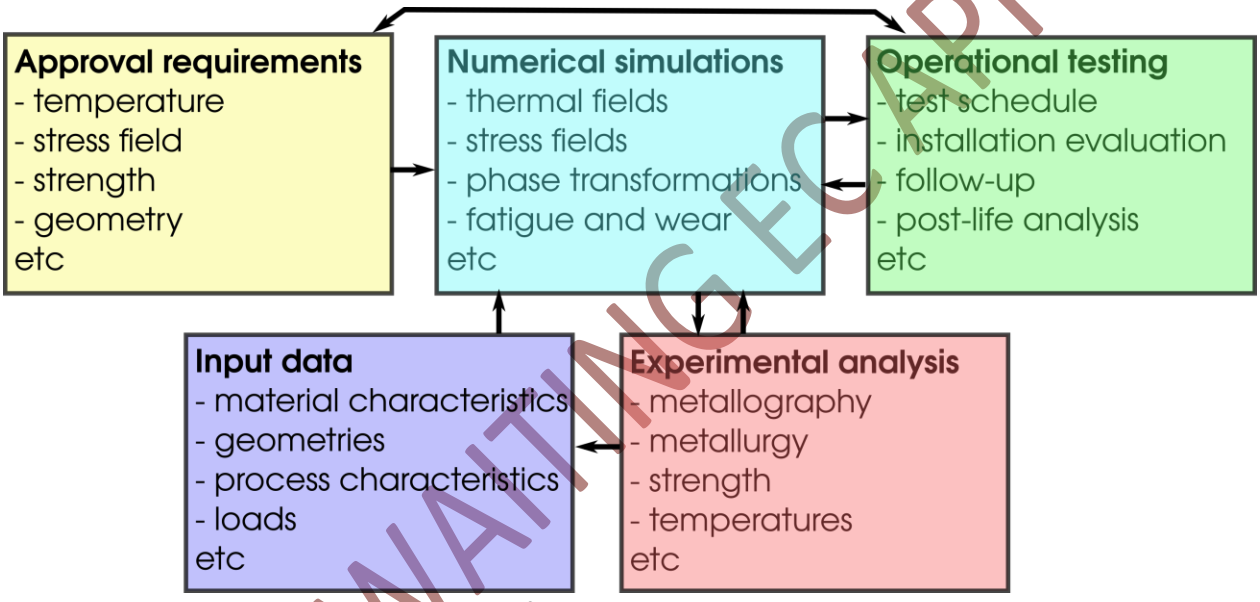

Figure 7.2: Schematics of a suggested streamlined approval process

The first step is to define the **approval requirements**. Since these will govern which welding repair methods will be approved, it is vital that these requirements are quantifiable and as precise as possible. The requirements can also be divided into general requirements and requirements for specific circumstances. One example of the first kind could be a limit on temperature evolutions. The temperature fields are reasonable straight-forward to characterise and relate subsequent material strength and residual stress field in the weld. A more direct requirement would be on the residual stresses, since too high residual stresses result in a large risk of rail fracture. An example of requirements for specific circumstances could be geometric tolerances where more geometry irregularities could (at least in theory) be allowed for a low speed line.

The second step is to compile required **input data** for numerical simulations. Which these data are depends on the simulations to be performed and which data that are available. A good

practice here is to estimate uncertainties in input data so that sensitivity analyses can be performed, see e.g. the investigation of the fill material temperature discussed in Chapter 5.4.

The third step is the **numerical simulations**. Here the robustness of the method can be assessed by varying process parameters, operational parameters etc. The extent of the simulations can be adjusted based on the extent of physical testing to be carried out. As an example, numerical simulations of phase transformations can (partly or fully) be replaced by metallographic/metallurgical examinations.

The outputs of the numerical simulations are contrasted towards **experiments**. As indicated above, there is a strong relation between the physical experiments and the numerical simulations: They can (partly) replace each other, the numerical simulations will indicate which experimental results that can be expected, and experiments can be employed to calibrate/validate simulations. Further, the experiments may also give additional input data that can be employed in subsequent numerical simulations.

The final step of the validation process is the **operational testing**. Since operational tests are costly and time consuming, it is vital to have a well-designed test and evaluation plan. This includes tests at installation (e.g. inspection of material defects) and follow-up tests (e.g. of geometry evolution). The tests should preferably conclude with a post-life analysis where the operational life of the weld is evaluated and contrasted to LCC estimations etc. This will also be a possibility for destructive testing of weld strength, material defects etc. Note that, if carried out correctly, the operational testing can provide very valuable input to improved definitions of approval requirements. It can also act as an “ultimate” validation of the numerical simulations.

One important part of operational testing is the use of (non-destructive) **validating testing**. Here the aim is to ensure that the weld is within allowable tolerances. Regarding geometry, this is fairly straight-forward (although evaluating local faults may be a challenge). To ensure correct temperatures and residual stresses is much more complicated: As discussed in Chapter 5.4 and Appendix 2, such evaluations are very sensitive to measurement positions and complicated by the high temperatures.

The current report includes parts of the suggested approval process. There are still significant efforts required to achieve full-fledged virtual homologation schemes where physical tests are only used for validation purposes. However, it should be kept in mind that virtual homologation schemes are currently essentially a reality for bridges, cars, airplanes etc. To implement such schemes also for rail welding is far from unrealistic, but would of course require both resources and determination.

7.4. Wider application of weld deposition processes

One of the seven recognised categories of “Additive Manufacturing” (AM) is Directed Energy Deposition (DED) which includes direct metal deposition. The DDR process is an example of AM and although the current application is for the restoration of a small defective area of the rail head, the technique could equally be employed to deposit degradation resistant materials at the active interface of many railway components. Some potential applications are discussed below.

7.4.1. Crossing nose

Figure 7.3 shows a crossing fabricated out of rails generally of Grade R260 and another crossing with austenitic manganese inserts. As the wheel rail contact locations through a crossing are well understood, AM techniques such as weld deposition can be used to deposit significantly more degradation resistant materials at exactly the locations they are needed while the remainder of the structure can be designed very cost-effectively in a supportive role. Hardfacing is a well-established technique for the deposition of a relatively thick coating of hard and wear-resistant material on a softer base metal substrate using one of the welding techniques or thermal spraying. A very wide range of hardfacing electrodes and welding wires are available from the major manufacturers that are generally used to restore worn components but the process has also been applied to new components to extend life expectancy. The DDR process could be adapted to either restore worn fabricated crossings or the manufacture of new crossings using highly degradation resistant deposits. It could also be used to refurbish or manufacture other components such as wing and check rails using the hardfacing approach to create a composite product.

Fully Fabricated Crossing

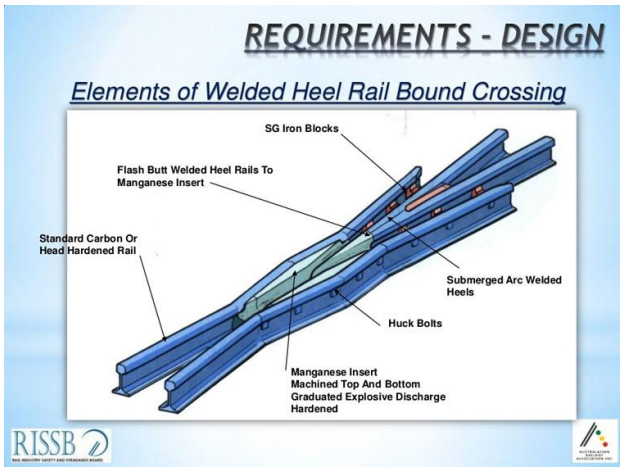

Rail Bound Crossing with Austenitic Manganese Insert [7-1]

Figure 7.3: Potential applications of additive manufacturing in railway crossings

7.4.2. Restoration of “cupped” welds

The differential wear across old aluminothermic and flash butt welds leads to “cupping” irregularity that gives rise to high dynamic forces onto the rail beyond the weld. The consequent damage to both rail and the track bed adjacent to the weld location in the direction of traffic reduces rail life, deteriorates ride quality, and increases the maintenance required. Furthermore, such cupped welds are generally associated with old regional tracks that do not attract the same degree of investment as high traffic density routes. Hence, removal of the vertical irregularity at welds would increase the life of rail and track in such routes. there are also no cost-effective techniques for restoring such localised differential wear. The DDR process could be adapted to excavate and weld restore the cupped area to one with wear resistance closely matched to the parent rail.

7.4.3. Batter resistant rail ends

A key cause of failure of IBJs is the batter of the rail ends leading to bridging of the gap. The use of weld deposition of a deformation resistant material is expected to enhance the life of IBJs. The DDR process could be used to deposit such a material.

7.4.4. Control of wear resistance and friction at gauge corner

Low preheat weld deposition has been used for the in-situ restoration of high carbon grooved rails as shown in Figure 7.4. An austenitic stainless deposit with a high rate of work hardening is used to restore a side worn embedded rail with the added bonus that the work hardening characteristic of the deposit increases the wear resistance of the deposit to enhance rail life further.

Figure 7.4: Gauge corner restoration using SAW and austenitic stainless wire. As deposited hardness of ~200HV and ~500HV after work hardening

Another additional benefit that stems from the stainless deposit is the observed reduction in squeal noise thought to be an effect of reduced rate of roughness growth. Although such benefits require controlled scientific validation, the technology hold promise for application at specific locations in main line railways such as within complex junctions at approach to stations.

8. Conclusions

The analysis of rail head defects with a focus on which defects that can be mitigated by repair welding was carried out in chapter 3. Statistics from the NR network indicate some 0.2 repairable defects per year and kilometre of track. From Trafikverket data, the corresponding amount is around 0.07, and for the SNCF network on the order of 0.2. The analysis thus indicates a large potential for rail repair, but also that there is a need to assess how well rail defect reporting is harmonised across Europe.

The assessment of different repair methods has highlighted benefits and drawbacks with all methods. In addition to the general qualities of the methods, the suitability will also depend on local conditions (that may affect track access, labour costs etc significantly). The evaluation in Chapter 5.1 provides a logical assessment scheme that can be employed also for future assessment of existing and innovative methods.

The analysis of consequences of imperfect weld geometries shows that better weld geometries are required in cases of high speeds and high support stiffness. In contrast altered unsprung mass has a moderate effect on the required weld geometry. The study also recommends that the use of 3D weld profile evaluation should be further investigated.

As for operational deterioration of weld geometry through wear, a methodology for assessment has been developed. The study indicates the need for improved indata, mainly in terms of wear coefficients. This is a particular issue if the weld material forms a microstructure that is not pearlitic (for which most available wear data is derived).

The in-depth investigation of the metallurgical integrity reported in Chapter 5.2 and Chapter 10(Appendix 1) showed that the DDR weld and the aluminothermic head repair welds had porosity well below maximum levels permitted in EN 15594:2009. The Sauron welds exceeded the levels specified in the standard in some areas. For MMA weld repairs, high levels of porosity are an acknowledged characteristic. The study showed that only a minimal preheat is required for the DDR process and that maintenance of interpass temperatures are not necessary as the weave technique inputs sufficient heat to slow the cooling rate. The higher temperatures in the aluminothermic weld repair processes resulted in the widest and deepest HAZ. The DDR and Thermit HR weld repairs completed 5 million cycles at a stress range of 105MPa.

The use of numerical simulations to assess heat transfer and thermal loading of the rail has been developed and demonstrated. The work indicated the influence of operational and modelling parameters. It showed how measured temperatures are severely influenced even by small deviations in the position of the thermocouples. It also indicated the need for input data to improve the analyses. Subsequent thermomechanical simulations evaluated the residual stress field due to the repair welding. In short, the investigation indicated needs for further

development, but proved that numerical simulations can be a viable part in the verification of welding methods. In particular the ability to compare thermal and residual stress fields between different methods, and to perform sensitivity analyses for various operational parameters provides new possibilities for the further development of repair welding techniques.

The report provides a description of desired attributes of a rail defect repair system. Based on this the discrete defect repair (DDR) method is considered to have the largest potential of the methods investigated. The most important scopes for development of this method are defined.

The report outlines a “streamlined” approval process for repair weld assessment. The evaluation process features a combination of numerical simulations, laboratory testing and validating field tests. If realised, such an approval scheme would significantly decrease cost and time, and enhance the quality for approval of innovative repair weld methods

The report finally discusses challenges and potentials for wider deployment of the investigated methods.

9. References

1. NRSPTRK057 Rail Failure Handbook Issue 4: October 2001.
2. Rail Defects: UIC Code 712: 4th edition, January 2002.
3. Guidelines for Shielded Metal Arc Welding (SMAW): Miller Booklet - 155 095 A July 2005.
4. The Manual Metal Arc Process: TWI Job Knowledge Booklet.
5. Manual Metal Arc (MMA) Welding: The Linde Group Website.
6. Maintenance Arc Welding of Rails, Switches and Crossings: Network Rail Specifications – NR/L2/TRK/0132, Issue 06, 4th December 2010.
7. Godfrey Dave: "Rail Repair using MMA", Welding Lines Issue 2, July 2002.
8. Electric Arc Welding Repair Procedure for Plain Line Repairs: Thermit Welding (GB) Ltd. Issue 1, 08 09 2003.
9. Ian Davison: Rail Welding – The Inside Story Part 2 Arc Welds, Welding Lines, Issue 24, July 2008.
10. Dahl B, Mogard B, Gretoft B, Ulander B: "REPAIRING RAILS IN SITU ON SWEDEN'S RAILWAYS"; WELDING REVIEW INTERNATIONAL; V15, No1, 1996, p19-23.
11. Bengt Dahl, Björn Mogard, Bibi Gretoft and Björn Ulander: "Repair of rails on site by welding"; ESAB Brochure XA00127720 , 1904-2004.
12. ESAB Brochure XA00102920 , 1904-2004.
13. Lincoln Electric Website – Technical support pages.
14. Chapman G: 16th Technical Seminar of IORW reported in Welding Lines Issue 29, February 2009.
15. Thomson D – InLine Welding – private communications.
16. AristoMig 400 – a strong work-horse in rail repair: Svetsaren no. 1-2006; p39-41.
17. Giving rails a new lease of Life: International Rail Journal; June 2015; p50-51.
18. Welding and preparing Equipment for repair works and maintenance for Rails: CTF France.com.
19. David Workman: Edison Welding Institute; Paper presented at AREMA 2011 Conference.
20. Gehrmann R and Keichel J: A simple approach to rail head repairs; Railway Gazette International; August 2011; P 42-43.
21. Recent Developments in track Welding part 1; Welding Lines: Issue 34; December 2011.
22. Banton I: Thermit GB Technical Report Technical Report – TR05-09; 15th June 2009.
23. The introduction of a new process for the aluminothermic weld repair of discrete rail surface defects: Welding Lines Issue 28; 26 February 2009, p4-6.
24. Goldschmidt Thermit Group Brochures.
25. Parker C: Repairing RCF; Rail Engineer; August 2015; P72-77.
26. Frédéric DELCROIX M: Head Wash Repair Welds Performing with Network Rail at RAILTECH; 14th Oct 2009.

27. Gutscher D; Effects of heavy axle loads on head repair welds at FAST; Railway Track & Structures; July 2009; p19-21.
28. Gutscher D & LoPresti J; Testing of innovative rail welds and methods under heavy axle loads; AREMA 2012.
29. Jerath V and Jaiswal S: A method of repairing or cladding a steel bloom rail or other part of a railway: EP1878528-A2.

References Chapter 4.

1. Steenbergen, M.J.M.M. and R.W. van Bezooijen, *12 - Rail welds*, in *Wheel–Rail Interface Handbook*. 2009, Woodhead Publishing. p. 377-408.
2. Mutton, P.J. and E.F. Alvarez, *Failure modes in aluminothermic rail welds under high axle load conditions.* Engineering Failure Analysis, 2004. **11**(2): p. 151-166.
3. Grassie, S.L., *Rail corrugation: Characteristics, causes, and treatments.* Proceedings of the Institution of Mechanical Engineers, Part F: Journal of Rail and Rapid Transit, 2009. **223**(6): p. 581-596.
4. Li, Z., et al., *An investigation into the causes of squats—Correlation analysis and numerical modeling.* Wear, 2008. **265**(9-10): p. 1349-1355.
5. Steenbergen, M.J.M.M. and C. Esveld, *Relation between the geometry of rail welds and the dynamic wheel-rail response: Numerical simulations for measured welds.* Proceedings of the Institution of Mechanical Engineers, Part F: Journal of Rail and Rapid Transit, 2006. **220**(4): p. 409-423.
6. Steenbergen, M.J.M.M., *Quantification of dynamic wheel–rail contact forces at short rail irregularities and application to measured rail welds.* Journal of Sound and Vibration, 2008. **312**(4): p. 606-629.
7. Jenkins, H.H., et al., *The effect of track and vehicle parameters on wheel/rail vertical dynamic forces.* Railway Engineering Journal, 1974. **3**(1).
8. European Committee For Standardization, *EN 14730-2 Railway applications - Track - Aluminothermic welding of rails - Part 2: Qualification of aluminothermic welders, approval of contractors and acceptance of weld*. 2006: Brussels.
9. European Committee For Standardization, *EN 14587-1 Railway applications - Infrastructure - Flash butt welding of rails - Part 1: New R220, R260, R260Mn, R320Cr, R350HT, R370LHT and R400HT grade rails in a fixed plant*. 2016: Brussels.
10. European Committee For Standardization, *EN 15594 Railway applications - Track - Restoration of rails by electric arc welding*. 2009: Brussels.
11. Australian Rail Track Corporation, *ETM-01-01 Rail Weld Geometry Standard* 2009.
12. Australian Rail Track Corporation, *ETI-01-04 P1 gauges* 2008.

13. Steenbergen, M.J.M.M. and C. Esveld, *Rail weld geometry and assessment concepts.* Proceedings of the Institution of Mechanical Engineers, Part F: Journal of Rail and Rapid Transit, 2006. **220**(3): p. 257-271.
14. ProRail, *Directives RLN00127 - 1 & 2*. 2007: Utrech.
15. RAILPROF, *User manual*. 2010.
16. Grossoni, I., Shackleton, P., Bezin, Y., *Longitudinal rail weld geometry control and assessment criteria.* Failure Engineering Analysis, 2017. **80**: p. 352-367.
17. WRIST, *Deliverable D1.4: Parametric studies to inform the optimum and pragnatic weld profile*. 2016.
18. MiniProf, *User manual*. 2009.
19. Grossoni, I., Shackleton, P., Bezin, Y., *RAIL WELD GEOMETRY: THE INFLUENCE ON VEHICLE/TRACK DYNAMICS AND ASSESSMENT CRITERIA*, in *25th International Symposium on Dynamics of Vehicles on Roads and Tracks*. 2017: Rockhampton, Australia.
20. Shen, Z.Y., J.K. Hedrick, and J.A. Elkins, *A comparison of alternative creep force models for rail vehicle dynamic analysis.* Vehicle System Dynamics, 1983. **12**(1-3): p. 79-83.
21. Yang, J., Thompson, D.J., Takano, Y., *Characterizing Wheel Flat Impact Noise with an Efficient Time Domain Model*, in *Noise and Vibration Mitigation for Rail Transportation Systems*, N.e. al., Editor. 2015, Springer-Verlag: Berlin.
22. Jendel, T., *Prediction of wheel profile wear—comparisons with field measurements.* Wear, 2002. **253**(1): p. 89-99.
23. Pavlina, E.J., Van Tyne, C.J. , *Correlation of Yield Strength and Tensile Strength with Hardness for Steels.* Journal of Materials Engineering and Performance, 2008. **17**(6): p. 888–893.
24. Hills, D.A., Nowell, D., Sackfield, A. , *Mechanics of Elastic Contacts*. 1993: Elsevier Ltd.
25. Johnson, K.L., *Plastic Deformation in Rolling Contact*, in *Rolling contact phenomena*, B. Jacobson, Kalker, J. J., Editor. 2000, Springer - Verlag: Wien.
26. Fretwell-Smith, S., Zhu, Ch., *Investigation of repair methods and welding techniques, Evaluation of Welding Feasibility of Head Repair Welds*. 2017, British Steel.
27. Hernandez, F.C.R., Demas, N.G., Davis, D.D., Polycarpou, A.A., Maal, L., *Mechanical properties and wear performance of premium rail steels.* Wear, 2007. **263**: p. 766–772.

References Chapter 5

1. CTF Sauron Company Brochure from Website
2. INNOTRACK Deliverable D1.2.5, Track segmentation, 22 pp (and 3 annexes 1+2+9 pp), 2009

References Chapter 7

1. Craig Bishop, VAE Railway Systems - Turnout Manufacture in Australia; Published on Apr 10, 2014
2. Skyttebol, A. Continuous Welded Railway Rails: Residual Stress Analyses, Fatigue Assessments and Experiments. PhD-thesis, Chalmers University of Technology, Gothenburg, 2004.

10. Appendix 1: Evaluation of welding feasibility of head repair welds

Fretwell-Smith, Sandra and Zhu, Chen, Evaluation of welding feasibility of head repair welds, Bitish steel report no BritishSteelRD_12, 49 pp, 2017.

11. Appendix 2: Numerical simulations of the Discrete Defect Repair method

Maglio, Michele Maria, Finite element analysis of thermal fields during repair welding of discrete rail defects, MSc-thesis, Chalmers University of Technology, Report 2017:17, 49 pp (and one appendix 4 pp), 2017. ISSN 1652-8557. http://publications.lib.chalmers.se/records/fulltext/250360/250360.pdf

BUILDING STRONGER FUTURES

EVALUATION OF WELDING FEASIBILITY OF HEAD REPAIR WELDS

Document Number:	BritishSteelRD_12
Revision Number:	V2
Status:	Final
Date:	

Authorisation Sheet

Client:	In2Rail, Innovative Intelligent Rail, Grant Agreement No 635900
Project title:	Investigation of repair methods and welding techniques, Evaluation of Welding Feasibility of Head Repair Welds

Prepared by

Name	Position
Sandra Fretwell-Smith	Lead Rail Researcher
Chen Zhu	Rail Researcher

Date: 27 January 2017

Checked by

Name	Position
Rob Lambert	Rail Technologies Manager

Date: February 2017

Authorised by

Name	Position
Rob Lambert	Rail Technologies Manager

Date: February 2017

Document history

Version No.	Date Approved	Description	Prepared by	Reviewed by	Approved by
V2					

Circulation

Customer name	Organisation
Carlos Hermosilla	Acciona
Jay Jaiswal	ARR Rail Solutions
Frédéric Fau	British Steel France
Anders Ekberg	Chalmers
Elena Kabo	Chalmers
Bob Cox	Network Rail
Charles Voivret	SNCF
Stefan Kallander	Trafikverket
Yann Bezin	University of Huddersfield

Confidentiality, Copyright & Reproduction:

Contents

1 Introduction

Work package 3.1 of the In2Rail EU funded project, 'Investigation of repair methods and welding techniques', included a demonstration and evaluation of the discrete defect repair (DDR) process under controlled conditions. Activity 5.2 of WP 3.1 necessitated the metallurgical evaluation of the trial weld produced during the demonstration in terms of internal soundness, microstructure and hardness. The full details of the trial were reported separately (1) so only those factors which could potentially influence the integrity of the weld will be discussed in detail in the current report. This report covers activity 5.2 and presents the results of the metallurgical evaluation of the DDR trial weld produced on the 14th June at Network Rail Training Centre in York (UK) and similar evaluations of head repair samples from Thermit Welding GB Ltd and Railtech. Results from 4-point bending fatigue tests of the DDR trial weld and a head repair weld from Thermit Welding (GB) Ltd. are also presented and discussed.

2 Summary of Welds Assessed

Three test welds were made during the trial at York in June 2016 via fully automated flux cored welding using the DDR (discrete defect repair) method patented by Corus in 2007 and the bespoke equipment developed by AAR Rail Solutions Ltd. All three welds were made using the flux cored welding wire ESAB Tubrodur 35 OM, 1.6mm diameter (previously branded Tubrod 15.43). The ESAB consumable was selected as it is approved for use by the major European railways and has been used previously for the repair of defects on plain high carbon rail steels. However, alternative consumables may need to be identified for the repair of defects in premium grade rail steels. The composition range for ESAB Tubrodur 35 OM welding consumable is given in Table 1 below.

Element, wt%								
C	**Si**	**Mn**	**P**	**S**	**Cr**	**Ni**	**Mo**	**Al**
0.12-0.50	0.50 Max	0.9-1.30	0.04 Max	0.04 Max	0.75-1.25	2.0-2.5	0.4-0.6	1.2-2.0

Table 1. Chemical Composition Range of ESAB Tubrodur 35 OM Welding Wire

Following milling of the 10mm x 100mm cavity pre-heating was applied using an oxy-propane pre-heating torch to an aim temperature of 60-80°C. Once the temperature was within this range welding commenced, with each layer of weld metal being deposited in a weave pattern across the full width of the rail head until the full 100mm length of the cavity had been filled (4 layers).

Operational problems were experienced during the production of welds 1 and 2, details of which have been covered in the independent audit report (1), with potential implications to the integrity of the weld and are thus outlined below to aid understanding of the resultant microstructures discussed later in this report:

Weld 1 The second layer was interrupted after approximately 35% of the layer had been deposited due to cessation of the torch movement, which resulted in a prolonged arc and subsequent creation of a large crater on the gauge corner. Welding was stopped but it was agreed that the weld should be examined to assess the microstructure beneath a single layer of weld deposit.

Weld 2 After approximately 70% of the layer had been deposited, the wire feed ceased at the weave reversal point, and the arc extinguished. The problem was identified as a build-up of spatter around the nozzle. The welding head was returned to the start position, and the nozzle cleared of spatter. The weld deposit was de-scaled, rail temperatures checked, and the next layer (layer 3) completed without incident. A fourth layer was deposited successfully (leaving a 3-layer deposit at the last 30% of the repair). Despite, the discontinuity caused by the failure to weld the whole cavity during the second layer, the overall resulting repair was considered acceptable and weld 2 was subsequently subjected to the planned 4-point bend fatigue testing.

Weld 3 The DDR procedure normally includes deposition of four layers. However, visual inspection indicated that the cavity had been filled after the third layer had been deposited, and to avoid the possibility of any further operational issues during welding of a subsequent layer the process was terminated after deposition of the third layer.

In order to assess the DDR trial weld against approved and well established industry head repair methods, head repair (HR) welds and a head wash repair (HWR) were received from Thermit Welding (GB) Ltd (one weld for metallurgical analysis, one for 4-point bending fatigue) and Railtech (one weld for metallurgical analysis) respectively.

In addition 3 welds supplied by SNCF made using a Sauron semi-automatic electric arc welding machine and flux cored welding wire were metallurgically assessed. The Sauron welds were made using SAF-FRO Steelcored 54 flux cored 1.6mm Ø welding wire, with an anticipated weld metal hardness of between 364-412HV; this is a broadly similar hardness range, albeit narrower, compared to that of the ESAB Tubrodur 35 OM welding consumable used in the making of the DDR trial welds, which is reported by the manufacturer to have an as-deposited hardness of between 300-400HV. However, the chemical composition of the two consumables are very different. The chemical analysis of the welding consumable using in the making of the three Sauron welds is given in Table 2 below.

Element, wt%				
C	**Si**	**Mn**	**Cr**	**Mo**
0.07	0.3	1.6	6.0	0.9

Table 2. Chemical Composition of Steelcored 54 SAF-FRO Consumable

A summary of the DDR trial outcome and the additional welds discussed in this report is presented in Table 3.

Weld No.	Weld Type	Tests Undertaken	Pre-heat Temp, °C		No. of Layers	Comments
			Strike-on	Strike-off		
1	DDR	Metallurgical/hardness examination	90	70	1 full layer Half layer	1st layer deposited successfully. Weld aborted after deposition of ~35% of 2nd layer due to cessation of torch movement, resulting in a prolonged arc which caused a large crater on the gauge corner. ***Sample used for examination of root bead and HAZ microstructure beneath a single layer.***
2	DDR	4-point bending fatigue	125	90	4 layers	1st layer deposited successfully. Wire feed ceased at the weave reversal point after deposition of ~70% of the 2nd layer due to build-up of spatter around the nozzle. After rectification of the issue the 3rd and 4th layers were deposited without incident. Despite failure to complete all of the 2nd layer, the overall resulting repair was considered acceptable and it was agreed that DDR 2 would be subjected to the planned fatigue testing. ***Sample subjected to 4-point bending fatigue test.***
3	DDR	Metallurgical/hardness examination	120	100		Three layers successfully deposited. Normal practice is to deposit a 4th layer but visual inspection indicated that the cavity had been filled, so the process was concluded. ***Sample subjected to detailed metallurgical analysis and hardness testing.***
4	HR Thermit Welding (GB) Ltd	Metallurgical/hardness examination				
5	HR Thermit Welding (GB) Ltd	4-point bending fatigue				
6	HWR Railtech	Metallurgical/hardness examination				

7 17TR10	Sauron, Automate TranslamaticTAC 2000 France: No.01/00/117/00 Control box No. 0001 0013 Weld No.1	Metallurgical/hardness examination	350	350	Single layer	Single layer in excavated cavity. V: 25/26 A: 175/180 Welding speed: 30 cm/min Heat input: 0.875-0.936 kJ/mm
8 17TR11	Sauron, Automate Translamatic TAC 2000 France: No.01/00/117/00 Control box No. 0001 0013 Weld No.3	Metallurgical/hardness examination	350	350	Single layer	Single layer in excavated cavity. V: 28 A: 170 Welding speed: 30 cm/min Heat input: 0.952 kJ/mm
9 17TR12	Sauron, Automate Translamatic 350 CTF France:No.11120452 Control box No. 12090534 Weld No.5	Metallurgical/hardness examination	350	350	Single layer	Single layer in excavated cavity. V: 24.6 A: 186 Welding speed 30 cm/min Heat input: 0.915 kJ/mm

Table 3. Details of Welds Examined

The DDR machine is shown in Figure 1a, while Figure 1b and 1c show the excavation of the cavity and a fully deposited weld layer respectively.

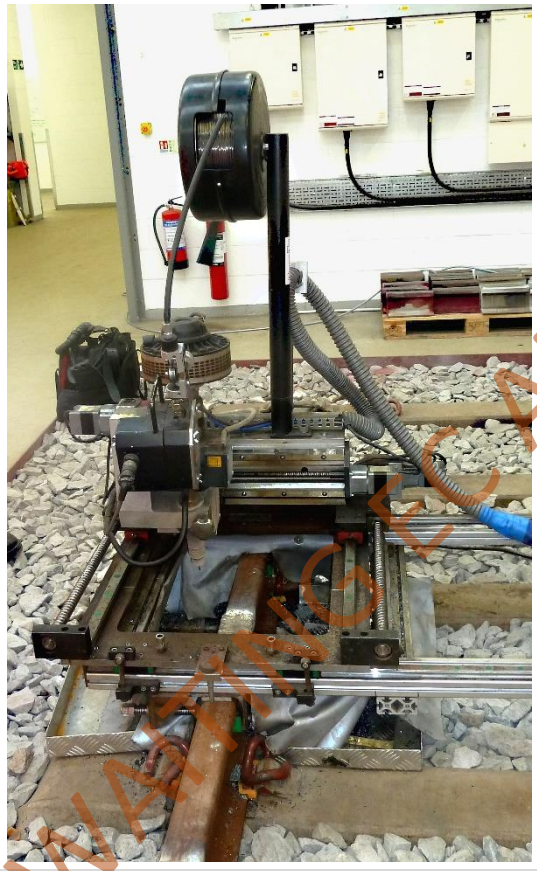

a. DDR Machine

b. Milling of Cavity

c. Deposited Weld Layer

Figure 1. Welding Trial in Progress

Figure 2a-2f shows the weld repair techniques after completion. Both the Railtech (Figure 2b) and Thermit Welding (GB) (Figure 2c) welds had been ground to profile so only the weld metal and the heat affected zone (HAZ) down the side of the head and into the web could be seen. The white paint on the Thermit Welding (GB) weld in Figure 2c is the residue from magnetic particle inspection carried out by Thermit Welding (GB) on completion of the weld. The depth of the weld metal, and presumably therefore that of the excavation, is substantially greater in the Railtech weld, extending beyond the lower fishing radius and into the top of the web. The resultant HAZ is as a consequence much deeper in the Railtech weld compared to the Thermit Welding (GB) weld. It is important to note that the Goldschmidt Thermit Group, of which Thermit Welding (GB) is a member, have two head repair welding procedures, the HR procedure used by Thermit Welding (GB) Ltd, which partially excavates the rail head, and the HRW process, which excavates the full rail head. For the current work package only, a HR weld from Thermit Welding (GB) Ltd. was available for examination.

The Sauron welds were carried out over a much longer length compared to the DDR and aluminothermic processes, the welded length being 300mm for each of the three welds (Figure 2d-2f).

a. DDR Weld

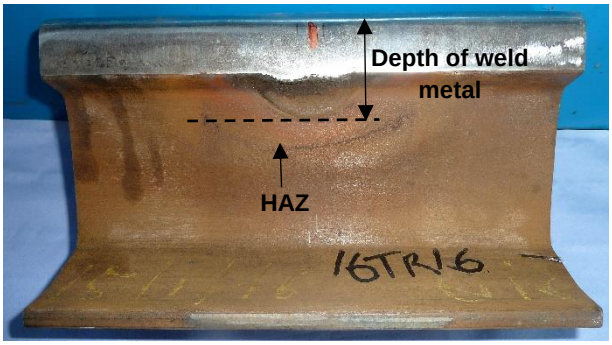

b. Railtech Head Wash Repair (HWR)

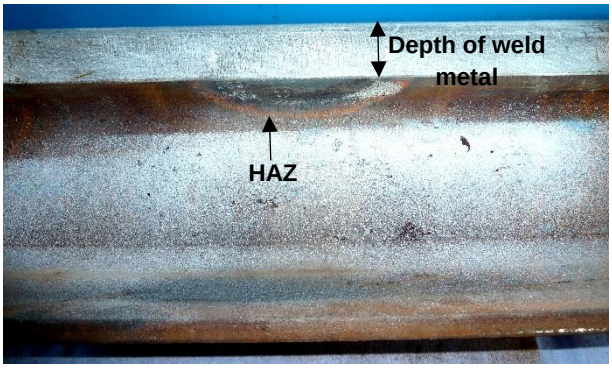

c. Thermit Welding (GB) Head Repair (HR)

d. Sauron, Automate TranslamaticTAC 2000 France: No.01/00/117/00, 25/26V, 175/180A

e. Sauron, Automate Translamatic TAC 2000 France: No.01/00/117/00, 28V, 170A

f. Sauron, Automate Translamatic 350 CTF France: No.11120452, 24.6V, 186A

Figure 2. Completed Welds

3 Metallurgical Examination

3.1 Macro Examination

Longitudinal-vertical sections were prepared from the DDR weld, aluminothermic head repairs and Sauron welds, including that from DDR weld 1 where the welding stalled halfway through deposition of the second layer. The locations of the samples taken from the DDR and Sauron welds are shown schematically in Figure 3, and were taken in a manner similar to that specified in the European standard EN 15594:2009 (2).

In addition, a transverse section was taken from the DDR and Sauron welds for subsequent hardness evaluation in line with the above standard. N.B. transverse samples were not taken from the aluminothermic head repairs as it wold not be appropriate to assess them against the same standard due to the significantly different weld and HAZ profile

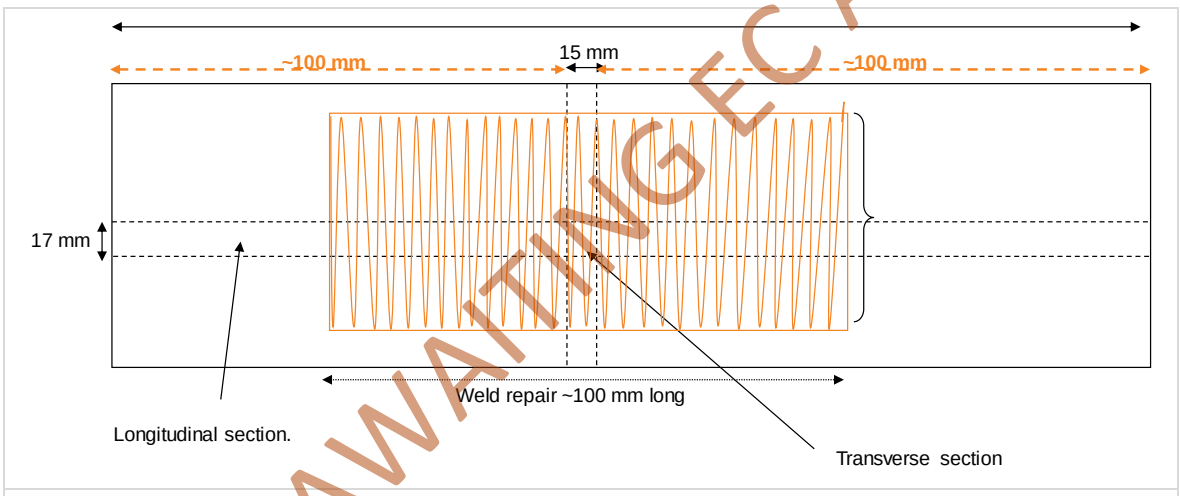

Figure 3. Schematic Diagram of Samples for Metallography

The samples were polished to a 1-micron finish and etched in 2% nital for examination under the optical microscope. Figure 4 shows the macrographs of the longitudinal-vertical sections from each weld. *N.B. the macrographs are not to scale so the lengths of the weld deposits have been highlighted to demonstrate the varying lengths of the deposits.* Due to the long length of the Sauron welds (300mm) it was not possible to take a longitudinal section through the full length of the weld. 100mm lengths were taken from the strike-on and strike-off of the welds, which included at least 20mm of parent rail at the respective ends of the welds.

The weld metal depth of the Sauron welds was very shallow as a result of only a single layer having been deposited (Figure 4e-4g).

The aluminothermic head repair techniques utilise a much deeper excavation than the 10mm deep cavity of the DDR process, although the DDR process does have options to excavate deeper cavities if required. This can be clearly seen in the macrographs (Figure 4), with the Railtech weld metal extending below the upper fishing radius in to the top of the rail web. The aluminothermic weld repairs both exhibit a wide HAZ, this being a product of the very high

temperatures and the volume of weld metal deposited in these two processes compared to the shallower and lower temperatures experienced during deposition of the DDR weld.

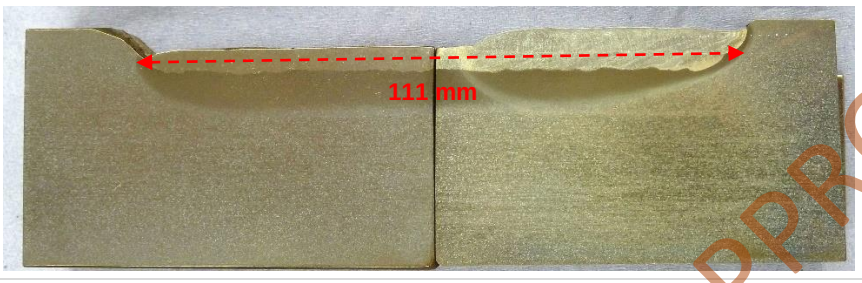

a. DDR, 1-layer weld - Weld 1

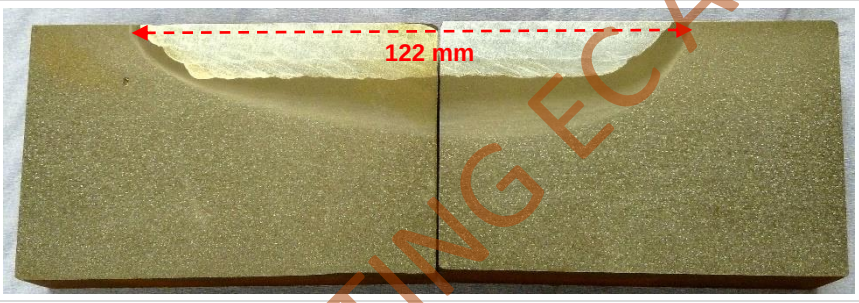

b. DDR, 3-layer weld – Weld 3

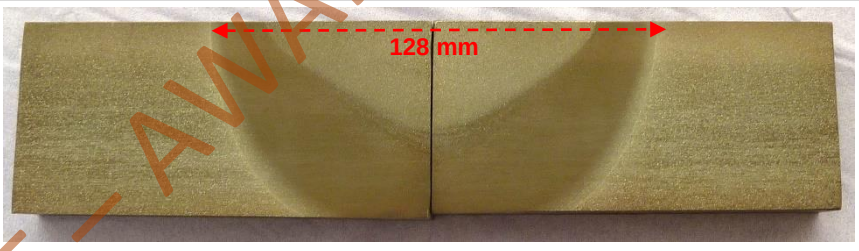

c. Thermit Welding (GB) Head Repair

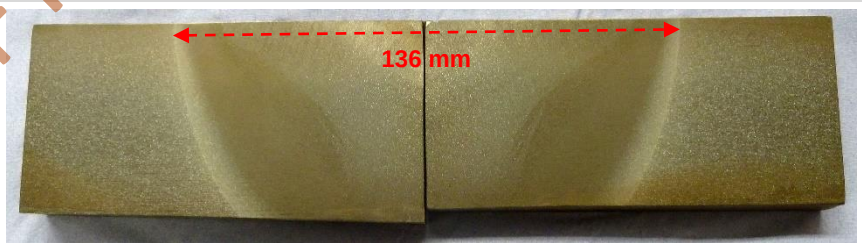

d. Railtech Head Repair

e. **Sauron, Automate TranslamaticTAC 2000 France: No.01/00/117/00, 25/26V, 175/180A**

f. **Sauron, Automate Translamatic TAC 2000 France: No.01/00/117/00, 28V, 170A**

g. **Sauron, Automate Translamatic 350 CTF France: No.11120452, 24.6V, 186A**

Figure 4. Macrographs of Longitudinal-Vertical Sections Through the Head Repair Samples

Surface hardness measurements taken on the completed welds after profile grinding are shown in Table 4. The DDR and Railtech welds were within the hardness range hardness stated in EN 15594:2009 of 290-340HB.

The Sauron welds, where only a single layer was deposited, had hardness levels in the range 320-377HB. For a single layer EN 15594:2009 specifies a maximum surface hardness of 380HB and all three Sauron welds fell within this range. However, the first Sauron weld 17TR10 was significantly harder than the remaining two welds or the DDR and aluminothermic repair welds.

It should be noted however, that aluminothermic weld head repairs are not assessed against the above standard and both were measured using portable hardness equipment, which generally produce greater variation in measured hardness values.

Weld Type	Max Surface Hardness, HB
DDR	337
Thermit Welding (GB)	286*
Railtech	316*
17TR10 Sauron, Automate TranslamaticTAC 2000 France: No.01/00/117/00, 25/26V, 175/180A	377
17TR11 Sauron, Automate Translamatic TAC 2000 France: No.01/00/117/00, 28V, 170A	320
17TR12 Sauron, Automate Translamatic 350 CTF France: No.11120452, 24.6V, 186A	325
* *Measured using calibrated Equotip portable hardness testing equipment*	

Table 4. Surface Hardness

3.2 Micro Examination Weld 1

It was agreed after weld 1 was aborted that it would be metallurgically assessed to determine the evolution of the microstructure after a single bead and application of a second layer.

Figure 5a shows the location of the micrograph. Figure 5b-e shows the microstructure of the weld metal down the chamfered edges of the excavation beneath the single layer at the strike-off and beneath the second layer at the strike-on. As neither of these layers had a subsequent weld layer deposited above them, it may be expected that the microstructures would be similar. However, the strike-on consisted of a microstructure predominantly of upper and lower bainite with a small proportion of untempered martensite (Figure 5e), whereas that of the strike-off consisted largely of untempered martensite with a small volume fraction of bainite (Figure 5c). Moreover, the microstructure at the weld metal/parent rail interface along the bottom of the excavation with 2-layers deposited consisted of a mixture of untempered martensite and bainite. The martensite beneath the second layer also appears to be untempered suggesting that deposition of the second bead has re-austenitised the underlying bead such that on cooling it has transformed to martensite once again with no tempering having occurred.

Figure 5g shows the typical weld metal microstructure of the two weld layers; the microstructure was comprised entirely of upper bainite.

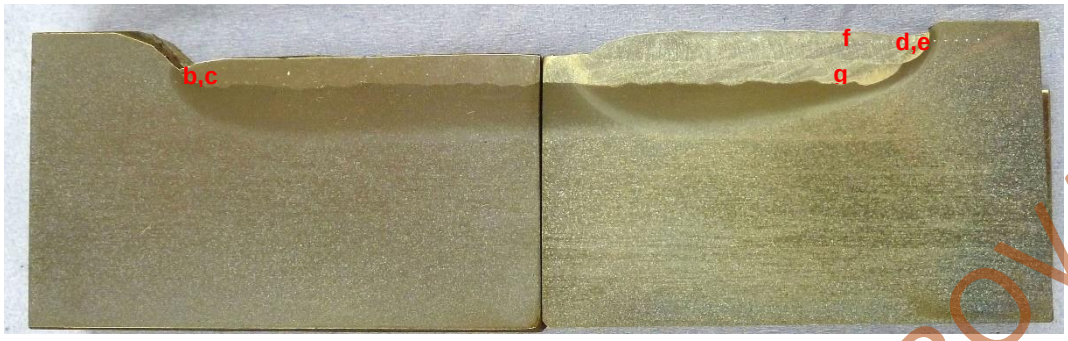

a. Location of Micrographs

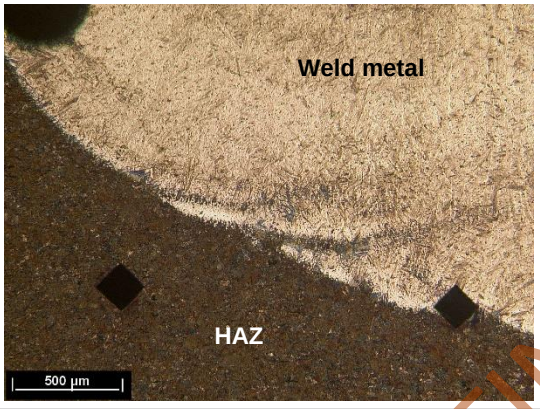

b. Single Layer, Strike-off,

c. Single Layer Interface Strike-off, Higher Magnification

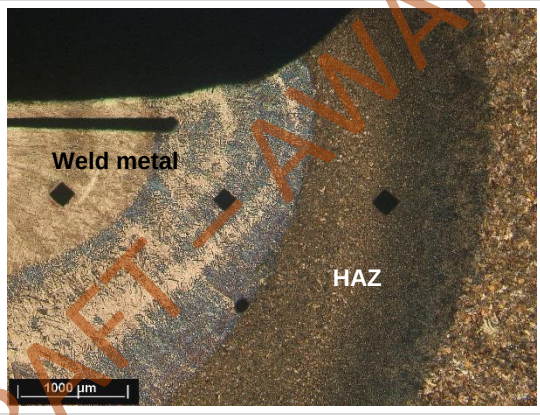

d. 2-layer Strike-on Low Magnification Surface Layer

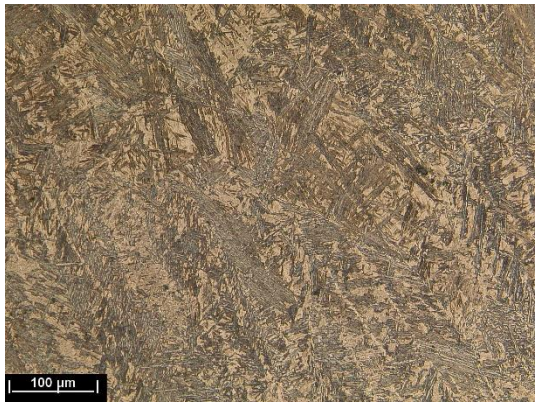

e. 2-layer Strike-on Higher Magnification Surface Layer

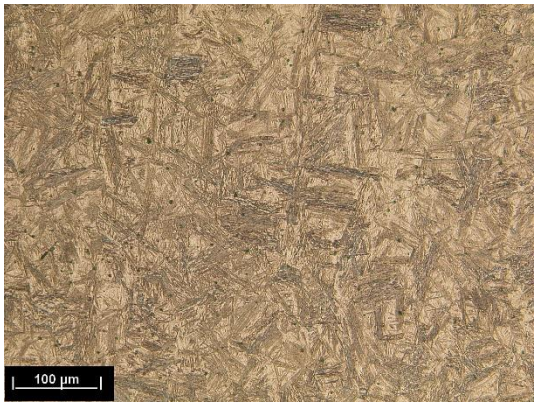

f. 2-layer Strike-on High Magnification Root Layer

g. 2-layer Strike-on Higher Magnification 2nd Bead

Figure 5. Interface of Weld 1 Beneath Single Layer and 2-Layer Deposit

The difference in the volume fraction of martensite at the strike-on and strike-off and the absence of tempering after application of the second layer can be explained by examination of thermal data measured on a previous DDR weld by BS (Tata Steel at the time of undertaking the work).

Longitudinal Vickers hardness traverses (10kg load) were carried out at the locations shown in Figure 7a and 7b, and the resultant hardness plots shown in Figure 7c-e. The hardness of the weld metal at the strike-off single bead was harder than that of the strike-on, at 508HV and 454HV respectively (Figure 7c and 7d); this is likely to be a result of the greater volume fraction of martensite at the strike-off and potentially the strike-on may have benefited from the additional heat from the second layer resulting in tempering of the microstructure. It should be noted that the measured hardness of the weld metal is lower than that which would be expected from untempered martensite for a steel of ~0.5% carbon (taking into account ~50% dilution into the weld metal from the parent rail). However, the microstructure is a mixture of martensite and bainite and the macro Vickers hardness test will evaluate the overall hardness rather than the hardness of individual phases.

The high hardness of the weld metal in the second layer of the 2-layer deposit (Figure 7e) is due to the relatively fast cooling rate of this exposed surface layer. There is much greater heat content underneath in a fully repaired section, which will slow down the cooling rate and potentially result in back tempering of the overlying weld metal. Moreover, the top layer is almost entirely removed during grinding to profile and largely serves as a sacrificial layer thus removing potentially harder weld metal at the surface.

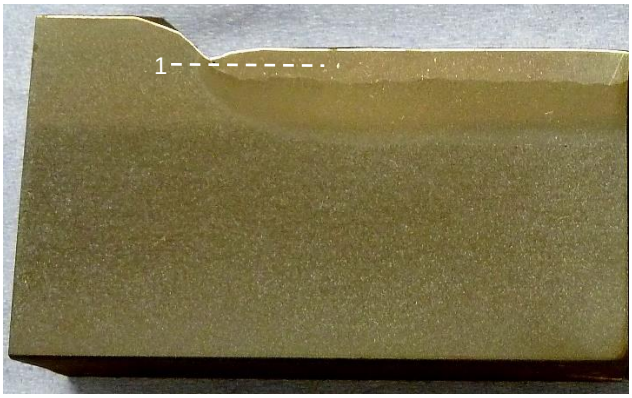

a. Root Bead Weld Metal/HAZ Traverse Strike-off

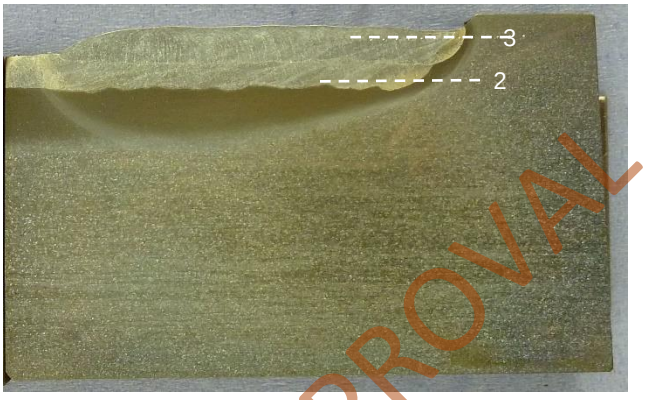

b. Root Bead and 2nd Bead Weld Metal/HAZ Traverse, Strike-on

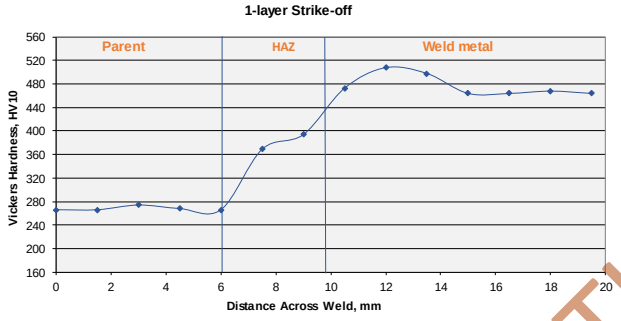

c. Traverse 1, 1-layer Root Bead

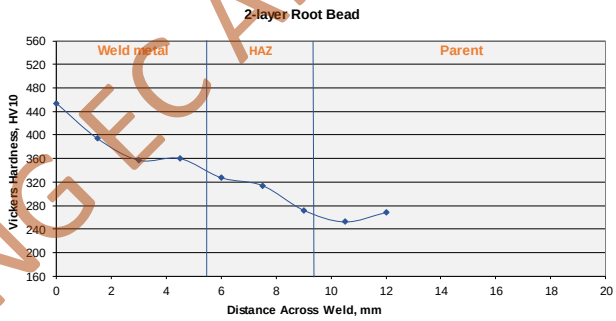

d. Traverse 2, 2-layer Root Bead

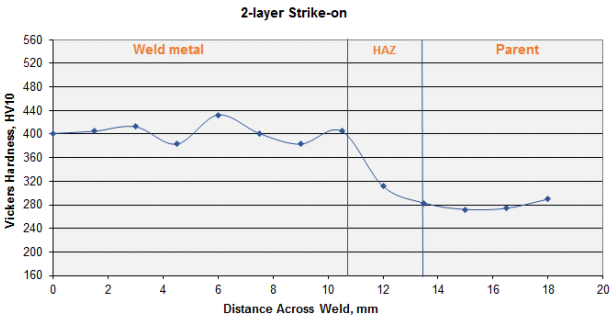

e. Traverse 3, 2-layer 2nd Bead

Figure 6. Longitudinal Vickers Hardness Traverses at Strike-on and Strike-off, Weld 1

3.3 Micro Examination Weld 3

Weld 3 was assessed largely against EN 15594:2009 (2) in terms of hardness, microstructure and the level of porosity. However, a more detailed examination beyond that required in the standard was carried out to understand better the integrity of the DDR weld.

The interface between the weld metal and the parent rail was continuous with no lack of fusion evident. The deposit contained only very small isolated pores visible of <0.1mm in diameter, which was well within the acceptance criteria of EN 15594:2009.

Location of the micrographs is shown in Figure 7a. The microstructure of the weld metal in Weld 3 at the strike-off close to the interface of the weld metal/parent rail down the chamfer and along the root bead consisted of an intermittent layer of martensite mixed with bainite similar to that observed in Weld 1 (Figure 8b and 8d). Again, only a small amount of martensite was observed at the strike-on, with the microstructure being predominantly bainite (Figure 8c and 8e).

a. Location of Micrographs

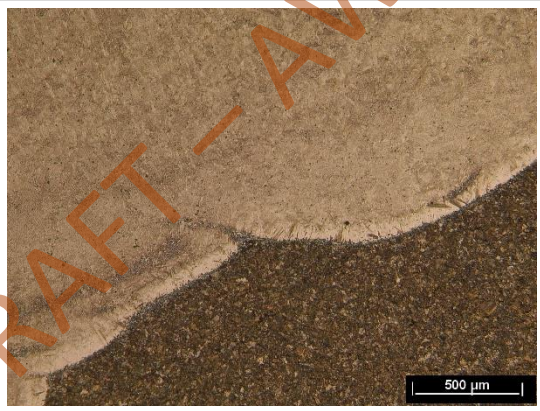

b. Strike-off Down Chamfer

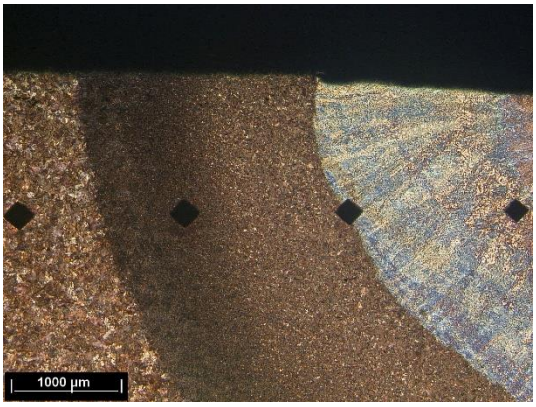

c. Strike-on Down Chamfer

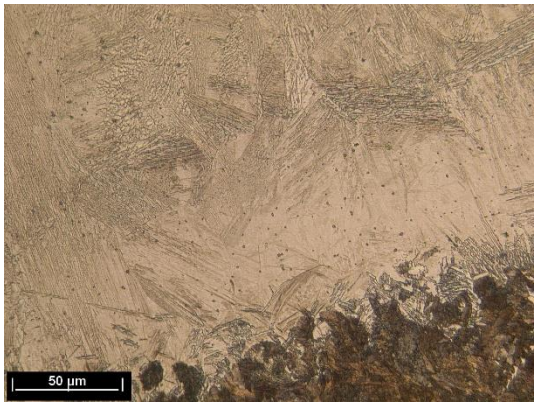

d. Strike-off, Martensite/bainite in Weld Metal at Interface, Higher Magnification

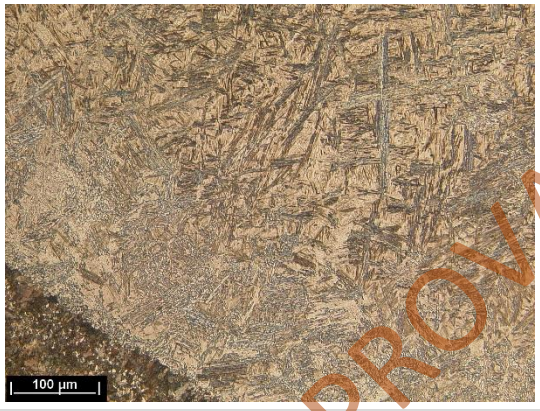

e. Strike-on, Predominantly Bainite With Some Martensite

Figure 7. Weld 3 Microstructure at Weld Metal/Parent Rail Interface

Figure 8a-d show optical and scanning electron (SEM) micrographs of the 3rd-layer and root layer. The uniformity of the upper bainite microstructure in the third layer is evident in Figure 8a and 8b. The electron micrograph in Figure 8d clearly shows the mixed microstructure of the root layer, consisting of lightly tempered martensite and bainite.

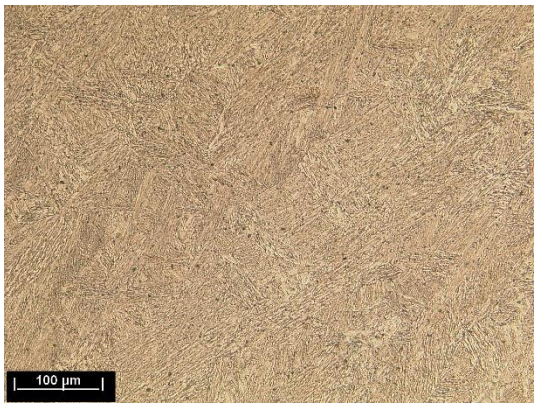

a. 3rd Layer Optical Micrograph

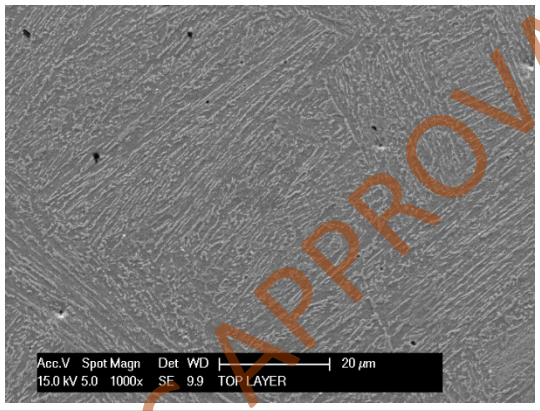

b. 3rd Layer SEM Micrograph

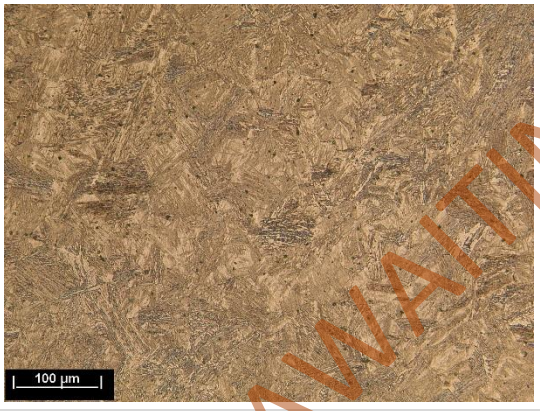

c. Root Layer Optical Micrograph

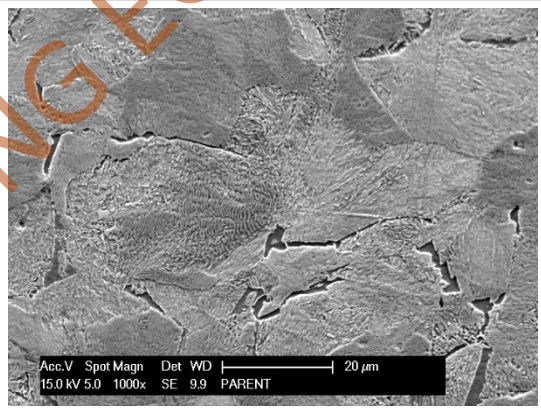

d. Root Layer SEM Micrograph

Figure 8. Optical and SEM Micrographs of Weld Metal Microstructures in DDR Trial Weld 3

In order to assess the hardness of the martensite at the strike-off adjacent to the interface, micro-hardness testing (100g load) was carried out at 5mm intervals in the weld metal from the strike-off to the mid-length of the weld. The hardness is shown superimposed on the weld macro of the strike-off in Figure 10.

The dilution of the root bead is typically around 50% and thus the weld metal adjacent to the interface will be much richer in carbon than the remaining weld beads ~0.5% cf ~0.18%max although will be simultaneously depleted of Cr and Ni. For a carbon level of ~0.5% the hardness of untempered martensite is nominally of the order of ~800 HV. The maximum measured hardness of 627HV suggests, therefore, that some degree of tempering has taken place, but the absence of the fourth layer has resulted in a harder than desirable microstructure at the interface.

As mentioned above, the presence of martensite in the weld metal adjacent to the interface with the parent rail is due to the carbon dilution from the parent rail. Thus, whether or not martensite is formed will depend on the chemistry of

the root bead close to the interface, the maximum temperature experienced and the cooling rate. The latter two parameters will vary with each successive welding pass. Figure 9a shows the thermal profile of a DDR weld carried out previously; locations of the thermocouples are shown in Figure 9b. Although the thermocouples measured the temperatures within the HAZ close to the interface, an assumption can be made that the temperatures within the root layer would be proportionally higher. The maximum temperatures after each pass was achieved at thermocouples TC3 (mid-length of weld) and TC4 (strike-off), although TC4 failed after the first pass. Even after deposition of the fourth layer the temperature at mid-length was above the austenite transformation temperature. Thus, whether or not transformation to martensite occurs at the interface will be dependent on the cooling rate of the weld and the localised composition as a result of the mixing of the weld metal and parent rail at the interface. At the strike-on the austenite transformation temperature was exceeded after the 2nd and 3rd layers, and thus the 4th layer is likely to temper any martensite present within the root bead at this location; it is not surprising, therefore, that only a very small amount of martensite was observed at the strike-on position. It is possible that some back tempering of any martensite generated may occur from the residual heat remaining in the weld after completion of the full weld build-up.

The integrity of the deposit and the microstructure in the root bead weld metal adjacent to the interface have undergone evaluation during the 4-point bending fatigue test regime, the results of which are presented in section 4 of this report.

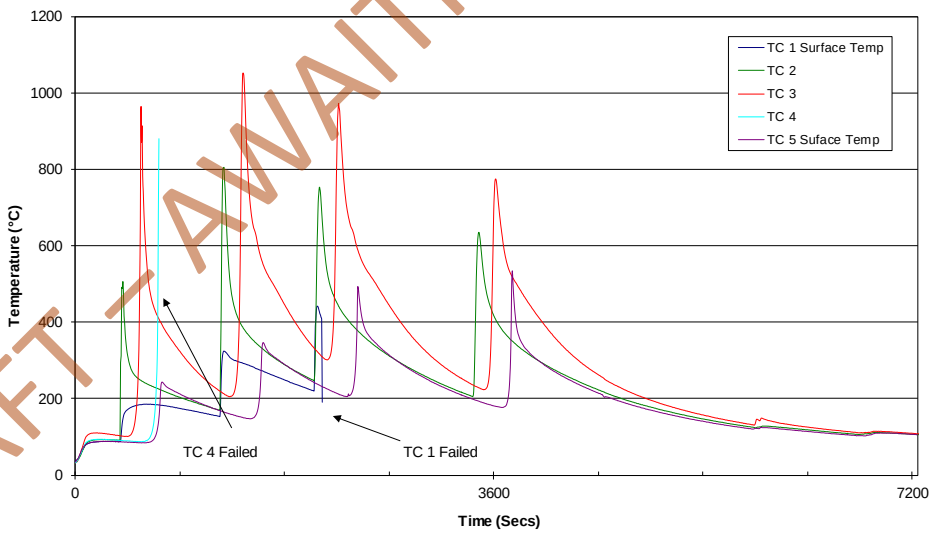

a. Thermal Data From R260 DDR Weld

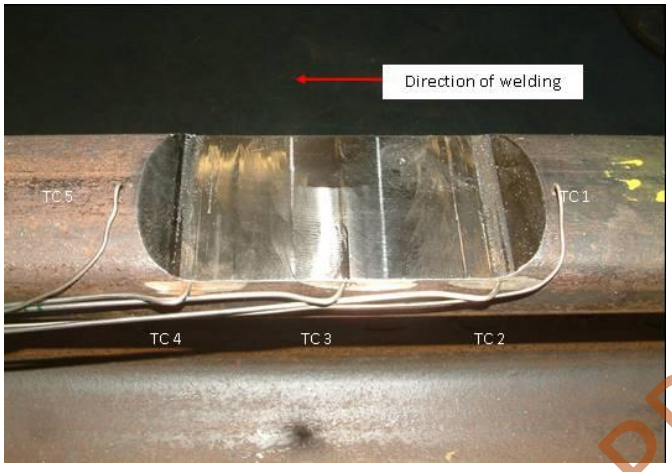

b. Location of Thermocouples

Figure 9. Instrumented R260 DDR Weld

Figure 10. Weld 3, Hardness of Weld Metal Adjacent to Interface

To determine whether the addition of a fourth bead would have reduced the sub-surface hardness (via tempering) a Vickers hardness traverse was carried out on the transverse sample as specified in EN 15594:2009 (10kg load) and compared to that of a weld made previously on the DDR machine using identical welding parameters, preheat and consumable (3). Figure 11a shows the hardness profiles of the 3-layer deposit (Weld 3) and the 4-layer deposit (12TR32) and the locations of the hardness traverses are highlighted by the red dashed lines in Figure 11b and11c. In both welds the maximum sub-surface hardness was within the root bead weld metal close to the interface with the parent rail. Maximum sub-surface hardness values of 394HV and 371HV respectively were recorded for the 3-layer (Weld 3) and 4-layer deposits. Both welds are below the maximum of 400HV stated in EN 15594:2009, however, the

3-layer weld was close to the maximum and some 23HV higher than that of the 4-layer weld, suggesting that some tempering may have occurred in the latter case during deposition of the fourth layer.

Vickers hardness traverses carried out on the longitudinal sample, 1mm below the rail running surface and through the parent rail, HAZ and into the weld metal (Figure 12) also confirmed that the hardness of Weld 3 with a 3-layer deposit was harder than that of the 4-layer deposit adjacent to the interface with the parent rail.

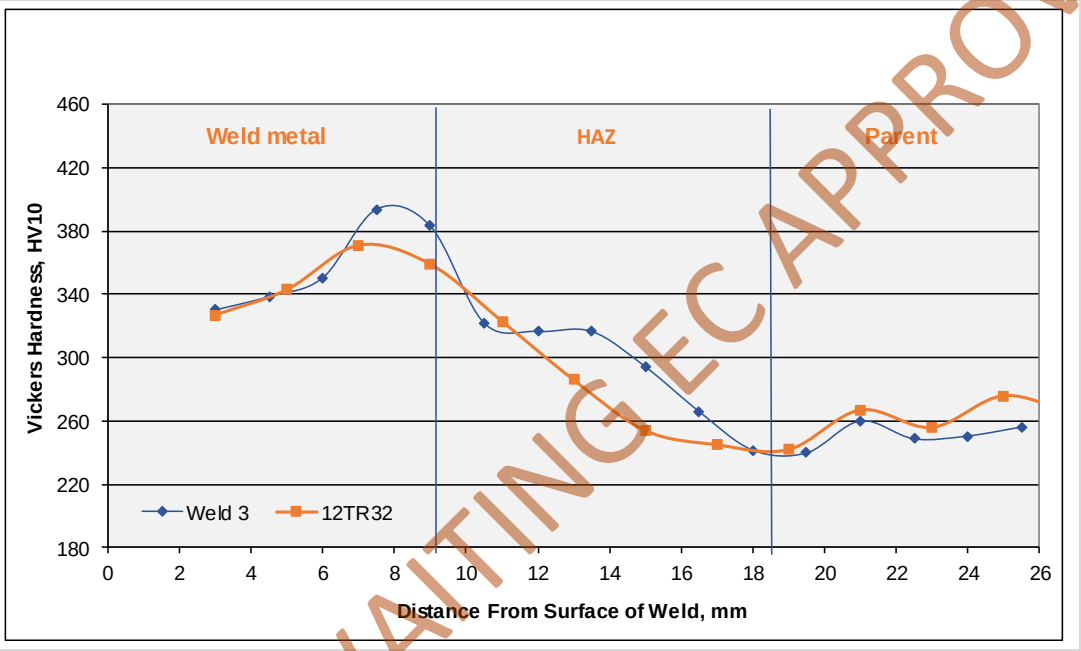

a. Vickers hardness Traverse on Transverse Samples

a. Weld 3, 3-layer Deposit

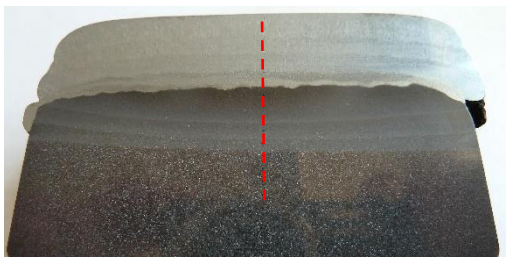

b. 12TR32, 4-layer Deposit

Figure 11. Vickers Hardness Traverses on Transverse Samples of Weld 3 and Earlier DDR Weld 12TR32

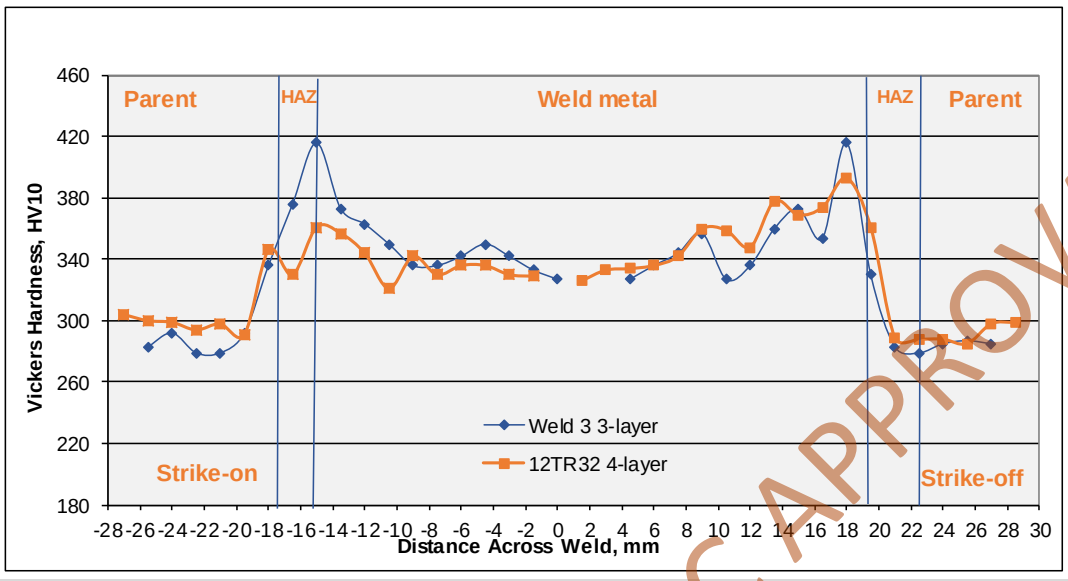

a. Hardness Profile Through Strike-on and Strike-off

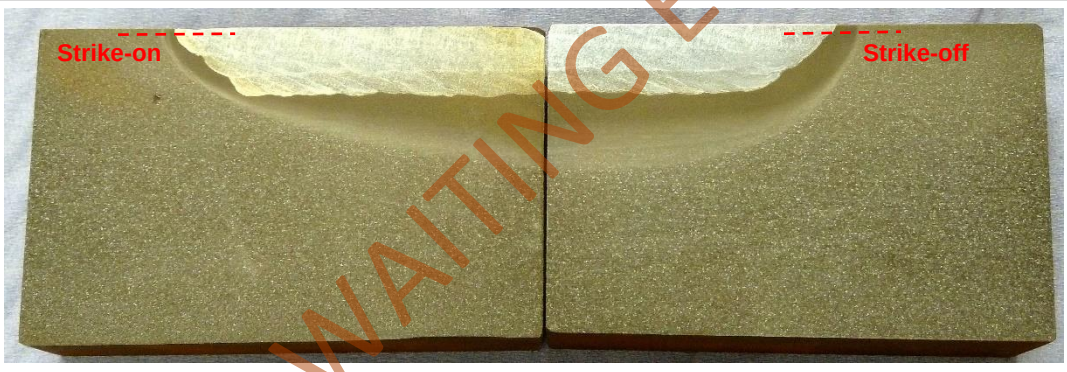

b. Weld 3, Showing Location of Hardness Traverses

Figure 12. Longitudinal Vickers Hardness Traverses at Strike-on and Strike-off

3.3.1 Laser Induced Breakdown Spectroscopy (LIBS)

Laser induced breakdown spectroscopy (LIBS) was carried out through the weld metal and in to the HAZ to determine the extent of elemental dilution in the root layer of the DDR repair. Figure 13 shows the line scan from the surface of the weld to ~0.5mm into the HAZ. It is clear from Figure 13 that any dilution effects only occur within 1mm of the fusion zone. Cr, Ni and Mn remain broadly unchanged through the third, second and a large part of the root bead but begin to decrease at a distance of ~1mm from the weld interface, dropping to ~50% of their nominal values close to the weld/rail interface, decreasing rapidly thereafter to residual levels within the HAZ. In contrast the carbon level within the root bead increases due to dilution from the higher carbon rail (~0.73%), achieving a level of around 0.55-0.6%C in the shallow zone immediately adjacent to the interface, i.e. the region corresponding to the shallow layer of martensite/bainite mix. The element distribution LIBS maps are shown in Figure 14.

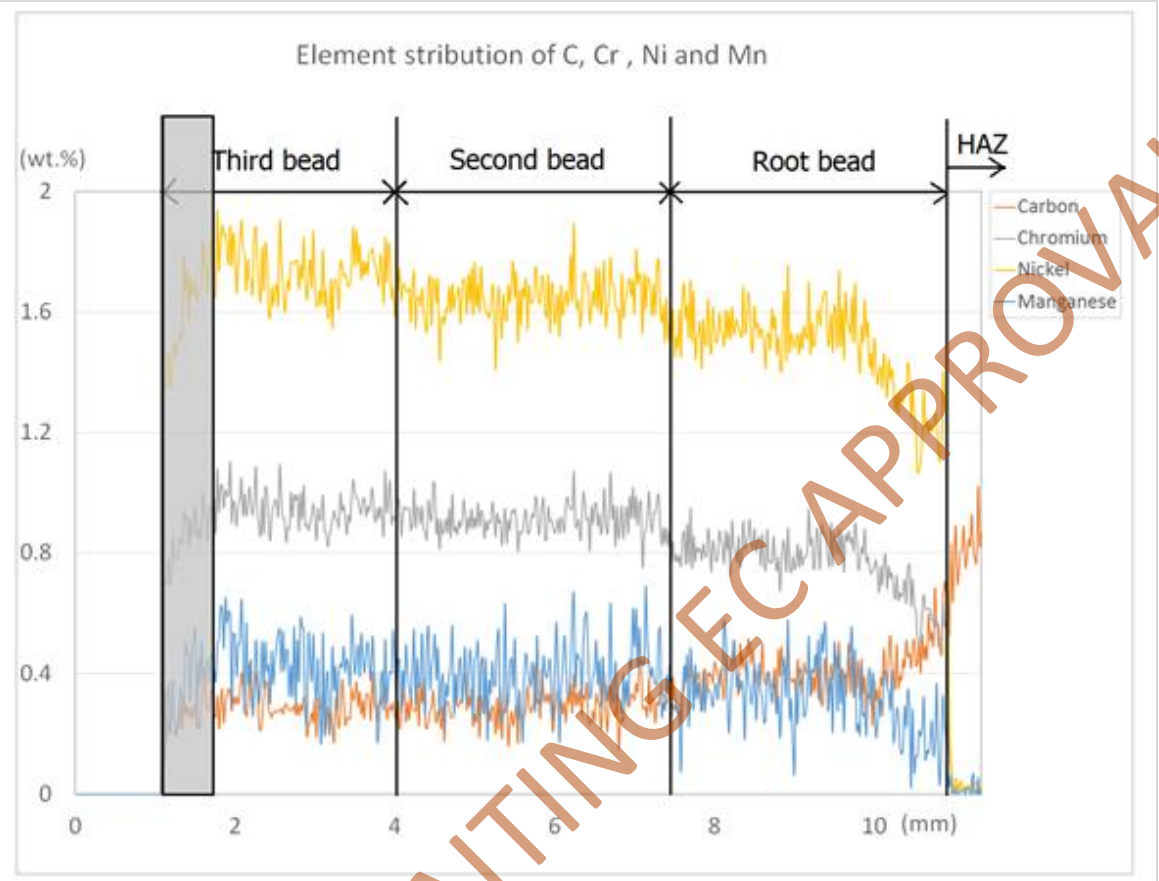

Figure 13. LIBS Results Showing Elemental Distribution in the DDR Trial Weld 3

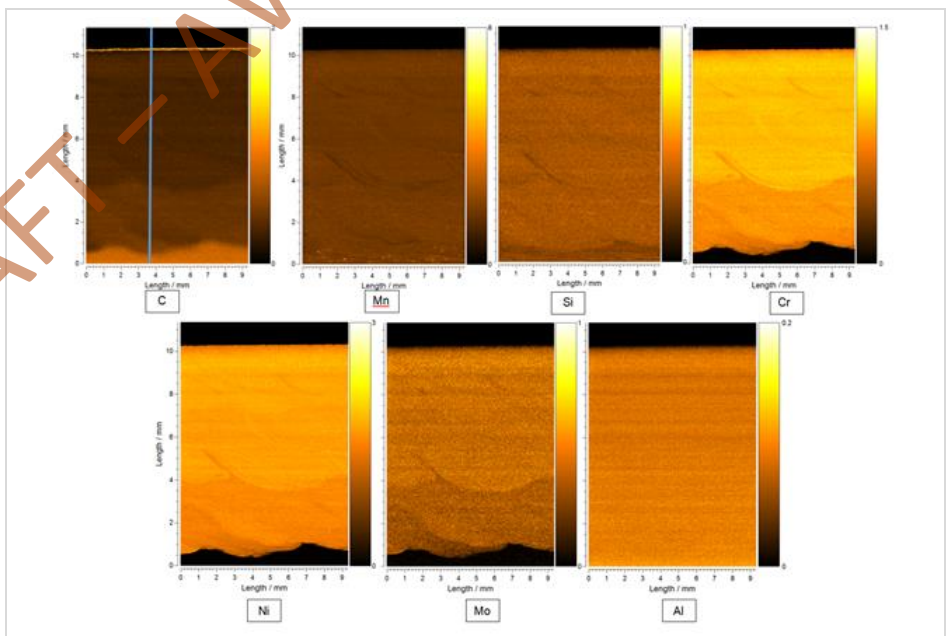

Figure 14. LIBS Maps Through Weld Metal and HAZ in DDR Trial Weld 3

3.4 Micro Examination of Aluminothermic Head Repairs

Micrographs of the aluminothermic head repairs from Thermit Welding (GB) and Railtech are shown in Figure 15a-Figure 15d. No porosity was observed within the weld metal of the Thermit Welding (GB) weld and only one isolated pore of <0.1mm observed within the Railtech weld.

The presence of ferrite around the prior austenite grain boundaries in the Thermit Welding (GB) weld metal Figure 15b suggests that the welding portion used had a lower carbon level than that of the almost fully pearlitic Railtech repair. Both welds had a continuous interface with no evidence of lack of fusion between the weld metal and parent rail. In fact, other than in the head close to the running surface, the interface of the Railtech head repair was difficult to locate under the optical microscope despite being clearly visible on the macro section (Figure 4d).

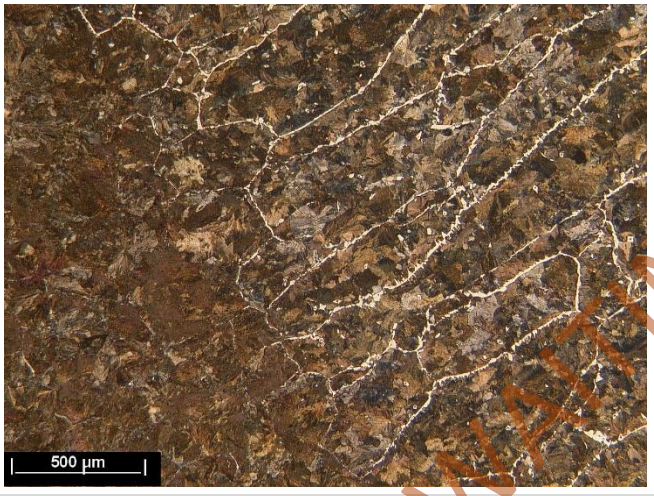

a. Thermit Welding (GB) Interface

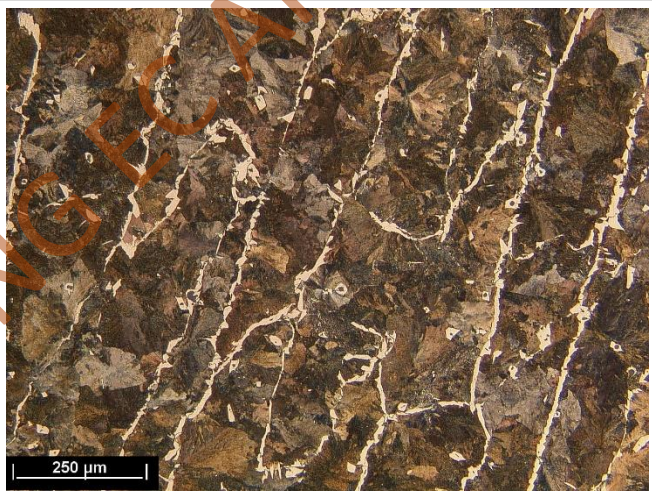

b. Thermit Welding (GB) Weld Metal

c. Railtech Interface in Head

d. Railtech Weld Metal

Figure 15. Micrographs of Aluminothermic Head Repairs

The critical HAZs (those regions closest to the weld metal/rail interface) for the three welds are compared Figure 16a-17d. Under the optical microscope the pearlite nodule size in the HAZ of the DDR weld appeared much finer than that in either of the aluminothermic welds, at least in part a consequence of the presumed significantly faster cooling rate of the DDR weld. This finer microstructure should be beneficial in terms of toughness of the HAZ. The reduced carbon concentration in the HAZ adjacent to the interface, as a result of some carbon diffusion into the root layer weld metal, is evidenced by the ferrite outlining the prior austenite grain boundaries (Figure 16b). A small amount of ferrite was also visible in the HAZ of the Thermit Welding (GB) head repair weld; again, this is likely to be due to dilution at the interface with the lower carbon weld metal.

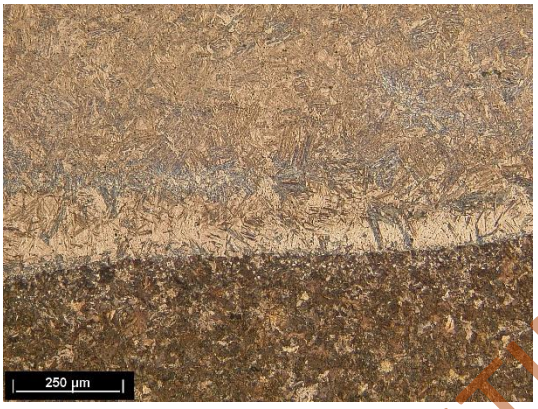

a. DDR HAZ Low Magnification, Weld 3

b. DDR HAZ High Magnification, Weld 3

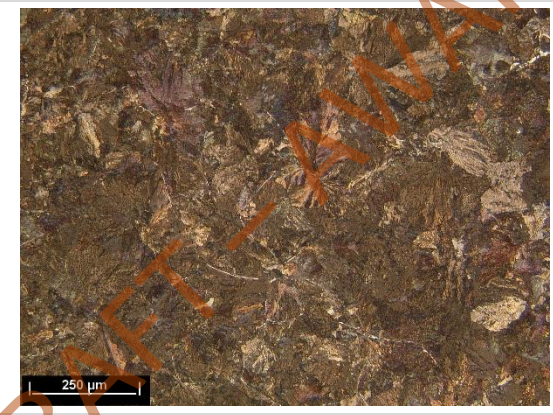

c. Thermit Welding (GB) HAZ

d. Railtech HAZ

Figure 16. Critical HAZ Microstructures in the Three Head Repair Techniques

The longitudinal hardness profiles of the two head repair techniques along with that of the DDR trial weld are shown in Figure 17a-18c (measured at 1mm below the running surface of the rail). The maximum hardness of the HAZ in the DDR weld of 416 HV is higher than the maximum sub-surface hardness permitted in EN 15594:2009 (400 HV). Had a fourth weld layer been deposited, as is normal practice for the DDR procedure, the HAZ at this position may have undergone some tempering thereby reducing the hardness. Moreover, some of the high hardness HAZ would

be removed during profile grinding following application of the fourth layer. As highlighted previously, the mean weld metal hardness of ~345 HV was around 60 hardness points higher than that of the parent rails of typically 285 HV. The choice of the consumables in the DDR process are based on practical experience of the wear resistance of bainitic microstructures that are not as resistant to wear as pearlitic microstructures of rail steels and thus require a higher hardness weld metal to achieve similar wear levels to R260 rail.

HAZ hardness values in the Thermit Welding (GB) head repair (Figure 17b) were typically ~35HV higher than those of the adjacent parent rails. Furthermore, the weld metal exhibited reasonably uniform hardness throughout, with a mean hardness in the central portion of the weld metal of ~260HV being slightly lower than that of the adjacent rails at 270 and 275HV respectively.

The Railtech repair has a higher hardness than the Thermit Welding GB repair and although both graphs show a short distance of higher than parent rail hardness values, a larger proportion of the weld metal region appears to have similar hardness to the parent rail.
In the case of the Railtech head repair, HAZ hardness values were also typically 35 hardness points above those of the adjacent parent rails. Not surprisingly, given the apparently higher C level of the Railtech weld, the mean weld metal hardness of 294 HV was higher than that of the Thermit Welding (GB) weld and slightly harder than that of the rail (Figure 17c). Worth noting, however, is the rather unusual hardness profile across the Railtech weld. In combination with features visible in the macrograph of Figure 4d, this could be, though unlikely, the result of an additional weld nugget of slightly richer chemistry in the centre of the weld. More probable, however, it may suggest localised post weld cooling to have been implemented at the centre of the weld, possibly to increase the hardness at the centre of the repair to reduce the hardness differential across the weld, resulting in a 'mini' sub-critical HAZ at a distance of ~20mm either side of the weld centreline.

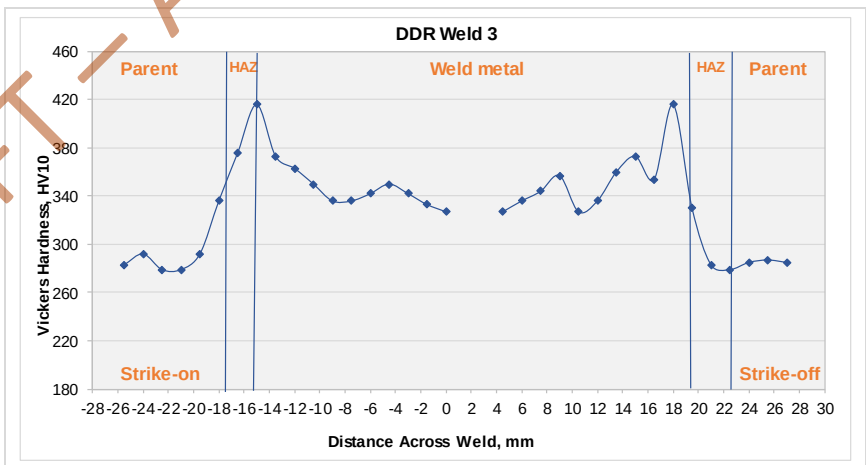

a. DDR Trail Weld 3

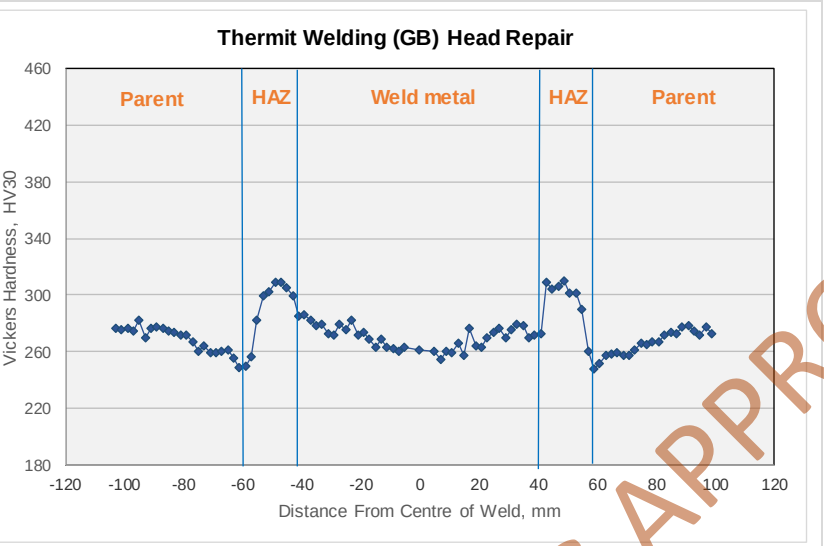

b. Thermit Welding (GB) Head Repair

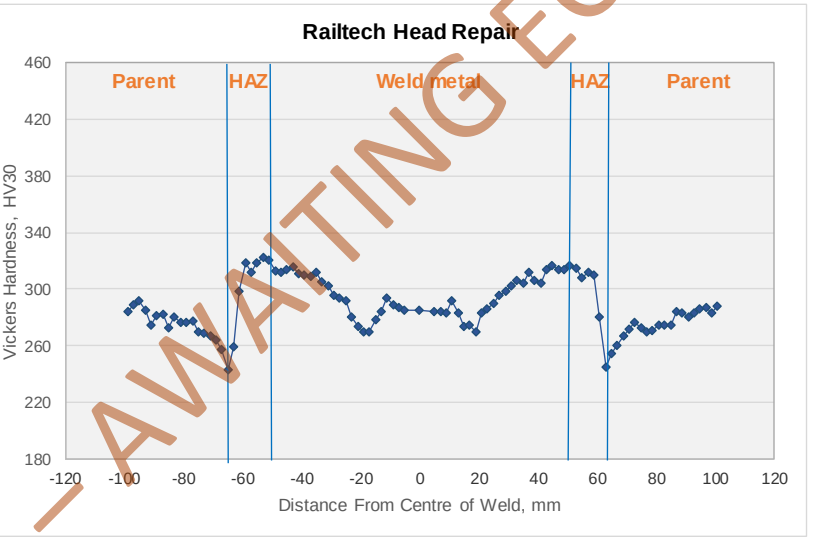

c. Railtech Head Repair

Figure 17. Longitudinal Vickers Hardness Profiles

3.5 Micro Examination of Sauron Automatic Flux Cored Welds

The Sauron welding was carried out using two different machines using different control boxes and some slight variation in welding parameters, although the calculated weld heat inputs were broadly similar (Table 3). Figure 18 shows the Sauron welding machine Translamatic TAC 2000 used in the making of welds 17TR10 (weld No.1) and 17TR11 (weld No. 3).

Figure 18. Translamatic TAC 2000 Welding Machine

In contrast to the weave technique used for weld deposition in the DDR welds the Sauron welds were made using the stringer bead deposition method.

The three Sauron welds were also assessed against EN 15594:2009 (2) in terms of hardness, microstructure and porosity but with a more detailed analysis of hardness than is required by the standard.

The interface between the weld metal and the parent rail was continuous with no lack of fusion evident. Small areas of porosity were visible in all three welds, the majority of which was within the limits specified in the above standard. Table 5 gives the porosity limits specified in EN 15594:2009 and Table 6 the measured porosity levels in the Sauron welds. However, weld 17TR11 was outside the requirements of the standard for porosity at porosity levels of 0.12mm-0.3mm, where only 3 areas of porosity within this dimension range is permitted.

Defect Type	Acceptance Criteria
Cracks	Not permitted
Crater cracks	Not permitted
Isolated porosity	0 mm – 0.12 mm not limited
	0.12 mm – 0.3 mm, 3 per sample max.
	0,3 mm – 1 mm, 1 per sample max.
	> 1 mm not permitted
Clustered porosity[a]	0.4 mm max, 3 clusters per sample max.
Linear porosity[b]	Not permitted
Elongated cavities/wormholes	Not permitted
Solid inclusions	None on polished sample to naked eye
Lack of fusion	Not permitted
Undercut	Not permitted
a = Porosity is considered to be clustered when the distance between two pores is less than the diameter of the smallest pore. b = Linear porosity is defined as three or more pores aligned in the same plane	

Table 5. Porosity Limits in EN 15594:2009

Weld No.	Porosity Dimensions			
	0-0.12mm	0.12-0.3mm	0.3-1.0mm	>1.0mm
17TR10	5	1	0	0
17TR11	4	5	0	0
17TR12	4	1	1	0

Table 6. Porosity Dimensions in Sauron Welds

Figure 19, 20 and 21 show the microstructures obtained within the three Sauron welds.

The microstructures of welds 17TR10 and 17TR11 had intermittent areas of untempered martensite present in the root bead weld metal adjacent to the interface with the parent rai (when examined at a magnification of X100 as required by the standard). 17TR10, which had the highest surface hardness had the greatest quantity of martensite in the root bead but the level was still only small, comparable to that observed within the DDR sample.

Figure 20d shows the microstructure along the bottom of weld 17TR11, where a crack can be seen in the weld metal adjacent to the interface. The crack in Figure 20d and the porosity on the interface in Figure 20g are both potential sites for fatigue crack initiation in service and previous rail break examinations have demonstrated that porosity on the interface in particular is very susceptible to fatigue crack initiation, which ultimately leads to either spalling of the weld deposit or failure of the rail itself.

In comparison 17TR12, made using a different Sauron welding machine, had no martensite visible at a magnification of X100.

a. Location of Micrographs

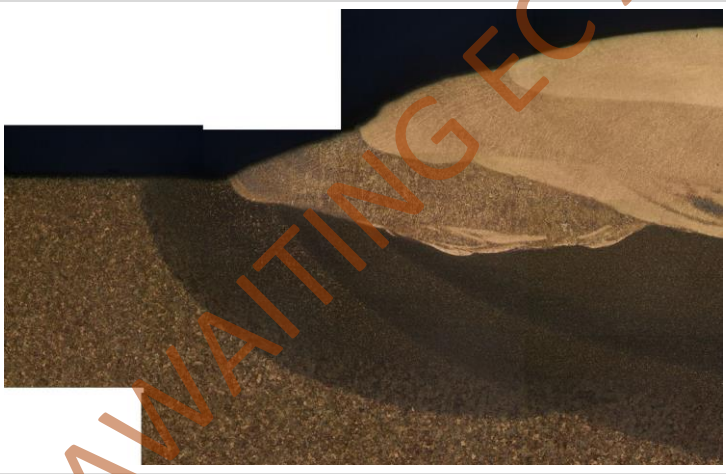

b. End of Weld

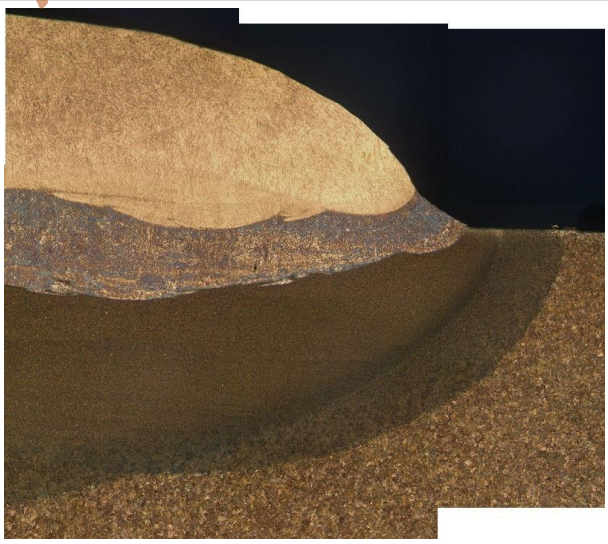

c. Opposite End of Weld

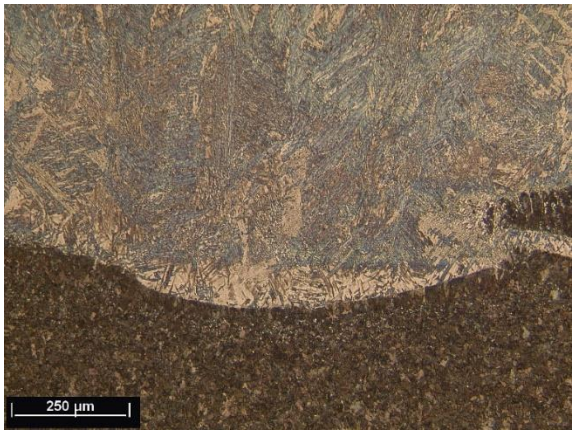

d. Along Bottom of Weld,
e. Low Magnification

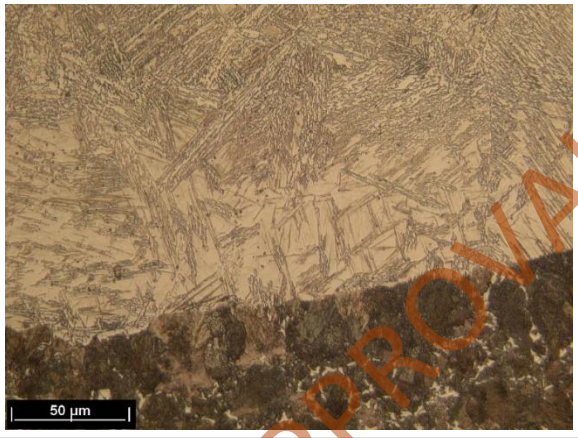

f. Along Bottom of Weld,
g. High Magnification

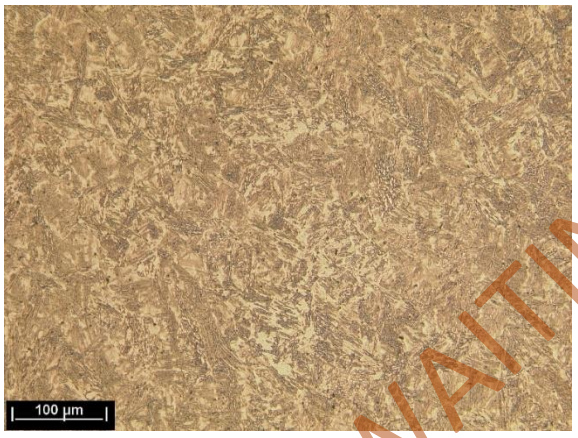

h. Weld Metal Near Top of Weld

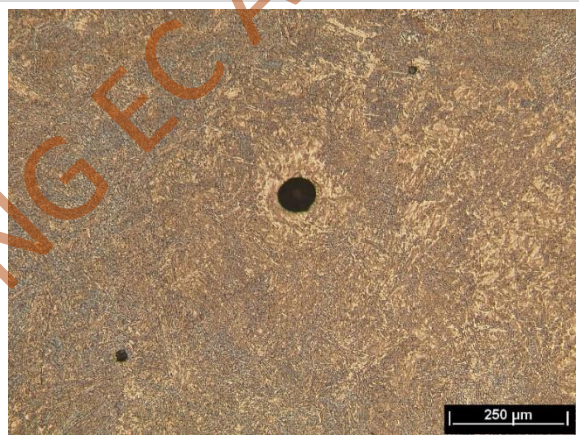

i. Porosity

Figure 19. Interface Microstructure of Sauron Weld,
Automate TranslamaticTAC 2000 France: No.01/00/117/00, 17TR10

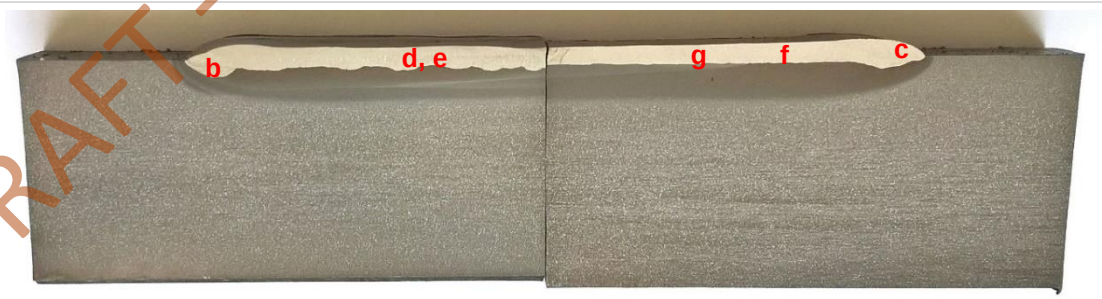

a. Location of Micrographs

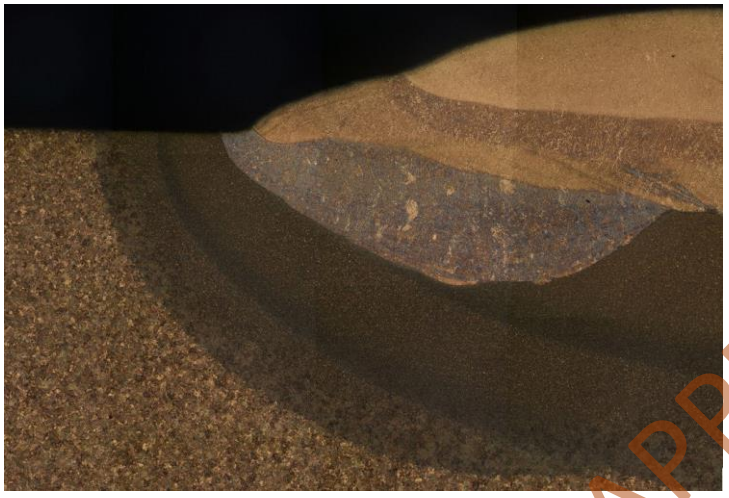

b. End of Weld

c. Opposite End of Weld

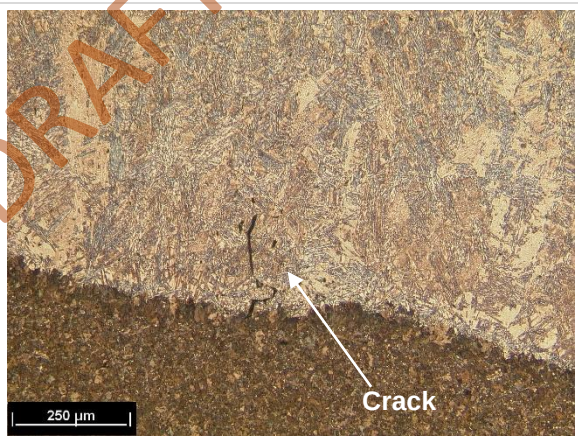

d. Along Bottom of Weld, Low Magnification

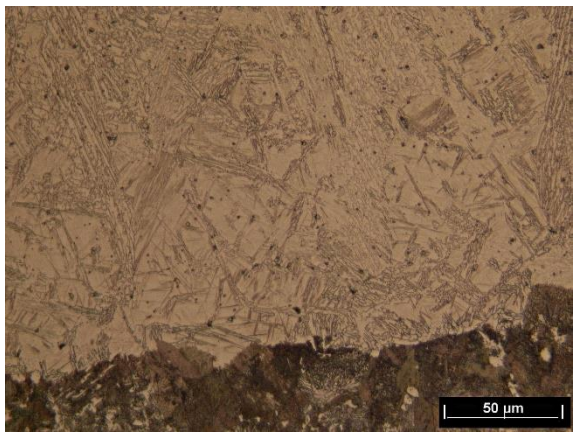

e. Along Bottom of Weld, High Magnification

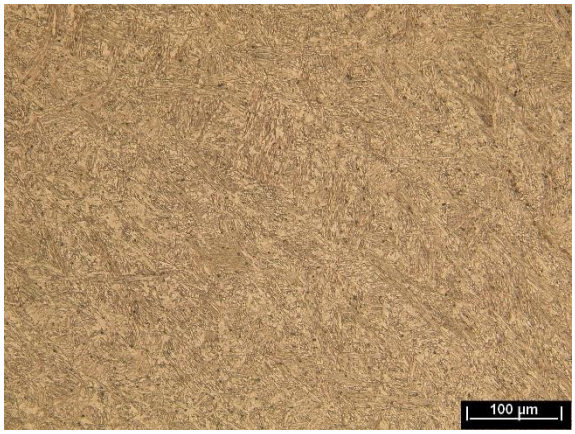

f. Weld Metal Near Top of Weld

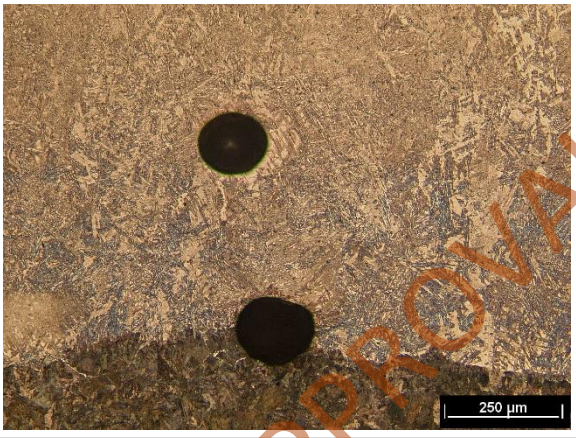

g. Porosity

Figure 20. Interface Microstructure of Sauron Weld,
Sauron, Automate Translamatic TAC 2000 France: No.01/00/117/00, 17TR11

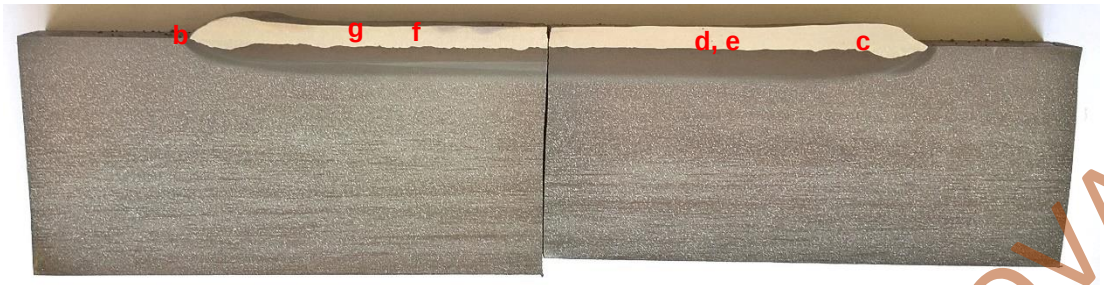

a. Location of Micrographs

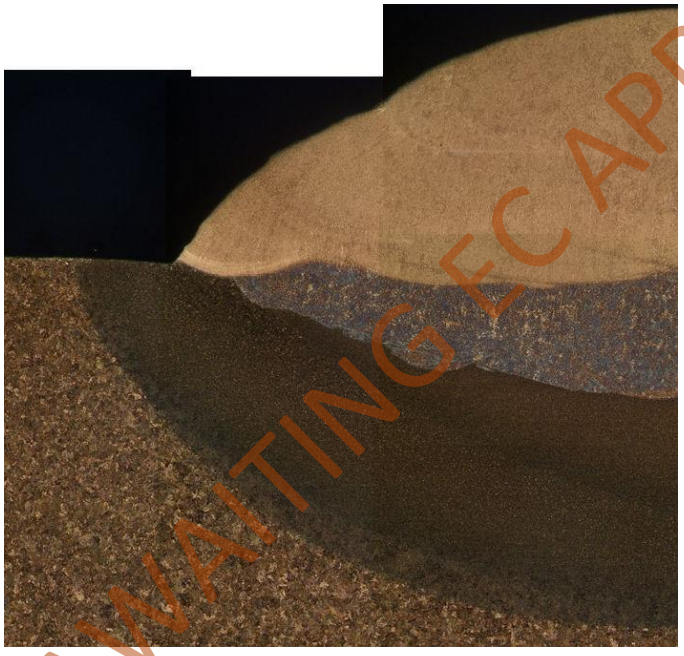

b. End of Weld

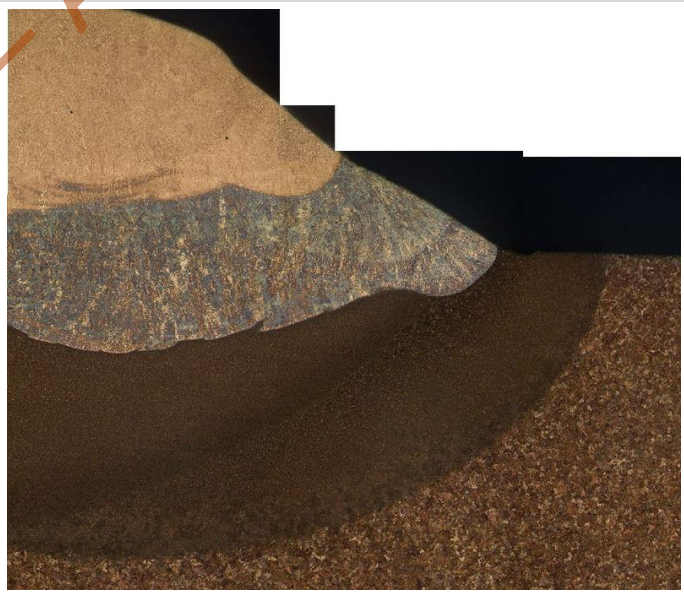

c. Opposite End of Weld

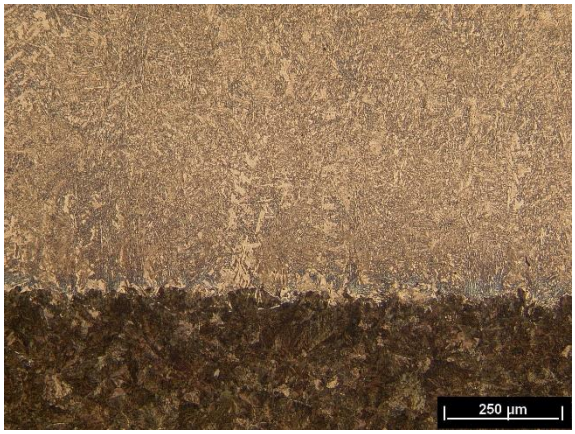

d. Along Bottom of Weld, Low Magnification

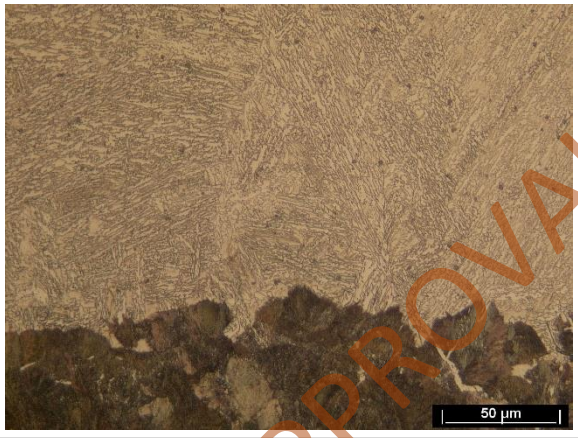

e. Along Bottom of Weld, High Magnification

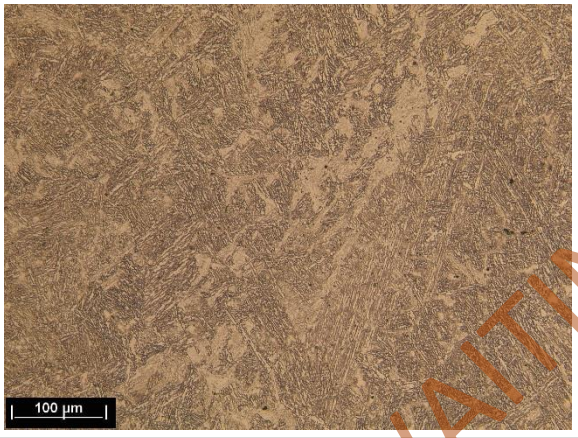

f. Weld Metal Near Top of Weld

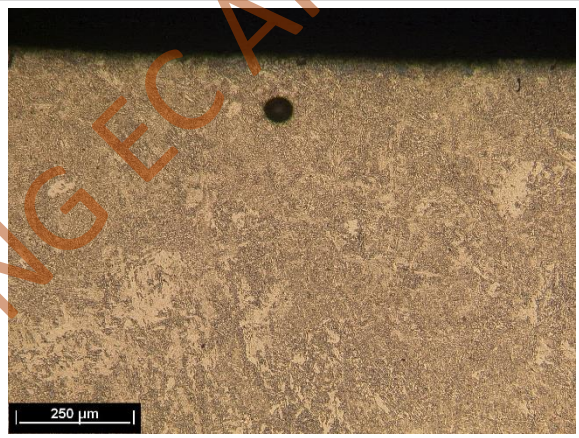

g. Porosity

Figure 21. Sauron, Automate Translamatic 350 CTF France:No.11120452, 17TR12

Vickers hardness traverses (HV10) were carried out on the transverse samples in accordance with EN 15594:2009 (2) for each of the three welds. Figure 22a-Figure 22f shows the macro samples and their associated hardness traverse; the location of the hardness traverse is shown by the red dashed line.

a. Macrograph of Weld 17TR10

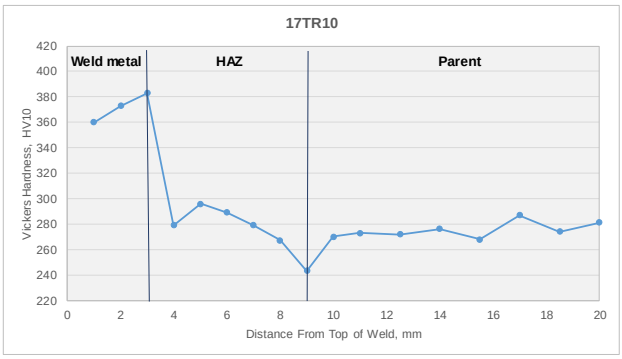

b. Vickers Hardness Traverse of 17TR10

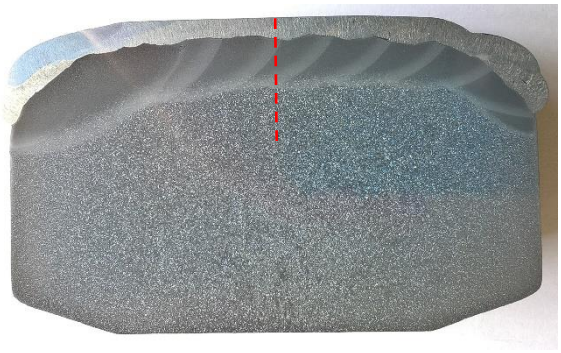

c. Macrograph of Weld 17TR11

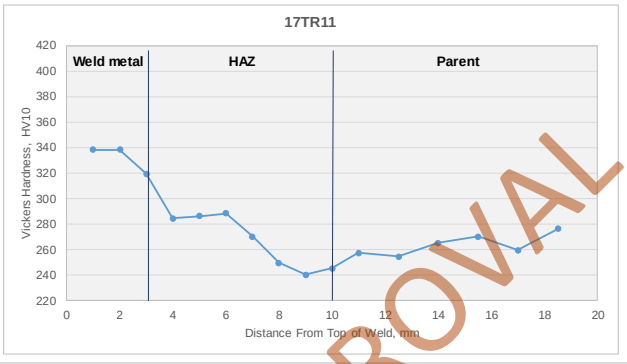

d. Vickers Hardness Traverse of 17TR11

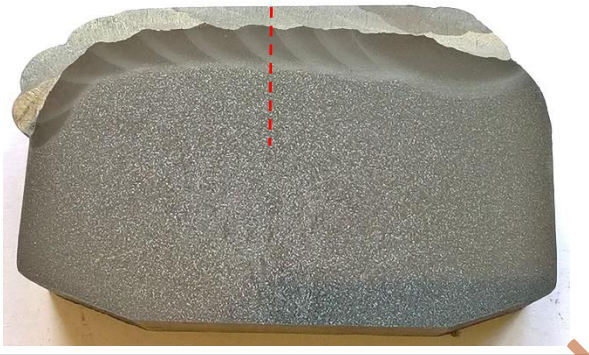

e. Macrograph of 17TR12

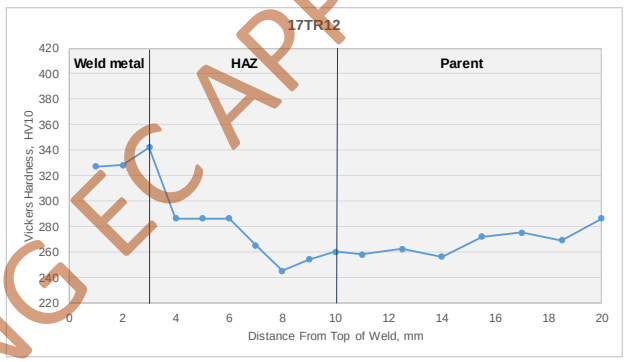

f. Vickers Hardness Traverse of 17TR12

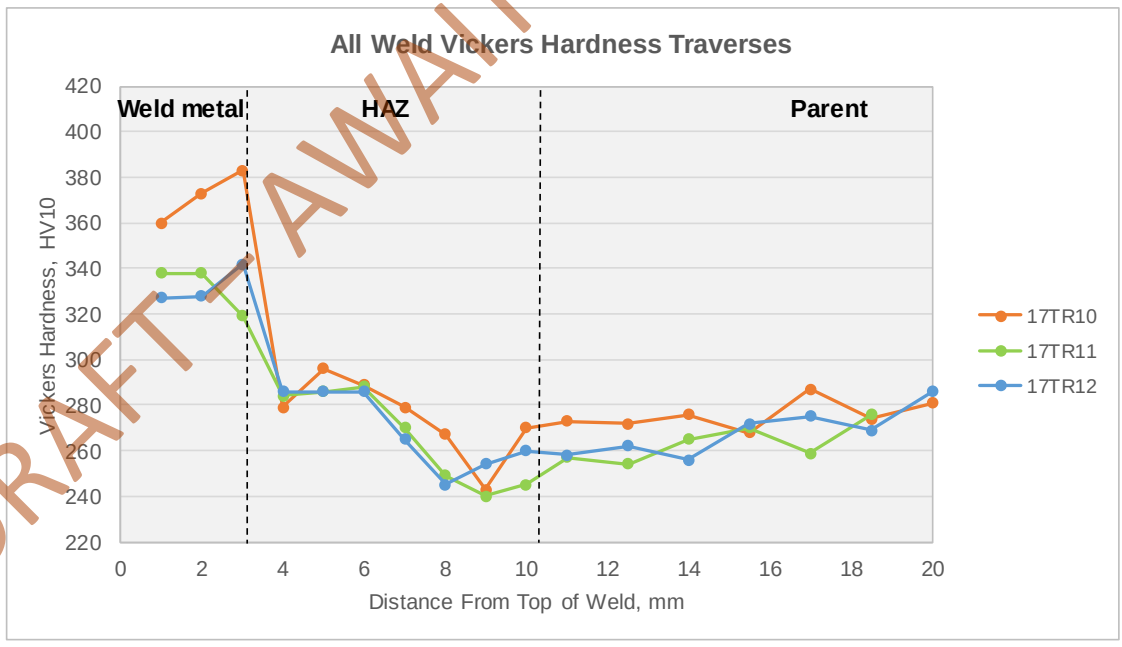

g. Vickers Hardness traverse of All Three Sauron Welds

Figure 22. Transverse Macrographs of Sauron Welds and Vickers Hardness Traverses

In Figure 22g all three of the weld hardness traverses are shown. The resultant HAZ hardness levels are very similar for all three welds. However, the weld metal hardness of weld 17TR10 was higher than that of the remaining two welds, in agreement with the surface hardness levels, which were in the region of 50HB higher for weld 17TR10.

Figure 23 shows the longitudinal hardness traverses carried out ~0.5mm below the rail running surface of DDR weld 3 and the Sauron welds. *N.B. The apparently low hardness of the parent rail on one side of weld 17TR12 is due to the traverse being partially within the zone of decarburisation below the running surface. This was unavoidable due to the cavity being very shallow resulting in a correspondingly shallow weld depth, which was thus close to the running surface.*

As would be expected due to the higher surface weld metal hardness 17TR10 had a higher overall weld metal hardness. Given that the 3 welds were made from the same batch of consumable and the heat inputs were not significantly different (which could affect the amount of dilution with the parent rail and hence increase the hardness) the higher hardness must be attributable to the post weld cooling rate.

Although the chemistries of the DDR and Sauron weld metal are different the resultant hardness levels, with the exception of 17TR10, were very similar. The DDR weld metal had a higher peak hardness close to the interface, which is most likely due to dilution effects and/or cooling rate due to the different angle/depth of the cavity. However, as demonstrated by Figure 12a, addition of a subsequent layer appears to have resulted in a certain degree of tempering thus producing a slightly softer microstructure immediately above the interface with the parent rail.

The HAZ widths at the extremities of DDR weld 3 and the Sauron welds were similar at around 3-4mm.

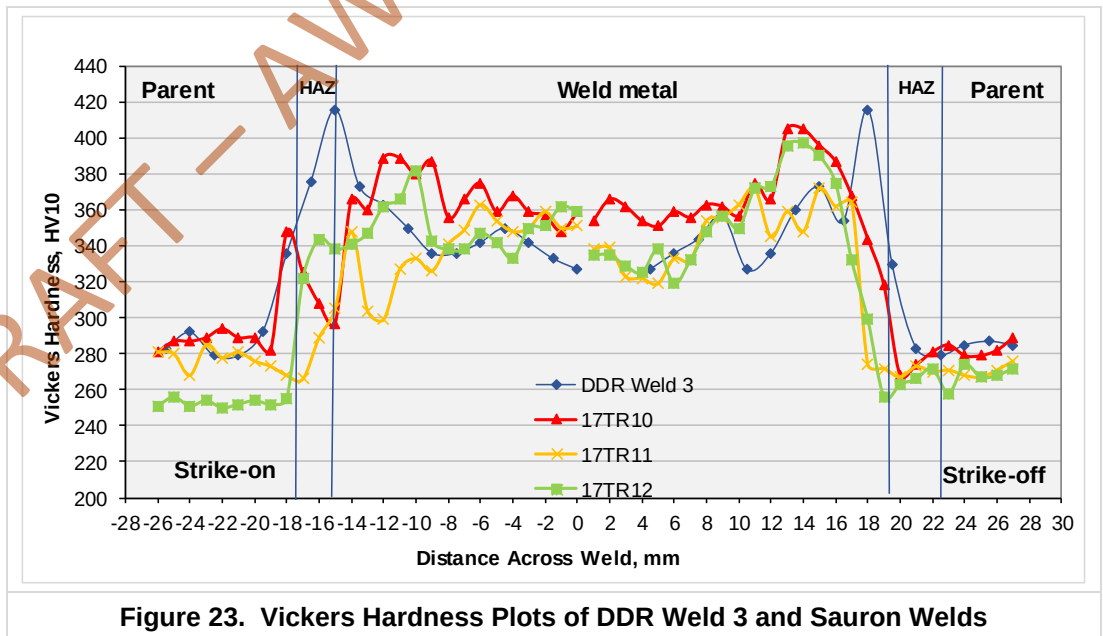

Figure 23. Vickers Hardness Plots of DDR Weld 3 and Sauron Welds

4 4-Point Bend Fatigue Testing

The bow wave effect created by passage of vehicles subjects the surface layers of the rail head to a cyclic stress range which, when coupled with the stress raising effects of defects such as internal porosity or slag inclusions can lead to fatigue cracks, particularly when such defects are associated with the parent rail/weld metal fusion zone. At greater depths from the rail surface, the passing vehicles subject the rail to bending fatigue and this phenomenon is more relevant to deeper weld repairs.

In order to evaluate the robustness of the head repair processes against such cyclic stresses 4-point bend fatigue testing was carried out.

DDR trial weld 2 was used for the fatigue test and a hear repair from Thermit Welding (GB) was also tested. Both welds were ground back to rail profile prior to testing. The arrangement of the fatigue test machine FF101 1500 kN static, 1000 kN dynamic (calibrated annually) is shown in Figure 24; testing was carried out with the head in tension, i.e. head down.

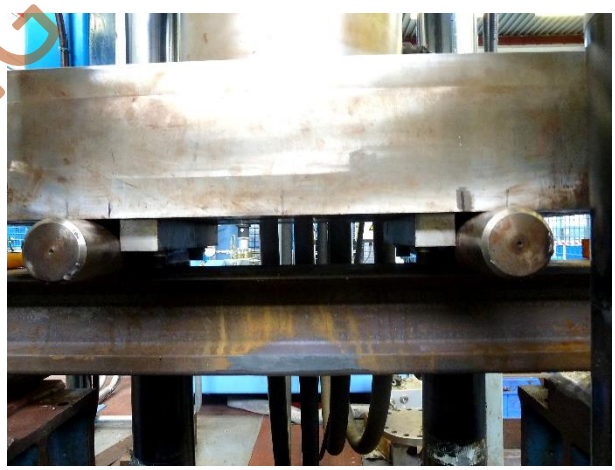

Inner span 465 mm
Outer span 1050 mm
Roller radius 35 mm

Figure 24. Arrangement of the 4-Point Bending Fatigue Test

Under typical track loading conditions, the weld metal/parent rail interface of the DDR weld will experience a stress cycle ranging from compressive when the wheels are directly on top of it, to tensile when the weld repaired section is either between the two axles of a bogie or in between two bogies. The estimated tensile stress range that could be experienced at the weld metal/parent rail fusion zone for an axle load of 25t is typically 35 MPa. It should be noted however, that this testing regime was designed to test the integrity of a weld repair interface with a depth of 10mm whereas in the aluminothermic process the orientation and depth of the interface is very different and the tests

undertaken were essentially assessing the integrity of the cast structure rather than the weld metal-parent rail interface for this weld. On this basis, the first fatigue test was carried out at a multiple of three times this stress range, i.e. 105 MPa, believed to be more representative of dynamic loading conditions, with a run out life set at 5 million cycles. Both the DDR and the Thermit Welding (GB) head repair fatigue tests at the105 MPa stress range ran out to 5 million cycles and therefore the tests were continued at a significantly more stringent stress range of 230 MPa, effectively representing dynamic loading conditions of six times those of static loading. At this higher stress range both head repairs failed, with the DDR head repair breaking at ~3.3 million cycles compared to ~176,000 cycles for the Thermit Welding (GB) weld.

A summary of the 4-point bend fatigue test results is shown in Table 7.

Weld Type	Stress Range, MPa	Run out/Fail (5 million cycles)	Number of Cycles to Failure
DDR Weld 2	105	Run out	-
Thermit Welding (GB)	105	Run out	-
DDR Weld 2	230	Broken	3,342.183
Thermit Welding (GB)	230	Broken	175,702

Table 7. 4-point Bend Fatigue Test Results

The fracture faces of the two broken fatigue tested welds are shown in Figure 25a-25d. The failure initiation point was below the excavated area and away from the weld deposit. Closer examination indicated that DDR trial weld 2 had failed from a surface feature which proved to be a sharp grinding facet created when the weld was ground to profile after completion of the deposition process (Figure 25b). It would appear, therefore, that the presence of stress raisers created by profile grinding of the rail head may play a more significant role in fatigue crack initiation than the small intermittent areas of martensite observed in the root bead weld metal adjacent to the interface. This highlights the importance of avoiding the creation of sharp grinding facets to avoid potential fatigue crack initiation.

In contrast, the Thermit Welding (GB) weld failed from an internal artefact, possibly an area of small porosity or a slag inclusion, although the precise nature of the initiation point has not been investigated (Figure 25d).

a. DDR Trial Weld 2

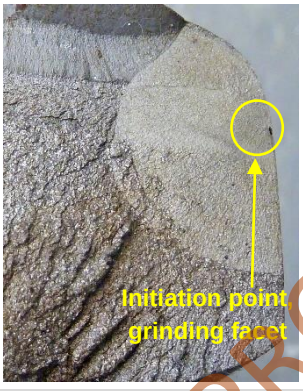

b. DDR Trial Weld 2
Initiation Point, Grinding Facet

c. Thermit welding (GB)

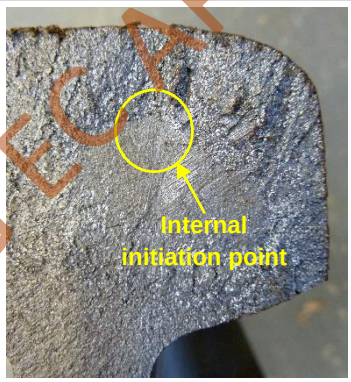

d. Thermit Welding (GB)
Internal Initiation Point

Figure 25. Broken Fatigue Test Fracture Faces

5 Discussion

The internal soundness in terms of porosity of both the DDR weld and the aluminothermic head repair welds was excellent, with all having levels of porosity well below the maximum levels permitted in EN 15594:2009. Some areas of porosity in two of the Sauron welds exceeded the levels specified in the above standard. The interface between the weld metal and parent rail for all three head repair techniques was continuous with no evidence of lack of fusion, and in the case of the Railtech weld the interface was difficult to identify under the optical microscope.

Although no MMA welds were examined during the course of this project examination of previous MMA trial welds have highlighted the shortcomings of the process. The porosity level in MMA welds is much greater than in semi-automatic flux cored welding due to the fact that the MMA weld quality is very much influenced by the experience and skill of the welder. The process is dependent on the operator in terms of deposition of the weld beads and maintenance of temperature, with the result that it is not uncommon to see large areas of porosity within both the deposit but more worryingly along the interface. In addition, the presence of martensite within the HAZ is sometimes observed as a result of either insufficient preheat or failure to maintain interpass temperature during the full deposition process (Figure 26) (3).

a. Porosity Within MMA Weld Repair

Figure 26. MMA Weld, Showing Porosity Within the Weld Metal and on The Interface

Defects such as those in Figure 26 have the potential to lead to either weld spalling or rail failure. Rail failures due to initiation from porosity at the interface between the weld metal and parent rail have been examined frequently, some examples of which are given in Figure 27 below (4), (5).

In terms of improvement of porosity level and reduction in the likelihood of failure, the semi-automatic process offered a significant advantage over the MMA process and in the case of the welds examined during this project the aluminothermic weld repairs also had a very low porosity level.

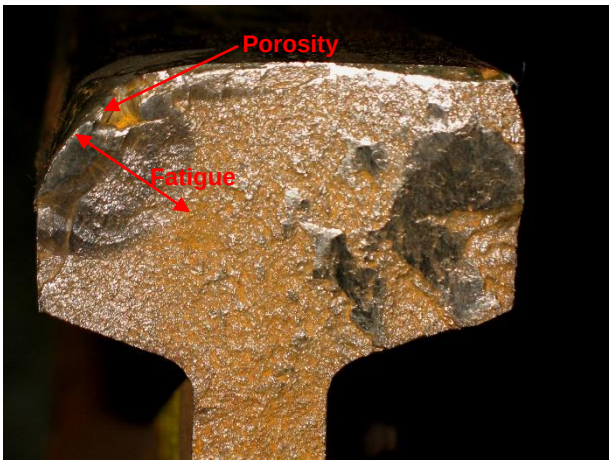

a. Fracture Face of Broken Rail With MMA Weld Close to Gauge Corner

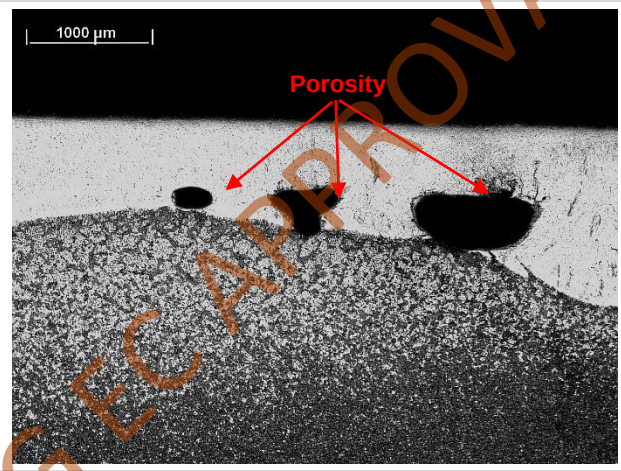

b. Gross Porosity Along Interface of Weld, Ultimately Leading to Rail Failure by Fatigue

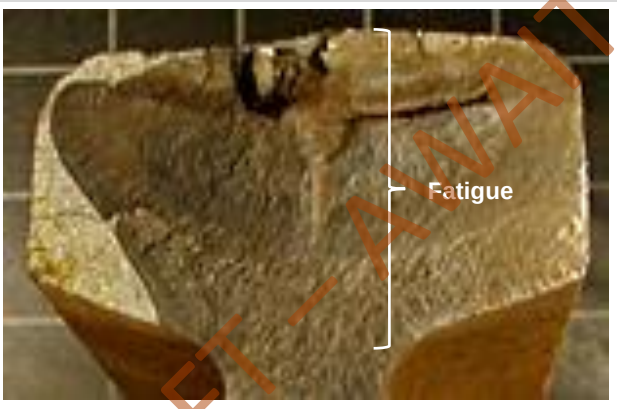

c. Fracture Face of Broken Rail with MMA Weld on Running Surface and Large Area of Fatigue

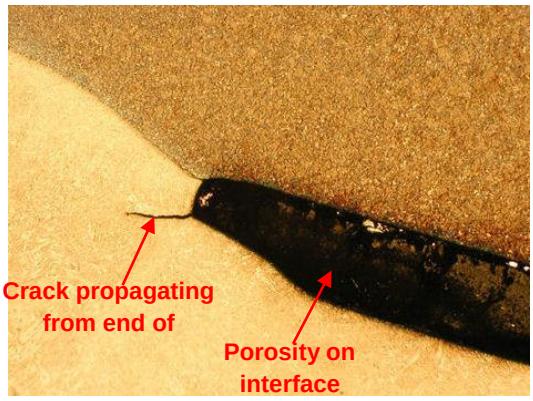

d. Porosity on Weld Interface With Parent Rail

Figure 27. Rail Failures Due to Defective MMA Welds

A higher hardness in the bainitic consumable compared to that of the parent R260 rail is necessary for the bainitic microstructure to have comparable wear resistance to the R260 rail. However, it should be noted that the wear behaviour of the aluminothermic repairs is not necessarily going to be equivalent to that of the parent rail despite having a similar hardness level or indeed to that of the bainitic welding consumable. The aluminothermic weld metal is in effect a cast product with a large elongated grain structure compared to the much finer equiaxed grain structure of the rolled rail. Currently no laboratory wear test data (twin disc testing) is available for aluminothermic weld metal

and it may be worth determining the difference, if any, in wear behaviour of cast aluminothermic rails to the rolled parent rail.

The sub-surface hardness of the DDR weld was assessed against EN 15594:2009 (2), which states that the subsurface hardness is measured on the transverse sample. Whilst the weld passed the hardness criteria stated in the standard of 400HV max, this assessment criterion did not reflect the hard microstructure observed in the weld metal immediately adjacent to the interface. Subsequent micro-hardness testing established the martensite within this mixed microstructure to have a maximum hardness of 627HV. For a carbon content of ~0.5%, i.e. that of the diluted weld metal immediately adjacent to the interface, untempered martensite would have a hardness of ~800HV and thus it can be concluded that some degree of tempering has occurred after deposition of the subsequent two weld layers.

One advantage of the aluminothermic welds is the similarity of the resultant weld metal in terms of composition and microstructure to that of the parent rail with the resultant microstructure within the weld metal adjacent to the interface free from any hard or brittle phases, which have the potential to initiate fatigue cracks during the cyclical loading experienced in track. However, as mentioned above, the effects of the cast aluminothermic weld metal structure on wear resistance compared to that of the rolled rail has not currently been assessed. The DDR procedure utilises a Network Rail approved consumable, ESAB Tubrodur 35 OM, which essentially produces a bainitic weld metal of higher hardness than that of the parent rail. Whilst this produces a hard weld metal beneficial to the wear behaviour in service, the compositions of the parent rail and weld metal, in particular the carbon content, are quite different. The microstructural examination and the LIBS analysis have demonstrated the effect of carbon dilution at the interface whereby the carbon content of the weld metal immediately adjacent interface has increased from circa 0.16%C to ~0.5%. This has undoubtedly resulted in a much harder microstructure in this region due to variation in the transformation behaviour of the higher carbon region compared to the remaining bulk of the weld metal; the dilution effect was minimal at distances of greater than ~1mm away from the fusion line.

The dilution effect at the weld metal interface will apply for any weld repair technique using a consumable of a significantly different chemical composition to that of the parent rail, and this is also the case with the Sauron welds where intermittent areas of martensite were present in the weld metal immediately adjacent to the interface. Again, some tempering may have occurred if subsequent layers had been deposited.

The weld metal microstructure in the intermittent narrow zone of approximately 90µm in width adjacent to the interface in the DDR weld consisted of a mixture of lightly tempered martensite and bainite. Given that the decision was taken during the trial in York not to deposit the fourth layer, it is possible that more significant tempering of the root bead microstructure may have occurred if the fourth layer had been deposited.

The finite element modelling of the DDR process may help in the optimisation of the welding parameters with a view to achieving the desired microstructure at the interface in the adjacent weld metal and parent rail HAZ. However, despite the presence of intermittent areas of martensite in the root bead of the weld adjacent to the weld metal/parent

rail interface, the 4-point bend fatigue tests have demonstrated that it has not had a significant effect in terms of generating fatigue cracking at loads well above those which would be expected in service.

The 4-point bending fatigue behaviour of the DDR trial weld and the Thermit Welding (GB) head repair were comparable with both achieving greater than three times the expected tensile stress range (105 MPa) at the weld metal/parent rail interface for an axle load of 25t.
After continuing testing at 230 MPa both welds failed, with the DDR weld possibly failing from a grinding facet on the rail surface and the Thermit Welding (GB) weld from an internal feature possibly a slag inclusion or porosity although this has not been confirmed. However, it should be noted that the shape and dimensions of the aluminothermic head repair cavity are significantly different from that of the DDR weld and as such the fatigue test was assessing the integrity of the cast weld metal structure rather than the weld metal/HAZ interface.

6 Summary/Conclusions

Assessment of the different welding techniques throughout this investigation has highlighted advantages and disadvantages of the different processes. The following section aims to summarise the findings for MMA, semi-automatic FCAW (CTF-Sauron), aluminothermic head repair techniques, and the novel DDR process.

- Porosity levels of MMA welds are very high and have been shown to lead to rail failure and this method has generally been considered the benchmark for developments over the years. The porosity levels of the remaining processes were much better with no porosity being observed in the aluminothermic weld repairs. However, although the porosity level was lower in the Sauron semi-automatic welds the process was still likely to produce porosity outside the limits stated in EN 15594:2009. The DDR process, using the weave technique produced a very low level of internal porosity well within the limits stated in EN 15594:2009.
- The DDR equipment offers a significant benefit in terms of the cavity excavation, producing consistent cavity dimensions and surface quality, which when combined with the slag removal between deposited layers, ensures very low levels of porosity compared to excavation of the cavity by grinding or gas burning (as is the case with the aluminothermic head repair).
- A further advantage of the DDR process is the very low preheat. Preheating and maintaining interpass temperature is one of the areas within semi-automatic flux cored and MMA welding that is dependent on the competence and diligence of the welder. The human interface inevitably brings variation in to the process and temperature control can frequently be poor or non-existent. Only a minimal preheat is required for the DDR process and maintenance of interpass temperature is not necessary as the weave technique inputs sufficient heat such that the cooling rate is sufficiently slow to avoid the production of low temperature transformation phases, i.e. martensite, within the HAZ.
- In terms of wear performance in track the aluminothermic head process has a wider HAZ than the DDR and Sauron welds and is more likely to result in cupped welds due to differential wear at the soft zones within the HAZ. The softer weld metal of the aluminothermic head repair processes compared to the bainitic consumables used in the DDR and Sauron processes may not provide wear resistance comparable to that of the parent rail and can lead to weld metal cupping, which in turn can lead to dynamic loading and potential weld failures where internal discontinuities are present (porosity, slag inclusions). However, the process is widely used and an industry standard of ~+20HB is factored in to the aluminothermic weld metal to alleviate any issue with preferential wear of the weld metal. One advantage of the aluminothermic process is that it uses existing equipment and aluminothermic portions and is relatively portable for easy transportation to site. Nevertheless, it is ultimately a casting process and is inherently prone to porosity and shrinkage due to the solidification of the large volume of molten weld metal.
- The behaviour of the DDR and Thermit HRW repaired samples under the cyclic loading conditions experienced in track was assessed using a bespoke laboratory test with imposed stress ranges that were several fold greater than those experienced in service. Both processes revealed high fatigue strength

suggesting failure through this mode was unlikely under track loading conditions. The DDR sample possessed showing higher endurance with the observed eventual failure occurring from an external manual grinding imperfection whereas the HRW sample failed from an internal casting flaw.

7 References

1. **Johnson, R S.** *The Repair of Discrete Rail Defects – Analysis of the method developed by ARR. INFERRICITY LTD. 2016.* 2016.
2. ***EN 15594:2009, Railway applications - Track - Restoration of rails by arc welding.***
3. C Zhu, L Roebuck. ***Manual Metal Arc Welding of HP335 Rails.*** **2015.**
4. Fretwell-Smith, S. ***Broken Rail Report B327_07.*** **2006.**
5. Thomas, S. ***Broken Rail Investigation Report, CRT/2003/021.*** **2003.**

CHALMERS
UNIVERSITY OF TECHNOLOGY

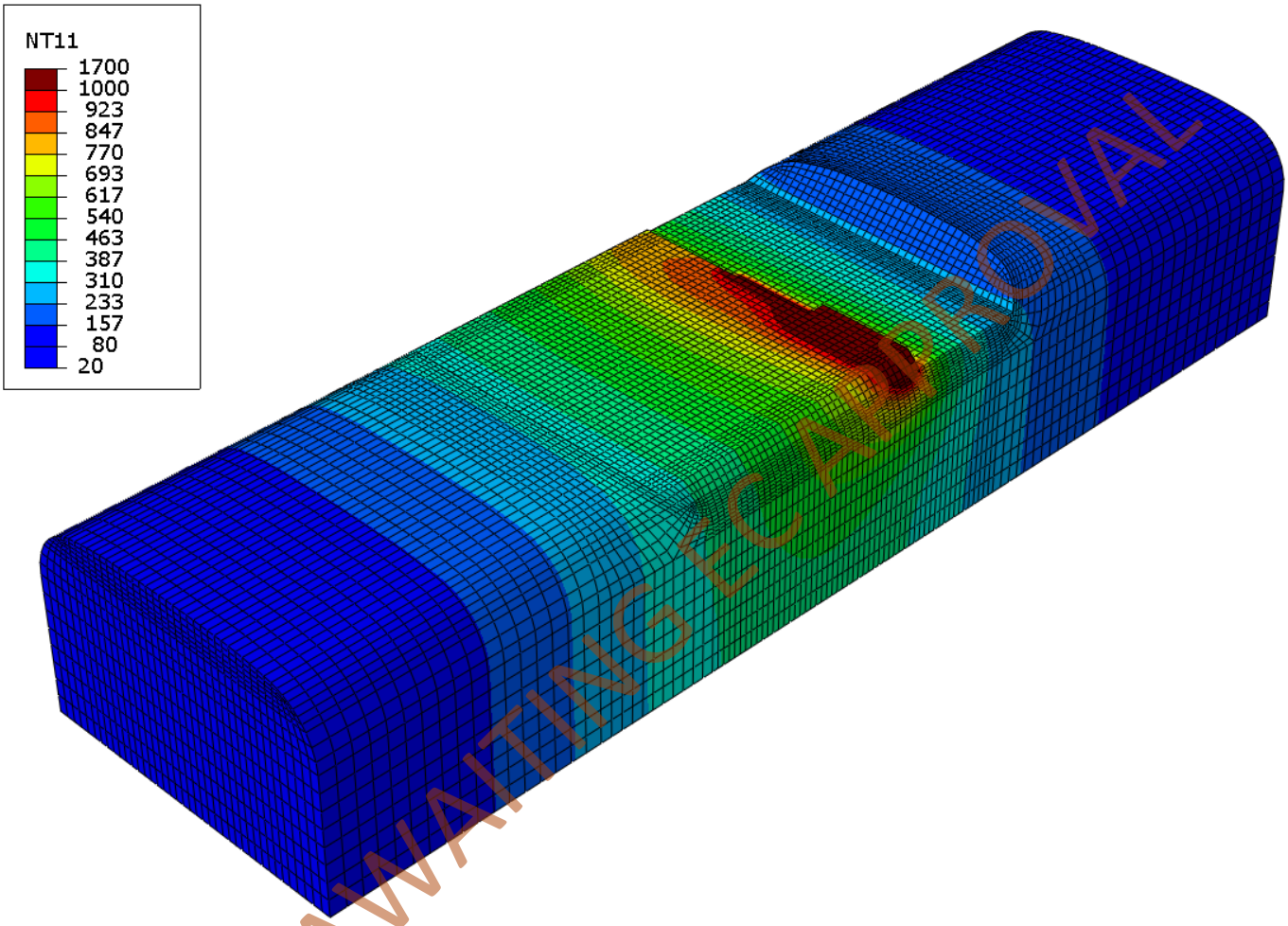

Finite element analysis of thermal fields during repair welding of discrete rail defects

Master's Thesis in Applied Mechanics, Chalmers Tekniska Högskola

MICHELE MARIA MAGLIO

Department of Applied Mechanics
CHALMERS UNIVERSITY OF TECHNOLOGY
Gothenburg, Sweden 2017

MASTER'S THESIS IN APPLIED MECHANICS

Finite element analysis of thermal fields during repair welding of discrete rail defects

MICHELE MARIA MAGLIO

Department of Applied Mechanics
Division of Dynamics
CHARMEC
CHALMERS UNIVERSITY OF TECHNOLOGY
Göteborg, Sweden 2017

Finite element analysis of thermal fields during repair welding of discrete rail defects

MICHELE MARIA MAGLIO

Supervisor: Elena Kabo
Examiner: Anders Ekberg

Master's Thesis 2017:17
ISSN 1652-8557
Department of Applied Mechanics
Division of Dynamics
CHARMEC
Chalmers University of Technology
SE-412 96 Göteborg
Sweden
Telephone: + 46 (0)31-772 1000

Cover:
Snap shot of evaluated temperatures during discrete defect repair welding

CHARMEC / Department of Applied Mechanics
Göteborg, Sweden 2017-06-12

Finite element analysis of thermal fields during repair welding of discrete rail defects

Master's thesis in Applied Mechanics, Chalmers University of Technology
Master's thesis in Mechanical Engineering, Politecnico di Torino
MICHELE MARIA MAGLIO
Department of Applied Mechanics
Division of Dynamics
CHARMEC
Chalmers University of Technology

Abstract

Discrete defects in a rail head may form due to aggressive wheel–rail contact in terms of thermal and/or mechanical loads, or due to indentations from foreign objects trapped in the contact. If large, such defects need to be repaired or the rail section removed. These are costly operations that cause operational disturbances. To decrease mitigation costs, discrete defect repair (DDR) procedures that include repair welding have been developed. These operations typically require high preheat temperature (350 °C) and long working process times.

This MSc-thesis work investigates a novel DDR rail welding procedure through numerical simulations. The new technique employs significantly lower preheat temperature (60–80 °C) and equipment that can easily be carried to the working place. However, the low preheating temperature introduces high temperature differences between the molten filler material and the surrounding rail steel. This may lead to the formation of defects, welding related cracks or martensitic areas.

The aim of the work is to simulate the DDR procedure and thereby be able to analyse the thermal history in the rail during the welding process. In this manner, cooling curves for critical locations in the rail head can be evaluated and the risk of weld related defects and metallurgical transformations to hard microstructures can be assessed. To achieve these ends, numerical models of a milled rail head were created in ABAQUS/CAE. The repair welding procedure was then simulated and the results compared to experimental data from the literature.

The results show temperature trends that are in line with temperature measurements from trials carried out some years ago. The simulations show the sensitivity to parameters such as the temperature of the molten filler and cooling times. There is thus a high potential in simulating operational procedures and thereby be able to e.g. investigate effects of various process parameters. However, to this end more high-quality test data are required. In particular the simulations show how sensitive a calibration is to the exact position of thermocouples. On the other hand, the simulations performed in the thesis have shown that small variations in the geometry of the numerical model of the repair process do not have a significant influence on the predicted cooling curves.

Contents

Preface

I would like to say thank you to my supervisor Elena Kabo for all the suggestions and support she has given to me in these five months. It was a real pleasure for me to work with her on the first “real engineering” project of my career. I would also like to thank her for making me aspire to perfection and professionality in this work and for teaching me to tackle problems “sakta men säkert”.

Thanks to my examiner Anders Ekberg for recommending this Master Thesis project to me, for providing me with all the literature material I needed and for all the precious suggestions, feedback and recommendations he gave on the analysis procedures and on the results.

I am grateful to both Elena and Anders for being so kind to me and for revising this report and giving a lot of suggestions on the content and the style, thus making it look much more professional and effective.

A huge thank you goes to all my Family members who have always made me feel their love and enthusiasm even if I was very far from home, at first in Turin and then in Gothenburg. They encouraged, supported and cheered me up in all the moments of my studies and they gave me strength when I was worried by exams or deadlines. A special thought goes to my beloved grandmother who passed away during this exchange year.

I would like to show my thankfulness to all the relatives and friends who visited me in Sweden this year. Thanks to my friends of a lifetime, the ones from Maglie and nearby, that I am always longing to meet again when I am away and with whom it is nice to have a chat when I am homesick. I also feel lucky to have met so many nice people in Gothenburg who made this Erasmus year so special and I would like to say thank you to them all and especially to the ones with whom I spent these fantastic five months of MSc thesis work.

Finally, I want to say thank you to my Turin “university projects friends” and to the people I had the privilege to meet on the third floor of Collegio Einaudi: After sharing hopes and worries, opinions and meals, lectures and holidays, exam sessions and party evenings for four years I really feel like I owe them a significant share of my academic achievements. They turned up to be my second big family from the rest of the world: I really wish I will keep in touch with them for the rest of my life.

MICHELE MARIA MAGLIO

Notations

AWI	Abaqus Welding Interface
BC	Boundary Conditions
DDR	Discrete Defect Repair
DOF	Degrees of Freedom
FCAW	Flux Cored Arc Welding
FE	Finite Element
HAZ	Heat Affected Zone
MMA	Manual Metal Arc repair
RCF	Rolling Contact Fatigue

1 Repair welding

1.1 Wheel–rail rolling contact and discrete defects

In railway applications, the rolling contact between the wheel and the rail is expected to cause material degradation in form of wear, rolling contact fatigue and possibly plastic deformations. This will lead to rail deterioration and eventually reduce the load carrying capacity of the rail. The contact behaviour of the mating surfaces is quite complex and unpredictable, and the rolling contact may lead to the formation of different discrete defects which can result in a substantial shortening of the rail life [1].

The most frequent kinds of discrete defects that can be found on many mixed-traffic railway networks are squats and wheel burns [2]. Examples of these damage types are shown in Figure 1.1.

Figure 1.1 – Rail surface affected by squats (picture courtesy A. Ekberg)

A squat is a local rolling contact fatigue. The creation of squats is a complex and not fully understood phenomenon where the contact stresses between wheel and rail is a key parameter, cf [3]. Cracks from squats grow in from the surface and degrade the rail head material.

Wheel burns are caused by slipping of wheels on rails [4]. The friction associated with the relative motion creates a very hot area which is rapidly cooled as the wheel moves away. This may cause the formation of a hard and brittle marten site layer on the rail surface.

There are a multitude of other kinds of damage types that may affect the rail head, see [5] and [6], however the above are the most common causes to discrete defects, which are the topic of the current thesis.

Even though most of the discrete damage areas are actually quite shallow and do not individually represent a threat to the rail integrity, it should be borne in mind that a frequent presence of them can eventually cause failures in the track as cracks form and grow from the discrete defects. When it comes to selecting a mitigating action, it

should be considered that substituting the entire rail is costly, requires significant time in track and introduces two cuts and welds to mount the replaced rails.

This is the reason why Discrete Defect Repair (DDR) methods are currently being investigated. These procedures involve an initial phase in which the worn part of the rail is trimmed away. After that, the original geometry is restored by filling the cavity with weld material and then grinding off excessive material.

1.2 Discrete defect repair methods

The work in this section relates strongly to the overviews in references [1], [2], [7] and [8], where further details may be found.

As discussed in the previous section, the presence of small defects can pose a potential risk for the integrity of the rail. Sometimes squats, wheel burns, etc. are clearly visible on the rail surface, whereas in other cases some more advanced inspection systems are required (e.g. magnetic inspection, ultrasound, etc.).

Appropriate actions are needed if defects are present. The replacement of the whole rail, as anticipated above, implies high costs and the need to distribute replacement rail to the site. The replacement rail then has to be mounted by means of cutting up the damaged part, replacing it and welding the new rail. The procedure should be carried out in a manner that avoids the introduction of vertical and lateral irregularities, and so-called "cupping" (local plasticity/wear close to the weld). Any such irregularities on the running surface of the rail causes faster degradation of the track due to the higher dynamic forces caused by local increases in the wheel–rail contact. Further it has to be ensured that the rail replacement does not affect the stress free temperature of the rail.

Although clear statistics are not available, the main European railway networks have to remove on average 0.48 defects per British mile of track per year [7]. It is thus clear that some alternative and cost-effective methods for the repair of discrete defects would be desirable. In particular, such techniques should allow a robust and reliable in-situ repair. Rapidity is another requirement since there is a strong desire among infrastructure managers to minimise the time in which the track availability is reduced in order to avoid delays or re-routing of train operations.

Different processes have been proposed for DDR, several of which are currently in use in the railway industry [2]. However, these procedures can differ significantly in the way they are performed, in the type of equipment that is required and in the metallographic structure of the repaired material. Some of these techniques are quite new, so no reliable control on the behaviour of the repaired area has been performed yet. Moreover, although some DDR processes were introduced in the railway track industry as early as in the 1920s [2], it was not until some years ago that major infrastructure managers started to approve them [2].

These are the reasons why the EU project *In2Rail* aims, among other things, at developing and evaluating different techniques for the repair of rail head defects, thus providing a benchmark to compare the efficiency of the different procedures.

Some of the most common DDR mitigation techniques in Europe are briefly described in the following sections.

1.2.1 Rail replacement

This method basically consists in replacing the defected rail with a new one. A replacement rail of at least 5 metres is usually required for such a replacement [8], [9].

As discussed above, this procedure is costly, time consuming and requires cutting and two vertical aluminothermic welds, which can cause further deterioration[1]. These are the reasons why this option is conveniently applicable only if the defected rail is close to the end of its life cycle.

1.2.2 Manual Metal Arc (MMA) repair

In this procedure (often referred to as Shield Metal Arc Welding), the defect is manually excavated by milling. The resulting cavity is subsequently refilled using manual metal arc techniques. The preheating temperature is at least 343°C and other parameters depend on the manufacturers' expertise [2].

Although this process is well established and generally robust, the correct outputs of the grinding and welding procedures depend on the ability of the welder. The whole procedure takes up to 4 hours. Among other downsides, there may be inconsistencies in the heat affected zone microstructure which can significantly shorten the fatigue life of the metal.

The industry has recently standardised the procedures and the consumables and has introduced assessment of the welder ability (standard EN 287-1) [2].

1.2.3 Flux Cored Arc Welding (FCAW)

This process is similar to MMA, but the welding operation is semi-automatic. The heat is given by an arc between the continuous electrode wire and the work piece. The flux cored electrode creates a slag layer which has to be brushed away manually.

The grinding phase is still manual, therefore the output does depend on the operator ability.

1.2.4 Wide gap aluminothermic weld

This technique is basically an extension of the aluminothermic welding process. This allows the welder to use an established technology but, as a consequence, the downsides of the casting technology are extended to weld (i.e. large heat affected zone, change in residual stresses, poor automation, cumbersome transportation of the equipment) [8].

[1] Note that all repair methods will introduce welds, in many cases larger than the aluminothermic welds, so this is not a uniqe problem for rail repacements.

1.2.5 Flash butt wedge repair

This process consists in welding a wedge of rail material into a slot which has been carved out to remove the defect, as shown in Figure 1.2. The internal integrity of the wedge gives excellent mechanical properties, but the procedure is complex and not well established according to [8].

Figure 1.2 – Carved slot (left) and completed flash butt weld (right) [8]

1.2.6 Thermit Head Repair (HR)

In this process, the defect is excavated using a cutting torch guided by a template. The resulting slot is then filled by means of casting in a specifically designed mould. This allows the removal of deeper defects and to work with overlapping repairs [8]. The resulting large cast structure might have a different wear resistance as compared to the original rail. Further, the repair equipment, as shown in Figure 1.3, is quite complex according to [8].

Figure 1.3 – HR process – mould preparation (left) and preheating phase (right) [2]

To be more specific, there are two different types of HR [2]:

- Head Repair Weld (HRW) (also known as Thermit Head Repair (THR))
- Head Wash Repair (HWR)

These two processes do not differ much in the defect detection and removal phases. Torch excavation is more common in the HRW process, whereas grinding is used in for HWR.

Preheating, the use of moulds and the pouring phases are common in the two methods, but different parameters are used. Different techniques for grinding and final testing have been developed too.

1.3 British Steel DDR process

The key characteristics of this process are the minimisation of the human interference and the very low preheat temperatures in comparison with other DDR methods [10]. To facilitate transportation and repair times, a single frame on which all the necessary equipment is mounted has been developed.

In this method, the defect is removed and a weld cavity is prepared by means of a computer controlled milling procedure. The cut-out is 100 mm long, 10 mm deep and it covers the full width of the rail head (72 mm). Its shape is seen in Figure 1.4.

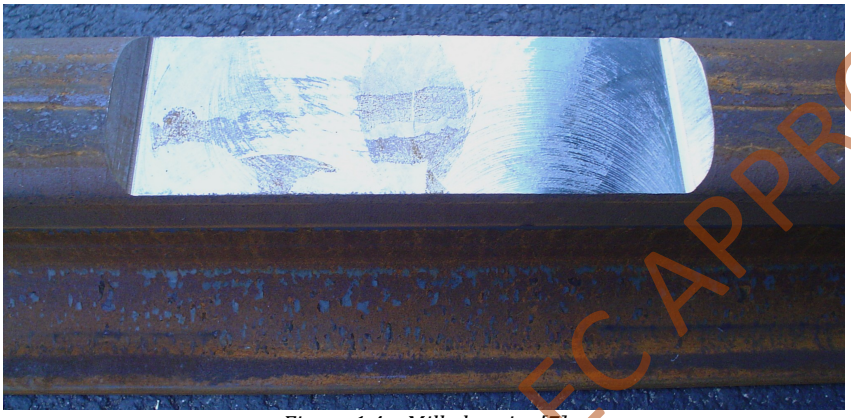

Figure 1.4 – Milled cavity [7]

One characteristic of this procedure is the use of a prototype unit in which the laser guidance, the milling tool and the FCAW welding head are all mounted. The unit is designed in such a way that it is easily possible to transport it to the place in which the repair procedure has to be performed, see Figure 1.5.

Figure 1.5 – Prototype unit employed during the DDR tests [10]

Before proceeding with welding operations, a preheat temperature of 80°C is applied to the rail. This preheat is considerably lower compared to other DDR welding techniques (where it is greater than 343°C). The use of such a low temperature eliminates the need for time consuming preheating to higher temperatures whilst preventing the completion of the transformation to martensite and retaining austenite. The deposition of subsequent beads tempers the martensite to a tough microstructure. In the case of the analysed DDR process, the weaved pattern permits the transformation to pearlite. In the penultimate layer, the start and end edges of the

cavity can create a HAZ that is susceptible to martensite formation but that can be tempered by a top sacrificial layer. [10][16]

The welding procedure is carried out as a semi-automatic open arc welding process under the guidance of a laser system. The consumable is deposited following a square weave pattern which, in this DDR procedure, is always perpendicular to the rail longitudinal direction [11]. The beginning of the path can be seen in Figure 1.6.

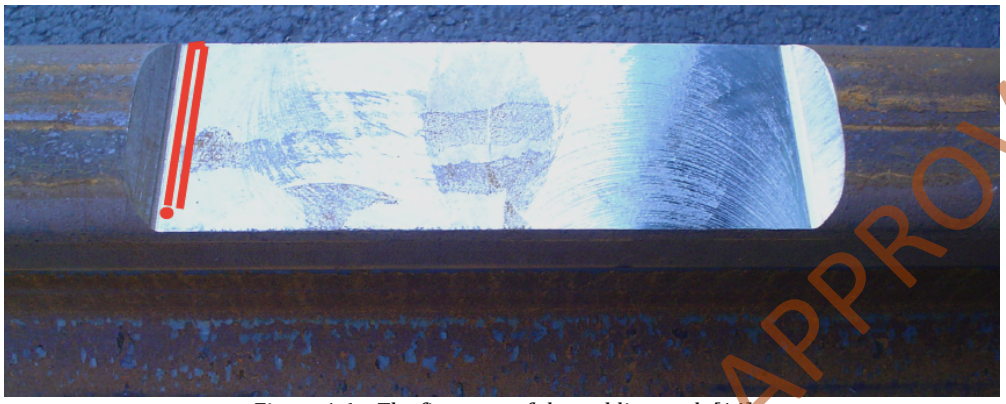

Figure 1.6 – The first part of the welding path [14]

Three layers are sufficient to cover the whole cavity, as shown in Figure 1.7, although a fourth sacrificial layer is used to ensure that the whole HAZ is tempered. Some time is spent after each layer deposition in order to manually remove slag using a pinning gun. This time frame allows the rail base material and the welding metal to cool down to an extent before a new layer is deposited.

The process is concluded with a manual grinding procedure in which the original rail head geometry is restored, see Figure 1.8. The efficiency of the grinding process is ensured by smoothness measurements on the restored surface and a visual inspection of the repaired rail.

Figure 1.7 – Appearance of the repaired area after the third layer is laid [10]

Figure 1.8 - Appearance of the repaired area after grinding [10]

1.4 Results from trials

Three sets of experiments were carried out in York, UK, in June 2016. Two of these experiments failed, the failure was due in one case to a problem with the software controlling the equipment and in the other case to an accumulation of spatter around the welding nozzle [10].

Since the aim of this report is to study the thermal effects of the whole welding procedure, the simulations will be based on results obtained in the third set. Normally four layers are deposited but on the experiment in June 2016 just three layers were used for the third experimental set [17].

As reported in Table 1.1, the preheating phase was accomplished in about 10 minutes by using an oxy/propane preheater. After that, the deposition phase, which used a 1.6 mm flux cored wire, started. The adopted consumable was named ESAB Tubrod 15.43, but it has lately been rebranded as ESAB Tubrodur 35 OM.

The rail was made of R260 steel. It took around 4 minutes to complete the weld run of each layer (slightly more for the third layer) and the slag removal phases in-between the different passes took about 3 minutes each.

The recorded rail temperatures during the DDR attempt are listed in Table 1.1 and are presented in the form of a graph in Figure 1.9.

DDR Process DDR weld 3	total process time actual	 elapsed	sequence time	weld time	rail temperature -deg C A	 B
	hr.min.sec	mins	mins	elapsed (s)		
Process start					16	17
Milling start	14.17.30	0.00			16	17
Milling finish	14.32.45	15.25	15.25		32	33
Preheat start	14.38.45	21.25		0.00	30	30
Preheat finish	14.48.50	31.34	10.09	605.40	120	90
Weld run 1-start	14.50.00	32.50		675.00	120	100
Weld run 1- finish	14.54.00	36.50	4.00	915.00	190	160
Weld run 2 - start	14.56.50	39.34		1085.40	190	160
weld run 2 - finish	15.01.00	43.50	4.16	1335.00	220	237
weld run 3 - start	15.04.10	46.80		1533.00	210	230
weld run 3 - finish	15.09.00	51.50	4.70	1815.00	250	260
weld run 4 - start						
weld run 4 - finish						
grinding start	15.26.40	1.09.20				
grinding finish	15.45.00	1.27.50	18.30			

Table 1.1 - Time and temperature history of the successful experiment [10]

Unfortunately no clear information is available regarding the exact location of the two points A and B. However, from the sketch shown in Figure 1.10 (from [10]), it could be assumed that they were placed close to the two corners of the cavity.

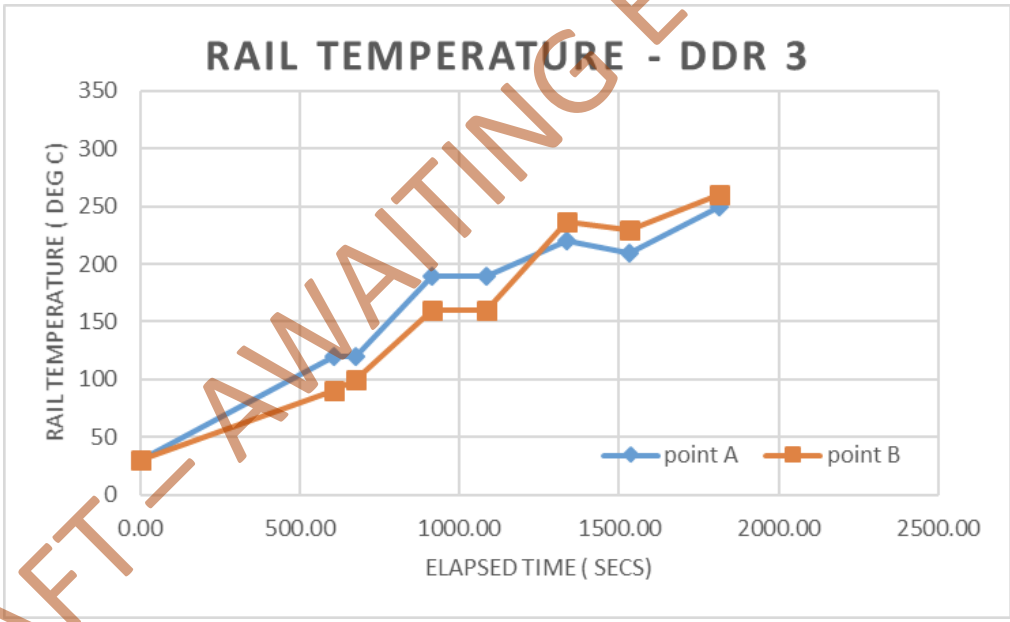

Figure 1.9 – Time–temperature graph for the complete trial in York [10]

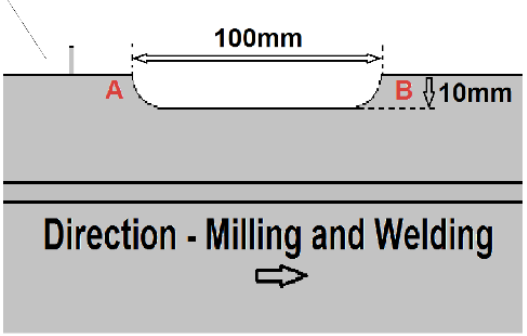

Figure 1.10 – Approximate positions of temperature measurement points A and B [10]

In comparison, Figure 1.11 shows the thermal history for a material point (located exactly at the centre of the cavity in the longitudinal direction and some 7.5 mm in from the gauge face of the rail) in a Flux Cored Arc Welding (FCAW) four-layer experiment carried out by British Steel in May 2008. Note that this graph refers to a different experiment than the one analysed in this Master Thesis. However, since the two repair processes have similarities, the data is still useful in providing a rough picture of the evolution of the thermal fields in the rail and estimate temperatures at which the filler material is deposited in the cavity.

Note the four peaks in Figure 1.11. This is due to the fact that the results refer to a trial in which four layers of welding material were used to fill the cavity. The numerical simulations that will be presented in this report consider three layers in order to match the conditions in the York experiments described above.

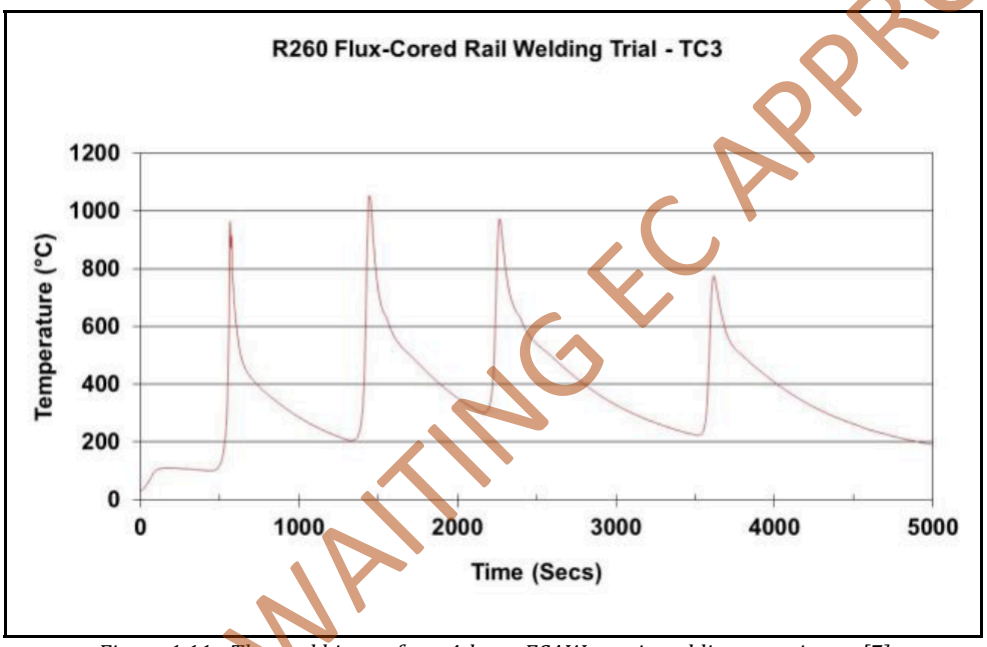

Figure 1.11 - Thermal history for a 4-layer FCAW repair welding experiment [7]

2 Scope & aims

The target of this Master Thesis work is to analyse the thermal history to which the rail material is subjected under the British Steel DDR welding procedure. The main aim in performing such analyses is the possibility of predicting the risk of phase transformations that the steel might undergo when the repair welding process is conducted.

It is indeed undesirable to have martensitic areas in a rail head since these tend to be hard and brittle, whereas an austenitic or pearlitic microstructure has more ductile mechanical properties. Knowing the trend of the rail temperature in time and especially in some critical points close to the weld allows contractors and infrastructure managers to identify where welding cracks or phase changes are more likely to occur, see Figure 2.1. This allows for more detailed inspections to identify and mitigate any such cracks.

Figure 2.1 – Fatigue initiation feature in a MMA weld repair of rail [5]

Some experimental data were obtained during the trial held in York in June 2016. These results are listed in section 1.4. To further investigate the temperatures during the trial, a computer model of the whole area affected by the repair procedure was developed. This model is used to predict the detailed temperature distribution throughout the experiment. Unfortunately due to the uncertainties related to the thermocouples position and reliability, it has not been possible to validate/calibrate the simulations in detail. This will be further discussed below.

The aim of the simulations is to find the thermal history of the rail during the whole welding procedure. Different conditions in which the experiments may be performed are analysed. Temperature fringe and history plots were created for each instant of analysis time. Moreover, temperature evolutions are evaluated for selected material points of interest. These include the centre and the corner points of the cavity where the formation of welding cracks is most likely, and possible positions of thermocouples for comparison towards experiments.

The interesting outcome from thermal histories lays in the possibility of extrapolating the cooling rates that different HAZ regions witness during the repair welding procedures. One can analyse these curves in order to assess whether the cooling rates are too high and the formation of martensite is likely or not.

It can be noted that a detailed transient analysis of this extended thermal process may lead to an excessive use of computer memory, very long computational times and, in the worst cases, numerical issues. Given these considerations, it was necessary to find a reasonable compromise between model accuracy and FE mesh density on one hand, and the computational times and memory usage on the other. This was always done by considering the convergence of results between models of increased detail, and also by comparing simulation outputs to experimental results. More details are presented in the next chapters.

3 FE-model

This section details the three-dimensional finite element model of the repair welding procedure consisting in the deposition of three welding layers. Most of the analysis is focused on studying temperature trends and cooling rates in the HAZ.

A reference case (in which the cavity has the geometry provided by British Steel) will be described in detail. Other models are then presented by highlighting differences with respect to the reference case.

The FE model was created with the software ABAQUS 6.14-2 [12] and most of the work was performed in the CAE interface. For the simulation of the welding process the ABAQUS Welding Interface (AWI) plug-in (version 2014) developed by Simulia South [13] was uses. More details about the numerical simulations are given in the following sections.

Different model configurations were considered. The output of the simulations was compared to the experimental results in order to evaluate robustness and reliability. Moreover, some sensitivity analyses were carried out.

3.1 Geometry

3.1.1 Rail

Rail dimensions are taken from the official definition of the rail profile 60E1 (UIC60) given by Banverket (which is nowadays part of Trafikverket, the Swedish Transport Administration), see Figure 3.1 and [15].

The York experiment was carried out on a 56E1 piece of rail, but the differences in dimensions are negligible from a thermal point of view. This especially relates to the rail head area [15], see Figure 3.1.

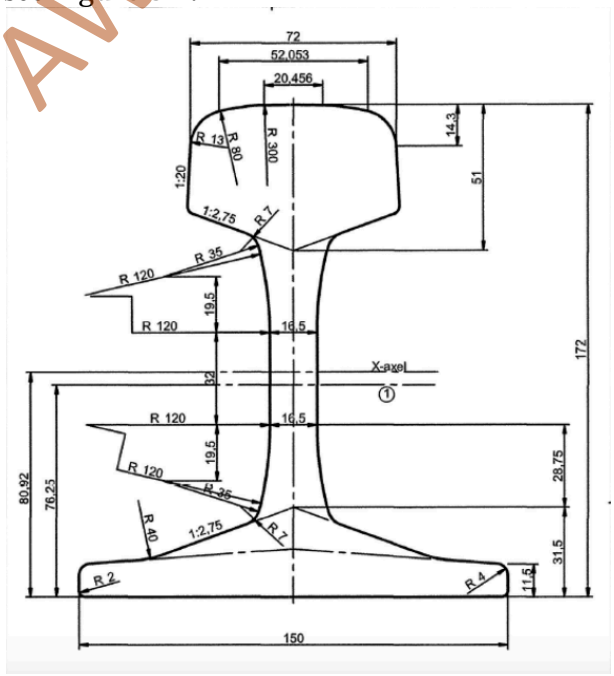

Figure 3.1 – Rail profile 60E1 (also known as UIC60) [15]

In order to keep the complexity of the model within an acceptable level, the rail foot has not been included in the model. Instead, a representative mechanical boundary condition was imposed on the rail head bottom surface. Moreover, the lower part of the head was assumed to be flat (the thermal gradients in this region are negligible with respect to those occurring close to the cavity, so the influence of the simplification is very minor).

The height of the rail head varies between 37.5 and 51 mm (see Figure 3.1).The modelled rail head employed the average height of 44 mm.

Since the model is aimed at simulating the thermal effects on the area surrounding the cavity, one of the problems was deciding the required length of the rail model. The deposition of the filler material warms up the metal below the cavity, but also leads to thermal conduction along the rail. Since the conduction acts as a thermal sink, it is important that the modelled length of the rail is sufficient to capture this effect. On the other hand, modelling a very long piece of rail would lead to significantly heavier simulations. Based on convergence studies, the final model employed length of 250 mm, see Figure 3.2. That means that 75 mm of rail were placed on each side of the 100 mm long cavity.

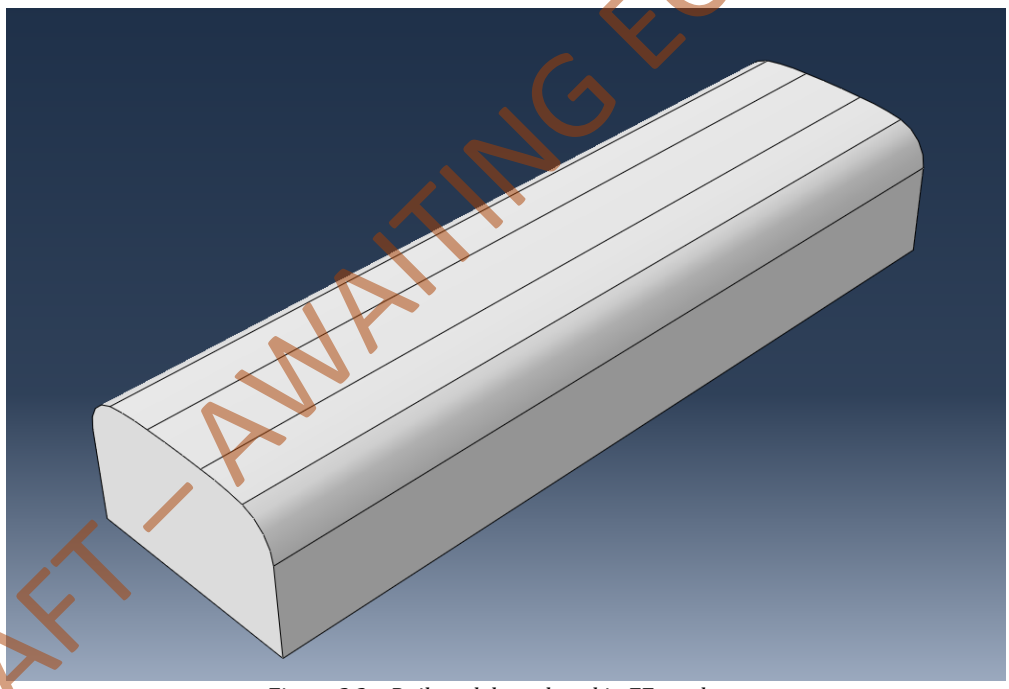

Figure 3.2 – Rail model employed in FE-analyses

3.1.2 Cavity

The shape of the cut-out was one of the main concerns that this Master Thesis work should have examined. The geometrical characteristics of the two corner points can be decisive from the point of view of cooling rates and the formation of welding cracks.

The modelling of the cavity was set out from the drawing in Figure 3.3, which illustrates the standardised dimensions of the cavity for the British Steel experiment [16] where the excavation is 100 mm long and 10 mm deep. It spans throughout the whole width of the rail (about 72 mm). The lateral walls are inclined 45° and transition to the bottom of the cavity is presented by two fillets with a 5 mm radius.

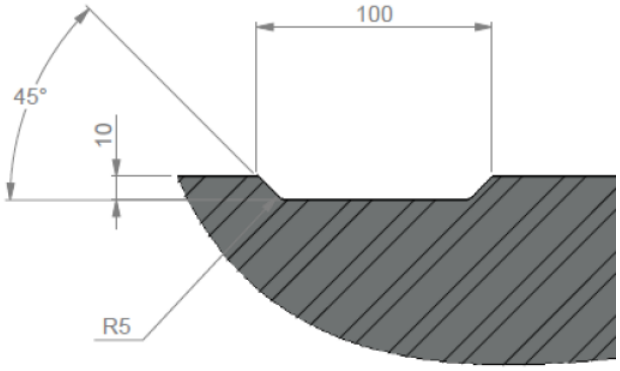

Figure 3.3 – The official geometry for the cut-out, dimensions are in millimetres [16]

However, from pictures taken during the day of the experiment (see e.g. Figure 3.4), it seems that the geometry differs significantly from the one in Figure 3.3. More specific, the corners look a bit sharper, as if the fillet had a radius smaller than 5 mm.

Figure 3.4 – Actual geometry of the cavity during the York experiments in June 2016 (picture courtesy Elena Kabo)

This uncertainty related to the actual dimensions of the cavity initiated the creation of three different models of the geometry of the cavity.

The first (and main) model was characterised by the geometry given in Figure 3.3. This was the geometry with which the main results were derived and further analyses (such as the sensitivity analyses) carried out. A FE-model featuring such a cavity can be seen in Figure 3.5.

(a)

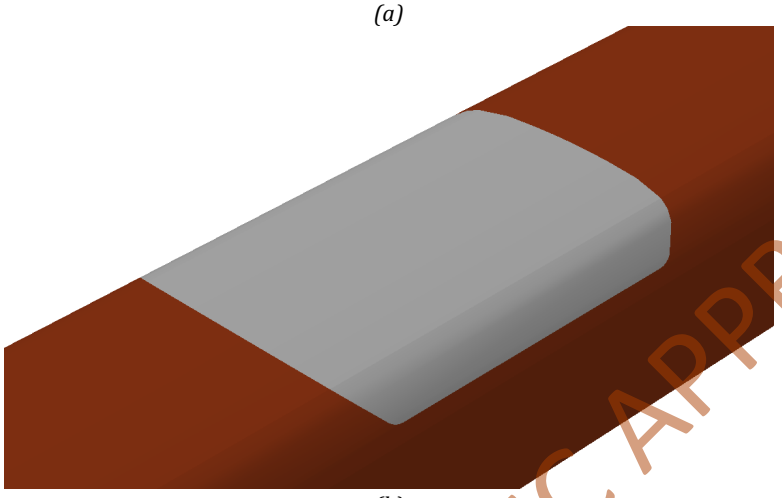

(b)

Figure 3.5 (a) and (b)– FE-model of a rail with a cavity as described in Figure 3.3

Two additional models were created in order to represent two extreme cases regarding the fillet radius: The first model lack inclined walls in the cut out. Instead two rounded fillets with a radius of 10 mm connect the bottom of the cavity to the rail head, see Figure 3.6.

(a)

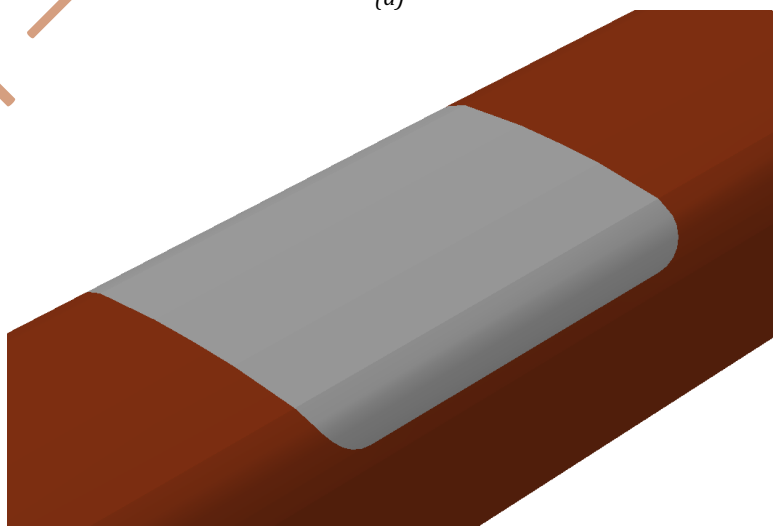

(b)

Figure 3.6 (a) and (b) – FE-model of a rail featuring a cavity with vertical walls built up with radii of 10 mm

The second case considers the theoretical possibility of having a sharp corner (in which the fillet radius is equal to zero) and lateral walls inclined 45° with respect to the base of the cavity, see Figure 3.7.

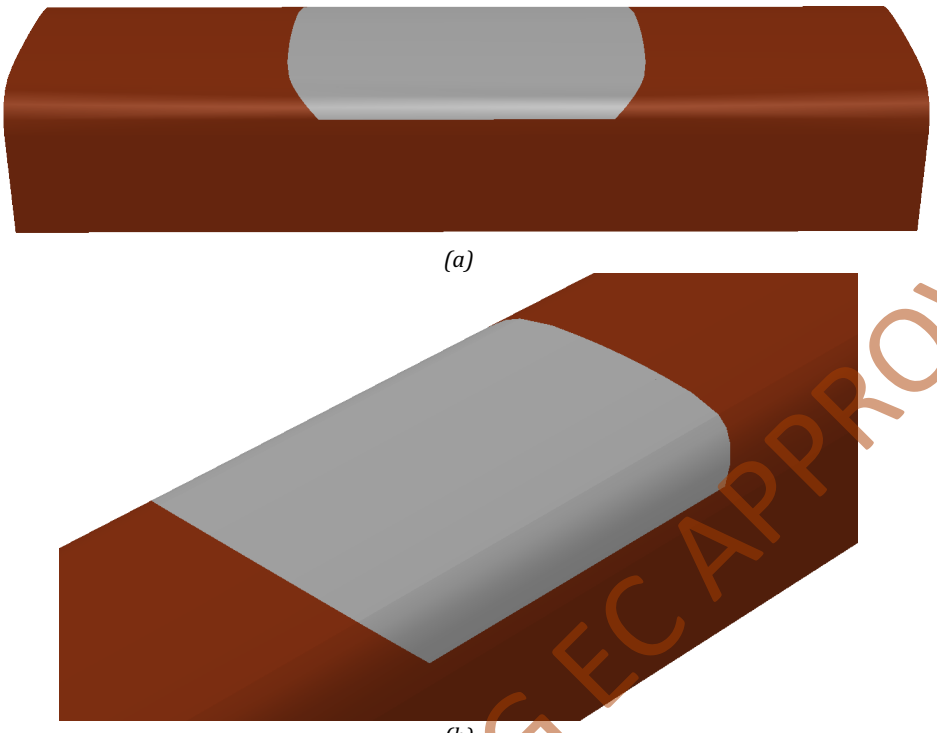

(a)

(b)

Figure 3.7 (a) and (b) – FE-model of rail with a cavity featuring 45° inclined walls with no transition radius

3.2 Boundary conditions

The model is characterised by a multitude of boundary conditions (BC). A small part of these are kept unchanged throughout the whole analysis, whereas the majority of the boundary conditions are activated and deactivated during the different stages of the welding process.

All BC are managed by the AWI plug-in according to instructions given by the user during the definition of the welding process characteristics. Most BC are described in detail in the following sections. In addition, some predefined fields are imposed by the AWI in order to define the initial temperature of the rail and of the filler material.

As for the permanent boundary conditions, it was mentioned in section 3.1.1 that the rail web and foot were not modelled. Instead, they were replaced by a mechanical boundary condition on a strip going through the bottom face of the rail head as seen in Figure 3.8.

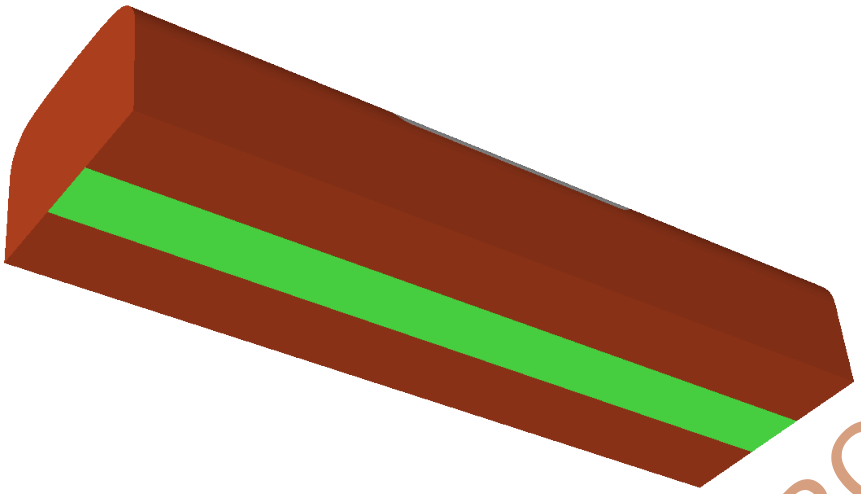

Figure 3.8 – Strip (highlighted in green) where the mechanical BC is applied

Since all analyses carried out for this thesis focused on heat transfer, temperature boundary conditions were extensively used.

First of all, in order to simulate the cooling effect the surrounding track structure has on the temperatures of the repaired area, fixed temperature BC of 20°C (considered as the ambient temperature) were imposed on the right and left vertical end posts of the rail model, see Figure 3.9.

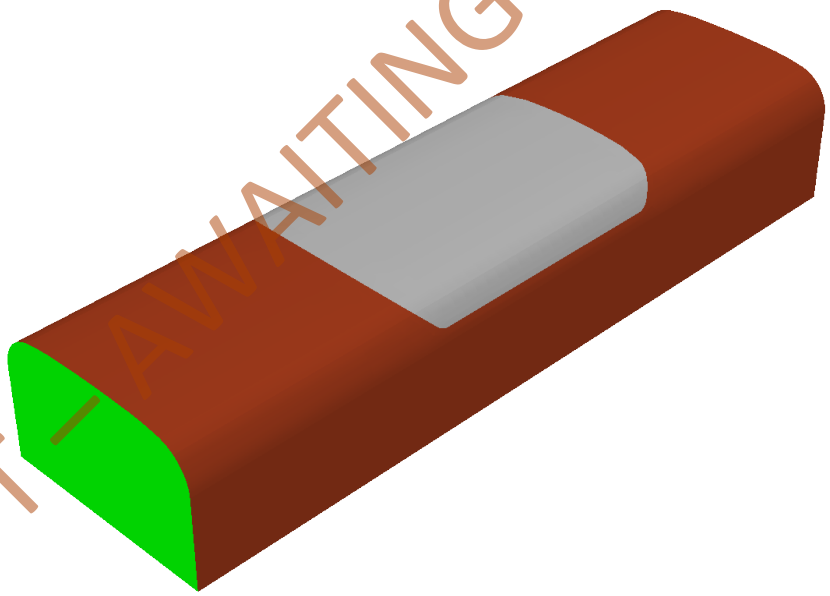

Figure 3.9 – One of the end posts on which the 20°C BC was applied (highlighted in green)

As discussed above, predefined fields were used to describe the initial conditions of the material. In order to simulate the preheating employed in the British Steel welding process, a 80°C field was imposed on the base material of the rail. It is important to consider this temperature since the very low preheat is a distinctive feature of this process as compared to the other methods. Moreover, one objective of the study is to obtain temperature trends in the area affected by the DDR procedure. Here the preheat temperature might have a strong beneficial or negative effect.

Regarding the welding material, no data were provided about the temperature at which it was laid onto the cavity. Some clues came from the temperature trends

registered by the central thermocouple in the 4-layer British Steel experiment shown in Figure 1.11. There it is possible to see that peak temperatures correspond to time instants in which the material is deposited and that the temperatures are always around 1000°C. However, the thermocouples that registered the temperatures were located at a depth of about 2.5 mm from the milled surface [16], therefore the temperature of the molten material must have been higher.

The graph refers to an experiment performed in March 2008 with another type of DDR procedure [7]. The melting temperature for the filler material employed during that experiment was 1510°C and as the material was laid on the cavity in a molten state, its temperature must have been equal or higher than that value [16] [17] (the temperature at which the welding metal is deposited was required by the Welding Interface in order to create appropriate temporary boundary conditions throughout the different analyses). Several temperatures have been employed in the analyses in this thesis. In additions, simulations comparing different filler material temperatures (using the same FE-model) have been performed. The resulting cooling curves have been compared in order to estimate the sensitivity of the analysis, see section 4.3.1.

3.3 Material properties

3.3.1 Rail material

The repair welding procedure on which the analyses are focused is meant to be performed on the conventional rail grades R220 and R260. The experiments were carried on a R260 piece of rail. Consequently R260 material data have been employed in the analyses. The main chemical composition of the R260 grade rail steel are presented in Table 3.1. The steel density is 7850 kg/m^3 according to [17].

Element	C	Si	Mn	P	S
wt. %	0.73	0.297	0.998	0.014	0.017

Table 3.1 – Chemical composition of R260 grade rail [17]

Regarding temperature dependent elastic properties, it was recommended by British Steel [17] to use values belonging to BS060A55, a medium carbon steel with a carbon content in the range between 0.3% and 0.5% in weight. The data used in the analyses are listed in Table 3.2.

Temperature [°C]	**Young's modulus [GPa]**	**Poisson's ratio**
20	210	0.280
50	209	0.282
100	207.5	0.284
200	202	0.289
400	186.5	0.299
600	165	0.310
650	158	0.314
700	136.5	0.326

Table 3.2 – Temperature dependent elastic properties of the BS060 A 55 medium carbon steel [17]

The thermal conductivity data, which are fundamental for the analyses, were taken from those of a 0.8% C eutectoid steel, see Table 3.3, since they are not expected to vary more than 0.07% with respect to the actual R260 grade ones [17].

Temperature [°C]	0	50	100	200	300	400	500	600	700
Thermal conductivity [W/m/°C]	49.8	49.4	48.1	45.2	41.4	38.1	35.2	32.7	30.1

Table 3.3 – Thermal conductivity for an eutectoid steel [17]

According to the recommendations from British Steel [17], additional thermal properties (specific heat capacity and expansion coefficient) should be similar to those of a medium carbon (0.55%) steel, see Table 3.4.

Temperature [°C]	**Specific heat capacity [J/kg/K]**	**Thermal expansion coefficient [10^{-6} °C^{-1}]**
20	430	
50	450	11.35
100	480	11.65
150	505	
200	530	
300	565	
400	610	13.70
500	670	
600	760	14.65
700	710	10.65

Table 3.4 – Specific heat capacity and thermal expansion coefficients for a medium carbon steel [17]

3.3.2 Filler material

The filler material comes from a self-shielded flux-cored wire. Its name was "OK Tubrodur 15.43", but has now been rebranded as "ESAB Tubrodur 35 OM". It is a common material for basic welding of railway and tram tracks.

According to the ESAB catalogue [18], the chemical composition of the all weld metals are as presented in Table 3.5:

Element	C	Si	Mn	Cr	Ni	Mo	Al
wt. %	0.14	0.3	1.1	1.0	2.2	0.5	1.5

Table 3.5 – Chemical composition for OK Tubrodur 15.43 [14]

The information in the catalogue was not focused on the thermo-mechanical properties which are important in heat transfer analyses. However, as stated in [19], the thermal characteristics of ESAB Tubrodur 35 OM are approximately similar to those of a low carbon steel. Consequently, data for a steel containing between 0.15% and 0.23% of carbon were used [17], these data are presented in Table 3.6 to Table 3.8. A typical density for steels (7800 kg/m^3) was presumed.

Temperature [°C]	Young's modulus [GPa]	Poisson's ratio
20	212.4	0.288
100	208.9	0.290
200	201.3	0.293
400	184.1	0.300
600	166.2	0.306
650	157.2	0.311

Table 3.6 – Elastic properties for a 0.15 % carbon steel [17]

Temperature [°C]	20	50	100	200	300	400	500	600	700
Thermal Conductivity [W/m/°C]	52.0	51.7	51.0	48.8	46.0	42.7	39.2	35.2	26.5

Table 3.7 – Thermal conductivity for a structural 0.20% carbon steel [17]

Temperature [°C]	Specific Heat Capacity [J/kg/K]	Thermal Expansion coefficient [10^{-6} °C^{-1}]
20	440	
50	450	11.92
100	480	12.18
150	505	
200	530	
300	565	
400	610	13.47
500	675	
600	800	14.41
700	1340	14.88

Table 3.8 - Thermal properties for a structural 0.20% carbon steel [17]

3.4 Discretisation

3.4.1 Weld beads

For the reasons described in section 3.3.2, three different geometries for the cavity were created. In all cases, the cavities were not modelled in ABAQUS/CAE as a separate part, but as a partition of the rail. The two materials (R260 grade and OK Tubrodur 15.43) were defined in the model with material properties given in section 3.3.

As for the different weld beads, they were modelled by means of rectangular chunks. Since the cavity was 10 mm deep and was fully covered with three layers as in the trials in York [10], the first two layers were partitioned in order to be 3 mm thick and the last layer featured a (maximum) height of 4 mm, see Figure 3.10. The depth was measured from the highest point of the rail head, as a consequence of the rounded rail head, the average thickness was therefore lower than 4 mm.

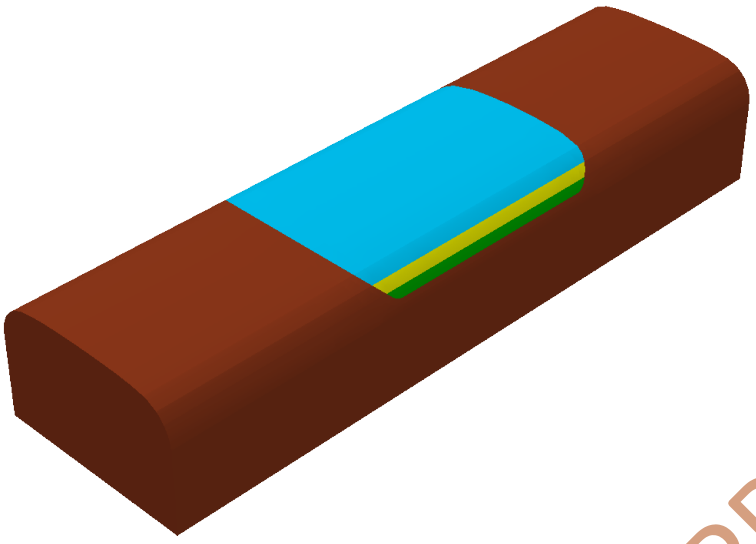

Figure 3.10 – The three welding layers represented in the main model

Another problem was estimating how many beads (i.e. welding segments) were used in the trial held in York in order to complete a layer. No exact information was provided from the experiments. A realistic estimation was made based on Figure 1.7 and other similar pictures taken during that day. The conclusion was that around 20 to 22 passes were needed to cover the surface of the cavity. For this reason the bottom layer was split in 20 parts by means of appropriate partitions in ABAQUS/CAE, see Figure 3.11.

Figure 3.11 – The different weld beads represented on the first layer of the main model

As can be noticed in Figure 3.5 to Figure 3.7, the surface covered by the welding layers increases as they get more distant from the bottom of the cavity. In order to keep the volume of filler material laid by each pass somehow constant, the two upper layers were modelled with 22 beads. This was useful also to take into account the longer time needed to complete the last layers, see Table 1.1.

As seen in Figure 1.7 and described in section 1.3, the final rail geometry cannot be reached by just filling the cavity with the welding material. Some slag has to be removed after each pass and the welding nozzle has to be carried back to its original position. Those operations took on average 3 minutes per pass, see Table 1.1, and allowed the repaired area to cool down. As a consequence, some intercooling steps of 180 seconds each were introduced in the simulation model after the completion of each welding layer. In addition, some material in excess is expected to be found on both the weld sides and the top, and that has to be taken away at the end of the process by means of grinding.

However, the final grinding phase (like the milling at the beginning of the process) has no significant effect on the thermal history, nor on the metallurgical transformation of the material. Therefore it will not be considered throughout the following numerical analyses. As a consequence, the computer model of the welding process will just assume that the exact geometry is reached directly after the three welding passes.

3.4.2 Finite element mesh

The fact that the different weld beads were modelled as partitions in ABAQUS/CAE was primarily due to the requirements set by the AWI. Some more complex partitions, were introduced in the areas of the cavity corners and close to the rail head radii (where the elements tend to be very distorted, see Figure 3.12).

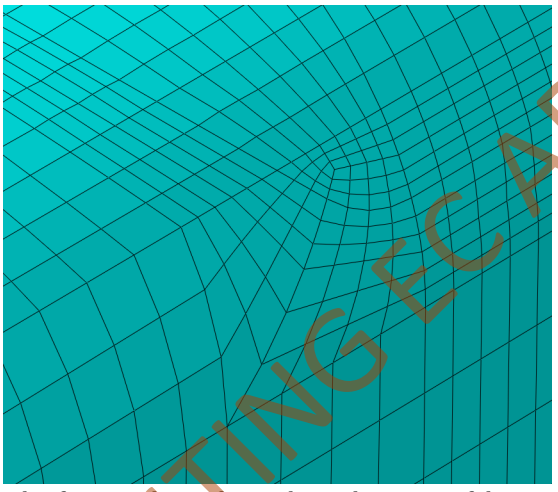

Figure 3.12 – An example of a critical area for meshing: the corner of the cut-out in the main model

Moreover, some vertical partitions were extended up to the base of the rail to keep the element shape as uniform as possible and to split the weld beads in smaller sections called chunks. This allowed improved simulations of the moving source of heat and the gradual addition of material.

The model was partitioned in such a way that the entire cut-out volume could be meshed by using either a structured or a swept mesh. A structured mesh is generated by Abaqus by adapting the mesh of regular and simple regions (such as squares, triangles, etc.…) onto the complex geometries of the models. A sweeping mesh is instead defined by creating a 2D mesh on a source side according to the instructions given by the user (e.g. element size, number of elements on specific areas, bias ratio, etc.) and copying these mesh nodes onto a series of layers until the mesh reaches the target side.

In order to use the AWI a swept mesh was necessary in the area filled by the welding material. The reason is that when the plug-in defines the different weld passes the paths of these are identified by using that the mesh is swept along the welding direction. For this reason, a swept mesh was used in the welded area. For the rest of the model (i.e. for the base material) a structured mesh was used.

Regarding the type of elements, heat transfer elements of DC3D8 type were chosen. These are 8-noded linear heat transfer bricks which belong to the ABAQUS' standard element library. They have the nodal temperature as their degree of freedom.

The main criteria for a good mesh were employed here:

- A finer mesh in areas of analytical interest and in the expected zones of stress concentration (or, in this case high temperature gradients). For the current analysis, this implied the cavity corners and the welded area.
- Low element distortion with aspect ratios below 5, element corner angles between 45° and 135°.

These characteristics were pursued by applying appropriate bias ratios on critical areas and by seeding the most important edges.

A vital aspect of the meshing process is the sensitivity analysis. It is well known that if the mesh is too coarse or the elements are too skewed then FE simulations may result in significant errors. The robustness of the output and the reliability of the mesh can be evaluated by comparing simulation results with the experimental ones and/or by performing a convergence analysis with gradually refined meshes. When the results of two consecutive meshes (essentially) converge, the coarser mesh is sufficient for the analysis.

A sensitivity analysis was carried out in the study. Details and output are presented in section 4.1.

3.5 Modelling of the welding process

The modelling of the thermal history of a welding process in ABAQUS/CAE requires the definition of many steps, introduction of boundary conditions with subsequent deactivation (and reactivation) of the different partitions in order to simulate the gradual addition of the welding material. This approach can get very time consuming, especially if the model is characterised by a large number of welding beads, such as in the current study.

In order to reduce computational times for repetitive actions (e.g. activating and reactivating temporary BCs, defining the surfaces on which conduction and radiation act on each step, etc.) the ABAQUS Welding Interface (AWI) plug-in can be employed. The AWI has been discussed in the previous sections of this report, but it will now be described in detail.

3.5.1 Weld definition

Once the model has been created, materials have been defined and the full geometry was meshed, the AWI could be employed for the welding process definition. First of all, it was necessary to define welding order and path. Since the interface expects weld passes to be straight, a swept mesh was required in the weld area (as discussed above).

Three different welds were defined (one for each layer) and the beads were chosen according to the welding order used to fill the cavity with a zig-zag path which moved from one wall of the cavity to the opposite one. Once the beads were defined, the interface automatically created chunks according to the vertical partitions of the rail.

The interface then used chunks in order to split each bead in smaller parts. The gradual addition of filler material can thus be discretised by a sequential activation of these small volumes.

3.5.2 Pass and job definition

The AWI required information on the single passes and on the characteristics of the analyses. With the term "pass", the interface considers a part of a weld bead that is activated in a single step during the analysis process.

As a consequence, the definition of a very high number of passes for each bead makes the analysis very close to the reality, i.e. to the gradual addition of the filler material. On the other hand, every time a pass is defined, the interface has to create a large number of steps, interactions, temporary boundary conditions, etc. Thus, the analysis gets extensive and slow. A trade-off analysis was made where it was found to be appropriate to define three passes for each weld bead, i.e. between 60 and 66 passes for each layer, see Figure 3.13. This can be compared to the fact that the interface tends to crash during the job definition phase if the number of passes goes above some 300–400.

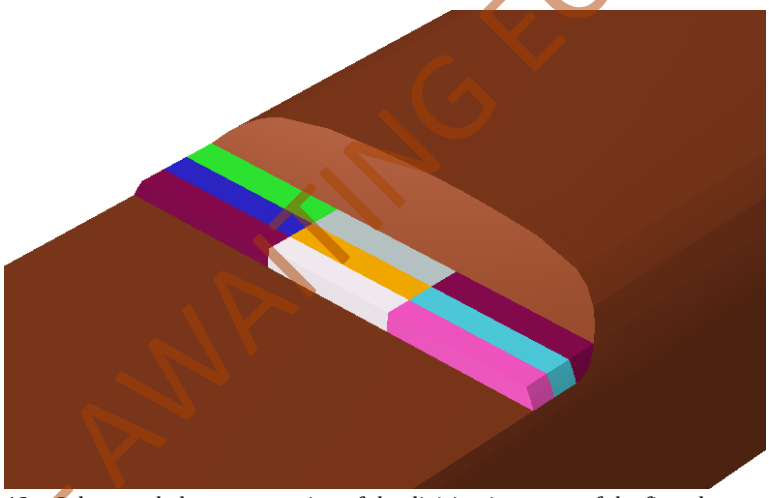

Figure 3.13 – Colour-coded representation of the division in passes of the first three weld beads

At this point, the interface requests information regarding the timing of the process. In order to keep the welding time around 4 minutes (or slightly above for the last layers, according to the trials in York [10]), each pass was set to have a time period of 4 seconds. This period was split in several time increments by the analysis software according to the temperature variation trend.

3.5.3 Temporary boundary conditions

After the different passes were defined, the AWI was provided with some data on the thermal characteristics of the process.

First of all, as discussed in the previous section, the temperature at which the molten welding metal is laid was requested. The technical staff from British Steel [16] estimated that temperature to be above 1510 °C, but the comparison between the numerical results and the thermal histories recorded during some trials [16] suggested that the filler material temperature could be as high as 1700 °C, see section 4.3.1.

The given values were used by the AWI to apply temporary temperature boundary conditions on the surfaces on which the filler was deposited, and for the amount of time that was required in order to complete each single pass (4 seconds in all the analyses described in this report). After that, the software activated the quantity of material corresponding to the filler deposit during the pass. The filler was applied at the requested predefined temperature according to what was specified in the interface settings. In the following step, the interface applied the same BCs on the areas affected by the subsequent pass, while the material belonging to the previous step was allowed to cool down.

Data regarding the metal-to-air convection were also needed. Unfortunately no precise information has been provided regarding this property for the R260 rail steel and for ESAB Tubrodur 35 OM. Instead, a reasonable value for steels was used (25 J/s/m^2/K) [13]. The convection interaction was applied on the whole free surface of the rail (apart from the bottom surface and the end posts, where an ambient temperature condition was imposed). Moreover, the plug-in created some small surfaces corresponding to the faces of the cavity and of the weld beads on which the convection interaction could be activated and deactivated. That depended on whether those areas were in contact with air or not during a certain stage of the repair process.

3.5.4 Intercooling steps

As mentioned in the description of the process, some time was spent in between the deposition of the different layers in order to remove the slag and to prepare the procedures needed for the completion of the next welding phase. Although, according to [10], the time required to carry this operation was not fixed, it was possible to notice that it was around 3 minutes (Table 1.1). During that time frame, the rail was allowed to cool down, which had an effect on temperature and, subsequently, on the thermal behaviour during the deposition of the following layer.

For the sake of precision and realism, three "cooling steps" of 180 seconds were defined after each welding phase in the simulations. To make the cooling process more realistic, these steps were characterised by the same boundary conditions and interactions which were active at the moment in which the last welding pass was laid. A final cooling step of 180 seconds was defined after the end of the whole filling process (i.e. at the end of the deposition of the third layer) in order to be able to predict the cooling characteristics of the whole repaired area after the completion of the welding procedure.

3.5.5 Thermal fluxes

Two different types of thermal fluxes were taken into account: thermal conduction within the material, and the convection between the air surrounding the rail and the filler material.

Regarding thermal conduction, its magnitude is mainly dependent on the thermal gradient and the conduction coefficient, see equation (1) [12].

$$q_c = -k \cdot \nabla\theta \qquad (1)$$

Here $q_c(x,t)$ is the heat flux density [W/m^2], $k(\theta)$ the material conduction coefficient [W/m/°C] (which depends on whether the heat flux is computed within the rail or the filler material and on the current temperature, as detailed in section 3.3), $\theta(x,t)$ [°C] is the temperature at a certain material point at a certain time.

According to the numerical results, thermal conduction was the main form of heat exchange within the model. However, convection between the rail material and the surrounding air has been fully considered in the analyses. Convection, q_s, can be estimated from

$$q_s = -\mathbf{n} \cdot h \cdot \nabla\theta \qquad (2)$$

This is the boundary term of the general convection law [12]. Here, h is the steel-to-air convection coefficient, whose average value is 25 [W/m^2/°C] [13] and $\mathbf{n}$ represents the normal vector of the surface which is affected by convection.

4 Results

4.1 Sensitivity analysis

As discussed in section 3.4.2, a sensitivity analysis was performed in order to evaluate the robustness of the mesh and of the whole modelling of the process. It was considered sufficient to perform these checks only on the reference model (with the cavity geometry defined by British Steel). All other models were then meshed using similar meshes to the sufficiently fine mesh identified by the sensitivity analyses.

Three different meshes were created for the model with the reference geometry. The "coarse" mesh was characterised by elements with a maximum size of 5 mm. In the most important areas (i.e. the corners of the cavity and the rounded surfaces at the sides of the third layer), the element edge was 0.51 mm. The "medium" mesh featured a maximum element size of 3.5 mm and an edge size of 0.35 mm in the vicinity of the corners. The "fine" mesh was characterised by a maximum element size of 2.5 mm which progressively decreased to 0.25 mm near the cavity. The mesh characteristics are summarised in Table 4.1.

Mesh type	Number of DOF in the whole model	Coarsest element size [mm]	Element size close to the corners [mm]
Coarse	29667	5	0.51
Medium	110259	3.5	0.35
Fine	160977	2.5	0.25

Table 4.1 – Characteristics of the three evaluated meshes

Figure 4.1 and Figure 4.2 show the differences between the three meshes in the corner areas

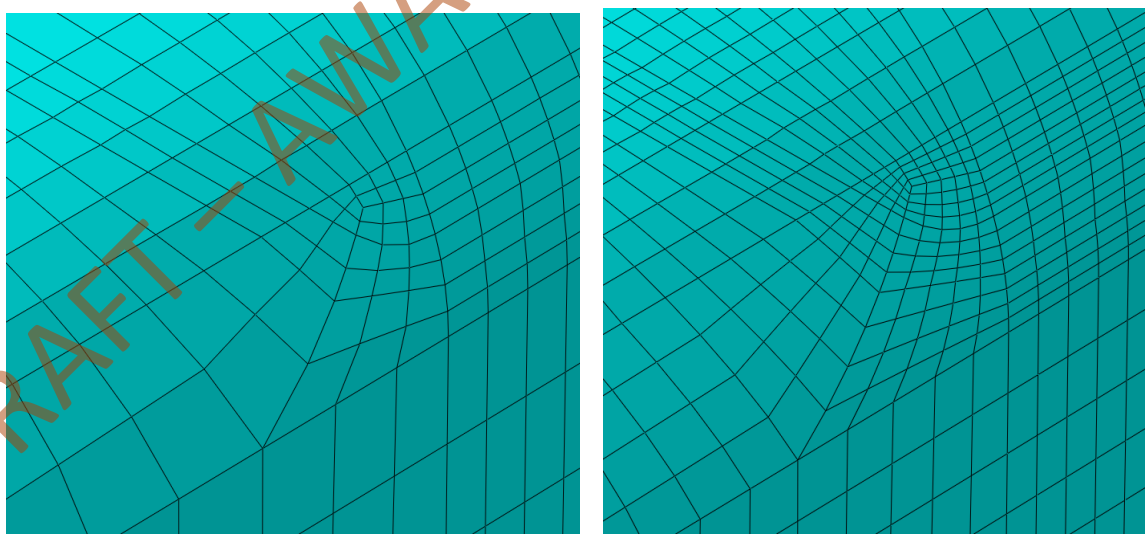

Figure 4.1 – The cavity corner with the "coarse" mesh (left) and the "fine" mesh (right)

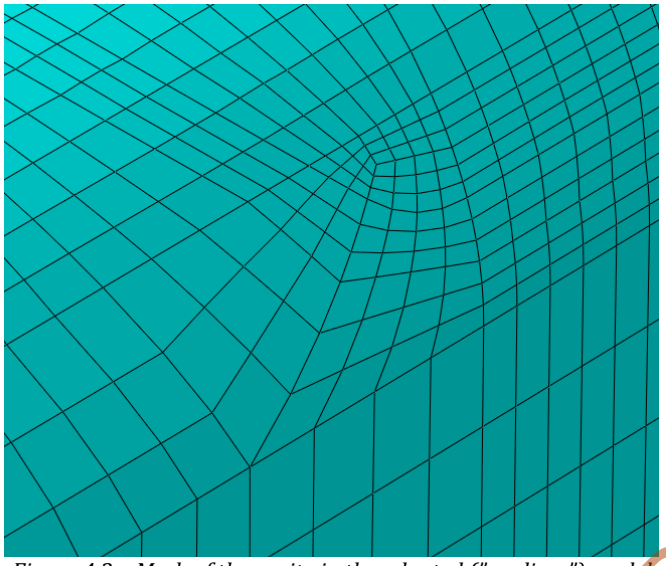

Figure 4.2 – Mesh of the cavity in the adopted ("medium") model

The way the whole rail head was meshed in the final model using the "medium" mesh is shown in Figure 4.3. It is possible to see that the areas with the finest mesh are the areas in the vicinity of the corners, the rounded surfaces and the border areas between the filled cavity and the base material.

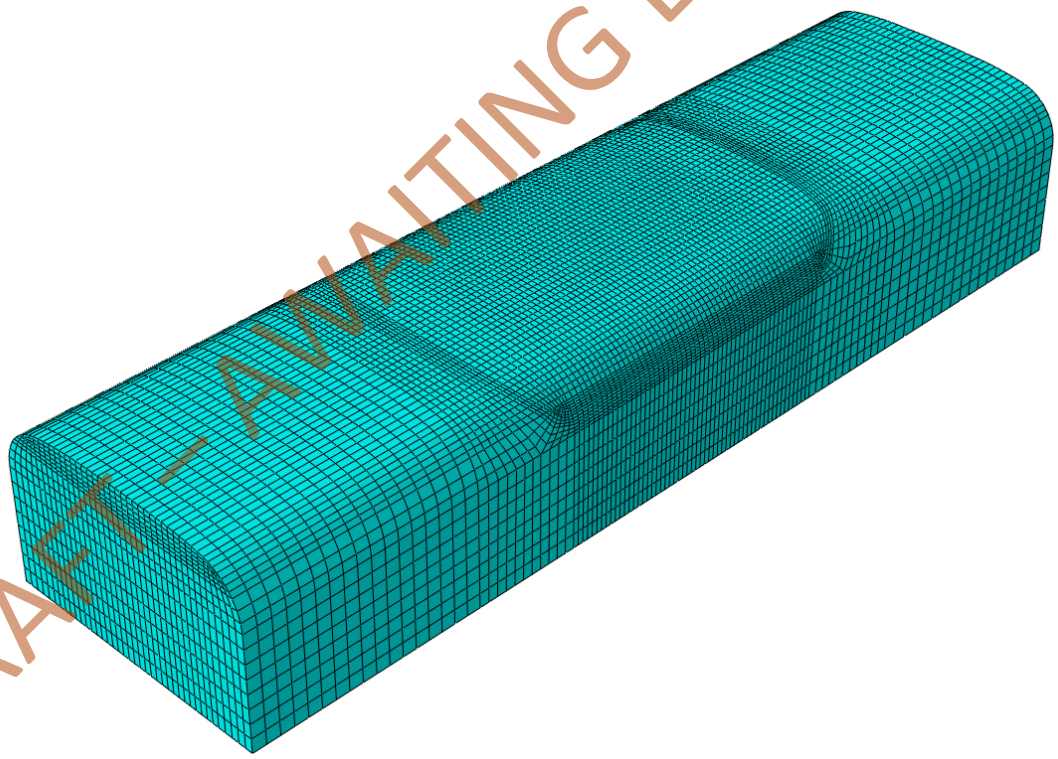

Figure 4.3 – Completed mesh of the "final" model

After applying the same steps, temperature fields, boundary conditions, etc. three different analyses were run on the three models. The results were compared in order to check the mesh convergence. To make this report more synthetic and easier to read, only some results are presented in this section. Remaining results are presented in Appendix A.

4.2 Robustness analysis

Three points in FE-models were chosen for the sensitivity analyses. These were located in some of the most interesting parts of the models, i.e. close to corners, close to the inclined walls and at the centre of the cavity, where the cooling effect due to convection is minimal.

The first point, here referred to as "SA-L" (which stands for "sensitivity analysis – left") was located close to the corner where the welding process started, exactly 2.4 mm from the cavity, see Figure 4.4. The sensitivity analysis focused not on the full thermal history, but data from significant instants in time. For this reason, only temperature peaks and minima in this point are compared for the three meshes. Evaluated temperatures are presented in Table 4.2:

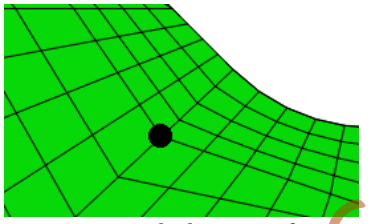

Figure 4.4 – The location of SA-L

Moment	Time instant [s]	Temperatures [°C] and mesh			coarse-medium difference [%]	medium-fine difference [%]
		coarse	medium	fine		
1st peak	8,4	567,7	562,2	561,1	0,97	0,20
1st minimum	421	161,3	157,9	156,6	2,11	0,82
2nd peak	429	479,3	473,9	474,2	1,13	0,06
2nd minimum	865	184,3	179,4	178,2	2,66	0,67
3rd peak	887	442,9	432,5	431,4	2,35	0,25
3rd minimum	1308	194,6	189	188,1	2,88	0,48

Table 4.2 – Temperature values for the FE-node SA-L for the three different meshes

It may be noticed that the difference in results between the meshes designated "coarse" and "medium" is around 2%. That value can already be considered acceptable, but since the element shapes for these meshes were slightly distorted in the areas close to the corners, a third "fine" mesh was prepared. Differences between this "fine" and the "medium" meshes at crucial points ranged between 0,06 and 0,82 per cent. At this point, it was clear that the "medium" mesh was reliable and robust enough to perform thermal analyses with.

It is worth mentioning that for the sensitivity analysis, a standard load case (e.g. employing a predefined temperature of 1150 °C) was used for the filler material. Since the robustness tests had given such a reliable output, it was not considered necessary to perform them again for every change in the analysis procedures.

The full thermal history of the SA-L node according to the medium mesh can be seen in Figure 4.5:

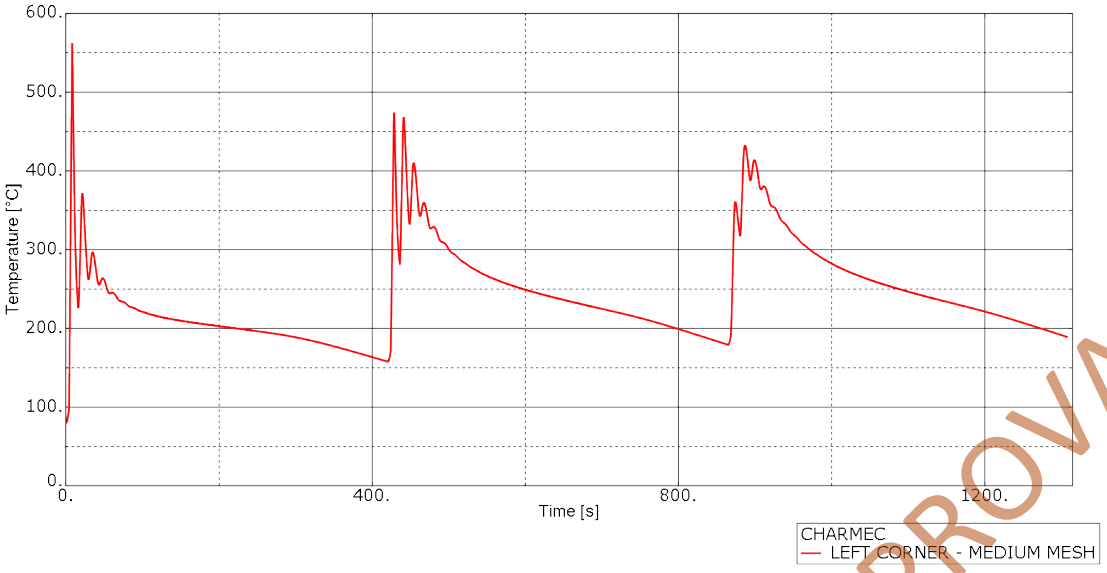

Figure 4.5 – Thermal history for the SA-L node in the final mesh

A comparison of the full thermal history of the point SA-L for all three meshes are presented in Figure 4.6 as the second layer is applied, and in Figure 4.7 as the third welding layer is deposited in the vicinity of the SA-L test node.

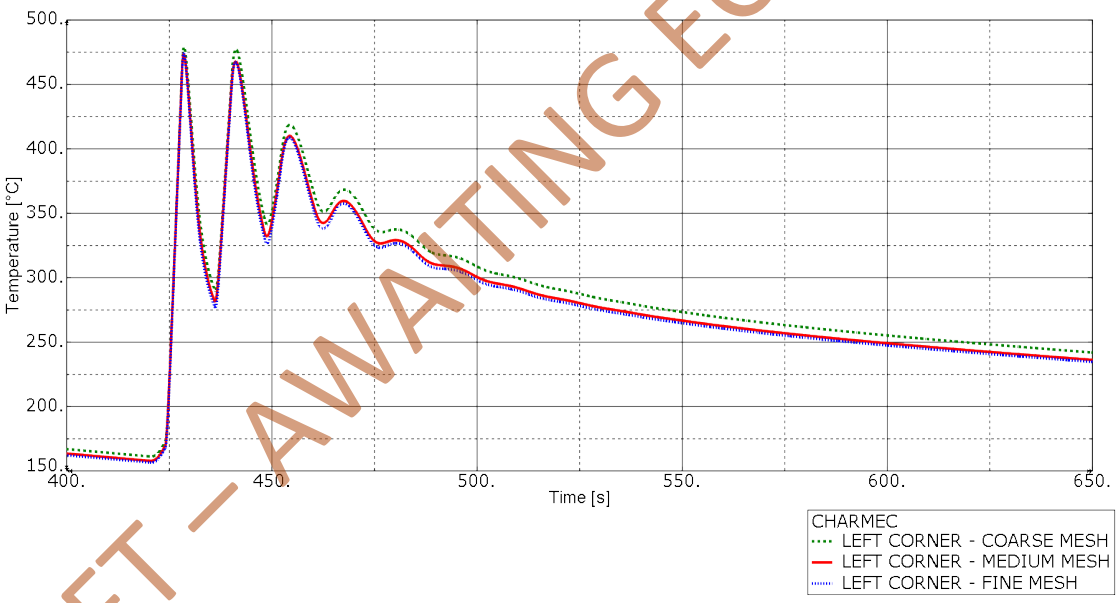

Figure 4.6 – Comparison of the time histories evaluated using the three meshes in point SA-L at instances in time associated to the second layer

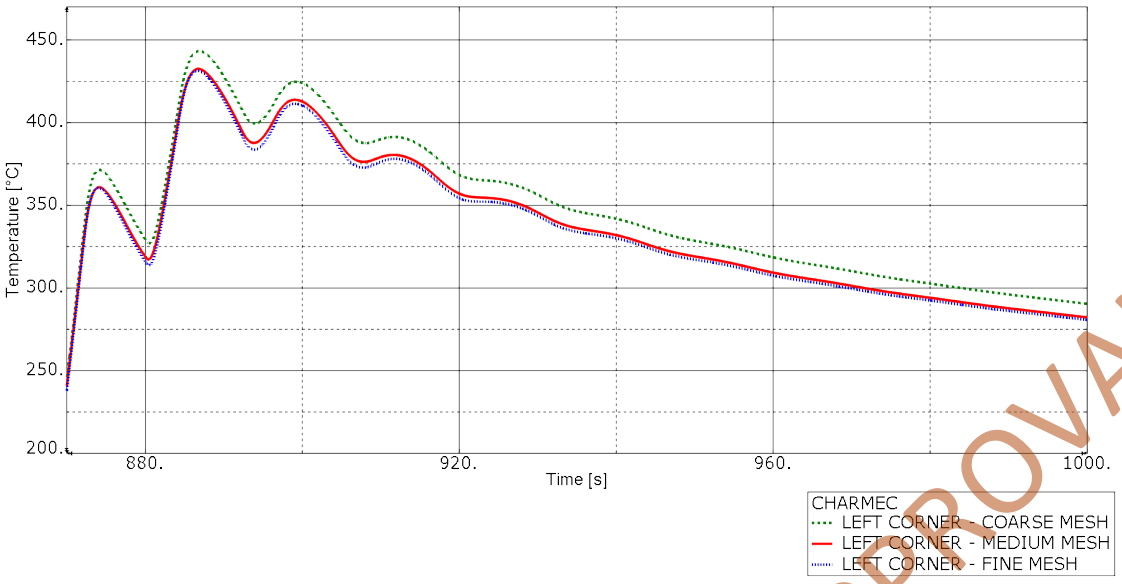

Figure 4.7 - Comparison of the time histories evaluated using the three meshes for the point SA-L for instances in time associated to the third layer

It can be easily noticed that the differences between the three meshes are only visible if the figures are zoomed in. In particular, the discrepancies between the ”medium” mesh and the ”fine” mesh are negligible.

Similar considerations were made for the other two test nodes. Results for these studies can be found in Appendix A.

4.3 Thermal history results

Different types of thermal history plots were produced during the analysis phase and results were compared with those of a similar experiment that was carried out on the same cut-out geometry by British Steel in 2008. That experiment, however, took a different amount of time with respect to the one simulated and analysed in the present study (according to the experiment in York in June 2016 [10]) and consisted of four welding passes [7].

The importance of the trials held in 2008 relates to the fact that five thermocouples were mounted in different points of the base rail material. In the experiment held in York in June 2016 no thermocouples were used and, as a consequence, there was no thermal data on which to calibrate the simulations and/or to validate the numerical results [10].

Figure 4.8 shows the position of the five thermocouples during the trials in 2008. The welding square weave path, in that case, started on the left-hand side of the picture (on the side corresponding to the thermocouple TC1) and proceeded towards the right (as in Figure 4.8), where the thermocouple TC5 was placed. In order to make the simulation results easier to compare, the same numbering order that was used for the thermocouples in the 2008 experiment was kept for the analysed nodes in the FE-models.

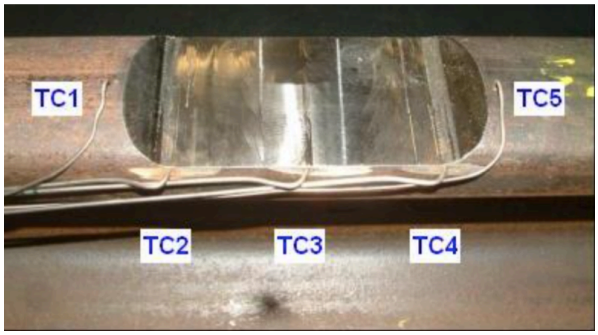

Figure 4.8 – Position of the five thermocouples for the experiment held in 2008 [7]

Two of the five thermocouples (TC1 and TC4) failed during the trial [16], but the other ones were still able to record the full thermal history in their respective locations. The positions of the thermocouples [16] can be seen in Figure 4.9, although it is important to consider that the actual locations might be slightly different due to uncertainties e.g. in hole drilling.

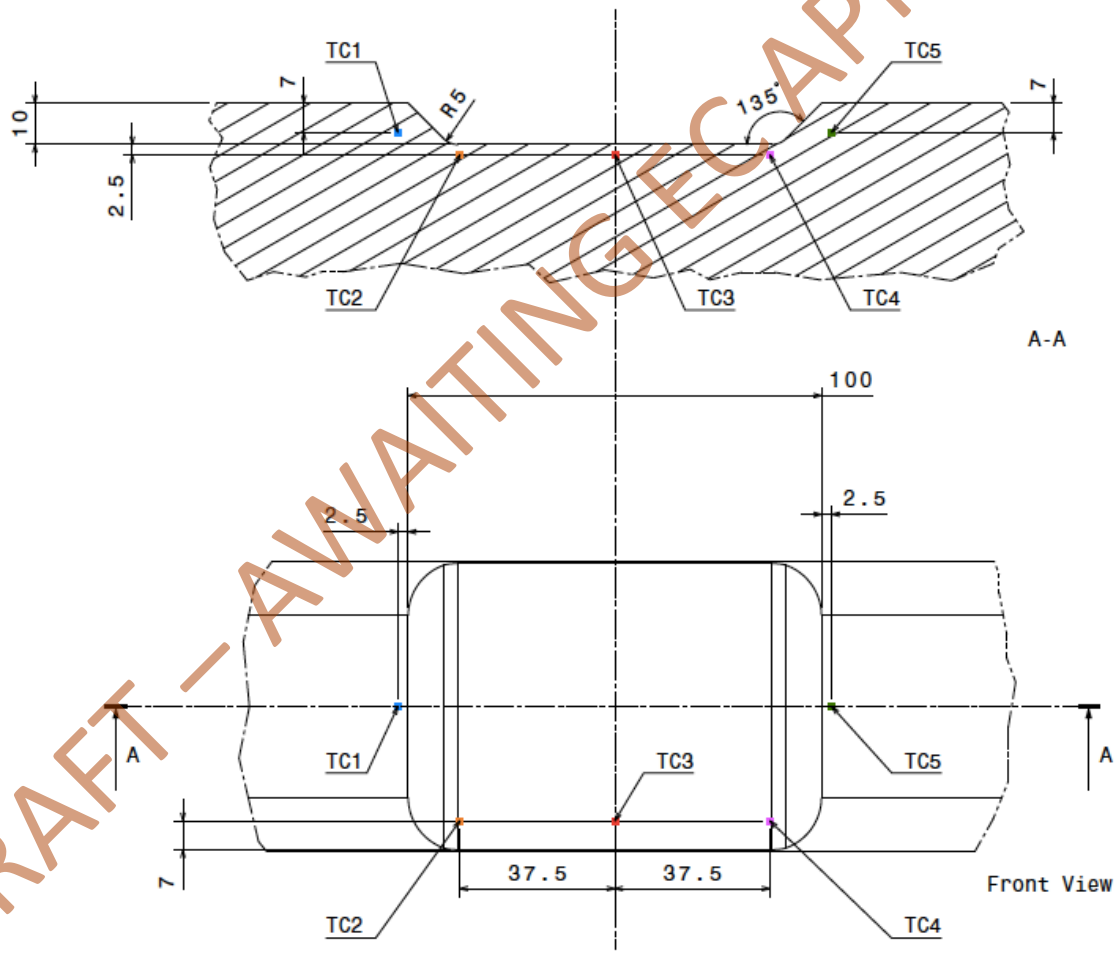

Figure 4.9 – Estimated positions of thermocouples during the experiments in 2008 [16]

4.3.1 Influence of the filler material temperature

The first analyses were aimed at studying the temperatures and the cooling rates in the areas corresponding to the thermocouple positions. Most of the attention was put in studying the effect that the temperature at which the filler material is deposited in the cavity has on the thermal history of the HAZ.

Two different temperatures were investigated for the welding material: 1700 °C and 1800 °C. These gave numerical results from the simulations which were closer to those actually obtained in the 2008 experiment [7].

In this section, just the results for the TC3 (the central thermocouple) and TC5 (the one located on the side of the cavity where the welding process terminates) will be compared. The results from the other TCs are not presented in the present report.

Before proceeding with results, more information about the analysis points will be provided: the node which approximated TC3 was located 3.1 mm below the cut-out, at a depth of 8.3 mm from the rail gauge surface, see Figure 4.10 (a value between 5 and 10 mm is generally used in this case in order to avoid the effect of the thermal convection between the rail surface and the surrounding air [16]).

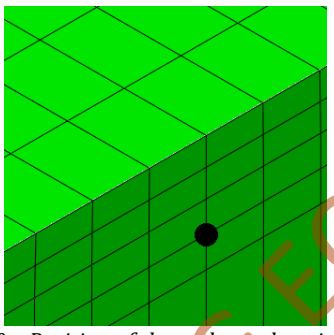

Figure 4.10 – Position of the node used to simulate TC3

The node used to approximate TC5 was located on the rail head centre line, at a depth of 10 mm from the running surface and at a lateral distance of 3.1 mm from the lateral side of the cavity, see Figure 4.11.

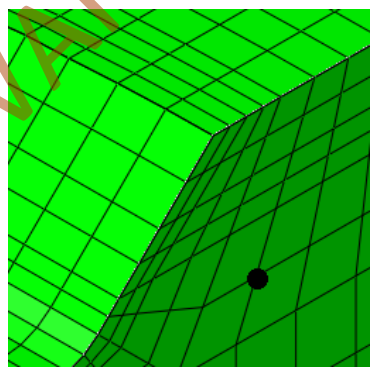

Figure 4.11 - Position of the node used to simulate TC5

At this stage of the analysis the attention was put on the dependency on the filler material temperature. The dependency on the exact location of the point of temperature evaluation (and therefore on the thermocouple position) will be studied in the next section.

Figure 4.12 shows the thermal history that TC3 recorded during the experiment in 2008. Figure 4.13 shows the thermal histories that were obtained in the FE analyses for the different filler material temperatures.

It is worth observing that the preheating phase (which is represented by the initial 400 seconds in Figure 4.12) is not included in the graphs describing the numerical results. That was due to the fact that preheating took 600 seconds, while the rest of the

process was about 1300 seconds long [10]. As a consequence, introducing such long extra time slots would have made graphs more difficult to read. Moreover, heating up the rail from the environment temperature to 80 °C does not have a significant impact on the thermal behaviour of the material, therefore it was not included in the simulations.

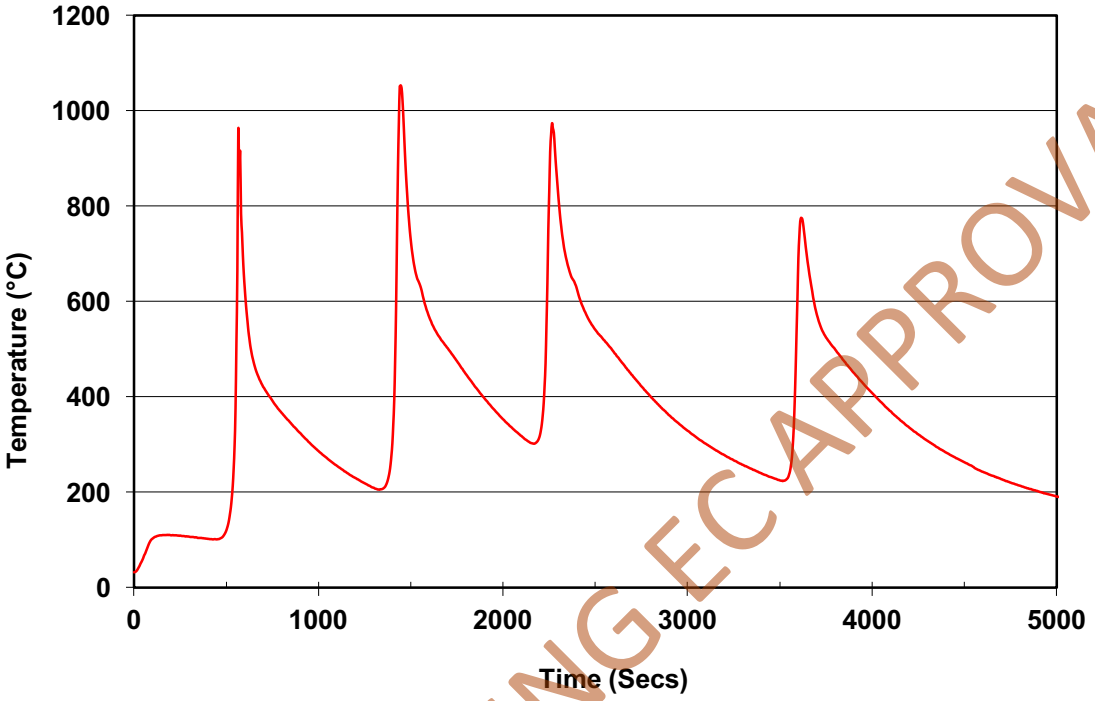

Figure 4.12 – Thermal history of TC3 for the experiment in 2008 [7]

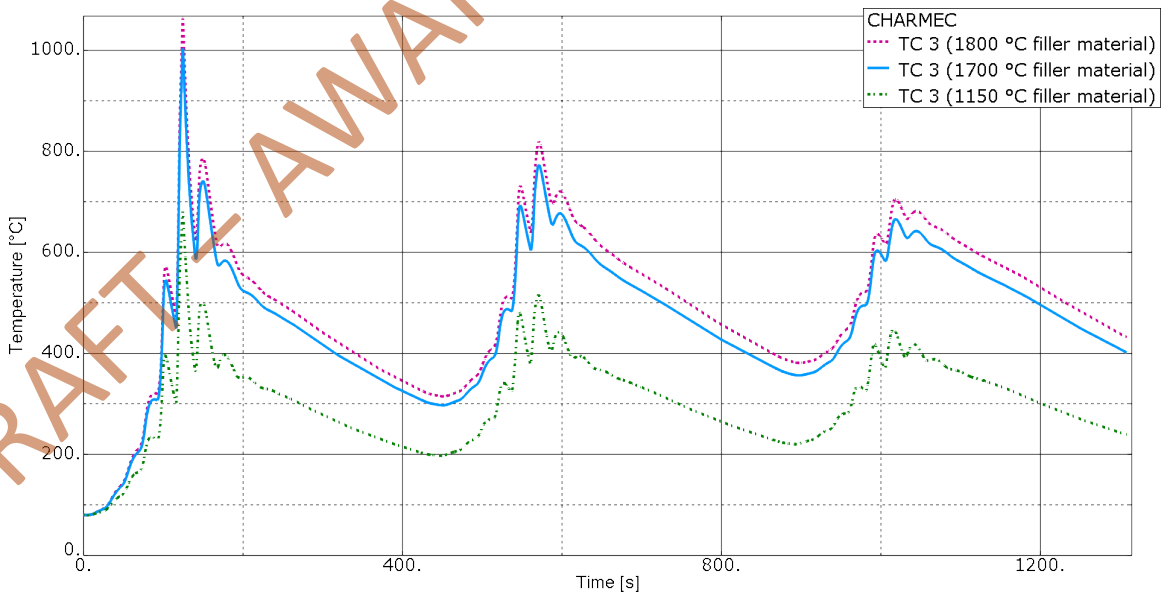

Figure 4.13 – Predicted thermal history for TC3 using different filler material temperatures

It can be seen in Figure 4.12 and Figure 4.13 that the temperature curves are shifted to higher values by the increase in temperature of the filler material.

Similarly, Figure 4.14 is a representation of the thermal evolution obtained by TC5 for the trial in 2008. Figure 4.15 shows predicted thermal histories for TC5 from FE

analyses featuring three different filler material temperatures and gives the same trends as noted from Figure 4.13.

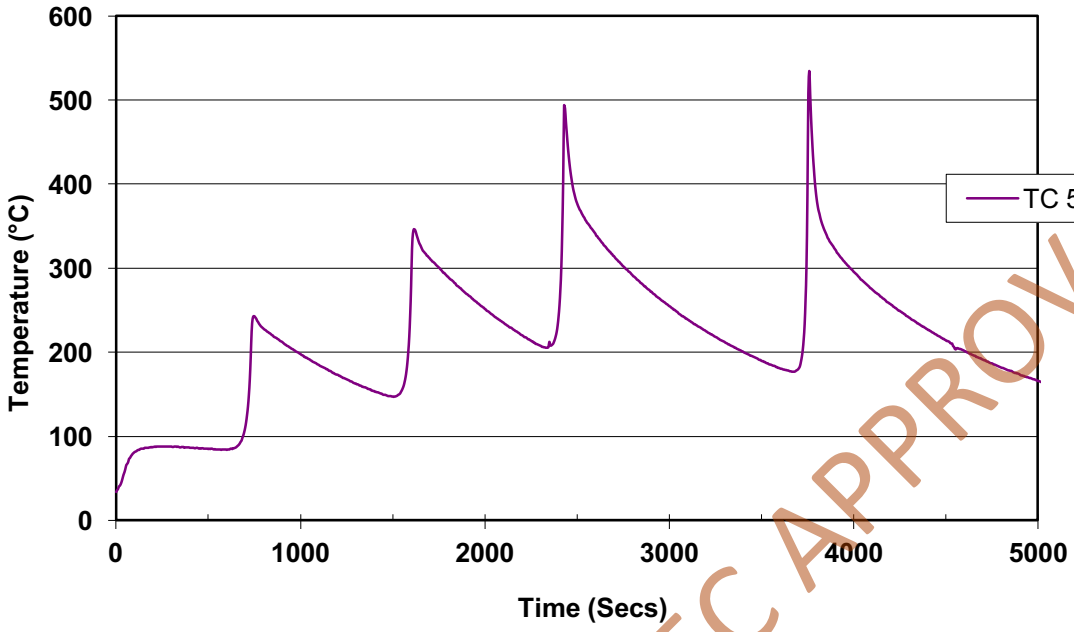

Figure 4.14 - Thermal history of TC5 from the experiment in 2008 [7]

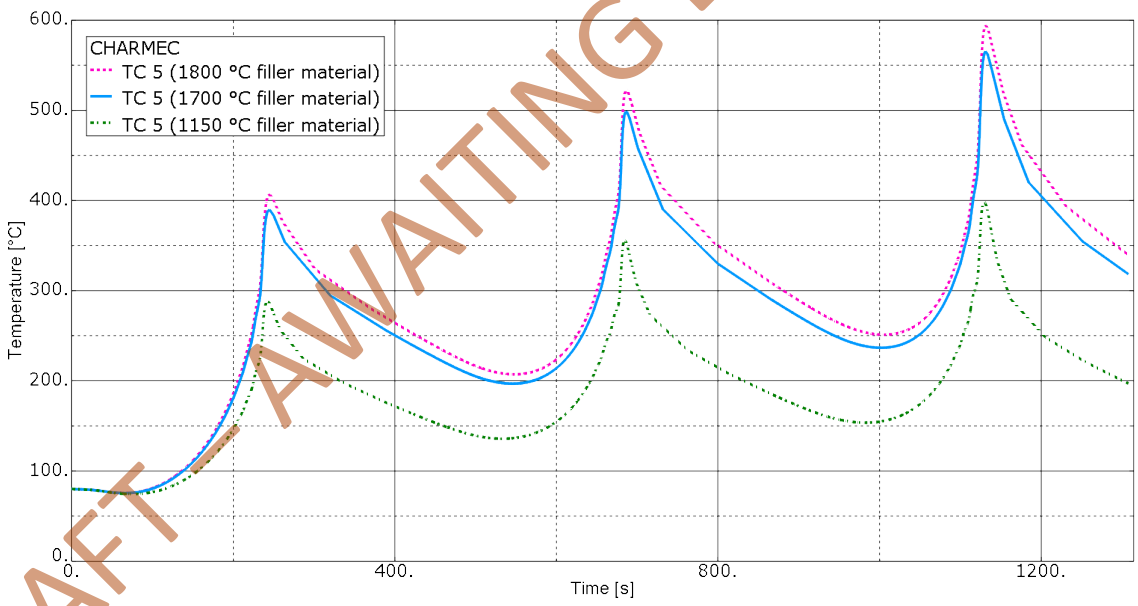

Figure 4.15 - Predicted thermal history for TC5 for different filler material temperatures

4.3.2 Influence of the thermocouple position

The second step of the analysis procedure consisted in studying the influence on the cooling curve of the position of the thermocouple. As a consequence, temperature evolutions for some different positions in the vicinity of the estimated thermocouple positions in the 2008 experiment have been derived.

In this analysis, the filler material was kept constant at 1700 °C (selected since it was the temperature which led to the closest results with respect to those obtained in the experiments of 2008, see section 4.3.1).

The three studied positions were all exactly in the middle of the cavity, at a depth of 8 mm from the rail gauge surface. The vertical distances from the cavity were 2.03 mm, 2.79 mm and 3.54 mm, see Figure 4.16.

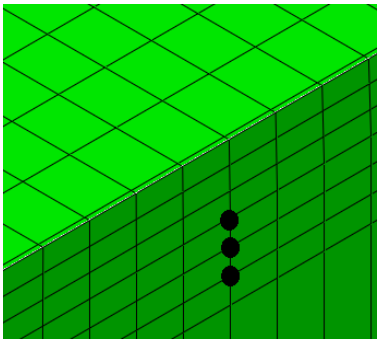

Figure 4.16 – The three analysed locations in the vicinity of TC3

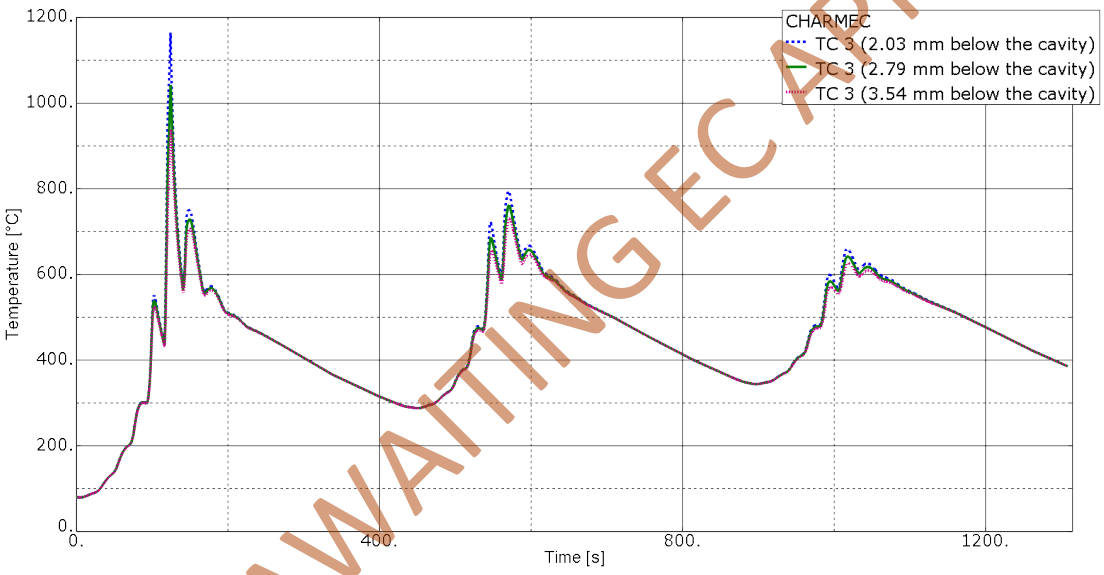

Figure 4.17 – Thermal histories for different positions in the vicinity of TC3 for a filler material temperature of 1700°C

Figure 4.17 shows that the disparity between the three curves is larger during the first pass, when the material volume between the thermocouple and the heat source is smaller. To make the graph more clear, Figure 4.18 and Figure 4.19 show zoom-ins of the first and in the second welding passes, respectively.

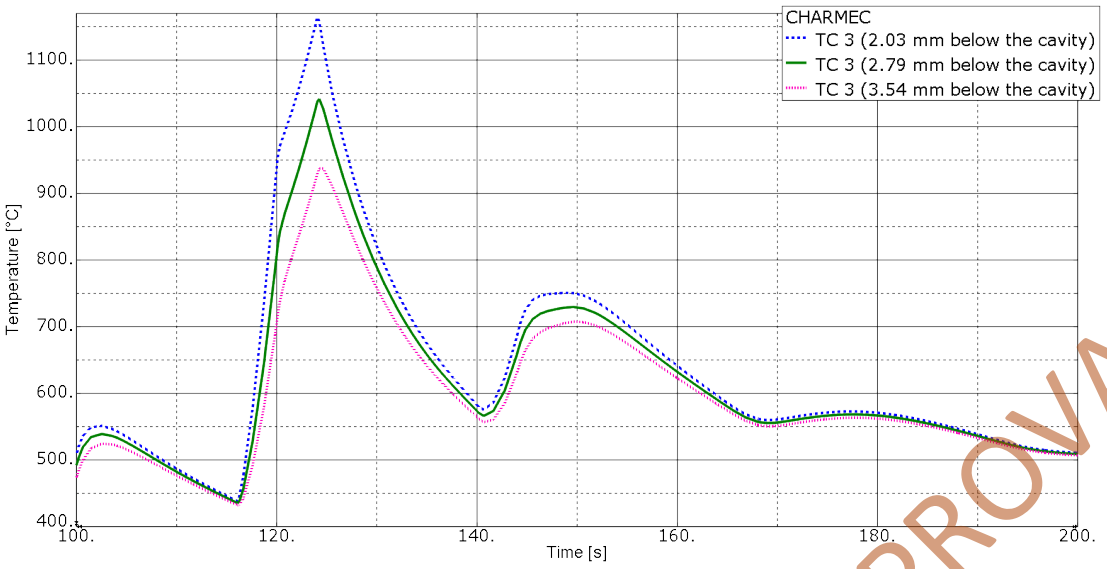

Figure 4.18 – First pass thermal history for different positions in the vicinity of TC3, for filler material temperature of 1700°C

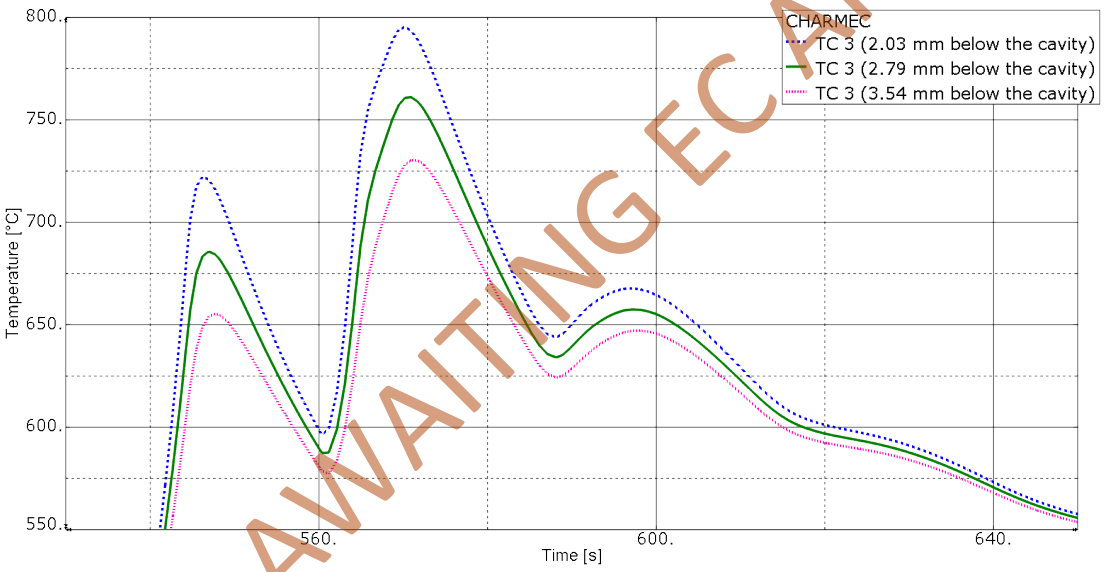

Figure 4.19 - Second pass thermal history for different positions in the vicinity of TC3, for filler material temperature of 1700°C

The same kind of study was performed for some possible locations of TC5. Here the studied position depended on both the vertical depth of the drilling and on the horizontal distance from the upper edge of the cavity. Thus, two degrees of freedom regarding the position of the analysis point were used. More information on the location of the points can be found in Table 4.3 and Figure 4.20.

Point	Drilling depth [mm]	Distance from the top cavity edge [mm]	Total distance from the cavity top corner [mm]
Point 1	5.00	2.28	5.49
Point 2	7.00	3.17	7.68
Point 3	9.43	2.03	9.65

Table 4.3 – The geometrical characteristics of the nodes used to approximate TC5

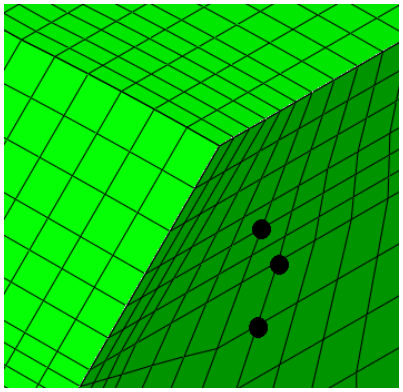

Figure 4.20 - The three analysed locations for TC5

Figure 4.21 shows the full thermal history for the three analysed locations in the vicinity of TC5, whereas Figure 4.22 to Figure 4.24 show in detail the peaks corresponding to the three passes.

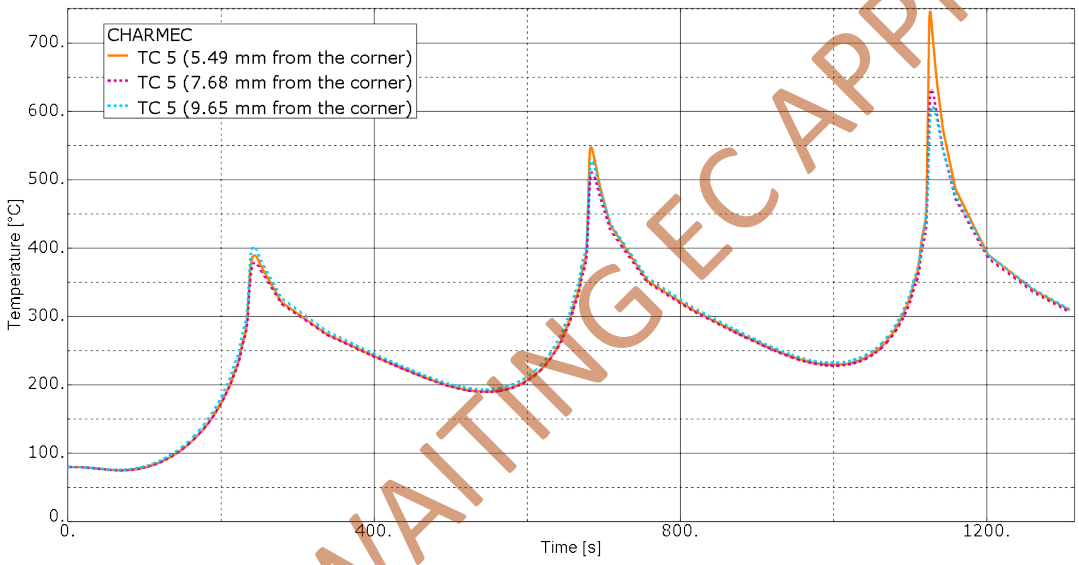

Figure 4.21 - Thermal histories for different positions in the vicinity of TC5 for a filler material temperature of 1700°C

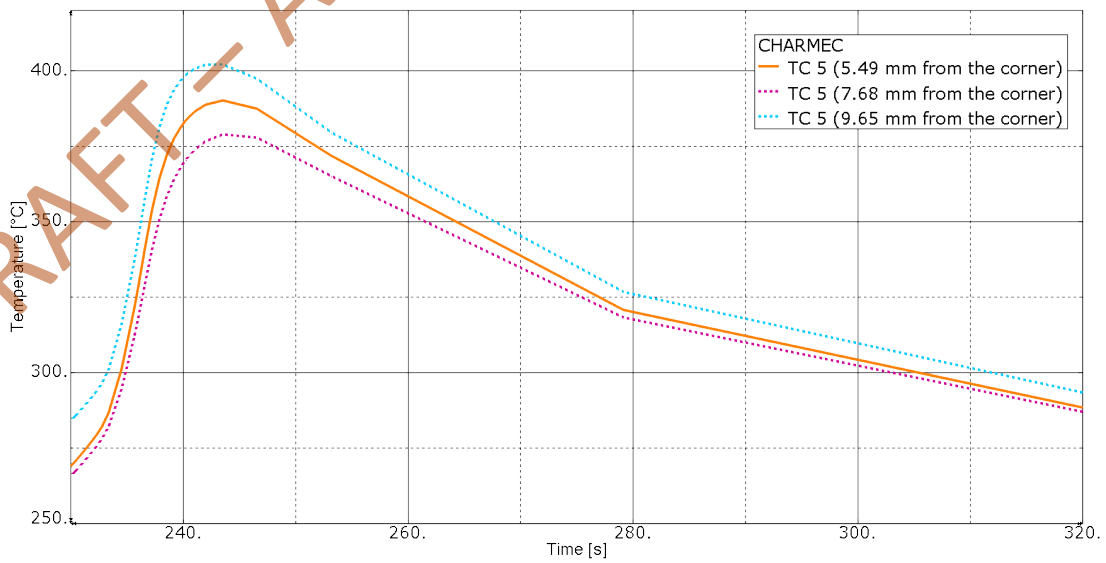

Figure 4.22 - First pass thermal history for different positions in the vicinity of TC5

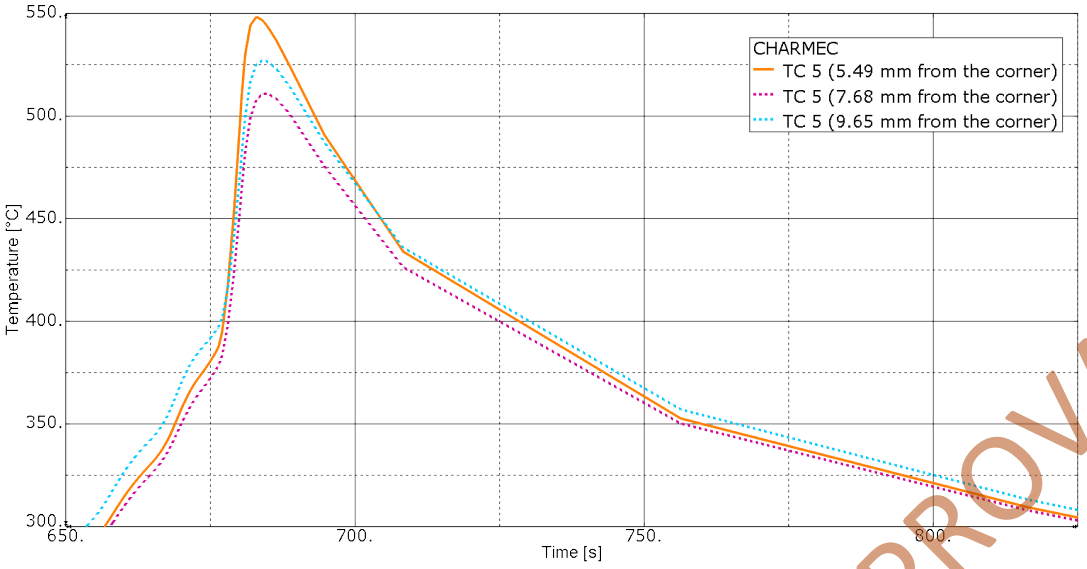

Figure 4.23 - Second pass thermal history for different positions in the vicinity of TC5

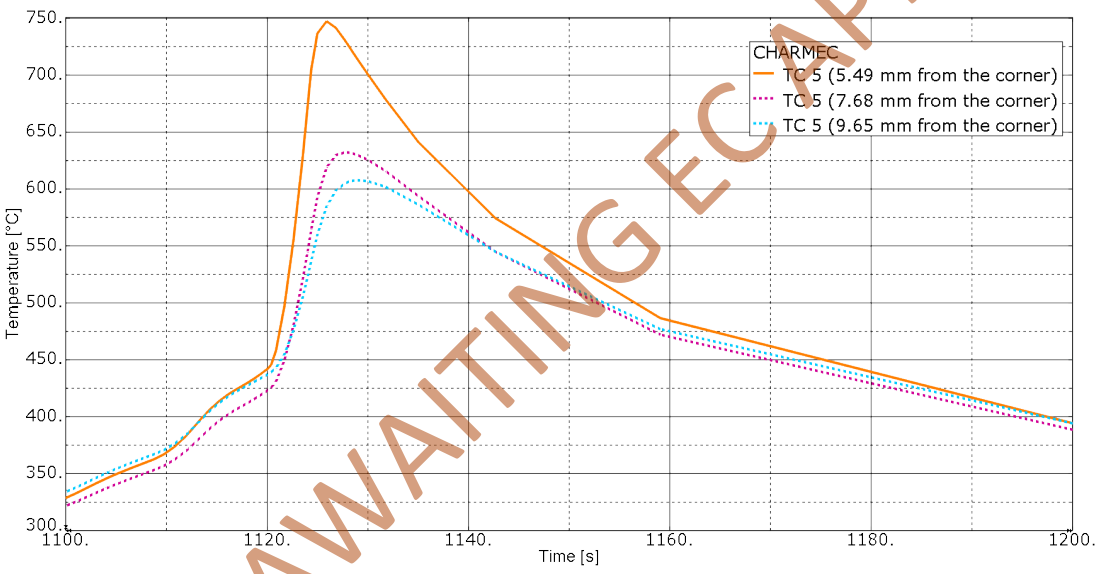

Figure 4.24 - Third pass thermal history for different positions in the vicinity of TC5

It can be noticed that in the case of the graphs referring to the temperature histories close to TC5 the location with the highest temperature was not always the same, as was the case of TC3. The magnitude of the peak indeed depended on the vertical depth of the thermocouple and the height of the deposited layer. For example, in Figure 4.22, the highest temperatures were recorded in the deepest point since the heat source was operating close to the bottom of the cavity. In Figure 4.24, on the other hand, the highest data were obtained on the most shallow point since the hot material was being laid on the top layer of the rail head.

The point which was located 7.68 mm from the cavity top corner, instead, followed a slightly different trend since it was located at a larger lateral distance from the cavity with respect to the other two test nodes. Nevertheless, the results were still within the range of the other analysed points and can therefore be considered consistent.

4.3.3 Influence of the corner geometry

The final step of this work focuses on the areas which were closer to the cavity corners to understand whether small changes in geometry could have any major influence on the cooling curves.

The studied points were chosen in such a way that their distance to the top cavity edge was very similar for all the analysed models (i.e. the reference geometry, the one with sharp corners and the one with rounded corners). Further, the points should be in the vicinity of the location of some thermocouples in the 2008 experiment.

The first point was in the vicinity of TC5. The position for the different cavity geometries are summarised in Table 4.4 where the drilling depth is from the running surface of the rail and the upper edge is the lateral side of the cut-out. A graphic representation of the location of the node in the case of the reference geometry is given in Figure 4.25.

Cavity corner geometry	Drilling depth [mm]	Distance from cavity top edge [mm]
Reference	7.00	3.16
Sharp	7.00	3.17
Rounded	6.99	2.94

Table 4.4 – Characteristics of the TC5 simulation points for the three geometries

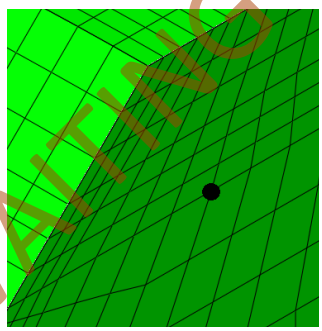

Figure 4.25 – The point used to simulate TC5 in the reference geometry

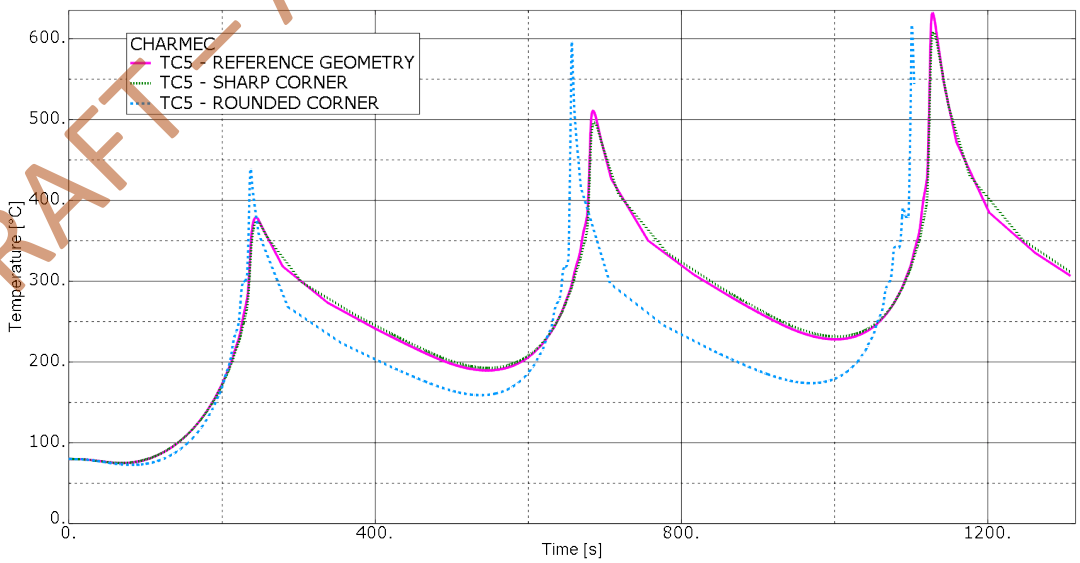

Figure 4.26 - Thermal histories in the vicinity of TC5 for different cavity corner geometries,with filler material temperature of 1700°C

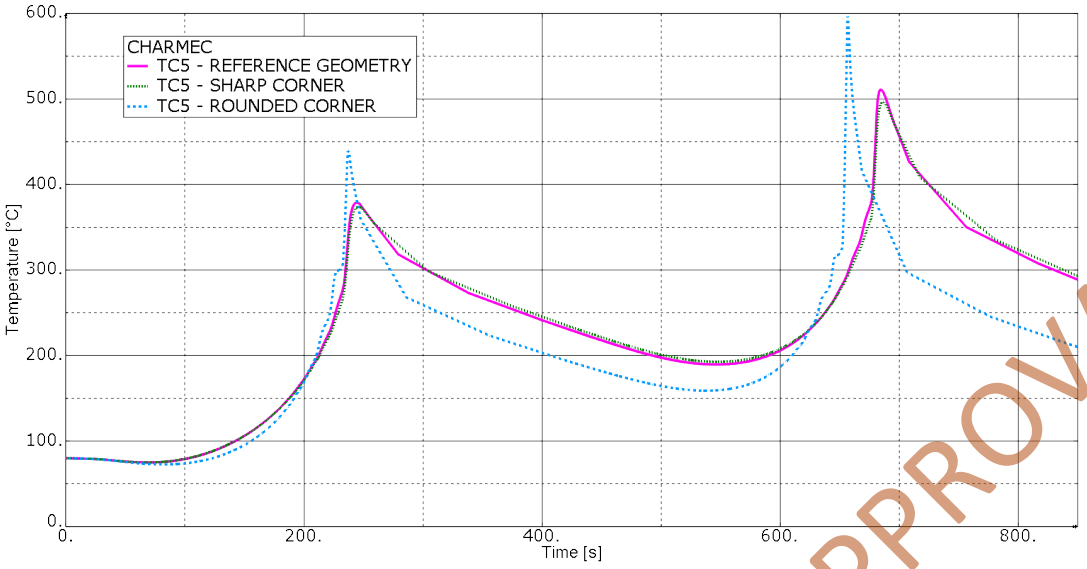

Figure 4.27 - Thermal histories in the vicinity of TC5 for the first two layers for different cavity corner geometries

Figure 4.26 and Figure 4.27 show the thermal histories at points close to TC5. It can be seen that the curves related to the reference model and to the one with the "sharp" corner follow a very similar path and their trends are hard to distinguish even in the zoomed-in version of the graphs.

The plot referred to the rounded corners model is slightly different. First of all, the time history is shifted: that is due to the fact that the variation in the cavity dimensions made the number of welding beads (and therefore the time required to complete them) slightly different.

Secondly, the peak temperatures for the first two passes in the rounded corners model are higher with respect to the other cases. That might be due to two reasons: the point of temperature evaluation in the model with the rounded corner was closer to the cavity (see Table 4.4) and the volume that the heat source had to fill in the reference and sharp corner cases was smaller than that of the circular one, see Figure 4.28, thus leading to a smaller heat input.

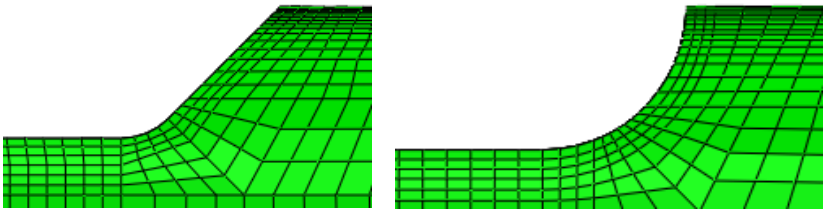

Figure 4.28 – Comparison between the corner shape in the reference geometry (left) and in the rounded one (right)

A similar comparison was done on some nodes representing TC4. Their positions with respect to the bottom of the cut-out are listed in Table 4.5 and the location in the reference geometry is depicted in Figure 4.29.

Corner geometry	Reference	Sharp	Rounded
Depth from the bottom of the cavity [mm]	2.03	2.11	2.00

Table 4.5 - Characteristics of the TC4 simulation points for the three geometries

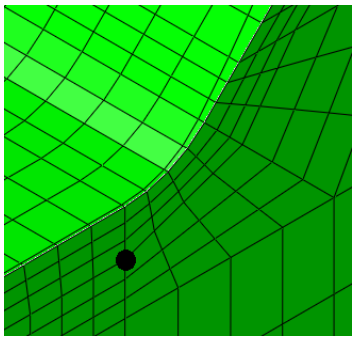

Figure 4.29 - The point used to simulate TC4 in the reference geometry analysis

The thermal history for TC4 showed its main differences in the first pass, see Figure 4.30.

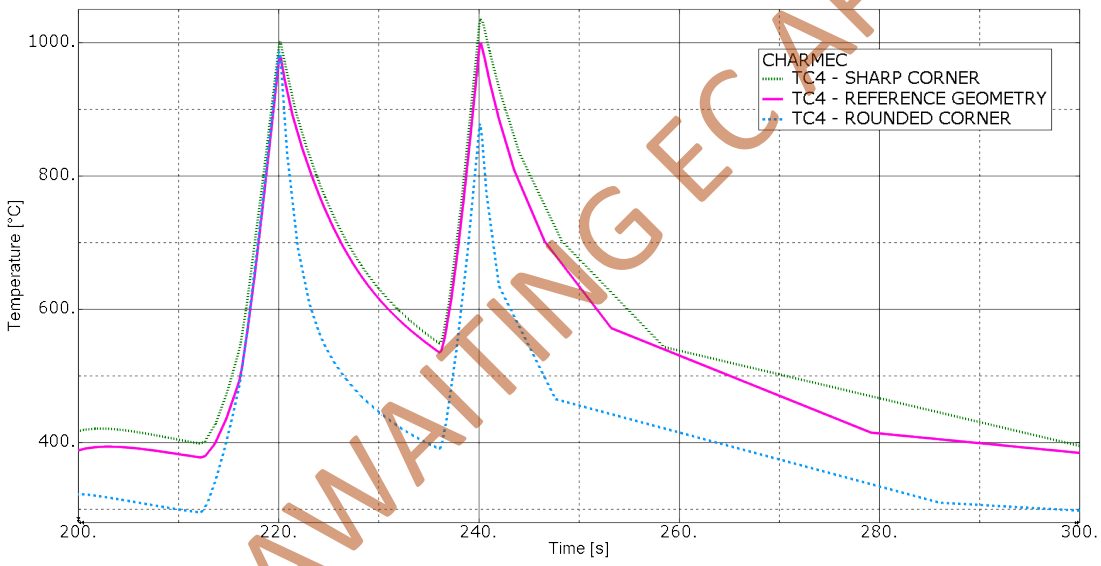

Figure 4.30 - Thermal histories for the first pass of TC4 for different corner geometries

Although the peak values for the three models were similar, the results show faster cooling rates for the rounded cavity corners model. That might be due to the fact that the curved corner geometry makes TC4 closer to the material zone which is unaffected by the welding procedure, see Figure 4.31.

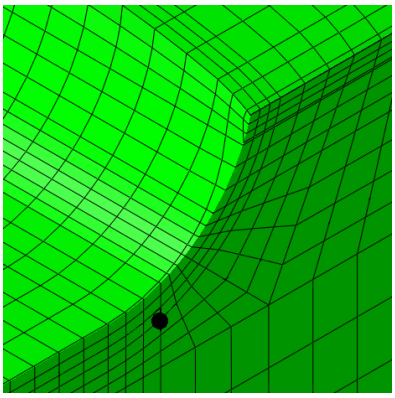

Figure 4.31 – The node representing TC4 in the rounded cavity corner model

5 Conclusions

The results presented in section 4 show the high potential of FE analyses in the field of heat transfer analyses applied to welding problems.

Firstly, the possibility to know the temperatures for all instants in time in every part of the repaired rail is a strong advantage. This is especially the case when (as happened in the trials held in July 2016) it is not possible to use thermocouples or similar devices during experimental processes. Another possible event that might push towards the use of numerical analyses might be the unexpected failure of the measuring equipment, as happened in the DDR experiments held in 2008. In addition, it is of course not possible to experimentally evaluate the temperatures in all points of the repaired weld even if all sensors operate as intended.

FE analyses also represent a tool to validate the metallurgical basis of the process developed by British Steel, as well. Today, preheating high carbon steels to temperatures above 343°C is considered necessary to slow down the cooling rates in the HAZ and to prevent the formation of martensite. The new DDR process tries to avoid hard microstructures by combining low preheat, optimum welding parameters and the weaved pattern [16]. Here FE-analyses are a useful tool in avoiding the difficulties in validating the new procedure by means of physical testing, which would require a very large number of samples to provide a statistically validated result. Instead, numerical simulations can be employed to verify that the formation of hard phases is not compatible with the evaluated cooling curves. Further, numerical analyses allows to test "what-if"-scenarios and thereby assess the robustness of the method.

On the other hand, simulations cannot completely take over trials and experimental results: the latter are fundamental in order to calibrate the analysis parameters and to validate the physical consistency of results. Another weak point of simulations is the necessity to make assumptions on some unclear aspects (e.g. boundary conditions, material properties) and the difficulty in taking into account all the phenomena which act during a process.

The consistency of the ways the FE-models were produced in this work was confirmed by both the results of the sensitivity analyses (see section 4.1) and the output of the different thermal histories.

As seen in section 4.3.1, the predicted temperature close to the cavity shows a clear dependency on the temperature of the filler material, thus providing a hint on the reliability of the numerical results. More in detail, an increase in the temperature of the deposited filler material (which is very hard to estimate or measure) from 1700 °C to 1800 °C resulted, during the first layer deposition, in a difference in temperature some 3.1 mm from the cavity of some 40 °C.

To further assess the validity of the numerical results, a comparison with experimental data collected in the 2008 trials was performed. As mentioned, those experiments featured a different process. On the other hand, that process is similar and the thermocouple results from the experiments the only sufficiently detailed results provided for validations.

Comparisons between experiments regarding temperature trends for layers 2 to 4 in Figure 4.12 and Figure 4.14 show similar peak values to those of simulated results for layers 1 to 3 in Figure 4.13 and Figure 4.15 when the molten material temperature is set to 1700 °C.

The most significant differences between the experimental and numerical results are the fact that in the experimental results, the peak temperatures for TC3 increase from the first to the second layer. Further, the cooling curves have different shapes where the predictions show some significant fluctuations, especially in the first passes.

The increase in peak temperatures when passing from the first to the second layer does not appear in the results of the FE model. However, provided the temperature of the applied fillet is consistent, an increase in temperature seems unlikely: Every time a welding layer is laid, the heat coming from the following layer has more material in which to be dissipated before reaching the thermocouple location. Thus, the predicted sequential decrease in peak temperatures is reasonable. However, an increase in peak temperature could occur if the welding is carried out so fast that the lower layer does not have time to cool down. As seen from the time scale of the experiment, this does not seem to be the case. The second reason could be that the conductivity is lower than assumed, which seems unlikely. A third reason could be that the preheating temperature is higher than 80°C (according to the experimental graphs, see Figure 4.12 and Figure 4.14, the area close to TC3 was preheated at about 110°C and the one close to TC5 reached a temperature of 88°C).

As for the fluctuations in the curves, these are due to the zig-zag path followed by the welding nozzle. The thermocouples are heated up when the filler material is deposited exactly above them (which is the moment that corresponds to the main peak in the graph), then the surrounding steel has some time (about 12–16 seconds, depending on the thermocouple position) to cool down before being heated up again by the deposition of a welding pass close to the location of the thermocouple. That these oscillations do not occur in the experiment measurements could be due to filtering of the measured temperature or that the process applies the filler in another pattern, but that does not seem to be the case according to the pictures in [7].

Those fluctuations are not present in the graphs referred to TC5 (Figure 4.15) as the latter is positioned after the end of the welding layer, so that the passing of the welding nozzle occurs just once per layer.

The second stage of this work, involved the study of the influence of the thermocouple position on the measured cooling curves. This study confirms the physical consistency of the simulations, as (not surprisingly) the highest temperatures occur when the heat source is close to the node where temperature is evaluated. Here it is seen that a shift in the location of temperature evaluation of 0.75 mm results in a difference in predicted (or measured) temperature for the first layer deposition in the order of 100°C. This discrepancy corresponds to a variation in the temperature of the filler material of some 200 °C.

An analysis of the influence of the detailed geometry of the cut-out and especially the corner areas revealed some interesting results. As already mentioned in section 4.3.3, the difference in the thermal history between the reference cut-out geometry and one with sharp corners is completely negligible. That can be easily explained with the

small differences in the actual geometry (see Figure 3.5 and Figure 3.7). Note that the simulations presume the fillet material to completely fill up the transition radius (or sharp corner in the case of no radius). In reality, the weld material may not completely fill a sharp corner. For that reason the geometry with a sharp corner could be unsuitable. However for simulation purposes they are as good as equivalent.

The model with the rounded geometry showed slightly different trends, but it is worth mentioning that the shape of its corners was considerably different from that of the previous two models, see Figure 3.6. The differences in temperatures can here be explained by this difference in geometry. It might also be useful to consider that such a notable variation in the geometry required a re-meshing and to the impossibility of finding a node located exactly in the same position (with respect to the heated filler material) as the ones used for the other models.

To sum up, the results obtained in the FE analyses performed in this MSc Thesis work are found to be physically consistent. The results should be of use to predict the behaviour of the steel in the heat affected zone. However, in order to improve the predictability, the model needs to be further calibrated and validated. For that reason there is a need for further experiments under controlled conditions. The thesis provides details on the experimental results that should be required for such a calibration/validation.

6 Future work

In general FE-analyses tend to provide results which are physically sound, but usually not fully exact. In particular for this study, some approximations were used and there are uncertainties in indata. For instance, the reliance of experimental data where the employed process is not the same as the one modelled and several parameters are unknown is not ideal. For this reason, further experimental data is required, as discussed in the conclusions. To this end, it would be wise to repeat the experimental procedure of the York experiments in June 2016, but equip the rail with thermocouples or other devices aimed at recording temperature-time curves.

Another limitation of the FE model is in the approximations which were made, especially with reference to material properties. In particular, several generic characteristic properties for low and medium carbon steels have been used. Moreover, the temperature dependency of those materials was only known up to 700 °C, while temperatures in the analysed models often reached 1700 °C. According to the way ABAQUS deals with temperature dependent material data, the values for material properties are interpolated if the analysis temperature falls within the range specified in the property definition. If the analysis temperature is below or above that interval, material properties are kept constant and respectively equal to the value at the minimum or maximum temperature in the specified interval. That implies that the material properties at 700°C were used to simulate the process where temperatures could reach values such as 1700°C. Experimental tests in order to quantify the specific properties of the welding and the rail steels on a wider temperature range would reduce the uncertainties in the numerical simulations.

The FE model can be refined by taking into account the effect that material phase transformations have on the cooling trends. This has been neglected throughout this study as no data were available on that, but including this phenomenon in more advanced FE models would make results more significant and complete.

Finally, performing the FE analyses on newer versions of the software and the welding interfaces would probably allow for a better discretisation, which might improve the accuracy somewhat.

Simulations which could be run in the future in order to better understand the effect of the investigated DDR procedure include thermomechanical analyses aimed at assessing the residual stresses in the HAZ after the material has cooled down.

Another interesting application is related to the case of the geometry with “sharp” corners. As stated in the previous sections, the differences in the thermal behaviour are not remarkable from a theoretical point of view. But, in reality, the welding procedure might not completely fill the sharp corners and some voids might form when the cooling process starts. Analysis that accounts for this phenomenon might provide a deeper knowledge on the relationship between the corner geometry, the cooling behaviour and the risk of weld defects.

7 Acknowledgements

The work performed within this Master Thesis is part of the Work Package 3.1 of the EU project In2Rail. The help of the following people and partners was fundamental for the completion of this work:

Jay Jaiswal, from ARR Rail Solutions Ltd and the Institute of Railway Research of the University of Huddersfield, who gave us feedback during the conference calls and provided us with literature and reports on repair welding procedures and in particular on the DDR method that is studied in this work.

Sandra Fretwell-Smith, from British Steel Ltd, who handed over the material data and some hints on how to approximate the real properties of the rail base and weld steels.

Stefan Kallander from Trafikverket.

The supervisor Elena Kabo and the examiner Anders Ekberg, the people at CHARMEC and at the department of Applied Mechanics of Chalmers University of Technology who shared opinions, material and information with me.

Finally, it is worth mentioning that this MSc Thesis project was carried within the Erasmus+ bilateral agreement between Chalmers University of Technology and Politecnico di Torino.

References

1. Jaiswal J. *Scope of Proposed Demonstration Trials*. EU project In2Rail report. Institute of Railway Research, University of Huddersfield, Huddersfield, United Kingdom, 8 pp, 2016
2. Jaiswal J. *Repair of Rail Head Defects – Status of Current Techniques*. EU project In2Rail report. Institute of Railway Research, University of Huddersfield, Huddersfield, United Kingdom, 19 pp, 2016
3. Grassie S L. Squats and squat-type defects in rails: the understanding to date. *Journal of Rail and Rapid Transit*, vol 226, p 235–242, 2011
4. NSW Transport RailCorp. *Rail Defects Handbook*, version 1.2, RailCorp Engineering manual, Sydney, Australia, 83 pp, 2012
5. UIC Code 712, *Rail Defects*, Union Internationale des Chemins de fer, Paris, France, 111 pp, 2002
6. Frick A, *BVH 524.100 – Katalog över rälsfel* (Catalogue of rail defects), Trafikverket, Borlänge, Sweden, 115 pp, 2015 (in Swedish)
7. Jaiswal J. *Cost Effective Repair of Rail Surface Defects – A Proposal for Demonstration of Developed Technology*. ARR Rail Solutions Ltd, Huddersfield, United Kingdom, 20 pp, 2016
8. Jaiswal J. *Repair of Rail Head Defects – Available Technologies*. IRR Report EU-I2R/31-01, Institute of Railway Research, University of Huddersfield, Huddersfield, United Kingdom, 8 pp, 2015
9. Frick A, *TDOK 2013:0393 Banöverbyggnad – Spårsvetsning* (Track structure – rail welding), Trafikverket, Borlänge, Sweden, 19 pp, 2015 (in Swedish)
10. Johnson R S. *The Repair of Discrete Rail Defects – Analysis of the method developed by ARR*. INFERRICITY Ltd, Doc. ref. V01-13-06-16, Derby, United Kingdom, 23 pp, 2016
11. Fretwell-Smith S, Zhu C. *Evaluation of welding feasibility of head repair welds*. Document number BritishSteelRD_12, British Steel Ltd, Scunthorpe, United Kingdom, 31 pp, 2016
12. ABAQUS. *ABAQUS/Standard*, version 6.14, Dassault Systèmes Simulia Corp., Providence, USA, 2014
13. ABAQUS, *ABAQUS extension for welding simulations*, Dassalult Systèmes Simulia Corp., Providence, USA, 2012
14. Jerath V, Smith H, Jaiswal J. *Discrete Defect Repair – A Novel Process*. TATA Steel Ltd and Corus Group, 15th technical meeting of the Institute of Rail Welding, Power Point presentation, 27 slides, 2009
15. Frick A, *BVH 524.12 – Måttuppgifter för räler och tungämnen. Standardprofiler samt äldre och utgångna profiler* (Dimensions for rails and switch blades. Standard, older and discarded profiles), Trafikverket, Borlänge, Sweden, 43 pp, 2015 (in Swedish)
16. Jaiswal J. *Personal communication on the shape of the cavity, on the filler material and on the experimental procedures*. ARR Rail Solutions Ltd, Huddersfield, United Kingdom, 2017

17. Fretwell-Smith S. *Personal communication on material properties regarding the rail material and the weld consumable.* British Steel Ltd, Scunthorpe, United Kingdom, 2017

18. ESAB. *Welding Handbook. Consumables for manual and automatic welding*, Eighth edition, ESAB North America, USA, 529 pp, 2016

19. Hlavaty I, Sigmund M, Krejčí L, Mohyla P. The bainitic steels for rails applications. *Materials Engineering*, vol 16, no 4, p 44–50, 2009

20. Andersson E, Berg M, Stichel S. *Rail Vehicle Dynamics*. Division of Rail Vehicles, Kungliga Tekniska Högskolan, Stockholm, Sweden, 2007

21. Liu G R, Quek S S. *The Finite Element Method, A Practical Course – Second Edition*. Butterworth-Einemann, Waltham, United States, 421 pp, 2015

22. Wen S. *Modelling rail head repair welding*. TATA Steel Ltd, Project number 11205-01, London, United Kingdom, 27 pp, 2015

23. Wen S, Smith H. *Modelling of heat affected zone cooling rates during the repair welding of grooved rail*. TATA Steel Ltd., Project number 7855/03, London, United Kingdom, 19 pp, 2010

24. Bray D P, Leggatt N A, Dennis R J, Smith M C, Bouchard P J. *Numerical Methods For Welding Simulation – The Next Technical Step.* Frazer-Nash Consultancy Ltd and British Energy Generation Ltd for the SIMULIA 2009 Customer Conference, United Kingdom, 15 pp, 2009

Appendix A – Sensitivity analysis

As anticipated in Section 4.1, the results regarding the sensitivity analysis on the other two nodal points (the "central" and the "right" ones) are presented in this appendix.

A1 Central Point

The "central node", here referred as "SA-C", was located exactly at the centre of the cavity, with respect to both the longitudinal and the lateral directions of the rail. Its depth from the bottom of the milled surface was 2.03 mm, see Figure A.1.

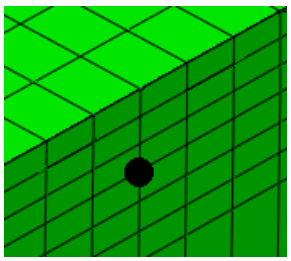

Figure A.1 – The position of SA-C node

Table A.1 summarises the main points of the thermal history for the FE-node SA-C:

Moment	Time instant [s]	Temperatures [°C] and Mesh			coarse-medium difference [%]	medium-fine difference [%]
		coarse	medium	fine		
1st peak	128	734,8	723,3	722,6	1,57	0,10
1st minimum	442	198,4	193,2	192,2	2,62	0,52
2nd peak	562	555,6	542,5	542,6	2,36	0,02
2nd minimum	888	221,6	215,3	214,3	2,84	0,46
3rd peak	1007	490,9	476,9	475,7	2,85	0,25
3rd minimum	1308	239,7	232,1	231,3	3,17	0,34

Table A.1 – Temperature values for the nodal point SA-C for the three different meshes

The temperature trend for the SA-C FE-node is depicted in Figure A.2. Figure A.3 represents the thermal history for the first layer deposition for SA-C.

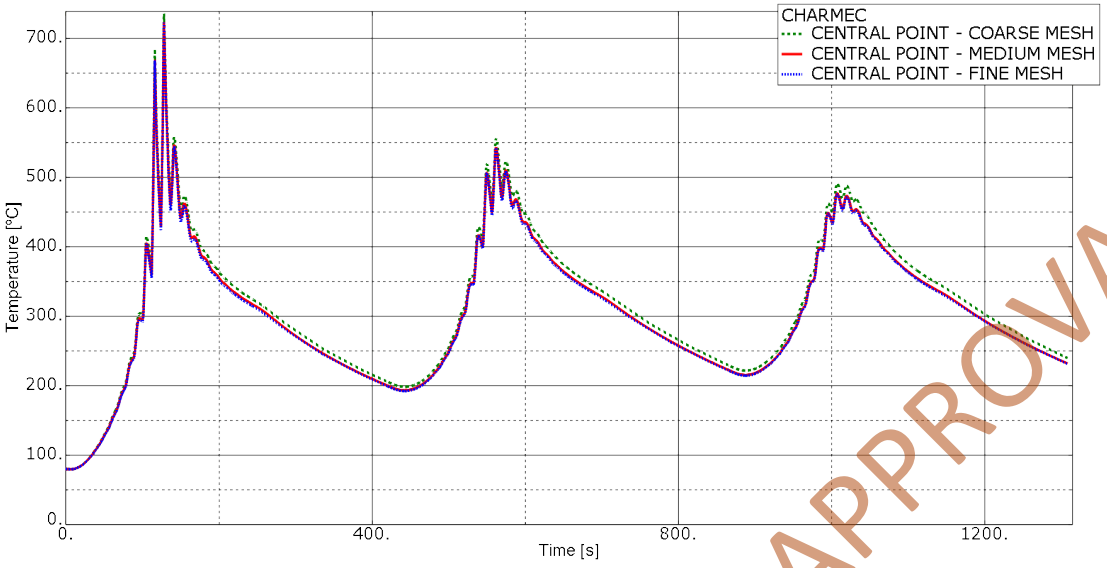

Figure A.2 – Thermal history for SA-C node for the three meshes

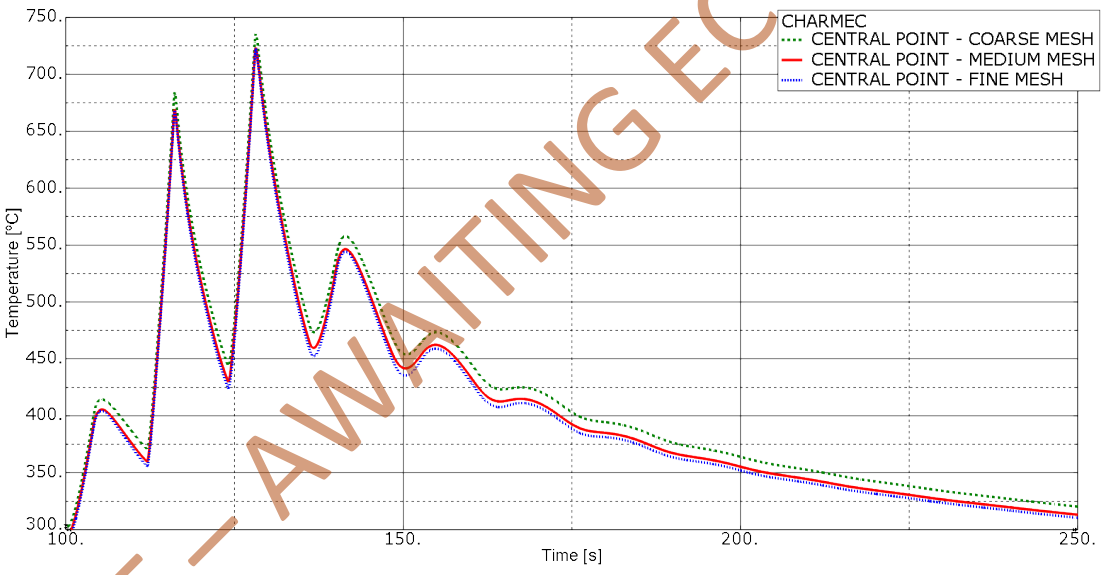

Figure A.3 – Comparison of the time histories evaluated using the three meshes in SA-C node for the time associated to the first layer deposition

A2 Right point

The "right node", here referred as "SA-R", was located close to the corner where the deposition of the three layers ends, at a depth of 7 mm, which is comparable to the one of the interface between the first and the second layer and along the longitudinal plane of the rail, see Figure A.4.

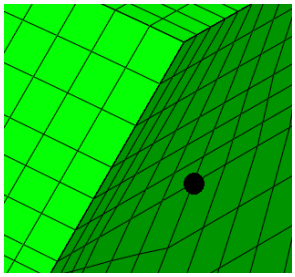

Figure A.4 - The position of SA-R node

The main points of its thermal history for the different meshes are shown in Table A.2:

Moment	Time instant [s]	Temperatures [°C] and mesh			coarse-medium difference [%]	medium-fine difference [%]
		coarse	medium	fine		
1st peak	240	317,4	308,6	306,4	2,77	0,71
1st minimum	533	137,1	133,8	133,1	2,41	0,52
2nd peak	682	429,7	416,8	415,4	3,00	0,34
2nd minimum	979	155,9	151,8	151,1	2,63	0,46
3rd peak	1126	512,8	502,5	502,6	2,01	0,02
3rd minimum	1308	239,7	232,1	231,3	3,17	0,34

Table A.2 – Temperature values for the nodal point SA-R for the three different meshes

The temperature trend for SA-R node is depicted in Figure A.5. Figure A.6 represents the thermal history for the first layer deposition for SA-C node.

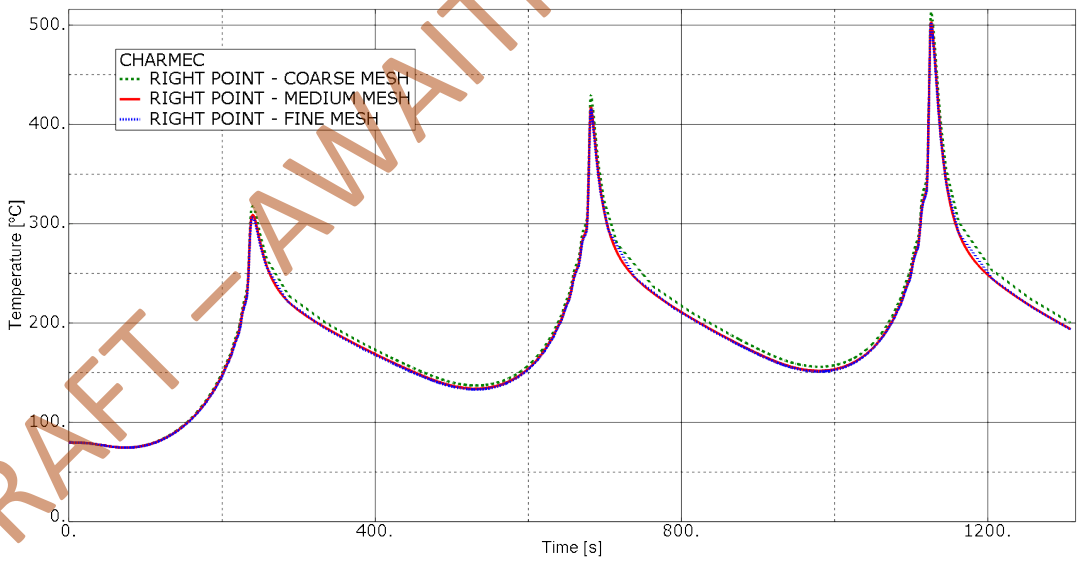

Figure A.5 - Thermal history for SA-R node for the three meshes

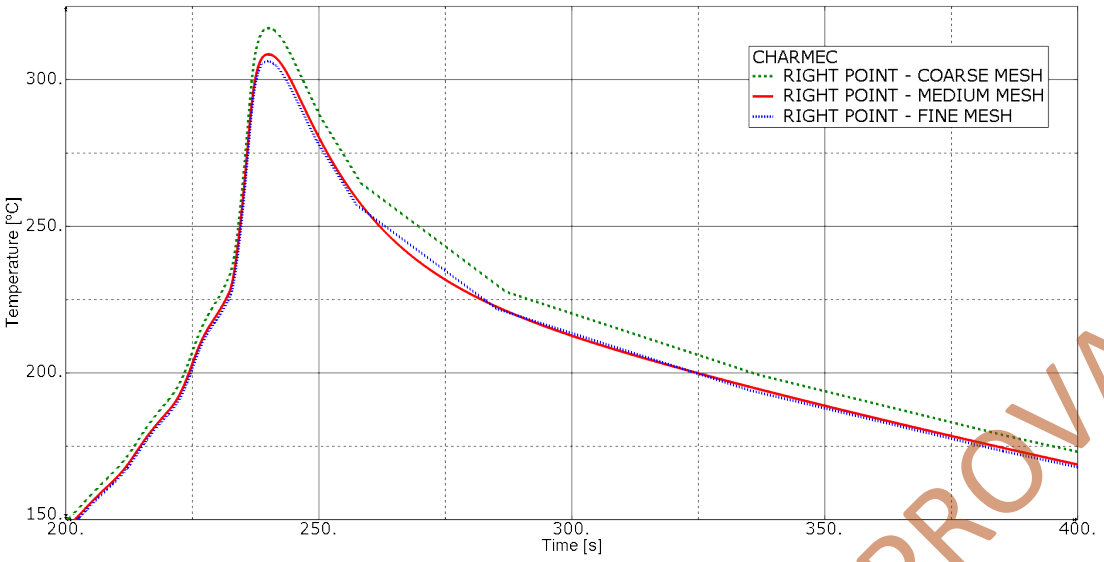

Figure A.6 - Comparison of the time histories evaluated using the three meshes in SA-R node for the time associated to the first layer deposition

The results in Table A.1 and Table A.2 confirm the ones obtained in section 4.1. The difference in output between the coarse and the medium mesh is in between 2% and 3%, whereas the one between the medium and the fine mesh is again around 0.4%.

The same trend is witnessed in Figure A.2 to Figure A.6, which confirm the results discussed in section 4.1.